GEOLOGICAL INVESTIGATION OF RARE EARTH ELEMENT AND URANIUM DEPOSITS OF THE BOKAN MOUNTAIN COMPLEX, PRINCE OF WALES ISLAND, SOUTHEASTERN ALASKA

J. Dostal [1], D. J. Kontak[2], J. Hanley[1] and V. Owen[1]

[1] Department of Geology, Saint Mary's University, Halifax, NS B3H 3C3, Canada
[2] Department of Earth Sciences, Laurentian University, Sudbury, ON P3E 2C6, Canada

Final Technical Report In Fulfillment of the Requirement under U.S. Geological Survey Grant G09PA00039.

Abstract

The Bokan Mountain complex is a small (6.5 km^2) Jurassic (~177. 2 ± 0.2 Ma, U-Pb zircon) peralkaline granitic intrusion located near the southern tip of Prince of Wales Island (Alaska). The complex hosts several uranium and thorium prospects, one of which was mined intermittently between 1957 and 1971. The uranium mineralization is structurally controlled and mainly occurs in a plunging pipe-like ore body up to 24 m in diameter with ~ 1 wt. % U_3O_8 and 3 wt. %ThO_2. In addition, there are several major rare earth element (REE) prospects related to the complex which predominantly occur as clusters of mineralized felsic dikes and alteration (metasomatically enriched) halos associated with NW-trending shear-fault zones, some of which can be traced for > 2 km. A recent mineral resource estimate has reported 3.7 million tonnes grading 0.75 wt. % ∑REE and Y oxides from two main zones.

The complex is a circular intrusive body composed of highly fractionated peralkaline granitic rocks hosted by a Paleozoic basement which includes granitoids dated at 469.2 ± 3.9 Ma (U-Pb zircon). In turn the complex was intruded by two suites of Cretaceous dikes dated at 150 and 105 Ma ($^{40}Ar/^{39}Ar$). The peralkaline granites are typically leucocratic with 2-10 vol. % of sodic amphibole (arfvedsonite) and sodic clinopyroxene (aegirine). The intrusion is composed of two main units: an outer ring made up predominantly of aegirine granite and a core composed of arfvedsonite granite; locally, a zone of mixed aplite-pegmatite borders the complex. The granitic rocks are high in alkalis (8-10 wt. %) with an agpaitic index [(Na+K)/Al] >1, are ferroan with high Fe_2O_3 (~3.5-5 wt. %) but low MgO (<0.04 wt. %) and with the (FeO*/(MgO+FeO*) ratio > 0.95. The rocks are characterized by high contents of high-field-strength-elements (HFSE), REE (particularly the heavy REEs), Th and U and low contents of CaO (<0.2 wt. %), Sr, Ba and Eu. The composition of the rocks reflects extensive fractional crystallization, in part due to the role of volatiles (including fluorine) and alkalis. Volatiles and alkalis are known to depress the solidus temperature and suppress crystallization of accessory minerals, which contain the bulk of HFSE and REE, until the latest stage of fractionation. The parent magma was likely derived from low degree partial melting of the lithospheric mantle metasomatically enriched in HFSE, REE, Th and U and possibly halogens during an earlier subduction zone related event, probably during the Ordovician. At an advanced stage of fractional crystallization, the magma became fluid-saturated and over-pressured, which led to the escape of a fluid-rich, highly fractionated melt and deposition of the major part of the U, Th, HFSE and REE mineralization. When these highly fractionated melts and aqueous fluids were exsolved they followed pre-existing zones of weakness (i.e., faults and shears) that penetrated through the complex and into the surrounding country rocks for up to several km from the intrusion. Although mineralization in the complex initially occurred in the zones of peralkaline granitic pegmatites and aplites, they and the surrounding host rocks were extensively overprinted at moderate temperature by hydrothermal fluids which caused a significant metasomatic remobilization of rare metals. Thus, most of the REE and HFSE mineralization reflect both an initial magmatic event, but more importantly a pervasive hydrothermal metasomatism which upgraded the mineralized zones.

Table of Contents

1. Introduction ---------- 1

2. Regional Geology of the Southern Prince of Wales Island ---------- 1

3. Geology of the vicinity of the Bokan Mountain Complex ---------- 2

4. Bokan Mountain Complex ---------- 3

5. Mineral Prospects ---------- 6

6. Mineralogy/Mineral Chemistry ---------- 8

7. Geochronology ---------- 10

7. 1. U-Pb zircon age ---------- 11

7. 2. $^{40}Ar/^{39}Ar$ age dating ---------- 11

8. Geochemistry ---------- 12

8. 1. Granitic Rocks ---------- 12

8. 2. Mafic and Intermediate Rocks ---------- 16

8. 3. Isotopes ---------- 17

9. Fluid Inclusion Study ---------- 19

10. Discussion ---------- 21

10.1. Petrogenesis of the Peralkaline Granites ---------- 21

10. 2. Origin of Mineralization ---------- 23

10. 3. Tectonic Setting: Geochemical Constraints ---------- 25

11. Conclusions ---------- 25

Acknowledgements ---------- 27

References Cited ---------- 27

Figures ---------- 36-75

Field Photographs ---------- 76-84

Tables ---------- 85-114

Appendix 1. History of Mining and Exploration ---------- 115

Appendix 2. Analytical Methods ---------- 117

Appendix 3. Sample Locations ---------- 120

1. Introduction

The Bokan Mountain complex is a small peralkaline granitic intrusion located near the southern tip of Prince of Wales Island (the southernmost island of Alaska), about 60 km SSW of Ketchikan, Alaska and 130 km NW of Prince Rupert, British Columbia, Canada (Fig. 1). It hosts several major uranium and thorium prospects, one of which, the Ross-Adams deposit, was mined intermittently between 1957 and 1971, thus it represents the only uranium production to date from Alaska (Thompson, 1988, 1997; Long et al., 2010). The Ross-Adams mine produced about 77,000 metric tons of high-grade uranium ore that averaged about 1 wt.% U_3O_8 and nearly 3 wt.% ThO_2 (Stephens, 1971; Long et al., 2010). The discovery and mining of uranium triggered further exploration in the area. Although most of the early investigations centered on the uranium mineralization, MacKevett (1963) reported unusually high concentrations of rare earth elements (REE), Y, Zr and Nb in the granitic rocks at Bokan Mountain. Subsequently, these resources (REE, Y, Zr, Nb and Ta) were evaluated by the U. S. Bureau of Mines (e.g., Warner and Barker, 1989) and U.S. Geological Survey (Philpotts et al., 1996, 1998; Long et al., 2010). Unlike many REE deposits, the Bokan Mountain complex is distinctly enriched in heavy REE (HREE that is Gd, Tb, Dy, Ho, Er, Tm, Yb and Lu as well as Y). However, there is only a limited amount of recent geological information on the intrusion and related dikes and detailed petrological-geochemical investigations are needed, particularly as the area may host strategic REE and high-field strength element (HFSE) resources (Warner and Barker, 1989; Long et al., 2010). The purpose of this report is to present data on the petrography, mineral chemistry, major- and trace element geochemistry, radiogenic and stable isotope geochemistry, geochronology and fluid inclusions. These data are then used to make some inferences regarding the genesis of the Bokan complex and related mineralization, as well as the tectonic setting of the intrusion.

2. Regional Geology of the Southern Prince of Wales Island

Prince of Wales Island (PWI), including the Bokan Mountain complex, is part of the allochthonous Alexander terrane of the northern Cordillera (Gehrels and Saleeby, 1987a), which extends from eastern Alaska and southwestern Yukon southward into southeastern Alaska and coastal British Columbia (Gehrels and Saleeby, 1987b; Colpron et al., 2007). The Alexander terrane is composed primarily of Late Proterozoic and Paleozoic volcanic and sedimentary units intruded by Paleozoic and Mesozoic plutonic rocks. All these units have juvenile (mantle-derived) isotopic characteristics, which are comparable to those of a primitive island arc (Samson et al., 1989), i.e. most of the rocks were derived from juvenile magmas that were essentially not contaminated by interaction with old continental crust. The terrane represents a Neoproterozoic-early Paleozoic island arc that originated off board from western North America (Laurentia) and was transported into the Cordilleran realm by accretionary tectonic processes (Nokleberg et al., 2000; Colpron et al., 2007).

The oldest recognized geological unit in the southern PWI is the Neoproterozoic to Lower Cambrian Wales Group (Gehrels and Saleeby, 1987a; Gehrels, 1992). The group consists of arc-related volcanic and volcanoclastic basaltic to andesitic rocks (Gehrels and Saleeby, 1987a; Slack et al., 2007) intercalated with greywacke, shale and rare limestone. These rocks, along with several enclosed plutons, were deformed and regionally metamorphosed to greenschist or amphibolites facies during the Middle Cambrian-Early Ordovician Wales orogenic event (Gehrels and Saleeby, 1987a).

The overlying and tectonically juxtaposed Ordovician-Lower Silurian Descon Formation (Redman, 1981; Slack et al., 2007) is composed of basaltic to andesitic, with subordinate rhyolitic, volcanic rocks and fine-grained marine clastic sedimentary rocks with Ordovician and possibly early Silurian conodonts and graptolites (Eberlein et al., 1983; de Saint-Andre et al., 1983). This sequence was intruded by dioritic to granitic plutons with ages ranging from 480 to 438 Ma (Gehrels and Saleeby, 1987a). The volcanic-plutonic complex has been inferred to be emplaced in an arc setting (Gehrels and Saleeby, 1987a). The Descon Formation and associated intrusions underlie most of the southern PWI and form the basement rocks that host the Bokan Mountain complex (Fig. 2). The formation is separated from the overlying Lower Devonian Karheen Formation by a regional unconformity, which records the Middle Silurian to early Devonian Klakas orogenic event. This event produced greenschist-facies mineral assemblages (Gehrels and Saleeby, 1987a; Slack et al., 2007) and was followed by the deposition of the Lower Devonian Karheen Formation, which ranges from mudstone and black shale in the upper parts of the sequences to conglomerate at the bottom and are intercalated with volcanic rocks of basaltic to andesitic composition (Gehrels and Saleeby, 1987a). These Devonian rocks, together with shallow marine carbonates, suggest a tectonically-stable environment which lasted until the Permian (Soja and Krutikov, 2008).

Mesozoic units in the southern part of PWI include the Jurassic alkaline/peralkaline intrusions, such as the Bokan Mountain and Dora Bay complexes, several generations of mafic to felsic dikes and mid-Cretaceous diorite and granodiorite plutons. Many of these rocks are related to igneous events associated with northeast and northwest strike-slip faults, whereas others were emplaced in an extensional environment (Gehrels and Saleeby, 1987a; Drinkwater and Calzia, 1994).

The subduction-related Cretaceous intrusions of the island belong to a belt of intrusive bodies of the Coastal plutonic complex of British Columbia and Alaska that formed during terrane convergence (Brew, 1988; Colpron et al., 2007). There is evidence for thrusting during the Cretaceous and of major, Tertiary age, regional strike slip faults which record transform faulting between the Pacific and North American plates.

3. Geology of the vicinity of the Bokan Mountain Complex

The country rocks in the vicinity of the Bokan Mountain complex (Bokan complex) are comprised primarily of rocks of the Descon Formation and associated intrusions (Fig. 2). The Descon rocks include slates and volcanic rocks. The slates form a crudely semicircular band around the western side of the Bokan complex. They are predominantly carbonaceous black slates with disseminated pyrite and contain bands of impure quartzites, metasiltstones and marbles. Around the Bokan complex, the slates are converted to hornfels.

Descon Formation volcanic rocks include both mafic and felsic types. The mafic rocks occur as flows, breccias, tuffs or dikes and are basaltic to andesitic in composition. The flows are fine-grained but porphyritic with phenocrysts mostly of plagioclase typically 1-3 mm in size enclosed in a recrystallized groundmass composed of chlorite, epidote and albite. In thicker units or dikes, the mafic rocks are coarser grained and resemble diabase dikes. Felsic rocks usually occur as rhyolitic breccias or tuffs.

MacKevett (1963) and Gehrels and Saleeby (1987a) recognized three different mappable units of Middle Ordovician-Early Silurian granitoid rocks in the vicinity of the complex, each of which has a distinct age: granodiorite (~462- 472 Ma), quartz diorite (~ 445-446 Ma) and quartz

monzonite (438 Ma), the latter of which is dominant around the Bokan complex (Fig. 2). However, quartz monzonite from the vicinity of the complex (near the Dotson Zone; Fig. 3) yielded an age of 469 Ma (this study), which indicates that the rocks of the older magmatic stage occur along the contact with the Bokan intrusion and suggests that the three Paleozoic granitoid units overlap in their age ranges.

The Middle Ordovician granodiorite is a medium to coarse-grained hypidiomorphic granular rock composed of quartz, plagioclase (oligoclase), hornblende (5-20 vol.%) and interstitial microperthite (MacKevett, 1963). Quartz diorite is fine to medium-grained and consists of plagioclase (andesine) and green hornblende (~ 25 vol. %) with subordinate biotite and interstitial quartz and K-feldspar. The rock passes to medium-grained diorites and gabbros composed mainly of hornblende and plagioclase. The colour index (volume % of Fe- and Mg-bearing minerals) of the gabbroic rocks reaches up to 80. Gabbroic to dioritic bodies that outcrop in the vicinity of the Bokan complex, particularly around the Dotson shear/fault zone, are probably a part of this unit (Gehrels and Saleeby, 1987a).

Quartz monzonite is medium to coarse-grained mainly hypidiomorphic granular and is composed of K-feldspar, plagioclase (oligoclase; Table 1c) and quartz with 5-25 vol. % mafic minerals (biotite, hornblende). K-feldspar forms microperthitic crystals in places (MacKevett, 1963). Compared to quartz diorite, both quartz monzonite and granodiorite contain higher proportions of quartz and K-feldspar. On the other hand, the quartz diorite contains a higher proportion of hornblende relative to biotite than do the granodiorite and quartz monzonite.

Mafic (basaltic-andesitic) and felsic dikes typically < 3 m thick, are widespread in the vicinity of the Bokan complex. Some of the mafic dikes are probably related to gabbroic bodies scattered throughout the area. MacKevett (1963) and Gehrels and Saleeby (1987a) distinguished several generations of dikes and dike swarms. Some dikes appear to be co-magmatic with Ordovician-Early Silurian plutonic rocks whereas others are younger and there are dikes that cut the Bokan complex. Most of these young dikes are mafic to intermediate in composition, fine-grained aphanitic and composed of hornblende and/or clinopyroxene and plagioclase (andesine), frequently with chilled margins. Other mafic dikes are typically porphyritic with phenocrysts of both plagioclase and amphibole or with only amphibole (i.e., the lamprophyre of MacKevett, 1963). There are at least two generations of lamprophyric dikes, as indicated by the crosscutting relationships and alteration patterns. Some lamprophyric dikes are biotite-rich. Likewise, the felsic dikes include rocks ranging from older, through coeval to younger than the Bokan complex.

4. Bokan Complex

The complex is a roughly circular intrusive body (a stock) of about 6.5 km^2, which forms a topographic high of ~ 700 m (Photos 1-3). This stock, which consists of peralkaline granites, was emplaced at a shallow depth based upon the contact metamorphic assemblages (including andalusite [chiastolite]-bearing hornfels) and field relations, such as ring dikes. The complex intruded Paleozoic slates of the Descon Formation as well as Paleozoic granitoid rocks (Fig. 3 – map). The contacts with the country rocks are generally sharp and invariably dip outward from the complex (40-70°). The country rocks along the contact are albitized and the slates are also hornfelsed.

Collot (1981) and Cuney and Kyser (2008) inferred that Bokan is the apex of a much larger, shallowly eroded composite intrusion at depth, whereas Thompson et al. (1982) interpreted the Bokan complex as a ring dike complex.

The peralkaline granites are characterized by the presence (2-10 vol. %) of subhedral, sodic amphibole (arfvedsonite) and sodic clinopyroxene (aegirine). The granites include diverse rock types that range from sacchroidal aplites to coarse-grained granites which dominate and lesser pegmatites and arfvedsonitic to aegirine augitic granite. Thompson et al. (1980, 1982) and Thompson (1988, 1997) recognized several mappable granitic units in the complex, which Gehrels (1992) and Warner and Barker (1989) grouped into three main zones: (1) a core made up of arfvedsonite granite to arfvedsonite granite porphyry with minor aplitic aegirine granite; the core forms the main part of the body, (2) an outer ring composed predominantly of aegirine granite porphyry, and (3) a discontinuous outermost border zone that contains pegmatite-aplite (Fig. 3). Thompson et al. (1982) proposed a genetic model for the intrusion whereby the subsidence or collapse of the core of the complex was followed by the emplacement of ring dikes, devolatilization of the magma and a change of crystallization from an early aegirine- to later riebeckite-type granite. The presence of fine-grained aegirine granite outcropping in the central part of the stock probably represents the preserved roof of the complex, which was the easliest phase to form (Cuney and Kyser, 2008).

The arfvedsonite granite and/or granite porphyry of the core contain phenocrysts of quartz, and subordinate K-feldspar (microperthite and microcline) and amphibole. Most of the aegirine granite, predominantly as aegirine granite porphyry, forms a nearly complete circular zone about 180 m thick around the core of the complex (Thompson et al., 1980, 1982). This granite passes into arfvedsonite granite transitionally over about 15 m. Although the latter unit is variable in modal composition and grain size, it is typically medium to coarse-grained.

The pegmatite-aplite border zone of a thickness of about 13 m consists of pegmatitic pods (i.e., stock scheider) enclosed in aplitic rocks. The pegmatite is composed of coarse-grained quartz and K-feldspar and contains aegirine and arfvedsonite crystals ≤ 3 cm. Of possible significance is that the border zone rocks appear to occur in two locals - at the SE and NW parts of the Bokan complex which are, coincidentally, at the extreme ends of the NW-trending zone of mineralization (Fig. 3).

The granitic rocks of the Bokan complex show some common characteristics (MacKevett, 1963; Thompson et al., 1980, 1982). They are generally leucocratic with about 2-10 vol. % of mafic minerals (aegirine and amphibole in various proportions) and the dominant textures are porphyritic and protoclastic. The porphyritic texture is defined by phenocrysts of subhedral to euhedral quartz and K-feldspar (0.5-2 cm) enclosed in a medium-grained quartzo-feldspathic groundmass with abundant albitic feldspar. The protoclastic textures are defined by broken or granulated (cataclasized) phenocrysts of quartz and feldspars. The protoclastic texture is also reflected by offsets and bending of the albite twinning and undulose extinction of quartz.

The petrography of the granitic rocks is illustrated in a series of plates (Figs. 4-9) and their features are summarized below. They are mainly composed of quartz (~25-40 vol. %) and K-feldspar (microperthite and microcline) (20-30 vol. %) with albite as both a separate phase and as a replacement of K-feldspar (30-50 vol. %). Quartz appears to have crystallized during two stages; the earlier megacrysts, as noted above, and then in the matrix and as vein-like features. Well developed early quartz crystals are intersected by the second generation, which typically forms veinlets or thin septae that cut the sodic amphibole. There are also at least two generations of K-feldspar. An early feldspar, now occurring as a cross-hatched microcline phase that is enclosed/ embayed by microperthitic K-feldspar that constitutes the dominant feldspar phase. This early K-feldspar is also commonly rimmed by albitic plagioclase (chess-board variety) and is variably replaced by albite. The albitic feldspar forms relatively fresh euhedral crystals,

probably postdating quartz of first generation quartz and K-feldspar. Albite pervasively replaces K-feldspar, both in phenocrysts (particularly along the fractures) and in the groundmass. The groundmass is dominated by albite and quartz with rare K-feldspar, but most of this is secondary with the primary assemblage overprinted by this metasomatic assemblage. There is a textural spectrum of plagioclase, of dominantly albitic composition, that reflects its formation from magmatic crystallization to later fluid mediated growth. The metasomatic nature of the feldspars is also indicated by the abundance of pitted textures present within these phases and the local abundance of fluid inclusions.

Although sodic amphibole and pyroxene are subordinate constituents, locally, they constitute up to about 30 vol. % of the rocks (i.e., some of the granites are mesocratic). The sodic amphiboles form subhedral prismatic crystals typically about 1-4 mm and, rarely to > 1 cm in size. The crystals are interstitial and may have fretted outlines indicating continued growth into the matrix, possibly at a subsolidus stage. An important feature of the amphibole is the presence of low-density fluid inclusions in the core of the grains; rarely melt inclusions also exist along with apatite grains. The amphiboles are distinctly pleochroic (lilac to blue), but commonly are replaced pseudomorphically by a mixture of secondary minerals that is most often quartz-hematite with lesser red and blue amphibole; rare element mineralization also occurs in these domains. Generally, both amphibole and pyroxene are spatially associated with one another, but in some samples only one or the other is present. Where both minerals are present, the anhedral to euhedral amphibole typically partly encloses and corrodes the pyroxene, but in rare cases pyroxene also post-dates amphibole. Notwithstanding the felsic composition of these rocks, the pyroxenes commonly display a (sub) ophitic texture (i.e., they enclose or partly enclose euhedral albite crystals) as can the sodic amphibole.

The aegirine has a range of shapes from equant grains to prismatic or skeletal shapes that occur as clots, aggregates or rarely spherulites. These features of aegirine also occur in the dike rocks. Philpotts et al. (1998) also noted the occurrence of aegirine as radiating spherulites and suggested that the mineral grew rapidly, probably due to the presence of fluids in the melts. Late-stage aegirine crystallized as needles along grain boundaries and other fractures or appears to be interstitial. Although not as common as amphibole, rarely low-density fluid inclusions also occur in this phase. The aegirine is also not altered to the extent of amphibole. In some samples, euhedral aegirine is enclosed by arfvedsonite, which itself is partly mantled by aegirine. This suggests overlapping crystallization of these Mg-Fe silicate phases. The matrix around the ferromagnesian minerals consists of variably perthitic microcline and subordinate albite (rarely oligoclase), with interstitial quartz. Arfvedsonite and aegirine are poikilitic with inclusions of quartz, albite and microcline with apatite present but rare.

The main accessory minerals in "unmineralized" granitic samples include allanite, F-apatite, zircon, monazite, xenotime, titanite, fluorite, and (Ti)-magnetite. Typically, they constitute <2 vol. % of the rocks. Importantly the zircon has a large range in textures from euhedral to anhedral and ameboid-like shapes.

Thompson et al. (1980, 1982) recognized an aegirine syenite which is closely associated with the U-Th mineralization at the Ross-Adams deposit. This rock type consists mainly of albite and aegirine with only a minor amount of fine-grained quartz. It is typically fine to medium-grained without phenocrysts of quartz and with accessory amounts of monazite, zircon and titanite.

In addition, the aplites and pegmatites related to the Bokan complex occur throughout the complex as well as outside. They typically form dikes (Photo 4), lensoidal bodies or elongated

pods, which are steeply dipping up to about 3 m (up to 6 m at the I&L Zone) thick and show "horse-tailing" with frequent branching and pinching out and with bifurcating and anastomosing characteristics (Photo 5), particularly away from the complex. These bodies commonly occur in small parallel groups (Fig. 10; Photos 6-8). Warner and Barker (1989) and Philpotts et al. (1998) used the term "vein-dike" for these veins and dikes including pegmatites, aplites and tabular bodies with quartz-cores and considered them to represent a system rather than individual bodies. Most of these vein-dikes are associated with NW-trending shear zones peripheral to the complex (Fig. 10). They include the Dotson, I&L and Geoduck zones (Fig. 3). The fine to medium-grained aplites are composed of quartz and K-feldspar with minor albite, rare fluorite, aegirine and amphibole. Pegmatite bodies frequently have aplitic border zones and cores consisting of massive quartz (Photos 9-10); the pegmatites are composed mainly of quartz and perthite with minor albite, fluorite and magnetite. There are also quartz veins up to about 1 m thick. Many of the felsic dikes contain elevated concentrations of Nb, Th, U, REE, Y and some other rare elements.

5. Mineral Prospects

MacKevett (1963) and Warner and Barker (1989) described a number of uranium-thorium and/or HFSE- and REE-bearing prospects within or proximal to the Bokan complex (Fig. 3) and recognized several types of mineralization. Most importantly is the presence of two structurally controlled types (Thompson, 1988): (1) the Ross-Adams deposit and (2) mineralized vein-dike systems associated with shear-fault zones, in particular the I&L and Dotson zones (Warner and Barker, 1989; Philpotts et al., 1996, 1998). Also of note is the observation that all the mineralized zones appear to define a NW-trending corridor that cut the Bokan complex, a structural theme that is also noted at the deposit scale (see below, Figs. 10 and 11).

The first type, the Ross-Adams deposit, includes veins, pods and pipe-like orebodies. The main ore pipe, up to 24 m in diameter with ~1 wt.% U_3O_8 and 3 wt. % ThO_2 and elevated concentrations of HREE, Y, Nb and Zr (Thompson, 1988; Warner and Barker, 1989; Long et al., 2010), has an irregular cylindrical shape and was mined along strike for over 300 m (Fig. 11; Photo 11). The pipe lies at the SE margin of the aegirine granite zone along the contact between desilicified and albitized aegirine syenite and aegirine-arfvedsonite granite, although the deposit appears to be structurally controlled (Photo 12; also Thompson et al., 1980). The pipe contained a core of high grade ore with >0.5 wt. % U_3O_8 surrounded by a lower grade (<0. 5 wt. % U_3O_8) ore zone, 0.6 - 6 m wide, which was not mined (Fig. 12). In addition, U-Th ore at the Ross-Adams deposit also forms lensoidal veins or pods in *en echelon* NW-striking shear zones (Thompson, 1988; Cuney and Kyser, 2008). The pods are up to 30 m long and 3 m wide (Thompson et al., 1980; Thompson, 1988, 1997). The ore zone displays extensive microfracturing, which may reflect a late-stage of magmatic devolatization of the magma chamber. Heavy REE, Y, Nb and Zr are enriched in the altered halo adjacent to the uranium mineralization (Thompson et al., 1980). The mineralization at the Ross-Adams deposit is typically accompanied by wallrock alteration within and adjacent to ore bodies that include intense albitization, silicification, chloritization and the calcite-fluorite or quartz-hematite replacement of aegirine. The advanced albitization is associated with the hydrothermal leaching of quartz from granites. Hematitization occurs in the outer parts of the ore zones and locally marks the position of shear and fault zones along which fluids travelled.

The second type of mineralization occurs in late-magmatic to hydrothermal felsic dikes and veins that cut the intrusion or are concentrated along the margin of the intrusion and in

adjacent country rocks (MacKevett, 1963). The dikes are steeply dipping and mostly associated with and oriented along the NW-trending faults and/or shear zones and contain mineralization of rare-earth elements, Y, Zr, Hf, Nb and Ta (total of 1-10 wt. %) accompanied by elevated concentrations of U and Th. Some of the bodies, such as those which are within the Dotson and Geoduck zones, occur outside the Bokan complex. Others including dikes of the I&L Zone (Staatz, 1978) crop out along the contacts or within the complex. Although most of the systems occur on the southeastern side of the complex, some zones are located on the northwestern side (Fig. 3).

The shear/fault systems hosting ore zones of lenses, dikes and veins can be followed on the surface for more than 2 km (Thompson et al., 1980). For example, the Dotson Zone can be traced for more than 2 km from Bokan Mountain to the West Arm of Kendrick Bay, whereas the Geoduck Zone, which crops out south of the Dotson Zone, can be followed along strike for another > 2 km (Fig. 3). The dike bodies are composite and texturally variable and consist of both aplites and pegmatites with quartz rich cores (Photos 9, 10, 13 and 14). They usually form a network or occur in groups. In these clusters, prominent dikes and vein-dikes are 25-250 m long (Cuney and Kyser, 2008). They are typically subparallel (Staatz, 1978; Warner and Barker, 1989) and away from the complex they bifurcate into many thinner dikes (Photo 5). In the dikes, the quartz-aegirine and aplitic ore lenses are up to 3 m thick and 30 m long (Cuney and Kyser, 2008). However, as documented by Warner and Barker (1989), the mineralization, particularly along the Dotson Zone, is also associated with shear/fault zones where it occurs as the ore dissemination in the country rocks (Photo 15). In the country rocks, the mineralization is typically accompanied by wallrock alteration.

The Dotson Zone intersected Paleozoic quartz diorite/diorite and quartz monzonite units (Fig. 10). Close to the contact with the zone, the latter rock type is locally silicified and/or albitized. The Dotson Zone is a steeply dipping structural lineament or zone of weakness (fault and/or shear zone) containing a network of at least 25 sub-parallel vein-dikes and numerous narrow veinlets (Photos 6-8 and 16). The zone has an average width of about 50 m and has been traced to a depth of about 450 m. There are typically two types of REE- and HFSE-rich vein-dikes. The first one includes relatively homogeneous unzoned aplitic dikes. The second type encompasses the dikes which are typically more than 10 cm thick and are symmetrically zoned with a core composed mainly of quartz (Photos 9-10). In addition to vein-dikes, the mineralization also occurs in arrays made up of numerous thin parallel veinlets over the interval of several meters (Photo 6) and/or is disseminated within the country rocks (Photo 15).

The I&L Zone consists of at least nine structurally-controlled NW-trending steeply-dipping pegmatitic dikes (Photo 4) hosted in the Bokan aegirine granites. The largest dike is > 300 m long and up to 6 m wide. The other dikes are sub-parallel, ranging in length from 30 to 150 m and are up to 2 m thick. The pegmatitic dikes are typically zoned (Photos 9, 10, 13 and 14) with a wide variety of REE-, HFSE-, U and Th-bearing minerals (Staatz, 1978). Compared to the Dotson Zone, the I&L has a different trace element composition suggesting that these two zones represent distinct dike systems.

The thorium-uranium, REE and HFSE mineralization is genetically related to the Bokan complex and is thought to be of magmato-hydrothermal origin (Thompson et al., 1980, 1982; Thompson, 1988; Warner and Barker, 1989; Philpotts et al., 1998). Warner and Mardock (1987) and Warner and Barker (1989) reported that in the aplites and pegmatites around Bokan Mountain, radioactive elements appear to be inversely correlated with REE, Y, Zr and Nb.

Compared to the Bokan granites, the mineralized dikes also have higher contents of rare earth-, yttrium-, niobium- and zirconium-bearing minerals.

6. Mineralogy/Mineral Chemistry

The granites and felsic dikes are composed primarily of quartz, K-feldspar and albite with subordinate sodic pyroxene and amphibole. The modal abundances of the rock-forming minerals of peralkaline granitic rocks from both the Bokan complex and the vein-dikes are well reflected by the normative mineralogy (Fig. 13) with the exception of acmite which can be represented in the mode by either pyroxene or amphibole.

Sodic pyroxene is near end member aegirine which shows a limited range of compositions (Aeg = 81-86%; Jad = 13-19%; Di $\leq$1.2%; Table 1a). Titanium contents are variable (0.5-2.0 wt. % TiO_2), whereas alumina contents are low ($\leq$0.8 wt. % Al_2O_3).

There has been a controversy about the nature of the sodic amphibole in the granitic rocks of Bokan. Whereas Thompson et al. (1982) considered this to be riebeckite, Collot (1981) and Philpotts et al. (1998) inferred the amphibole to be arfvedsonite. Our data confirm that the amphibole is arfvedsonite (Fig. 14; very close to the Fe end member). Using the classification scheme of Leake et al. (2004) and WinAmphcal software (Yavuz, 2007), with Fe^{3+} contents calculated from the mean of normalization schemes providing minimum (15exNK) and maximum (13exCNK) values for this parameter, most of the amphiboles are fluorian-potassian arfvedsonites (Table 1b). These arfvedsonites average 1.0 wt% F (0.45 ions per formula unit [pfu] based on a 23 oxygen unit cell); A-site alkalis (Na+K) range between 0.7 and 1.5 ions pfu. As with aegirine, titanium contents are variable (0.5-1.7 wt. % TiO_2). They have an average calculated oxidation ratio (X_{Fe3+}) of 0.1. A few samples contain ferroeckermannite or fluorian ferroeckermannite; the latter is rare and occurs as the core of fluorian-potassian arfvedsonite grains. It contains less F (0.45 ions pfu) than the arfvedsonite, has A-site alkalis (=0.8 ions pfu) near the low end of the range for these sodic amphiboles and a very low oxidation ratio (0.06). In contrast, the rare ferroeckermannite is enriched in A-site alkalis (2.7 ions pfu) and has an oxidation ratio of zero. The samples with ferroeckermannite also contain riebeckite, which has only traces of F (<0.1 wt.%), and a small amount of A-site alkalis (0.38 ions pfu) compared with the other sodic amphiboles in the complex, but they have relatively high oxidation ratios (X_{Fe3+} = 0.28). Mafic dikes contain magnesiohastingsite that lacks F, has low A-site alkalis (0.45-0.50 ions pfu), and an oxidation ratio of 0.6 in one sample (LM143 - mafic dike associated with the Geoduck Zone), and 1.0 in another (LM-79 - lamprphyric dike near the I&L Zone).

Alkali feldspar contains between 1.8 and 5.0% Ab (Table 1c) and it coexists with nearly pure albite (An_1). In contrast, the country rock quartz monzonite contains calcic albite/sodic oligoclase (An_{10-13}). Mafic (lamprophyric) dikes even rarely contain ternary feldspar (An_{7-13} Ab_{60-85} Or_{8-26}).

The primary uranium-thorium minerals in the Ross-Adams deposit are uranothorite and minor uraninite; brannerite and coffinite are rare (Thompson, 1988). They are typically associated with < 2 vol. % of sulphides (pyrrhotite, pyrite, chalcopyrite, galena, sphalerite, molybdenite). The ore resembles strongly altered host peralkaline granite with numerous ore-bearing microveinlets typically between 0.1 and 1 mm thick and ore ovoids that are 0.2 to 2 mm in size (Thompson, 1988). The ore frequently seems to replace original aegirine. Uranium minerals are also disseminated. Cuney and Kyser (2008) noted that uranothorite forms fine crystals (~50-500 μm in size) disseminated in secondary albite. Gangue minerals are mainly

quartz and feldspar with minor hematite, calcite, fluorite, chlorite and clay minerals (MacKevett, 1963). Secondary uranium minerals are rare and include gummite, sklodowskite, beta-uranophane, bassetite and novacekite (Staatz, 1978; Thompson, 1988). Abundant REE-bearing minerals around the Ross-Adams deposit are britholite and/or abukumalite, which frequently occur as fillings of microfractures.

The bulk of the uranium and thorium in the dikes outside of the Ross-Adams deposit reside in the uranothorite, uraninite and coffinite (Table 1d; Philpotts et al., 1998). The analytical data indicate that uranothorite and coffinite also contain a significant amount of REE (Table 1d; Fig. 15). The composition of coffinite from the I&L Zone resembles that of REE-bearing coffinite from New Mexico (Hansley and Fitzpatrick, 1989) and its chondrite-normalized REE pattern is enriched in HREE. The composition of thorite/uranothorite is highly variable with respect to U and Th, which are negatively correlated. It ranges from a crystal with 64 wt. % ThO_2 and 14.3 wt. % UO_2 to that with 16.7 wt.% ThO_2 and 59.3 wt.% UO_2.

The Bokan complex has been known for nearly half a century as a locality with a wide range of unusual minerals of REE, Y, Nb, Th and U (e.g., MacKevett, 1963; Staatz, 1974, 1978; Staatz et al., 1979; Floran, 1983; Mariano, 1983; Foord et al., 1984; Philpotts et al., 1998). Images of some of these phases, in particular the occurrence of zircon, are provided in Figure 8.

In the dikes of the Bokan complex, the Dotson and I&L zones, REE and Y are present in various accessory minerals including xenotime, allanite, britholite, abukumalite, bastnaesite, synchysite, iimoriite, monazite and zircon, whereas Nb occurs in euxenite and columbite (Staatz, 1978; Warner and Barker, 1989; Philpotts et al., 1998). We have also seen Nb enrichment in rutile and ilmenite phases, sometimes accompanied by Sn. The abundances of these minerals are higher in the dikes than in the granites of the complex. In addition to the minerals noted above, thalenite, gadolinite, fergusonite, gittinsite, andradite, rowlandite, plumbopyrochlore, taeniolite and samarskite were identified in the Dotson Zone (Warner and Barker, 1989; Philpotts et al., 1998) and thalenite, fergusonite, gadolinite, parasite, coffinite and uranothorite in the I&L Zone (Staatz, 1978). A. Mariano also identified kainosite and elpidite in these two zones (personal communication, 2009) and we have also noted the presence of elpidite coexisting with zircon as an intergranular phase in the granites. The chemical analyses of some of these minerals are given in Table 1d, including accessory minerals from nonmineralized granites (allanite, zircon). Fluorite is a frequent accessory mineral, which occurs typically along grain boundaries; it contains ~ 2.4 wt. % Y_2O_3 (Table 1d). Most of the Ca in the Bokan granites is probably hosted in this phase.

The REE and HFSE mineralization typically occurs along microfractures of the dikes or in the intergranular groundmass among the larger silicate grains (Warner and Barker, 1989). Some of these REE-bearing minerals such as zircon, monazite and iimoriite occur as euhedral crystals up to 1 mm in size, but anhedral shapes are more common. Other REE-bearing minerals form complex intergrowths of two or more phases with variable grain size ranging from 10 µm to ~ 1 mm. The minerals of the intergrowths have tabular or acicular subhedral habits although even these minerals also occur as single crystals. These minerals appear to be secondary and typically occur in pseudomorphs whose outline suggests the replacement of pre-existing aegirine and arfvedsonite. In fact, many rocks show evidence of the partial to complete replacement of pre-existing minerals or mineral assemblages. Many REE-bearing minerals such as bastnaesite and sychysite, frequently occur within pseudomorphs which apper to show a prismatic to rhombic habit. The aggregates of these accessory minerals seem to have grown from the wall inwards, suggesting open space-filling. The secondary REE-Nb-Zr mineral assemblage appears

to be also replacing euhedral prismatic crystals of elpidite. These ore minerals also occur as clusters or as banded veins within the quartz-feldspar matrix. From the Dotson Zone, Philpotts et al. (1998) described abundant and interconnected, irregularly-shaped cavities up to 1 mm in diameter that are filled or coated by µm-grain sized REE-bearing minerals. Relatively abundant bastnaesite forms mm-size patches which appear to replace K-feldspar and aegirine.

A. Mariano (personal communication, 2009) identified two generations of zircon in the I&L Zone. Zircons of the first magmatic generation are dominant and form tetragonal prismatic crystals characterized by a high Hf content and by high HREE. The second generation zircon occurs as sub-microscopic polycrystalline grains intergrown with quartz as pseudomorphs probably after euhedral elpidite. These secondary polycrystalline zircon microcrystals are high in Th, Y and Fe. We also note that F may also occur in some of these zircons. Similarly two types of zircon populations were described from highly fractionated granitic intrusions by Erdmann et al. (2011) who related the second zircon generation to magmatic fluid exsolution. The interpretation may also apply to the Bokan complex.

In the I&L Zone, three major REE-bearing minerals - bastnaesite, synchysite and iimoriite, have distinct chondrite normalized patterns. Bastnaesite is enriched in light REE, synchysite is enriched in both LREE and HREE, whereas iimoriite is enriched in HREE (Fig. 15a). In general, the REE mineralogy of the Bokan peralkaline rocks shows some similarities to other mineralized peralkaline granitic bodies such as the Strange Lake complex (on the Quebec-Labrador border).

7. Geochronology

The dating of the country rocks has provided a relatively wide set of ages. The Middle Ordovician to Early Silurian U-Pb zircon ages of granitoid plutons (480-438 Ma) outcropping in the vicinity of the Bokan complex were reported by Gehrels and Saleeby (1987a). The ages are comparable to conventional K/Ar ages of 431 ± 21 Ma and 446 ± 22 Ma for hornblende from the quartz diorite and quartz monzonite of the nearby plutons (Lanphere et al., 1964), a Rb-Sr whole rock age of 432 ± 19 Ma (one-sigma uncertainties) of Armstrong (1985) and within the age ranges of graptolites and conodonts from the sediments of the Descon Formation (Auyso et al., 2007). To refine the age of the Paleozoic granitic rocks in the vicinity of the complex, we determined the U-Pb zircon age of the country rocks (1 sample) next to the Dotson Zone.

There is some controversy regarding the ages of emplacement of the Bokan complex, which has previously been dated by several methods. Lanphere et al. (1964) reported K/Ar amphibole ages of 181 ± 8 Ma and 186 ± 8 Ma (one-sigma uncertainties) for the Bokan granite, whereas Thompson et al. (1980) obtained a K/Ar age for albite of 182 Ma from granite/syenite of the Ross-Adams deposit, which likely records the age of precursor K-feldspar in the sample. De Saint-Andre et al. (1983) determined U-Pb zircon ages for two samples from the Bokan complex - the fine-grained aegirine granite and metasomatized albite-rich syenite which was closely associated with the U-Th mineralization. These data provided a Concordia intercept age of 171 ± 5 Ma. Subsequently, de Saint-Andre and Lancelot (1986) revised their data and inferred an age of 167 +7/-5 Ma (two-sigma uncertainties) for the emplacement of the complex and 101 ± 3 Ma for the Th-U mineralization. Armstrong (1985) obtained a whole rock Rb-Sr age of 151 ± 5 Ma for the Bokan complex and suggested that the age discrepancy with the K-Ar data was due to excess of Ar in the samples and also considered the U-Pb data of suspect quality (see also Gehrels and Saleeby, 1987a). Philpotts et al. (1998) tried to use Nd isotopes to date the complex, but the whole rock data did not yield an isochron within acceptable error. Thus, the previously

available geochronological data suggest that the Bokan complex is of Jurassic age, but there are poor constraints of these data compared to modern methods. In order to reconcile the discrepancies in the previously reported age dates and to provide a more precise and accurate age for the complex both U-Pb zircon (1 sample) and Ar-Ar (three amphibole and two whole-rock samples) dating methods were employed. The results of these analyses are discussed separately below.

7. 1. U-Pb zircon age

Zircon for dating from the Bokan complex was separated from an arfvedsonite granite (G245) collected from the central part of the complex. The zircon separate consists of colourless to pale yellow crystals (Fig. 16). Five single grain fractions of chemically-abraded zircons were analyzed. Uranium-lead isotopic data for these fractions of zircons (Table 2) are shown graphically in Figure 17. The data are concordant and overlapping with a mean $^{206}Pb/^{238}U$ age of 177.2 ± 0.2 Ma (2 sigma; see Fig. 17; note that the thicker-than-normal Concordia curve reflects decay-constant uncertainties). This age is interpreted as the time of zircon crystallization and, therefore, a good approximation of the time of emplacement of the Bokan complex. Importantly, this age is significantly older than those presented by de Saint-Andre and Lancelot (1986) and Armstrong (1985, 1986), as discussed previously.

Zircons from a quartz monzonite country rock collected near the Dotson Zone were separated and dated by laser-ablation ICP-MS. The data give a U-Pb zircon age of 469.2 ± 3.9 Ma (2 sigma; Fig.18; Table 3). The age is within the range for Paleozoic granitic rocks from the vicinity of the Bokan (480-438 Ma; Gehrels and Saaleby, 1987a) but indicates that rocks of the older magmatic period of Gehrels and Saaleby (1987a; ~472-462 Ma) occur along the contact of the complex.

7. 2. $^{40}Ar/^{39}Ar$ age dating

The results of the $^{40}Ar/^{39}Ar$ analyses are presented in Table 4 and the results are plotted in standard age versus $\%^{39}Ar$ in Figure 19. Fresh amphibole separated from a peralkaline granite (G-242) of the Bokan complex yielded an excellent plateau age of 175.5 ± 0.6 Ma that incorporated 75% of the gas released. The age is identical to both the correlation (175.0 Ma) and integrated (175.2 Ma) ages calculated for the sample. This age is interpreted to indicate the time of crystallization of the granite and is in agreement with the U-Pb zircon age of the peralkaline granite.

A fresh amphibole separate (LM24) from a mesocratic (amphibole ~20 vol. %) granitic dike closely associated with the mineralization at the Ross-Adams deposit yielded a hump-shaped age spectrum with a plateau age of 176.3 ± 0.8 Ma. This age is defined by 54% of the gas released and is identical to the correlation age of 176.2 Ma for the same steps. However, it is noted that the last step, incorporating some 35% of the gas released, had an age only slightly younger than the plateau at 174.2 Ma. The lower temperature gas fraction has a stepwise increase in ages with the lower temperature steps (i.e., three to five) yielding ages near 160 Ma. The sample is interpreted to indicate a primary crystallization age of 176 Ma with a later overprinting thermal event at <157 Ma.

Sample LM73 is a fresh biotite (30 vol. %) - rich lamprophyre dike with minor quartz that cuts the I&L Zone. The nearly pure biotite separate yielded an age spectrum that increases monotonically from about 120 Ma to near 150 Ma. This spectrum is interpreted to indicate a minimum age of ca. 150 Ma for this sample with an overprinting event at <120 Ma.

Fresh amphibole set in an altered, sericite-rich matrix was separated from an amphibole-bearing (10-15 vol. %) dike (lamprophyric) rock (LM79) which crosscuts the Dotson granitic dikes. This amphibole yielded an irregular age spectrum from which a plateau age of 105.2 ± 0.6 Ma is calculated. Importantly, the shouldering steps for this sample are only slightly older than the plateau age and range between 107 and 109 Ma. The age is interpreted as recording emplacement of the dike rock at about 105 Ma.

A fine-grained diorite dike (?) rock (LM143) associated with the Geoduck Zone and consisting of intergrown plagioclase (70%) and amphibole (30%) was run as a whole rock since it was not possible to produce an adequate high-purity mineral separate of the amphibole. The sample yielded a U-shaped profile with a minimum age of 117 Ma (3.5% of gas released) and a maximum age of near 325 Ma that is defined by the last two steps which incorporate 21% of the gas released. This sample is clearly anomalous, departing markedly from the other samples analyzed in this study, and likely records the presence of excess radiogenic argon derived from older basement rocks in the area. The sample is, therefore, cautiously interpreted to indicate a minimum age of 325 Ma for its formation with a thermal overprinting event at < 117 Ma. The basement is composed of the Paleozoic granitoids (U-Pb zircon ages of 480-438 Ma; Gehrels and Saleeby, 1987a; this study; see Figs. 2 and 3).

Collectively, the Ar-Ar and U-Pb dating of the selected samples indicates that the Bokan complex was emplaced at 177 Ma (U-Pb zircon age) into a basement of ~ 469 Ma (U-Pb zircon age). The complex was intruded by similar age dike rocks (LM24), but also by younger suites of lamprophyric dike rocks at two times during the Cretaceous, one at around 150 Ma (LM73) and the other at 105 Ma (LM79). Importantly, the emplacement of these later dikes partially reset the Ar-Ar age spectra in some of the samples (i.e., low-temperature gas fractions) with the ca. 150 Ma event possibly recorded in a sample of the Bokan granitic dike (LM24) and the ca. 105 Ma event recorded in a samples of the basement (LM143) and a dike rock (LM73). This Cretaceous magmatism accounts for the age of the hydrothermal event of de Saint-Andre and Lancelot (1986) estimated to take place at 101 ± 3 Ma.

The LA-ICP-MS age of zircon from U-Th-REE mineralization (~177 Ma; our preliminary and unpublished data) as well as the Ar-Ar age of amphibole (LM24) from Ross-Adams and K/Ar age of albite from syenite (Thompson et al., 1980) associated with the Ross-Adams deposit coincide with the age of the peralkaline granite intrusion, suggesting the near contemporaneity of the magmatic evolution of the complex and REE and U-Th mineralization in the Dotson and I&L zones and the Ross-Adams deposit. This supports the conclusions of MacKevett (1963), Thompson et al. (1980) and Thompson (1988) that mineralization and alteration coincided with the emplacement of the complex.

8. **Geochemistry**

8. 1. Granitic Rocks

8.1. 1. *Major Elements*

The granitic rocks of the Bokan complex (Table 5a) have SiO_2 contents in the range of 72 to 78 wt. % accompanied by high alkalis (8-10 wt. %); K_2O and Na_2O concentrations are similar and the rocks are iron-rich ($Fe_2O_{3(total)}$ ~3.5-5 wt. %). Alumina contents vary from 10 to 13 wt. % and TiO_2 ranges between 0.05 and 0.2 wt. %. On the other hand, these rocks are low in MgO (< 0.04 wt. %) and CaO (<0.2 wt. %). The QAP (quartz-alkali feldspar-plagioclase) diagram (Fig. 13) of LeMaitre et al. (1989) shows that the rocks are "true" granites; they have a peralkaline composition with both the aluminum saturation index (A/CNK [molar

$Al_2O_3/(CaO+Na_2O+K_2O)$]) and agpaitic index A/NK [molar $Al_2O_3/(Na_2O+K_2O)$] < 1 (Fig. 20). According to de la Roche et al.'s (1980) compositional discrimination diagram (Fig. 21), the rocks are mainly alkaline granites. Their alkali characteristics are also indicated by the total alkalis-silica and Zr/TiO_2 versus SiO_2 diagrams (Fig. 22). The latter diagram shows that the rocks have compositions comparable to the volcanic equivalents of peralkaline granites (comendites and pantellerites).

Using the parameters of de la Roche et al. (1980), Batchelor and Bowden (1985)'s tectonic discrimination classification (Fig. 21) indicates that the Bokan rocks are anorogenic (A-type granite). The rocks have also high $FeO_{(tot)}/(FeO_{(tot)}+MgO)$ ratios due to their low MgO concentrations and correspond to the ferroan (A-types) granites of Frost et al. (2001) (Fig. 23). The Bokan granitic rocks are compositionally similar to other peralkaline A-type granites (e.g., Eby, 1990, 1992; Whalen et al., 1996), although they are more fractionated/evolved than most others. There is no obvious systematic variation in chemical composition across the complex, which is not unexpected given the small size of the intrusion at present level of erosion. In fact, Cuney and Kyser (2008) noted that the limited chemical variation for the major elements in the Bokan complex is not related to magmatic fractionation.

The felsic dike rocks of the I&L and Dotson zones (Table 5b) are compositionally similar to those of the Bokan complex. Their SiO_2 contents range from 73 to 77.5 wt. % and the alkali contents range from 7.5 to 9.5 wt. % with Na: K near unity for fresh samples. Like the Bokan granites, the samples have high $Fe_2O_{3\,(total)}$ (3-5 wt. %) and low MgO (<0.03 wt. %) and CaO (<0.5 wt. %) contents. Their major element composition is also typical of A-type peralkaline granites.

The Bokan rocks are distinct from the Paleozoic granitic country rocks (Fig. 13; Table 5c). These country rocks are typical subalkaline granitoids (Fig. 22) and are peraluminous (Fig. 20) and magnesian (Fig. 23).

8.1. 2. *Trace Elements*

Like other typical peralkaline granites, the Bokan rocks are distinctly enriched in HFSE, REE, Th and U, but depleted in Ba, Sr and Eu. The concentrations of Sr (< 20 ppm) and Ba (< 80 ppm) are very low compared to the host Paleozoic granites and to various granitic averages (e.g., Dostal and Chatterjee, 1995; Abdel-Rahman, 2006). The abundances of Rb (150-350 ppm) are relatively high and are accompanied by low K/Rb ratios (100-250) relative to the typical crustal average (~ 240; Shaw, 1968). The depletion of Ba, Sr and Eu in peralkaline granitic rocks is usually attributed to the fractionation of feldspars whereas Rb is gradually enriched in late-stage melts (Cerny et al., 1985; Abdel-Rahman, 2006). The Bokan peralkaline granites have high Rb/Sr ratios (>5), and their distribution in the Rb/Sr vs K/Rb plot (Fig. 24) supports their anorogenic character. In contrast, granites from orogenic tectonic regimes have Rb/Sr ratios < 1 (Abdel-Rahman, 2006).

Shaw (1968) demonstrated that granitic rocks with a K/Rb ratio < 160 were probably affected by hydrothermal-magmatic processes. Thus, the low K/Rb ratios in some Bokan rocks are consistent with the inference of Philpotts et al. (1998) that many of the rocks were modified by late-stage- magmatic-hydrothermal fluids.

The abundances of Zr (800-3,000 ppm) and Nb (35-85 ppm) are high compared to typical orogenic granites (Linnen and Cuney, 2004). Enrichment in HFSE, which are typically hosted in accessory phases, is a characteristic feature of peralkaline granites in general (e.g., Whalen et al., 1996; Schmitt et al., 2002). The Zr/Hf ratio typically varies from 37 to 50 and Nb/Ta ratios from

12 to 15. They are comparable to the ratios of other anorogenic granitic complexes (e.g., Yemen - Capaldi et al., 1987; Egypt - Abdel-Rahman and El-Kibbi, 2001, Abdel-Rahman, 2006 and Namibia - Schmitt et al., 2002), as well as to many peraluminous granites (e.g., Dostal and Chatterjee, 2000).

The Bokan granites also have high Ga (37-47 ppm) contents and Ga/Al ratios (with Ga/Al x10^4 ranging from 6 to 8), which are values typical of A-type granites (Fig. 25; Eby, 1992; Whalen et al., 1987, 1996). The abundances of Th and U vary between 10 and 60 ppm and between 6 and 30 ppm, respectively (Fig. 26a), with average Th and U contents of about 24 and 12 ppm (Cuney and Kyser, 2008). The Th/U ratio, which is mostly between 1 and 4, decreases with increasing U. These radioactive elements in the fresh Bokan rocks show a weak positive correlation with some incompatible trace elements (Fig. 26b). The fluorine content is high and variable (200-3,200 ppm, Cuney and Kyser, 2008, Thompson et al., 1980, 1982) and is reflected in the widespread occurrence of fluorite, which occurs as a late-stage phase. The periodic high volatile content of magma is indicated by the presence of fluid inclusions in magmatic pyroxene and amphibole, as noted above.

The REE abundances of the Bokan granites, particularly of the HREE, are high. The contents of La range from 5 to 150 ppm, Yb up to 55 ppm, Dy up to 60 ppm and Y up to 300 ppm. The shapes of the chondrite-normalized REE patterns (Fig. 27) are variable and range from those with nearly flat (unfractionated) HREE [$(Gd/Yb)_n$ ~1 and slight LREE enrichment [$(La/Sm)_n$ ~1-2] to shapes with a distinct LREE enrichment [$(La/Sm)_n$ ~4-5], but a positive slope for HREE [$(Gd/Yb)_n$ ~0.2]. The chondrite-normalized patterns of all the Bokan granites display a distinct negative Eu anomaly (Eu/Eu*), typically ~ 0.3, which suggests extensive fractionation of feldspars. The size of the Eu anomaly is similar in all the Bokan granites suggesting that they underwent a similar degree of feldspar fractionation.

The REE shapes are similar to some of the characteristic patterns of the peralkaline A-type granites the world over (e.g., Whalen et al., 1996; Schmitt et al., 2002; Vander Auwera et al., 2003; Abdel-Rahman, 2006), but contrast with typical REE patterns of orogenic granites (e.g., Linnen and Cuney, 2004). The chondrite-normalized REE patterns of the host Paleozoic granites (Fig. 27c) show an enrichment of LREE $(La/Sm)_n$ ~3.5-4, $(La/Yb)_n$ ~5-16) and flat unfractionated HREE [$(Gd/Yb)_n$ ~1-1.4] with or without a small negative Eu anomaly. They resemble granitic rocks of relatively primitive island arcs.

On the primitive mantle normalized plots (Fig. 28), the Bokan peralkaline granites exhibit moderate enrichment in most of the HFSE and REE, as well as Th and Rb, but marked depletion in Sr, Eu, Ba and Ti. These trace element profiles are comparable to those of typical A-type granites world wide (e.g., Whalen et al., 1996; Schmitt et al., 2002; Vander Auwera et al., 2003; Abdel-Rahman, 2006). In contrast, the mantle-normalized trace element patterns of the Paleozoic granitic country rocks are typical of arc rocks with a distinct depletion of Nb-Ta and Ti, enrichment of incompatible trace elements, including Th and La, and slight enrichment of Zr-Hf relative to REE (Fig. 28c).

The granitic (including aplitic) rocks from the I&L and Dotson zones have trace element characteristics similar to those of the Bokan complex. They are low in Sr (<30 ppm) and Ba (< 60 ppm), but high in Th, U, HFSE and REE. The I&L rocks resemble the more evolved Bokan granites. For example, they are typically enriched in HREE with $(Gd/Yb)_n$ <1 in some samples. However, the Eu/Eu* values are about 0.3, comparable to those of the Bokan granites, suggesting that the granites from the complex and dikes underwent a similar degree of feldspar fractionation. The concentrations of Th and U are also elevated relative to typical continental

crust values (Rudnick and Gao, 2003) but are highly variable (Th ~ 10-80 ppm; U ~6-40 ppm) with Th/U ratio ~0.8-4 (Fig. 26a).

Although the peralkaline granites of the Dotson Zone are comparable to those of the I&L Zone, the average trace element concentrations of the mineralized sections differ (Fig. 29). The average concentrations of the mineralized parts of the I&L Zone are distinctly enriched in heavy REE with $(La/Yb)_n$ ~0.7, $(La/Sm)_n$ ~2 and $(Gd/Yb)_n$ ~ 0.4 whereas the similar average for the Dotson Zone yields $(La/Yb)_n$~3, $(La/Sm)_n$ ~1.4 and $(Gd/Yb)_n$ ~1.7 (samples with cutoff grade of 0.2 wt.% REE+ Y; Robinson et al., 2011). Both averages have a comparable negative Eu anomaly (~Eu/Eu*~0.3).

8.1. 3. *Granitic Rocks at Ross-Adams Deposit*

The peralkaline granitic rocks in the proximity of the Ross-Adams deposit (Table 5d) show distinct compositional variations, which, in general, are related to mineralization and alteration and thus provide an opportunity to investigate the relation between the mineralization and the composition of the host Bokan granites. The fresh Ross-Adams granites are compositionally within the range of the granitic rocks of the Bokan complex. They plot in the granite field of the QAP diagram, whereas the major element compositions of the altered and mineralized samples reflect some compositional modification due to interaction with fluids. Some mineralized samples have lower content of SiO_2 (~65 wt. %) and correspond to trachyte/syenite (Figs. 21 and 22). The fresh granitic rocks generally have equal proportions of Na_2O and K_2O, whereas the samples from the mineralized zones or their vicinity have significantly higher Na_2O contents, which related to the variations in albite/K-feldspar ratios with the albite-rich samples having lower quartz contents (Collot, 1981; Cuney and Kyser, 2008). Variations of the quartz contents relative to K-feldspar and plagioclase in the fresh and altered granitic rocks associated with the U-Th mineralization is shown in Fig. 30, which helps to evaluate the effects of the secondary processes on the major element compositions of the rocks. The compositional trends indicate two stages of post-magmatic evolution. The variations of the K-feldspar/albite (P-parameter; Fig. 30) versus quartz contents (Q parameter) show that the first stage of alteration (the horizontal arrow) includes replacement of K-feldspar by albite at constant quartz content, followed by the second stage (the inclined arrow) where albitization is accompanied by de-silicification leading to quartz-undersaturated compositions (negative Q values). More specifically, de-silicification led to the formation of the syenites which are associated with the Ross-Adams U-Th deposit (Thompson et al., 1980, 1982; Cuney and Kyser, 2008). These chemical changes are consistent with petrographic observations. The SiO_2 vs FeO*/(FeO* +/MgO) diagram (Fig. 23) indicates that the secondary processes also modified the Fe/Mg ratio.

The alteration also leads to the modification of trace elements, particularly alkalis (Fig. 31). The secondary processes, which probably involved hydrothermal fluids, led to a significant enrichment in Zr (up to 7,000 ppm) and Nb (>200 ppm), but most notably Th (from 10-200 ppm in nonmineralized samples to >20,000 ppm Th in mineralized granites) and U (5-50 ppm in nonmineralized samples to >5,000 ppm in mineralized granites). In both fresh and altered rocks, Th and U show a positive correlation (Fig. 26a). However, the mineralized samples are enriched in Th relative to U as well as some other incompatible trace elements such as Y (Fig. 26b).

The REE abundances of the altered and mineralized rocks also reflect modification due to secondary processes that resulted in a variety of REE patterns. Their $(La/Yb)_n$ ranges from <0.1 to > 4 and correlates with La (Fig. 32), the abundances of which reaches >200 ppm. The variety

of the REE patterns is also reflected in the ranges of $(La/Sm)_n$ (0.1- >4) and $(Gd/Yb)_n$ (0.1 to 1.5). Although the shape of these patterns and the REE abundances are variable, the granitic rocks including the fresh, altered and mineralized from the complex and dikes have approximately the same negative Eu anomaly (Eu/Eu* ~0.3), indicating that all these rocks underwent about the same degree of feldspar fractionation and that the secondary processes did not modify the size of the Eu anomaly.

There are differences in alteration and mineralization between the Ross-Adams and Dotson zones. In the Ross-Adams deposit, hydrothermal alteration of granites reached a stage of pervasive albitization accompanied by leaching of quartz leading to the transformation of granites to syenite composed dominantly of albite. The altered granites of Ross-Adams plot either outside of the fields for anorogenic granites or show a significant dispersion on various diagrams using the elements generally considered to be immobile during the alteration processes (Fig. 31). The mineralization of the Ross-Adams deposit has higher concentrations of U and Th but lower REE and HFSE compared to the Dotson Zone.

8. 2. Mafic and Intermediate Rocks

8. 2. 1. *Younger Dikes*

Mafic to intermediate dikes which crosscut the Bokan granitic rocks including the I&L and Dotson zones and the Ross-Adams deposit (Table 5e), have SiO_2 ranging from ~ 50 to 60 wt.% and an Mg# (molecular proportion 100xMgO/[MgO+FeO*]) from 47 to 33. Their SiO_2 and Mg# are negatively correlated. The rocks correspond to subalkaline basalts and andesites (Fig. 33a) and display a calc-alkaline differentiation trend of decreasing TiO_2 with increasing FeO_{tot}/MgO ratio (Fig. 33b); these rocks probably include the lamprophyres of Thompson (1988, 1997) and Thompson et al. (1980, 1982). Their chondrite-normalized REE patterns (Fig. 33c) show a slight enrichment in LREE with $(La/Yb)_n$ ~2.5-4, $(La/Sm)_n$ ~1.5-2 and $(Gd/Yb)_n$ ~ 1-1.6. The primitive mantle-normalized patterns are typical of magmas derived from a subcontinental lithospheric mantle with negative Nb-Ta and Ti anomalies (Fig. 33d). The patterns also show a minor relative depletion of Zr and Hf. The field relations, differences in alteration and Ar/Ar dating indicate that the dikes are not all of the same age. Some of these dikes, particularly those which appear to be coeval with the peralkaline granites, might have been derived from a source similar to that of the Bokan complex.

8.2. 2. *Paleozoic Mafic Rocks*

In order to evaluate the effects of hydrothermal fluids on the country rocks and their mineralization, mafic bodies of Paleozoic age hosted in quartz monzonite along the Dotson Zone were investigated. Drilling along the Dotson Zone intersected several thick mafic bodies hosted by Paleozoic quartz monzonite. These bodies are crosscut by the Dotson Zone (Fig. 10). The mafic rocks (Table 5c) are compositionally similar to the diabase dike (sample G249 in Table 5c) collected away from the complex and to the diabase dike described by Philpotts et al. (1998). The mafic rocks have SiO_2 contents ranging from 47 to 53 wt. %, have an Mg# that varies between 67 and 48 and display typical tholeiitic characteristics (Fig. 34). The REE patterns of many of these rocks, particularly those away from the contact (e.g. sample G249), are rather flat without a noticeable negative Eu anomaly and with the La concentrations ~5-20 ppm. However, this contrasts with the mafic rocks close to the contact with (or within) the Dotson Zone, the trace element contents of which were apparently modified by infiltration of high temperature

fluids related to the complex. These metasomatised mafic rocks have trace element contents similar to those of the mineralized granitic rocks of the Dotson Zone [e.g., La ~200-600 ppm and with a significant negative Eu anomaly (Eu/Eu* ~ 0. 3)]. The presence of the enrichment halos around the mineralized dikes and shear zones implies that high temperature fluids played an important role during the mineralization processes.

8. 3. Isotopes

8.3.1. *Neodymium Isotopes*

Nd isotopic ratios for the rocks of the Bokan complex, related dikes and lamprophyres are given in Table 6. The Bokan data were aged-corrected to 177 Ma, although some of the lamprophyre dikes might be younger. The new data are in agreement with the values reported by Philpotts et al. (1998).

The high positive ε_{Nd} values for the granitic rocks of the Bokan complex and the dikes indicate that the rocks were derived from a reservoir with a history of LREE depletion, such as depleted upper mantle, and were not affected by contamination of ancient continental crust. However, the enrichment of LREE accompanied by positive ε_{Nd} values suggest that the mantle source was metasomatically enriched (e.g., Menzies and Murphy, 1980). The similarities of the ε_{Nd} values of the Bokan complex and the Dotson and I&L dikes suggest that these rocks are genetically related. Some of the mineralized samples have slighltly lower ε_{Nd} values indicating that secondary processes modified the Nd isotopic values. On the other hand, the lamprophyres have higher ε_{Nd} values than the granites implying that the rocks might not be closely genetically related.

The high positive ε_{Nd} values of the granitic country rocks reported by Philpotts et al. (1998) imply that these rocks were also derived from a juvenile source, consistent with the inference of Samson et al. (1989) that the crust of the Alexander terrane is mantle-derived, and probably formed in an oceanic or primitive volcanic arc setting. The mafic country rocks with positive ε_{Nd} values (e.g., Philpotts et al., 1998) were also derived from a depleted mantle source and were not affected by contamination of old continental crust.

8.3.2. *Lead Isotopes*

Eleven whole rock samples of granitic and dike rock material from Bokan as well as two lamprophyres were analyzed for their Pb isotopic composition and U and Th contents. The results are summarized in Table 7a, where the Pb isotopic ratios for all samples are age-corrected to 177 Ma, the preferred time of emplacement for the complex. It is worth noting that since there are several ages for dike rocks present in the complex, one of the lamprophyre dike rocks in the data set (LM-92) may be younger than the 177 Ma age for the complex, hence over-corrected for U and Th decay. Also included in the data set are analyses of two galena samples (Table 7b), one of which was reported by MacKevett (1963). Our sample (2009) is shown in the plot (solid symbol), whereas the other (MacKevett's) is too radiogenic to fit into the area of the plots.

The granitic data set (Table 7a) indicates an age-corrected range for $^{207}Pb/^{204}Pb$ of 15.49 to 15.19, for $^{206}Pb/^{204}Pb$ of 17.28 to 18.95, and for $^{208}Pb/^{204}Pb$ of 37.05 to 38.59. These data are also summarized on conventional $^{207}Pb/^{204}Pb$ versus $^{206}Pb/^{204}Pb$ and $^{208}Pb/^{204}Pb$ versus $^{206}Pb/^{204}Pb$ diagrams in Figure 35, where the data are compared to the various lead evolution curves of Doe and Zartman (1979). Of note in these diagrams is the large spread of the data due to the large range in $^{206}Pb/^{204}Pb$ values. Compared to the lead isotope evolution curves, the data

fall below the orogene model growth curve in terms of $^{207}Pb/^{204}Pb$ versus $^{206}Pb/^{204}Pb$. In this same plot the data clearly define a slope (0.07356) which equates to a $^{207}Pb/^{206}Pb$ age of 1034 Ma. Although this regression has no significance in terms of absolute age, it does reflect possible mixing of reservoirs. Importantly, the less radiogenic of the two galena samples plots at the radiogenic end of the array.This is interpreted to approximate the "real" lead isotopic composition of the Bokan magma when it was emplaced. Thus, the lead isotopic characteristics in this galena sample (2009) were derived from the Bokan melt and can be inferred to be of magmatic hydrothermal origin.

For comparative purposes, the data from Bokan are contrasted with a few suites in Figure 35, which include a variety of source reservoirs. The lead isotopic data for the Cretaceous Cassiar Batholith of the Canadian Cordillera overlap the upper crust evolution curve, which is consistent with the dominance of upper crustal source rocks based on whole rock chemical and isotopic (O, Sr, Nd, Pb) data (Driver et al., 2000). In contrast, the Devonian South Mountain Batholith of Nova Scotia, Canada, has a less radiogenic signature and overlaps the orogene curve, consistent with a source of mixed metasedimentary and metavolcanic rocks (Dostal et al., 2004; Dostal and Chatterjee, 2010). Finally, the lead isotopic data for the Cretaceous Josephine intrusive suite of California, interpreted to have been emplaced in continental margin arc, reflects a mixture of mantle and crustal sources, although the latter is more dominant (Barth et al., 1995). Also relevant in regard to the data set is the limited scatter in the data for two of the suites (Cassiar and Josephine), which reflect either a homogeneous source or mixing of melts, but a spread for the South Mountain Batholith, which reflects partial involvement of a Precambrian source rock and fluid fractionation in the petrogenesis of this suite. Based on the above discussion, the spread of the Pb isotopic data of the Bokan complex indicates that the melt was either not homogenized with respect to lead or it was variably contaminated, either during ascent or at the site of emplacement. The uniform petrology and geochemistry favors the latter interpretation which likely occurred during the subsolidus evolution of the complex which involved fluid: rock interaction, as recorded in the petrographic features of the rock. The lead isotopic system thus was significantly disturbed by hydrothermal fluids/metasomatic processes.

The least radiogenic galena sample (2009) is considered to be the best approximate of the primary lead composition of the Bokan melt. Thus, whole rock samples with a similar lead isotopic composition record limited contamination, whereas the rest of the samples reflect increasing amounts of lead derived from hydrothermal fluids. The galena sample (McKevett) with the highly radiogenic composition is consistent with its location within the Ross-Adams deposit and reflects the enrichment of both U and Th.

8.3.3. *Oxygen Isotopes*

Seven samples of quartz from granitic material were analyzed for ^{18}O. Quartz came from two samples of amphibole granite (LM66, LM78) and five samples of vein quartz and pegmatite (LM58, LM61, LM70, LM71, LM77). The results of the analyses are summarized in Table 8. The $\delta^{18}O$ values for quartz from the two granitic samples are essentially identical with $\delta^{18}O$ values of +9.0 and +8.9‰, whereas values of quartz from the second group range from +8.9 to +11.3‰ and average +9.7‰.

In terms of the granitic samples, it is important to note that $\delta^{18}O$ values of quartz do not generally vary much as a result of magmatic crystallization (Taylor and Sheppard, 1986), thus it can be inferred that the data for the two quartz samples are a good approximation of $\delta^{18}O_{quartz}$ for the Bokan granites. Furthermore, quartz is considered to be robust and not easily reset due to

later interaction with fluids, especially under conditions of low fluid: rock interaction at moderate to high temperatures (e.g., >400°C). Thus, this quartz value is used to estimate the original composition of the melt. This allows us to avoid using whole rock data, an unappealing alternative given the evidence that feldspars were altered (e.g., albitization, sericitization) by fluids during the cooling history. Based on a compilation of whole rock and quartz $\delta^{18}O$ values for variety granitic intrusions, Kontak and Kyser (2009) estimated Δ quartz-whole rock = +1.2‰, which is consistent with the expected small crystal-melt partitioning of ^{18}O at a high temperature in magmas (Taylor and Sheppard, 1986). Thus, for the average Bokan quartz this suggests the melt had a $\delta^{18}O$ value of +7.8‰. This value falls above the range of +5 to +7‰ for mantle-derived melts (Kyser, 1986) and is, instead, more typical of I-type or anorogenic granites (Taylor, 1986).

The quartz data for the pegmatite and vein samples can be used to infer the isotopic composition of the fluid in equilibrium with the quartz and indirectly assess the source of such a fluid. In this manner, it is possible to see if the mineralizing fluid may have been exsolved directly from the granite. This procedure is done with reference to a plot of $\delta^{18}O_{quartz}$ versus Temperature (°C) (Fig. 36) that is contoured for values of $\delta^{18}O_{H2O}$, as calculated using the quartz-H_2O fractionation equation of Matsuhisa et al. (1979). If the $\delta^{18}O_{quartz}$ value of +9‰ from the granite is used, then at 600°C a $\delta^{18}O_{H2O}$ value of about +7.5‰ is inferred and for 500°C a value of +6.7‰, as summarized in Table 8. These temperatures are considered valid for the generation of pegmatite-vein systems in such settings. As can be seen on the diagram (and also in Table 8), the pegmatite-vein data are consistent with quartz having crystallized from a fluid which had an original $\delta^{18}O_{H2O}$ value near +8‰ at high temperatures. If the pegmatite-vein samples originated at lower temperatures from the same fluid, then much higher $\delta^{18}O_{quartz}$ values are required (e.g., about +15‰ at 300°C). The sample with a higher $\delta^{18}O_{quartz}$ value (+11.3‰, LM73), would be consistent with it having crystallized at a lower temperature, probably near 450°C (Fig. 36). Thus, the $\delta^{18}O$ data for the pegmatite-vein quartz samples are consistent with generation of a magmatic fluid from a closed system. Furthermore, the current data set does not indicate the incursion of an external fluid during the early stage evolution of the Bokan complex, either of meteoric or metamorphic origin. This is also in an agreement with the oxygen and carbon isotopic data for carbonates from the Ross-Adams deposit reported by Thompson (1988), which indicate a magmatic origin.

9. Fluid Inclusion Study

Fluid inclusions reported here are hosted in quartz phenocrysts and are typically in the 10-15 μm range, with some inclusions up to ~ 40 μm. Generally, with the exception of only a few specific lithologies, the fluid inclusion record within the Bokan area is limited. Inclusions were identified in felsic dikes of the I&L zone associated with mineralization and in their immediate wall rocks (Ordovician-Silurian). No workable inclusions were identified in the main intrusive units of the Bokan suite. Inclusions are generally small and and texturally ambiguous, making phase change measurements and petrographic determination of origin challenging.

Three types of fluid inclusions are present: (i) type I (NaCl-KCl-CO_2-H_2O) inclusions of primary origin, found only in syn-mineralization dikes; (ii) type II (NaCl-KCl-H_2O) inclusions of secondary origin found in the wall rocks and syn-mineralization dikes examined; and (iii) type III (CO_2) inclusions of secondary origin occurring the wall rocks and syn-mineralization dikes. Microthermometric data are summarized in Table 9.

Type I inclusions appear either two-phase (aqueous liquid [L] + vapour [V]) or, rarely, three-phase (with visible CO_2 phase) at room T. However, the presence of CO_2 was confirmed in all type I inclusions by observation of clathrate melting, even when no visible CO_2 phase was present. Type I inclusions show clathrate melting (T_m^{clath}) between 2.6 and 7.4°C, with ~95 % of inclusions showing $T_m^{clath} > 4°C$ (n = 68). The inclusions homogenize completely to liquid between 178 and 296°C ($T_h^{L+V>L}$). When present, homogenization of the CO_2 phase (to liquid) occurs between 24.5°C and the critical point for CO_2 (31.1°C). Bulk salinities for type I inclusions, range between 5.0 and 12.4 wt. % $NaCl_{eq.}$, with the bulk of inclusions showing a narrow range in salinity between ~7 and 9 wt. % $NaCl_{eq}$. Single assemblages (small groups of inclusions trapped along single growth features) show narrow ranges in bulk salinity and homogenization characteristics (Fig. 37). Type II inclusions with anomalously high T_h values that occur with other inclusions in single assemblages that have overall lower T_h values may have experienced leakage or refilling (reopening, mixing, resealing).

Type II inclusions appear two-phase at room temperature and show final ice melting temperatures (T_m^{ice}) between –18.7 and –1.7°C, corresponding to a range in bulk salinity from 2.8 to 20.3 wt. % $NaCl_{eq}$ (n = 102). Homogenization to liquid ($T_h^{L+V>L}$) occurs between 140 and 345°C, with an average $T_h^{L+V>L}$ slightly lower than for type I inclusions. Single assemblages of inclusions (i.e., along single fractures) show much narrower ranges in salinity and $T_h^{L+V>L}$, but variations from one fracture to another indicate significant fluctuations in the bulk composition and T of this late-stage aqueous fluid. Many type II inclusions contain accidentally-trapped (partially-included) solid phases that were identified by LA-ICP-MS to be Y-REE minerals (e.g., yttrian fluorite, allanite). These phases grew earlier but were intersected by fractures that later healed to trap type II fluid.

Type III inclusions yielded CO_2 final melting (T_m^{CO2}) and homogenization temperatures (T_h^{CO2}) within uncertainty of -56.6°C (indicating pure CO_2), and 10.4 to 25.3°C, respectively (homogenizing to CO_2 liquid or by supercritical behavior; indicating a wide range in entrapment P; n = 16).

Analyses of 26 individual type I and II inclusions from one of the pegmatitic dike samples were obtained by LA-ICP-MS at ETH Zurich (Elan 6100 MS-GeoLas Ar-F 193 nm) utilizing a short menu (fewer elements, longer dwell times) to optimize limits of detection. Type I and type II inclusions contain K as a major secondary cation (~3,000-6,000 ppm) in addition to Na. Trace elements detected, quantified and common to both inclusion types I and II were B (10s-100s ppm), Cs (10s ppm), Rb (10s-100s ppm), Sr (10s-100s ppm), Ba (1-10s ppm), and Pb (10s ppm). Notably, in addition to the elements listed above, type I inclusions contain significant concentrations of Y (most commonly observed; 10s ppm), LREE (Ce; 1-10s ppm), and U-Th (1-10s ppm); these elements are below detection limits in type II inclusions. This is a significant finding since the bulk salinities of type I and type II inclusions are similar, suggesting that differences in composition are not an artifact of differential detection capability (mass load entering the ICP-MS) but instead represents a true composition difference. Additionally, Rb, Cs and B concentrations are higher in the type I inclusions, indicating that these highly melt-incompatible are preferentially enriched in the primary aqueous-carbonic phase compared to the late-stage, post-magmatic aqueous phase.

The results of the fluid inclusion study suggest that aY-REE-U-Th-rich, aqueous-carbonic fluid of moderate salinity was exsolved as a magmatic volatile phase at some stage during the evolution of the Bokan dike rocks. The exsolved magmatic volatile phase could have been responsible for localized ore metal enrichment, or the secondary redistribution of Y-REE-

U-Th originally occurring in accessory (primary, magmatic) minerals. Entrapment conditions for type I inclusions were estimated by finding the intersection of isochores with the solidus curve for fluid-saturated granitic liquid. This intersection occurs at very high entrapment pressures in the range of ~8-9 kbar (Fig. 38), entirely inconsistent with the depth of emplacement for the dikes. The reason for this discrepancy is not clear at present. Significant post-entrapment modification, impacting the bulk density of the inclusions, is unlikely since no direct petrographic evidence for this could be found. However, variations in pyroxene/amphibole mineralogy does suggest fluctuations in fO_2 during cooling and, therefore, post-entrapment water loss from the inclusions by H_2 diffusion out of the inclusions cannot be ruled out. Continuing work is attempting to resolve this uncertainty.

The transition from early magmatic aqueous-carbonic to late aqueous fluids was not associated with a change in bulk salinity but was associated with a decrease in CO_2, dissolved ore metal, and incompatible LILE content. The lack of ore metals in this late aqueous fluid suggests that either melts by this late stage had already lost their metal endowment to earlier exsolved fluids or crystallized accessory minerals, or that the presence of carbonate-based ligands in the earlier fluids favoured higher dissolved ore element concentrations.

Later stage fluids may have been fluoride-rich, as indicated by the near F end-member composition of apatite in equilibrium with biotite in the metasomatized wall rocks hosting the late felsic dikes. Biotite-apatite halogen-exchange thermometry (electron microprobe; Dalhousie University) yielded anomalously low final equilibration temperatures (270-400°C; n = 87 from three different gabbroic and granodioritic wall rock samples) broadly consistent with the microthermometric data for type II inclusions. This metasomatic event was associated with REE enrichment/redistribution in apatites in those wall rocks, which contain 0.86 wt. % LREE compared to apatites in the country rocks at a distance of several km from the Bokan dike rocks which contain little REE.

10. Discussion

Although they constitute only a small volume of the Earth's crust, alkaline/peralkaline felsic intrusive complexes have attracted a large amount of attention in the geological literature where their petrology, geochemistry, mineralogy and mineralization have been discussed extensively. The attention these complexes have received is due in part to their distinct enrichment in REE, HFSE and radioactive elements (Th, U), which in many cases (such as in the Bokan complex) is of economic significance. However, controversy remains regarding the origin of these silica-oversaturated alkaline magmas, as well as whether the contained HFSE, REE, Th and U mineralization is due to extensive fractional crystallization or is associated with late-stage magmatic-hydrothermal processes. These topics will be discussed in turn.

10.1. Petrogenesis of the Peralkaline Granites

10.1. 1. *Magma Evolution*

The granitic rocks of the Bokan complex are peralkaline with an agpaitic index (i.e., whole rock atomic [(Na+K)/Al]) greater than unity and in addition are characterized by high contents of HFSE, REE, Th and U, as well as halogens (F), and low contents of Sr, Ba and Eu. The trace elements showing the greatest enrichment are highly incompatible; they do not easily enter into the crystal structure of the common rock-forming minerals and are progressively enriched in the residual magmas as a consequence of fractional crystallization. However, a model of simple fractional crystallization of a primitive basaltic magma cannot produce the

observed enrichment of the incompatible trace elements. The compositional characteristics of these rocks, which are suggestive of extensive fractional crystallization, are consistent with a model of protracted evolution of an alkaline felsic magmas leading to an extremely fractionated melt composition at relatively low temperatures (e.g., Markl et al., 2001) in part due to the role of volatiles which depress the solidus in the rock systems. The presence of fluorine is well known to decrease the solidus temperature of felsic rocks, thus extending the duration of crystallization to low temperature (Markl et al., 2001). Alkalis and fluorine also increase the solubility of HFSE, REE, Th and U in volatile-bearing peralkaline felsic magmas (Linnen and Keppler, 1997, 2002). Thus, fractionation was probably enhanced by high concentrations of alkalis and some fluorine enrichment in the peralkaline magmas, which led to an increase of the solubility of these trace elements and also contributed to the suppression of crystallization of HFSE- and REE-bearing accessory minerals until the latest stages of fractionation (Keppler, 1993; Linnen, 1998). The absence of xenocrystic zircon in the granites and zircon inclusions within any of the magmatic phases may indicate that most of the zircons in the Bokan complex nucleated and crystallized near the liquidus. Low REE- HFSE-, U-, Th-solid-liquid partition coefficients of typical rock-forming mineral phases in alkaline/peralkaline melts also contribute to the extreme enrichment of these elements during fractional crystallization. Finally, volatiles and high P (fluid) expand the field for quartz and alkali feldspar, thereby making the residual melt more sodic-rich.The generation of a sodic-rich melt towards the terminal part of the crystallization of the Bokan complex probably relates to the abundance of albite as a late-stage phase which overprints the intrusion, much like it does in evolved rare-element pegmatite systems (e.g., Li-Cs-Ta type).

Negative anomalies of Ba, Sr and Eu on the primitive mantle-normalized spidergram plots for the Bokan rocks reflect the fractionation of feldspars, whereas the depletion of Ti probably reflects the fractionation of ilmenite. Such spider diagrams suggest that these granites solidified from highly fractionated melts that underwent extensive low-pressure feldspar-dominated crystal fractionation, which is further supported by petrographic observations. The lack of obvious correlations among various incompatible trace elements, together with the distinct differences in REE among the rocks of rather similar major element compositions, are consistent with an important role of accessory minerals during the evolution of these rocks.

10.1.2. *Source Rock Composition*

Peralkaline felsic magma, such as the Bokan complex, cannot be readily derived by partial melting of common crustal source rocks which are typically peraluminous. Instead, peralkaline magmas are conventionally considered to be derived by low degrees of partial melting of a mantle source. These magmas subsequently undergo extensive fractional crystallization during their ascent, possibly accompanied by crustal contamination. A comparison with recent volcanic rocks of similar composition (e.g., Pecerrrilo et al., 2003) suggests that the Bokan granites plausibly represent products of extreme fractionation of transitional basaltic magma.

In order to account for the tectonic setting and chemical composition of these rocks, several source-related models/processes can be considered for the genesis of Bokan: (1) crustal contamination of silica-undersaturated alkaline magmas (e.g., Goodenough et al., 2000; Marks et al., 2003); (2) melting of lower crustal material (e.g., Cerny, 1992; Lentz, 1996; Martin and De Vito, 2005); (3) melting of primitive mantle (Fowler and Doig, 1983); and (4) melting of metasomatically enriched lithospheric mantle (Upton et al., 2003; Halama et al., 2004).

-*(1) Crustal contamination of silica-undersaturated alkaline magma*.
Although crustal contamination of basaltic magma at depth cannot be ruled out, the consistently high positive ε_{Nd} values and oxygen isotopic ratios argue against crustal contamination. The observed enrichment of incompatible trace elements and unusual composition of the peralkaline granitic rocks indicate that crustal involvement was insignificant.

-*(2) Melting of lower crustal material*.
Lower crustal rocks such as granulites, charnockites and tonalities are considered to be depleted in radioactive elements U and Th. Thus, it is highly unlikely that melting of such a source rock would generate parent magma rich in U and Th unless some very unusual and rare process was involved, thus we exclude this mechanism.

-*(3) Low degree of melting of primitive mantle source.*
Melting of a primitive mantle (e.g., Sun and McDonough, 1989) would produce a melt with relatively low concentrations of incompatible trace elements. Geochemical modeling of such melts indicates that even after extensive fractionation, these melts would have significantly lower concentrations of incompatible trace elements than those observed in the Bokan granites. Also, this process would not account for the negative Nb-Ta anomalies on the primitive mantle-normalized graphs, which predicate a source showing such depletion.

-*(4) Melting of metasomatically enriched lithospheric mantle*.
Melting such a source, which has a prior history of elemental depletion (i.e., Nb and Ta relative to light REE) and metasomatism leading to enrichment of incompatible trace elements, including the light REE and positive ε_{Nd} values, seems to be consistent with the data in hand and can be invoked for the origin of the parent melt of the Bokan complex. The enrichment of the mantle source is probably associated with earlier subduction-related processes, part of the long-lived tectonic regime in this part of North America during the Paleozoic-Mesozoic period. The Nd model ages suggest that the mantle enrichment took place during the Ordovician.

10. 2. Origin of Mineralization

The genesis of the HFSE and REE mineralization associated with the peralkaline rocks is not well understood and debate remains as to whether the mineralization is magmatic, hydrothermal or a combination of the two (e.g., Richardson and Birkett, 1995; Salvi and Williams-Jones, 1990, 1996, 2004; Salvi et al., 2000; Linnen and Cuney, 2004; Cerny et al., 2005). The magmatic model assumes that the enrichment is mainly due to extensive fractional crystallization. In this model, protracted differentiation is probably related to magma composition, particularly its high content of volatiles and alkalis. Important in this context are the high levels of Zr and REE enrichment both within pegmatites and the intergranular (i.e., late crystallization volumes) parts of some granites, which may reflect the high levels of rare element enrichment attained during magmatic fractionation. However, mineralization is typically associated with altered parts of peralkaline intrusions, which suggests that the metal enrichment is also related to hydrothermal activity, unless the association is only coincidental.

It has been documented elsewhere (e.g., Salvi and Williams-Jones, 2004) that the volatiles play an important role in the evolution of highly evolved peralkaline rocks. The parent

melts of the peralkaline felsic rocks are generated under dry conditions (Salvi and Williams-Jones, 2004), as attested here by the low modal abundance of amphibole and its late-stage appearance in the crystallization history of the complex. Consequently, when these magmas undergo extensive fractionation they become saturated with aqueous fluids only very late in their crystallization history. The presence of low-density fluid inclusions in the amphibole at Bokan may be evidence of such volatile enrichment in the late-stage magmatic evolution of the complex. At the advanced stage of fractionation, the aqueous fluids escape from the magma which, at this point in its evolution, is also highly enriched in incompatible elements (such as REE, HFSE, Th and U) and, in addition, may contain significant amounts of halogens, particularly fluorine. Thus, the hydrothermal fluids, which are enriched in all these elements, can play an important role in further concentrating the HFSE, REE, Th and U, as well as during autometasomatism (e.g., Abdel-Rahman, 1994; Salvi and Williams-Jones, 2004). Such a model, where both magmatic and hydrothermal processes are likely to have contributed to mineral deposit formation, can probably be applied to the Bokan complex and associated dikes, where the mineralization is normally associated with altered zones and much of it is composed of secondary minerals, some of which pseudomorphically replaces primary minerals.

The U-Th mineralization of the Ross-Adams deposit is associated with intense alteration including hematization, albitization and silicification (Thompson et al., 1980; Collot, 1981) suggesting that the mineralization is at least in part hydrothermal. Likewise, in the Dotson, I&L and other zones, the occurrences of REE and HFSE mineralization in the aplitic dikes is accompanied by alteration and mineralization of the country rocks, including the diorites and gabbros and by the occurrences of fluorite veinlets rich in REE in the hornfelses. These features indicate that the mineralization was accompanied by hydrothermal and metasomatic activities.

In Bokan, the initial enrichment of HFSE, REE, Th and U by magmatic processes was followed by late magmatic-hydrothermal processes, which played an important role in producing the concentrations of metals observed in the mineralized sites. This hydrothermal alteration is considered to have coincided with the devolatilization of the magma at depth and the sites of mineralization reflect the highly fractionated nature of these late-stage fluids/melts. Unaltered granite of the Bokan complex has an average of U and Th contents of around 12 ppm and 24 ppm, respectively, whereas the corresponding grades in the Ross-Adams deposit (~0.85 wt. % U and 2.5 wt. % Th; Thompson et al., 1980; Cuney and Kyser, 2008) indicate that the hydrothermal enrichment factor was between 700 and 1,100.

Thompson et al. (1980) and Thompson (1988) concluded that the mineralization was rapid and essentially contemporaneous with hydrothermal alteration and both were closely related to the emplacement of the complex. This is also supported by our geochronologic data. Fluid saturation of the magma resulted in rapid degassing of the magma chamber and an escape of highly fractionated, silica-saturated melts and related fluids, which were subsequently focused along zones of structural weakness with precipitation of the U, Th, REE and HFSE mineralization due to fluid-wall rock interaction and changes in the fluid chemistry. An important observation that supports this model is that the mineralized aplite dikes along the Dotson Zone probably formed penecontemporaneously with fluid separation/escape during crystallization of the granitic magma.

Fluorite commonly occurs in the mineralized parts of the rocks and even forms veinlets in the hornfelses around the contact with the complex. The presence of fluorite indicates an appreciable amount of fluorine in the aqueous fluids, suggesting that HFSE and REE might have been transported in hydrothermal fluids mainly as fluoride complexes. The interaction of such

Ca-poor, F-rich fluids with Ca-bearing rocks or fluids would lead to the deposition of REE- and HFSE-bearing minerals, as well as fluorite (Salvi and Williams-Jones, 2004).

10. 3. Tectonic Setting: Geochemical Constraints

The Bokan granites display the characteristics of the A-type or within-plate granites (e.g., Whalen et al., 1987; Eby, 1990; Pearce et al., 1984). These traits include the presence of alkali amphibole and pyroxene in the mode, acmite in the CIPW norms, and a peralkaline nature. The rocks have low Al, Ca and Mg, high Ga/Al ratio and are strongly enriched in HFSE, REE, U and Th relative to typical continental crust (Rudnick and Gao, 2003) and orogenic calc-alkaline granitoids (Dostal and Chatterjee, 1995). Using standard tectonic discrimination diagrams, the Bokan granites plot in the A-type granite field (Fig. 31c,d) of Whalen et al. (1987) and in the field of within-plate granite (WPG, Fig. 31a,b) of Pearce et al. (1984). These characteristics are also consistent with the major element discrimination plots (Fig. 21). However, on average, the Bokan complex is more fractionated than the majority of the peralkaline felsic intrusions.

Anorogenic peralkaline granites are typically shallow seated intrusives or ring-dike complexes emplaced in rift or proto-rift environments, such as Nigeria (Bowden, 1985), the Oslo Graben (Neuman, 1978) and parts of the Arab Shield associated with the opening of the Red Sea (Stoeser, 1986). The more fractionated parts of these intrusions host disseminated types of HFSE, REE, Th, U and Sn mineralization (e.g., Kinnaird, 1985; Jackson, 1986, Linnen and Cuney, 2004; Salvi and William-Jones, 2004) and resemble the Bokan complex. Like other A-type peralkaline intrusions, the Bokan complex was emplaced during a rifting event.

The southern PWI hosts several alkaline plutons ranging in age from early Paleozoic through late Paleozoic and Jurassic to Early Cretaceous (Drinkwater and Calzia, 1994). They appear to have elevated concentrations of U-Th, REE and HFSE and a potential for hosting rare-earth element mineralization (Barker, 1990; Barker and Mardock, 1988; Warner, 1989; Drinkwater and Calzia, 1994). Some, particularly the Middle Jurassic pluton at Dora Bay (possibly coeval with the Bokan, but located about 30 km to the north), are compositionally similar to the Bokan complex. Drinkwater and Calzia (1994) grouped all these intrusions into a metallogenic belt of alkali plutons. This suggests that the intrusion of the Bokan complex was not an isolated event, but instead, was related to a regional rifting event and it might, therefore, reflect the presence of enriched lithospheric mantle under this part of the Alexander terrane.

On the other hand, the Paleozoic granitic country rocks plot in arc/orogenic fields on all these diagrams. The data on the Paleozoic granites, including the ε_{Nd} values of + 3.9 reported by Philpotts et al. (1998), are consistent with a model where the Paleozoic rocks of PWI were emplaced in a primitive island arc environment.

11. Conclusions

The Bokan Mountain complex is composed of highly fractionated peralkaline granitic rocks of Jurassic age (~177.2 Ma) that are hosted by the Paleozoic basement associated with granitoids dated at 469.2+/-3.9 Ma. In turn the complex was intruded by younger dikes at two times during the Cretaceous, one at around 150 Ma and the other at about 105 Ma.

The proposed model for the evolution of the Jurassic Bokan complex invokes the parent mafic magma which was derived from a lithospheric mantle metasomatically enriched in HFSE, REE, Th and U and possibly halogens during an earlier subduction zone related event, suggesting that these source rocks were phlogopite-or amphibole-bearing. The melts (possibly

transitional basalt - Frost and Frost, 2011) underwent fractional crystallization during their ascent and in so doing achieved a felsic composition. These melts were emplaced into a high-level magma chamber at crustal levels. The magma underwent further differentiation such that extremely fractionated magma was generated and subsequenty accumulated in the uppermost part of the chamber. Batches of this highly fractionated magma rose to form either a high-level stock or, alternatively (as Collot [1981] suggested), the complex might represent the apex of the chamber. As the magma was very poor in Mg, the mafic minerals (aegirine and arfvedsonite) were very close to the Fe end members and as such they were the last minerals to crystallize from the magma. These minerals typically enclose accessory HFSE- and REE-bearing minerals. The early-formed phases of the evolved felsic magma, alkali feldspar and quartz, do not contain any significant amounts of HFSE, REE, Th and U, thus their crystallization led to the further increase of their concentrations in the residual melt. At an advanced stage of fractional crystallization, the magma became fluid-saturated and over-pressured which led to the fluid and fractionated melt escape and to the deposition of the major part of the U, Th, HFSE and REE mineralization. It was probably a protracted event with two or more stages of rare metal enrichment (Photo 8). The alkaline fluid, released during the last stage of crystallization, is a potent agent for the late mobilization of these incompatible trace elements.

The primary mineral assemblage of peralkaline granites was iron-rich and oxidized, as indicated by near end member aegirine (e.g., Markl et al., 2010; Marks et al., 2011). The late stages of crystallization were more reducing (but accompanied by higher water pressure) leading to crystallization of arfvedsonite (with high proportion of Fe^{2+}) in lieu of aegirine and local replacement of aegirine by magnetite. However, late stage hydrothermal replacement of magnetite by hematite, replacement of mafic minerals by association of hematite and quartz and extensive hematitization associated with mineralization indicate a subsequent return to oxidizing conditions.

The initial stage of the intrusion was emplacement of the outer part of the stock which cooled relatively quickly. Magmatic fractionation, nonetheless, continued inward. As there are no significant compositional variations across the stock (Cuney and Kyser, 2008), the fractional crystallization likely occurred in the deeper part of the magma chamber. At a deeper central level of the magma chamber, the magma became more fractionated leading to fluid saturation. Subsequently, fluids were released from the hotter, deeper central part and migrated towards the cooler, marginal part of the intrusion (Cuney and Kyser, 2008). Highly fractionated melts and aqueous fluids highly enriched in Th, U, HFSE and REE escaped and followed zones of weakness. These fluids not only produced mineralization, but also extensive microfracturing and alteration of the granites. The alteration included, but was not restricted to the ubiquitous albitization of the K-feldspars and partial dissolution of the quartz. Fluids also penetrated the country rocks along fractures and fault/shear zones for up to several km from the stock. The occurrence of mineralized aplitic quartz-aegirine lenses within the vein-dikes suggests that the process already started during the magmatic stage. The mineralized bodies in these zones initially crystallized as peralkaline granitic pegmatites and aplites but were extensively overprinted at moderate temperatures by hydrothermal fluids which also produced a significant metasomatic remobilization of rare metals. It was during this fluid-rock interaction that most REE and HFSE minerals were formed.

The key factors in the formation of the Bokan deposits include (1) melting of a metasomatically enriched lithospheric source; (2) the formation of a highly fractionated magma with commensurate build up of volatiles; (3) an initial stage of late-magmatic mineralization

with coincident release of metal-enriched fluids; and (4) focusing of the fluids into structurally prepared zones where the bulk of the mineralization occurs.

Acknowledgements

This study was supported by the U. S. Geological Survey grant G09AP00039. The report would not be possible without the support of Ucore Rare Metals - the management of the company has allowed the authors to access their samples, drill cores and files and even more provided generous logistic and financial support for the study. Some of the laboratory work was also funded by the Natural Science and Engineering Research Council of Canada (Discovery grants to JD, DK and JH). Numerous discussions with Ucore geologists Harmen Keyser, Jim Barker, Roger Hulstein, Mike Power and Jim Robinson helped us to appreciate the geology and mineral potential of the Bokan Mountain. We also thank Sue Karl and Richard Goldfarb of U.S. Geological Survey and Tony Mariano for encouragement and numerous advices. Mike Hamilton from the University of Toronto, Greg Shellnutt from Academia Sinica, Taipei and Douglas Archibal from Queen's University, Kingston helped with geochronological analyses. We thank Randy Corney for cheerful technical support.

References Cited

Abdel-Rahman, A.M., 1994. Alkali amphibole: a potential source of rare earth elements in felsic alkaline rocks: Exploration and Mining, v. 3, p. 81-94.

Abdel-Rahman, A.M., 2006. Petrogenesis of anorogenic peralkaline granitic complexes from eastern Egypt: Mineralogical Magazine, v. 70, p. 27-50.

Abdel-Rahman, A.M., and El-Kibbi, M.M., 2001. Anorogenic magmatism: chemical evolution of the Mount El-Sibai A-type complex (Egypt), and implications for the origin of within-plate felsic magmas: Geological Magazine, v. 138: 67-85.

Anderson, T., 2002. Correction of common lead in U-Pb analyses that do not report ^{204}Pb: Chemical Geology, v. 192, p. 59-79.

Armstrong, R.L., 1985. Rb-Sr dating of the Bokan Mountain granite complex and its country rocks: Canadian Journal of Earth Sciences, v. 22, p. 1233-1236.

Armstrong, R.L., 1986. Rb-Sr dating of the Bokan Mountain granite complex and its country rocks: Reply: Canadian Journal of Earth Sciences, v. 23, p. 743-744.

Ayuso, R.A., Karl, S.M., Slack, J.F., Haeussler, P.J., Bittenbender, P.E., Wandless, G.A., and Colvin, A.S., 2007. Oceanic Pb-isotopic sources of Proterozoic and Paleozoic volcanogenic massive sulfide deposits on Prince of Wales Island and vicinity, Southeastern Alaska: Alaska Science Centre, U.S. Geological Survey Professional Paper 1732-E.

Barker, J.C., 1990. Rare earth element- and yttrium-bearing pegmatite dikes near Dora Bay, southern Prince of Wales Island: U. S. Bureau of Mines, Open-File Report 19-90, 41 p.

Barker, J.C., and Mardock, C.L., 1988. Lithophile metal, REE-Y-Nb deposits on southern Prince of Wales Island, Alaska. *In:* Carson, D.J.T. and Vassiliou, A.H. eds., Process Mineralogy VIII: The Minerals, Metals and Materials Society, p. 139-157.

Barth, A.P., Wooden, J.L., Tosday, R.M., and Morrison, J., 1995. Crustal contamination in the

petrogenesis of a calc-alkaline rock series: Josephine Mountain intrusion, California: Geological Society of America Bulletin, v. 107, 201-212.
Batchelor, R.A., and Bowden, P., 1985. Petrogenetic interpretation of granitoid rock series using multicationic parameters: Chemical Geology, v. 48, p. 43-55.
Bodnar, R.J., 1994. Synthetic fluid inclusions. XII. Experimental determination of the liquidus and isochores for a 40 wt% H_2O-NaCl solution: Geochimica et Cosmochimica Acta, v. 58, 1053-1063.
Bowden, P., 1985. The geochemistry and mineralization of alkaline ring complexes in Africa: Journal of African Earth Sciences, v. 3, 17-40.
Brew, D.A., 1988. Latest Mesozoic and Cenozoic magmatism in southeastern Alaska- a synopsos: U.S. Geological Survey, Open-File Report 88-405, 41 p.
Brew, D.A., Drew, L.J., Schmidt, L.M., Root, D.H., and Huber, D.F., 1991. Undiscovered locatable mineral resources of the Tongass National Forest and adjacent areas, southeastern Alaska: U.S. Geological Survey, Open-File Report 91-10, 370 p, 16 maps.
Capaldi, G., Chiesa, S., Manetti, P., Orsi, G., and Poli, G., 1987. Tertiary anorogenic granites of the western border of the Yemen plateau: Lithos, v. 20, p. 433-444.
Chiu, H.Y., Chung, S.L., Wu, F.Y., Liu, D., Liang, Y.H., Lin, I.J., Iizuka, Y., Xie, L.W., Wang, Y., and Chu, M.F., 2009. Zircon U-Pb and Hf isotopic constraints from eastern Transhimalayan batholiths on the precollisional magmatic and tectonic evolution in southern Tibet: Tectonophysics, v. 477, p. 3-19.
Cerny, P., 1992. Geochemical and petrogenetic features of mineraliztion in rare-element granitic pegmatites in the light of current research: Applied Geochemistry, v. 7, p. 393-416.
Cerny, P., Meintzer, R.E., and Anderson, A.J., 1985. Extreme fractionation in rare element granitic pegmatites: Selected examples of data and mechanisms: Canadian Mineralogist, v. 23, p. 381-421.
Cerny, P., Blevin, P.L., Cuney M., and London, D., 2005. Granite-related ore deposits: Economic Geology, v. 100, p. 337-370.
Clarke, A.H., Archibald, D.A., Lee, A.W., Farrar, E., and Hodgson, C.J., 1998. Laser probe $^{40}Ar/^{39}Ar$ ages of early- and late-stage alteration assemblages, Rosario porphyry copper-molybdenum deposit, Callahuasi district, I Region, Chile: Economic Geology, v. 93, p. 326-337.
Clayton, R.N., and Mayeda, T.K., 1963. The use of bromine pentafluoride in the extraction of oxygen from oxides and silicates for isotopic analysis: Geochimica et Cosmochimica Acta, v. 27, p. 43-52.
Collot, B., 1981. Le granite albitique hyperalcalin de Bokan Mountain (S.E. Alaska) et ses mineralisations U-Th. Sa place dans la cordilliere canadienne. Doct. 3 degree cycle thesis, Montpellier II University, Montpellier, France, 238 p.
Colpron, M., Nelson, J.L., and Murphy, D.C., 2007. Northern Cordilleran terranes and their interactions through time: GSA Today, v. 17, p. 4-10.
Coney, P.J., Jones, D.L., and Monger, J. W. H., 1980. Cordilleran suspect terranes: Nature, v. 288, p. 329-333.
Cuney, M., and Kyser, T.K., 2008. Deposits related to magmatic differentiation. *In*: Cuney, M., and Kyser, K., eds., Recent and Not-so Recent Developments in Uranium Deposits and Its Implications for Exploration. MAC Short Course, v. 39, p. 55-77.

de la Roche, H., Leterrier, J., Grandclaude, P., and Marchal, M., 1980. A classification of volcanic and plutonic rocks using R1-R2 diagram and major element analyses: Its relationships with current nomenclature: Chemical Geology, v. 29, p. 183-210.

Debon, F., and LeFort, P., 1988. A cationic classification of common plutonic rocks and their magmatic associations; principles, method, applications: Bulletin de Mineralogie, v. 111, p. 493-519.

DePaolo, D.J., 1988. Neodymium isotope geochemistry: an introduction: Springer Verlag, New York, 187p.

de Saint-Andre, B., Lancelot, J.R., and Collot, B., 1983. U-Pb geochronology of the Bokan Mountain peralkaline granite, southeastern Alaska: Canadian Journal of Earth Sciences, v. 20, p. 236-245.

de Saint-Andre, B., and Lancelot, J.R., 1986. Rb-Sr dating of the Bokan Mountain granite complex and its country rocks: Discussion: Canadian Journal of Earth Sciences, v. 23, p. 743-744.

Doe, B. R., and Zartman, R.E., 1979. Plumbotectonics, the Phanerozoic. *In*: Barnes, H.L. ed., Geochemistry of hydrothermal ore deposits (2nd ed.). Wiley-Interscience, New York, p. 22-70.

Dostal, J., and Chatterjee, A. K., 1995. Origin of topaz-bearing and related peraluminous granites of late Devonian Davis Lake pluton, Nova Scotia, Canada: Chemical Geology, v. 123, p. 67-88.

Dostal, J., and Chatterjee, A. K., 2000. Contrasting behaviour of Nb/Ta and Zr/Hf ratios in a peraluminous granitic pluton (Nova Scotia, Canada): Chemical Geology, v. 163, p. 207-218.

Dostal, J., and Chatterjee, A. K., 2010. Lead isotope and trace element composition of K-feldspars from peraluminous granitoids of the Late Devonian South Mountain Batholith (Nova Scotia, Canada): Implications for petrogenesis and tectonic reconstruction: Contributions to Mineralogy and Petrology, v. 159, p. 563-578.

Dostal, J, Chatterjee, A. K., and Kontak, D. J., 2004. Chemical and isotopic (Pb, Sr) zonation in a peraluminous granite pluton: role of fluid fractionation: Contributions to Mineralogy and Petrology, v. 147, p. 74-90.

Drinkwater, J.L., and Calzia, J.P., 1994. Geochemical reconnaissance of alkali plutons on Prince of Wales Island, Southeastern Alaska: Alaska Department of Natural Resources, Geological and Geophysical Surveys, U. S. Geological Survey Bulletin 2107, p. 173-184.

Driver, L.A., Creaser, R.A., Chacko, T., and Erdmer, P., 2000. Petrogenesis of the Cretaceous Cassiar batholith, Yukon–British Columbia, Canada: Implications for magmatism in the North American Cordilleran Interior: Geological Society of America Bulletin, v. 112, p. 1119-1133.

Eby, G.N., 1990. The A-type granitoids: a review of their occurrence and chemical characteristics and speculations on their petrogenesis: Lithos, v. 26, p. 115-134.

Eby, G.N., 1992. Chemical subdivision of the A-type granitoids: Petrogenetic and tectonic implications: Geology, v. 20, p. 641-644.

Eberlain, G.D., Churkin, M., Carter, C., Berg, H.C., and Ovenshine A.T., 1983. Geology of the Craig quadrangle, Alaska: U. S. Geological Survey, Open-File Report 83-91, 50 p.

Erdmann, S, Wodicka, N., Jackson, S., and Corrigan, D., 2011. Zircon textures and composition: sensitive recorder of magmatic fluid exsolution?: GAC/MAC Annual Meeting, Abstracts, v. 2011, p. 59.

Foord, E.E., Staatz, M.H., and Conklin, N.M., 1984. New data for iimoriite: American Mineralogist, v. 69, p. 196-199.
Fowler, A.D., and Doig, R., 1983. The age and origin of Grenville province uraniferous granites and pegmatites: Canadian Journal of Earth Sciences, v. 20, p. 92-104.
Floran, R.J., 1983. Yttrium mineralogy of samples from the Bokan Mountain peralkaline igneous complex, southeastern Alaska: Technical Memorandum, Union Oil Company of California, E&P Geology 83-65M, 41 p.
Frost, B.R., Barnes, C.G., Collins, W.J., Arculus, R.J., Ellis, D.J., and Frost, C.D., 2001. A geochemical classification for granitic rocks: Journal of Petrology, v. 42, p. 2033-2048.
Frost, C. D., and Frost, B.R., 2011. On ferroan (A-type) granitoids: their compositional variability and modes of origin: Journal of Petrology, v. 52, p. 39-53.
Gehrels, G.E., 1992. Geologic map of the southern Prince of Wales Island, southeastern Alaska: U. S. Geological Survey, Miscellaneous Investigations, Map 1-2169, scale 1:63,000.
Gehrels, G.E., and Saleeby, J.B., 1987a. Geology of southern Prince of Wales Island, southeastern Alaska: Geological Society of America Bulletin, v. 98, p. 123-137.
Gehrels, G.E., and Saleeby, J.B., 1987b. Geologic framework, tectonic evolution, and displacement history of the Alexandra terrane: Tectonics, v. 6, p. 151-173.
Goodenough K.M., Upton, B.G.J., and Ellam, R.M., 2000. Geochemical evolution of the Ivigtut Granite, South Greenland: a fluorine-rich "A-type" intrusion: Lithos, v. 51, p. 205-221.
Gutierrez-Alonso, G., Murphy, J.B., Fernandez-Suarez, J., and Hamilton, M.A., 2008. Rifting along the northern Gondwana margin and the evolution of the Rheic Ocean: A Devonian age for the El Castillo volcanic rocks (Salamanca, Central Iberian Zone): Tectonophysics, v. 461, p. 157-165.
Halama, R., Marks, M., Brugmann, G., Siebel, W., Wenzel, T., and Markl, G., 2004. Crustal contamination of mafic magmas: evidence from a petrological, geochemical and Sr-Nd-Os-O isotopic study of the Proterozoic Isortoq dike swarm, South Greenland: Lithos, v. 74, p. 199-232.
Hansley, P.A., and Fitzpatrick, J.J., 1989. Compositional and crystallographic data on REE-bearing coffinite from the Grants uranium region, northwestern New Mexico: American Mineralogist, v. 74, p. 263-270.
Holtz, F., Pichavant, M., Barbey, P., and Johannes,W., 1992. Effects of H_2O on liquidus phase relations in the haplogranite system at 2 and 5 kbar: American Mineralogist, v. 77, p. 1223-1241.
Jackson, N.J., 1986. Mineralization associated with felsic plutonic rocks of the Arabian Shield: Journal of African Earth Sciences, v. 4, p. 213-228.
Jackson, S.E., Peason, N.J., Griffin, W.L., and Belousova, E.A., 2004. The application of laser ablation-inductively coupled plasma mass-spectrometry to in situ U-Pb zircon geochronology: Chemical Geology, v. 21, p. 47-69.
Jaffey, A.H., Flynn, K.F., Glendenin, L.E., Bentley, W.C., and Essling, A.M., 1971. Precision measurement of half-lives and specific activities of ^{235}U and ^{238}U: Physical Review, v. 4, p. 1889-1906.
Kent, S., and Sullivan C., 2004. 2004 Preliminary assessment/site inspection report, Ross-Adams uranium mine, Prince of Wales Island, Alaska: Private report for U. S. DA Forest Service.
Keppler, H., 1993. Influence of fluorine on the enrichment of high field strength trace elements

in granitic rocks: Contributions to Mineralogy and Petrology, v. 114, p. 479-488.
Keyser, H.J., and McKenney, J., 2007. Geological report on the Bokan Mountain Property, Prince of Wales Island, Alaska: Private report for Landmark Minerals Inc., 48 p.
Kiffer, D., 2005. There's Giegers in them thar hills - Bokan Mountain and the Alaska uranium "boom". Stories in the News, Ketchikan, Alaska. http://www.sitnews.us/Kiffer/BokanMountain/071005_bokan.html
Kinnaird, J., 1985. Hydrothermal alteration and mineralization of the alkaline anorogenic ring complexes of Nigeria: Journal of African Earth Sciences, v. 3, p. 229-252.
Kontak, D.J., and Kyser, T.K., 2009. Nature and origin of an LCT-suite pegmatite with late-stage sodium enrichment, Brazil Lake, Yarmouth Country, Nova Scotia. II. Implications of stable isotopes ($\delta^{18}O$, δD) for magma source, internal crystallization and nature of sodium metasomatism: Canadian Mineralogist, v. 47, p. 745-764.
Krogh, T.E., 1973. A low contamination method for hydrothermal decomposition of zircon and extraction of U and Pb for isotopic age determinations: Geochimica et Cosmochimica Acta, v. 37, p. 485-494.
Kyser, T.K., 1986. Stable isotope variations in the mantle. *In:* Valley, J.W., Taylor, H.P., Jr, and O'Neil, J.R., eds., Stable Isotopes in High Temperature Geological Processes. Reviews in Mineralogy 16, Mineralogical Society of America, p. 141-164.
Lanphere, M. A., MacKevett, E. M., and Stern, T. W., 1964. Potassium-argon and lead-alpha ages of plutonic rocks, Bokan Mountain area, Alaska: Science, v. 145, p. 705-707.
Leake, B.E., Woolley,A.R., Birch, W.D., Burke, EAJ, et al., 2004. Nomenclature of amphiboles: additions and revisions to the International Mineralogical Association's amphibole nomenclature: European Journal of Mineralogy, v. 16, p. 191-196.
Le Maitre, R.W., Bateman P., Dudek A., Keller J., Lameyre J., Le Bas M.J., Sabine P.A., Schmid R., Sorensen H., Streckeisen A., Wooley A.R., and Zanettin B., 1989. A Classification of Igneous Rocks and Glossary of Terms: Blackwell, Oxford. 193 p.
Lentz, D.R., 1996. U, Mo and REE mineralization in late tectonic granitic pegmatites, southwestern Grenville province, Canada: Ore Geology Review, v. 11, p. 197-227.
Linnen, R.L., 1998. The solubility of Nb-Ta-Zr-Hf-W in granitic melts with Li and Li-F: Constraints for mineralization in rare-metal granites and pegmatites: Economic Geology, v. 93, p. 1013-1025.
Linnen, R.L., and Cuney, M., 2004. Granite-related rare-element deposits and experimental constraints on Ta-Nb-W-Sn-Zr-Hf mineralization. *In:* Linnen, R.L., and Samson, I.M., eds., Rare-element geochemistry and mineral deposits. Geological Association of Canada Short Course Notes, v. 17, p. 45-68.
Linnen, R. L., and Keppler, H., 1997. Columbite solubility in granitic melts: Consequences for the enrichment and fractionation of Nb and Ta in the Earth's crust: Contributions to Mineralogy and Petrology, v. 128, p. 213-227.
Linnen, R. L., and Keppler, H., 2002. Melt composition control on Zr/Hf fractionation in magmatic processes: Geochimica et Cosmochimica Acta, v. 66, p. 3293-3301.
Long, K.R., Van Gosen, B.S., Foley, N.K., and Cordier, D., 2010. The principal rare earth element deposits of the United States-a summary of domestic deposits and a global perspective: U.S. Geological Survey, Scientific Investigations Report 2010-5220, 96 p.
Ludwig, K.R., 2003. User's manual for Isoplot 3.00, a geochronological toolkit for Excel: Berkeley Geochronological Center Special Publication 4, 71p.

MacKevett, E.M. Jr., 1963. Geology and ore deposits of the Bokan Mountain uranium-thorium area, southeastern Alaska: U. S. Geological Survey Bulletin 1154, 125 p.

Mariano, A.N. , 1983. Some characterization data on the Strange Lake Complex of Quebec-Labrador and Bokan Mountain, Alaska. Private Report to Molycorp.

Markl, G., Marks, M., Schwinn, G., and Sommer, H., 2001. Phase equilibrium constraints on intensive crystallization parameters of the Ilmaussaq Complex, South Greenland: Journal of Petrology, v. 42, p. 2231-2258.

Markl, G., Marks, M.A., and Frost B.R., 2010. On the controls of oxygen fugacity in the generation and crystallization of peralkaline melts: Journal of Petrology, v. 51, p. 1831-1847.

Marks, M., Vennemann, T., Siebel, W., and Markl, G., 2003. Quantification of magmatic and hydrothermal processes in a peralkaline syenite-alkali granite complex based upon textures, phase equilibria, and stable and radiogenic isotopes: Journal of Petrology, v. 44, p. 1247-1280.

Marks, M.A., Hettmann, K., Schilling, J., Frost, B.R., and Markl, G., 2011. The mineralogical diversity of alkaline igneous rocks: critical factors for the transition from miaskitic to agpaitic phase assemblages: Journal of Petrology, v. 52, p. 439-455.

Martin, R.F., and De Vito, C., 2005. The patterns of enrichment in felsic pegmatites ultimately depend on tectonic setting: Canadian Mineralogist, v. 43, p. 2027-2048.

Maas, K. M., Bittenbender, P.E., and Still, J.C., 1995. Mineral investigations in the Ketchikan mining district, southeastern Alaska: U.S. Bureau of Mines, OF Report 1-95, 606 p.

Matsuhisa, Y., Goldsmith, J.R., and Clayton, R.N., 1979. Oxygen isotopic fractionation in the system quartz-albite-anorthite-water: Geochimica et Cosmochimica Acta, v. 43, p. 1131-1140.

Menzies, M.A., and Murphy, V.R., 1980. Mantle metasomatism as a precursor to the genesis of alkaline magma-isotopic evidence: American Journal of Science, v. 280-A, p. 622-638.

Miyashiro, A., 1974. Volcanic rock series in island arcs and active continental margins: American Journal of Science, v. 274, p. 321-355.

Middlemost, E.A. K., 1985. Naming materials in the magma/igneous rock systems: Earth-Sciences Reviews, v. 37, p. 215-224.

Neumann, E.R., 1978. Petrology of plutonic rocks: Norges Geologiske Undersokelse Bulletin, v. 45, p. 25-34.

Nockleberg, W.J., Parfenov, L.M., Monger, J.W.H., Norton, I.O., Khanchuk, A.I., Stone, D.B., Scotese, C.R., Scholl, D.W., and Fujita K., 2000. Phanerozoic tectonic evolution of the circum-North Pacific: U. S. Geological Survey Professional Paper 1626, 122 p.

Peccerillo, A., Barberio, M.R., Yirgu, G., Ayalew, D., Barbieri, M., and Wu, T.W., 2003. Relationships between mafic and peralkaline silicic magmatism in continental rift settings: a petrological, geochemical and isotopic study of the Gedemsa volcano, Central Ethiopian rift: Journal of Petrology, v. 44, p. 2003-2032.

Pearce, J.A., Harris, N.B., and Tindle, A.G., 1984. Trace element discrimination diagrams for the tectonic interpretation of granitic rocks: Journal of Petrology, v. 25, p. 956-983.

Philpotts, J.A., Taylor, C.D., and Baedecker, P.A., 1996. Rare-earth enrichment at Bokan Mountain, southeast Alaska. *In*: Moore, T.E. and Dumoulin, J.A., eds. Geologic studies in Alaska by the U.S. Geological Survey, 1994: U. S. Geological Survey Bulletin 2152, p. 89-100.

Philpotts, J.A., Taylor, C.D., Tatsumoto, M., and Belkin, H.E., 1998. Petrogenesis of late-stage granites and Y-REE-Zr-Nb-enriched vein dikes of the Bokan Mountain stock, Prince of Wales Island, southeastern Alaska: U.S. Geological Survey, OF Report 98-459, 71 p.

Redman, E., 1981. Keete Inlet thrust faul, Prince of Wales Island: Alaska Division of Geological and Geophysical Surveys Report, v. 73, p. 17-18.

Richardson, D.G., and Birkett, T.C., 1995. Peralkaline rock-associated rare metals. GSA Geology of North America, vol.P-1, p. 523-540.

Robinson, R.J., Power, M.A., and Barker, J.C., 2011. Technical report on the exploration program and mineral resources estimate for the Bokan Mountain property, Prince of Wales Island, Alaska. Report to Ucore Rare Metals, 159 p.

Rudnick, R.L., and Gao, S., 2003. Composition of the continental crust. *In:* Treatise On Geochemistry. Elsevier Ltd, Amsterdam, v. 3, p. 1-64.

Salvi, S., and Williams-Jones, A.E., 1990. The role of hydrothermal processes in the granite-hosted Zr, Y, REE deposit at Strange Lake, Quebec/Labrador: Evidence from fluid inclusions: Geochimica et Cosmochimica Acta, v. 54, p. 2403-2418.

Salvi, S., and Williams-Jones, A.E., 1996. The role of hydrothermal processes in concentrating HFSE in the Strange Lake peralkaline complex, northeastern Canada: Geochimica et Cosmochimica Acta, v. 60, p. 1917-1932.

Salvi, S., and Williams-Jones, A.E., 2004. Alkaline granite-syenite deposits. *In:* Linnen, R.L. and Samson, I.M., eds. Rare-element geochemistry and mineral deposits. Geological Association of Canada Short Course Notes, v. 17, p. 315-341.

Salvi, S., Fontan, F., Monchoux, P., Williams-Jones, A.E., and Moine, B., 2000. Hydrothermal mobilization of high field strength elements in alkaline igneous systems: Evidence from the Tamazeght Complex (Morocco): Economic Geology, v. 95, p. 559-576.

Samson, S.D., McClelland, W.C., Patchett, P.J., Gehrels, G.E., and Anderson, R.G., 1989. Evidence from neodymium isotopes for mantle contributions to Phanerozoic crustal genesis in the Canadian Cordillera: Nature, v. 337, p. 705-709.

Schmitt, A.K., Trumbull, R.B., Dulski, P. and Emmermann, R., 2002. Zr-Nb-REE mineralization in peralkaline granites from the Amis complex, Brandberg (Namibia): Evidence for magmatic pre-enrichment from melt inclusions: Economic Geology, v. 97, p. 399-413.

Shaw, D.M., 1968. A review of K/Rb fractionation trends by covariation analysis: Geochimica et Cosmochimica Acta, v. 32, p. 573-601.

Slack, J.F., Shanks, W.C., Karl, S.M., Gemery, P.A., Bittenbender, P.E., and Ridley, W.I., 2007. Geochemical and sulfur-isotopic signatures of volcanogenic massive sulfide deposits on Prince of Wales Island and vicinity, southeastern Alaska: Alaska Science Centre, U. S. Geological Survey Professional Paper 1732-C.

Soja, C.M., and Krutikov, L., 2008. Provenance, depositional setting, and tectonic implications of Silurian polymictic conglomerates in Alaska's Alexander terrane: Geological Society of America Special Paper, v. 442, p. 63-75.

Staatz, M.H., 1974. Thorium veins in the United States: Economic Geology, v. 69, p. 494-507.

Staatz, M.H., 1978. I&L uranium and thorium vein system, Bokan Mountain, southern Alaska: Economic Geology, v. 73, p. 512-523.

Staatz, M.H., Armbrustmacher, T.J., Olson, J.C., Brownfield, I.K., Brock, M.R., Lemons, J.F, Coppa, L.V., and Clingan, B.V., 1979. Principal thorium resources in the United States: U.S. Geological Survey Circular 805, 42 p.

Steiger, R.H., and Jäger, E., 1977. Subcommission on geochronology: convention on the use of decay constants in geochronology and cosmochronology: Earth Planetary Science Letters, v. 36, p. 359-362.

Stephens, F.H., 1971. The Kendrick Bay project: Western Miner, v. 44, p. 151-158.

Stoeser, D.B., 1986. Distribution and tectonic setting of plutonic rocks of the Arabian Shield: Journal of African Earth Sciences, v. 4, p. 21-456.

Sun, S. S., and McDonough, W. F.,1989. Chemical and isotopic systematics of oceanic basalts: implications for mantle composition and processes. *In:* A. D. Saunders, A. D., and Norry, M. J., eds., Magmatism in the Ocean Basins. Geological Society London Special Publication, v. 42, p. 313-345.

Tanaka, T. and 18 others, 2000. JNdi-1: a Neodymium isotopic reference in consistency with La Jolla Neodymium: Chemical Geology, v. 168, p. 279-281.

Taylor, H.P. Jr., 1986. Igneous rocks: II. Isotopic case studies of Circumpacific magmatism: *In:* Valley, J.W., Taylor, H.P. Jr., and O'Neil, J.R., eds., Stable Isotopes in High Temperature Geological Processes: Reviews in Mineralogy 16, Mineralogical Society of America, p. 273-317.

Taylor, H.P. Jr., and Sheppard, S.M.F., 1986. Igneous rocks: I. Processes of isotopic fractionation and isotope systematics. *In:* Valley, J.W., Taylor, H.P. Jr., and O'Neil, J.R., eds., Stable Isotopes in High Temperature Geological Processes: Reviews in Mineralogy 16, Mineralogical Society of America, p. 227-271.

Thompson, T.B., 1988. Geology and uranium-thorium mineral deposits of the Bokan Mountain granite complex, southeastern Alaska: Ore Geology Reviews, v. 3, p. 193-210.

Thompson, T. B., 1997. Uranium, thorium, and rare metal deposits of Alaska: Economic Geology, Monograph 9, p. 466-482.

Thompson, T.B., Lyttle, T., and Pierson, J.R., 1980. Genesis of the Bokan Mountain, Alaska, Uranium-Thorium Deposits: U.S. Department of Energy Report (Bendix Field Engineering; subcontract 78-245-E), Grand Junction, Colorado, 232 p.

Thompson, T.B., Pierson, J.R., and Lyttle, T., 1982. Petrology and petrogenesis of the Bokan granite complex, southeastern Alaska: Geological Society of America Bulletin, v. 93, p. 898-908.

Todt,W., Cliff,R.A., Hanser,A., and Hofmann, A.W., 1996. Evaluation of a ^{202}Pb-^{205}Pb double spike for high precision lead isotope analysis. *In:* Basu, A. and Hart, S.R. eds., Earth Processes: Reading the isotopic code. American Geophysical Union, Geophysical Monograph, v. 95, p. 429-437.

Upton, B.G.J., Emeleus, C.H., Heaman, L.M., Goodenough, K.M., and Finch, A.A., 2003. Magmatism of the mid-Proterozoic Garder Province, South Greenland: chronology, petrogenesis and geological setting: Lithos, v. 68, p. 43-65.

Yavuz, F., 2007. WinAmphcal: A Windows program for the IMA-04 amphibole classification: Geochemistry, Geophysics, Geosystems, v. 8, Q01004, doi:10.1029/2006GC001391.

Vander Auwera, J., Bogaerts M., Liegeois, J.P., Demaiffe, D., Wilmart, E., Bolle, O., and Duchesne, J.C., 2003. Derivation of the 1.0-0.9 Ga ferropotassic A-type granites of southern Norway by extreme differentiation from basic magma: Precambrian Research, v. 124, p. 107-148.

Warner, J.D., 1989. Columbium-, rare earth element-, and thorium-bearing veins near Salmon Bay, southeastern Alaska: U. S. Bureau of Mines, Open-File Report 06-89, 15 p.

Warner, J.D., and Barker, J.C., 1989. Columbium and rare earth-bearing deposits at Bokan Mountain, Southeast Alaska. U. S. Bureau of Mines, Open-File Report 33-89, 196 p.

Warner, J.D., and Mardock, C.L., 1987. Rare earth element-, niobium-, thorium-, and uranium-bearing dikes at Bokan Mountain, southeast Alaska [abs.]: Geological Society of America Abstracts with Programs, v. 19, n. 6, p. 461.

Whalen, J.B., Currie, K.L., and Chappell, B.W., 1987. A-type granites: geochemical characteristics, discrimination and petrogenesis: Contributions to Mineralogy and Petrology, v. 95, p. 407-419.

Whalen J.B., Fyffe, L.R., Longstaffe, F.J., and Jenner, G.A., 1996. The position and nature of the Gander-Avalon boundary, southern New Brunswick, based on geochemical and isotopic data from granitoid rocks: Canadian Journal of Earth Sciences, v. 33, p. 129-139.

Winchester, J.A., and Floyd, P.A., 1977. Geochemical discrimination of different magma series and their differentiation products using immobile elements: Chemical Geology, v. 20, p. 325-343.

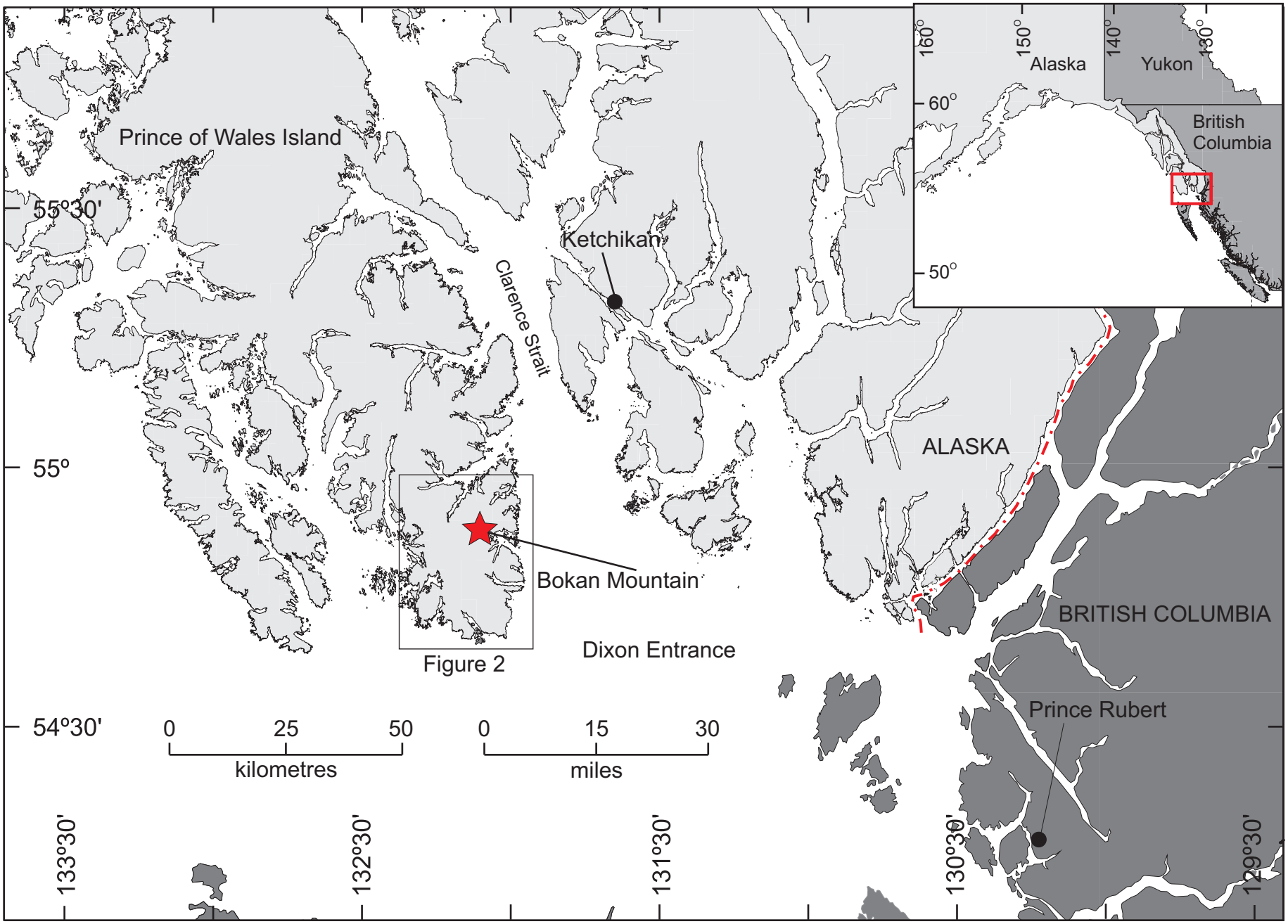

Figure 1. Map showing the location of Bokan Mountain. The solid box represents the geographic area covered by Figure 2 whereas the inset (upper right) shows the general location of the Figure 1 map in NW North America.

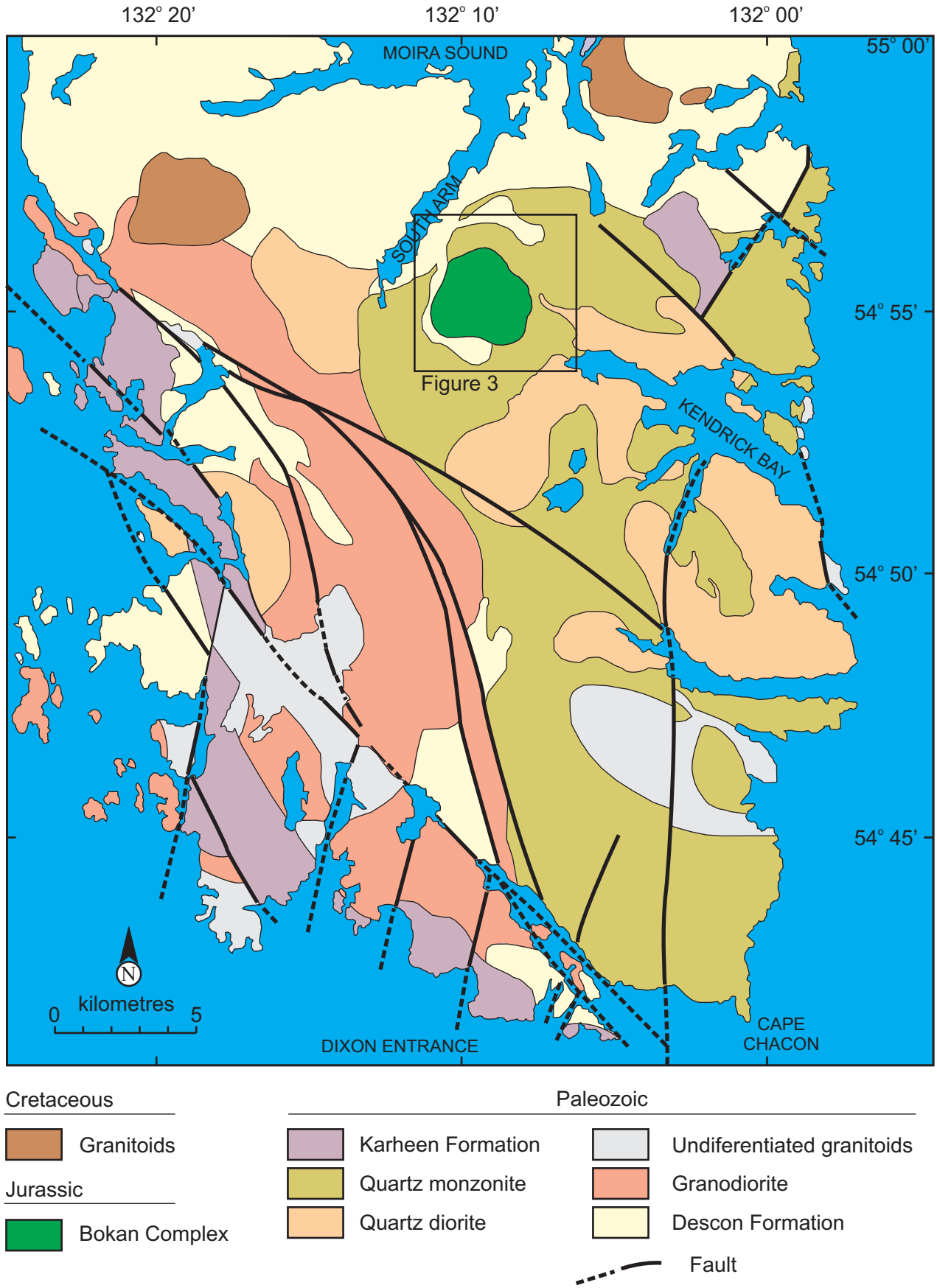

Figure 2. Geological sketch map of southern Prince of Wales Island. Modified from MacKevett (1963), Thompson et al. (1982), Warner and Barker (1989), Gehrels (1992), Gehrels and Saleeby (1987a), Brew et al. (1991) and Mass et al. (1995). The solid box represents the area covered by Figure 3.

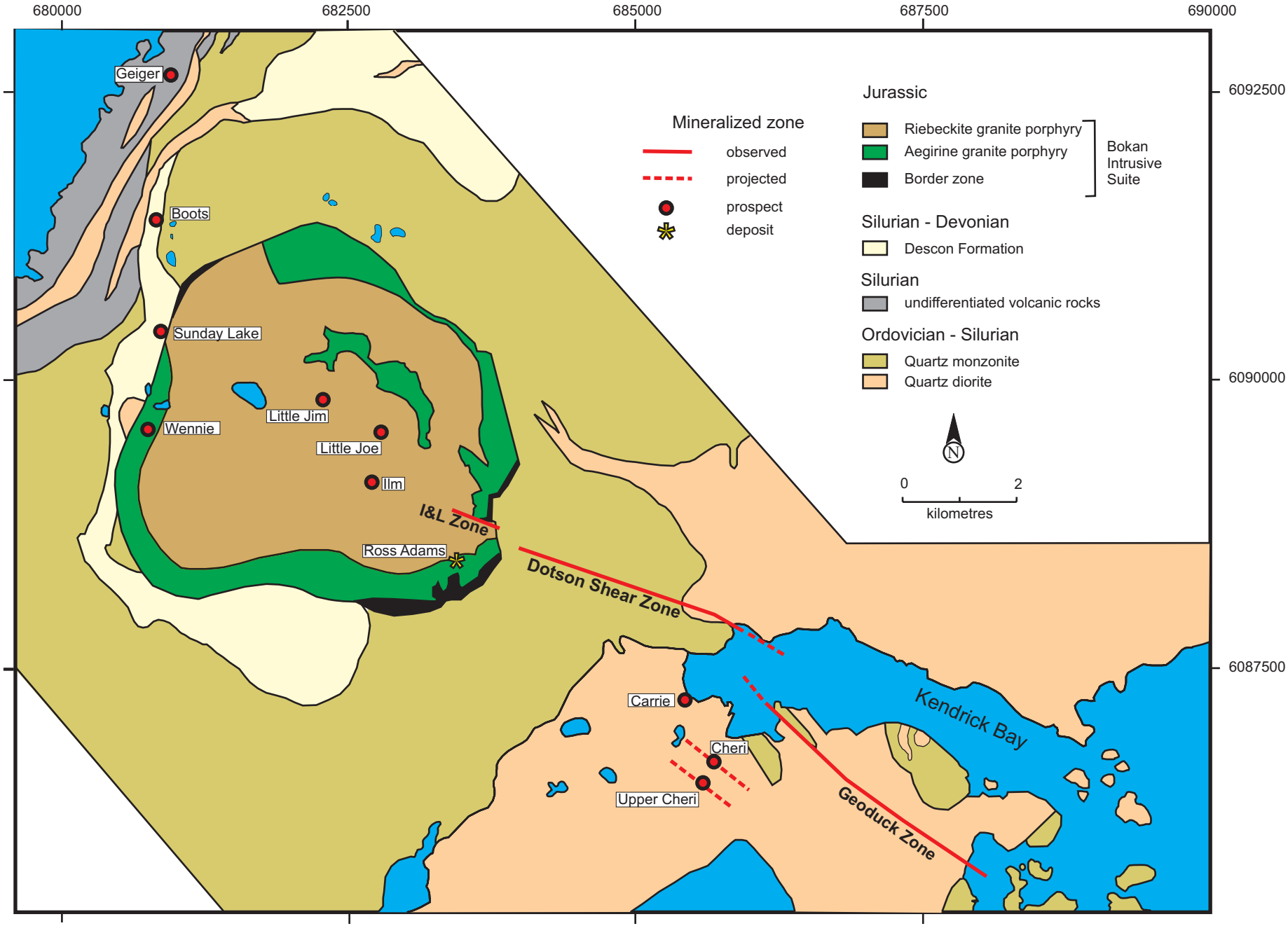

Figure 3. Geological sketch map of the Bokan complex area and the locations of the main mineralized zones and prospects. Modified after MacKevett (1963), Thompson et al. (1982), Gehrels (1992) and Keyser and McKenney (2007).

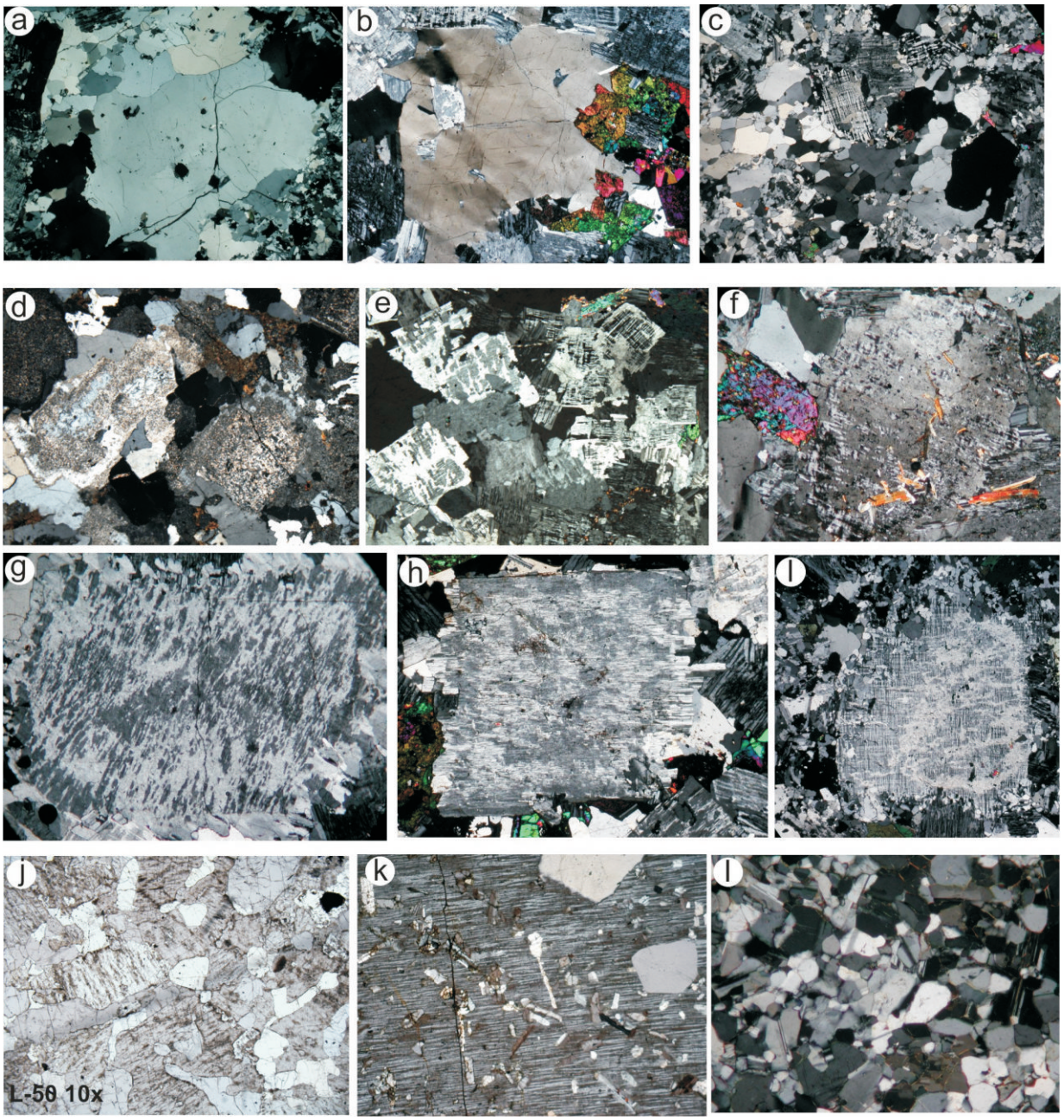

Figure 4. Photomicrographs of granitic rocks from the Bokan complex taken in crossed nicols, except for j (plane polarized light). (a, b) Typical hypidiomorphic granular texture of Bokan granite with coarse, mosaic-textured quartz in a quartz-two feldspar (plagioclase, microcline) matrix. Note the presence of aegirine in the right side of image b. (c) Anhedral, rod-shaped quartz grains intergrown with microcline-quartz matrix and two subhedral grains of amphibole. (d) Rare example of igneous texture in a granite sample with subhedral to euhedral plagioclase (An20) intergrown with quartz and with only minor alteration, in this case saussuritization of plagioclase. (e) Typical metasomatic texture in the Bokan granites with extensive development of secondary albite after earlier K-feldspar, now microcline. (f) Sodic (albite) alteration of the microcline with the preservation of the crystal outline. Aegirine is on the left side and the matrix is quartz rich. (g) Sodic (albite) alteration of K-feldspar. (h) Sodic (albite) alteration of the core of a K-feldspar with a rim of chessboard-type albite forming a pseudorapakivi texture. Note the presence of small, late-stage grains of aegirine in the matrix. (i) Veins of secondary albite invading the microcline with the initial development of chessboard albite on the margin. (j) Granophyric intergrowth of quartz and microcline perthite with anhedral to subhedral shapes of the quartz. (k) Part of a coarse (cm-size) grain of microcline perthite in a pegmatite with grains of euhedral albite laths and quartz. Note the well developed film to flame type perthite lamellae in the microcline. (l) Hypidiomorphic granular matrix of a dike rock sample showing a lack of alteration and preserved igneous textures. Scales (field of view - FOV): (a-e, g-i) FOV = 7 mm, (f) FOV = 3.5 mm, (j) FOV = 1.7 mm, (k) FOV = 3.5 mm, (l) FOV = 1.7 mm.

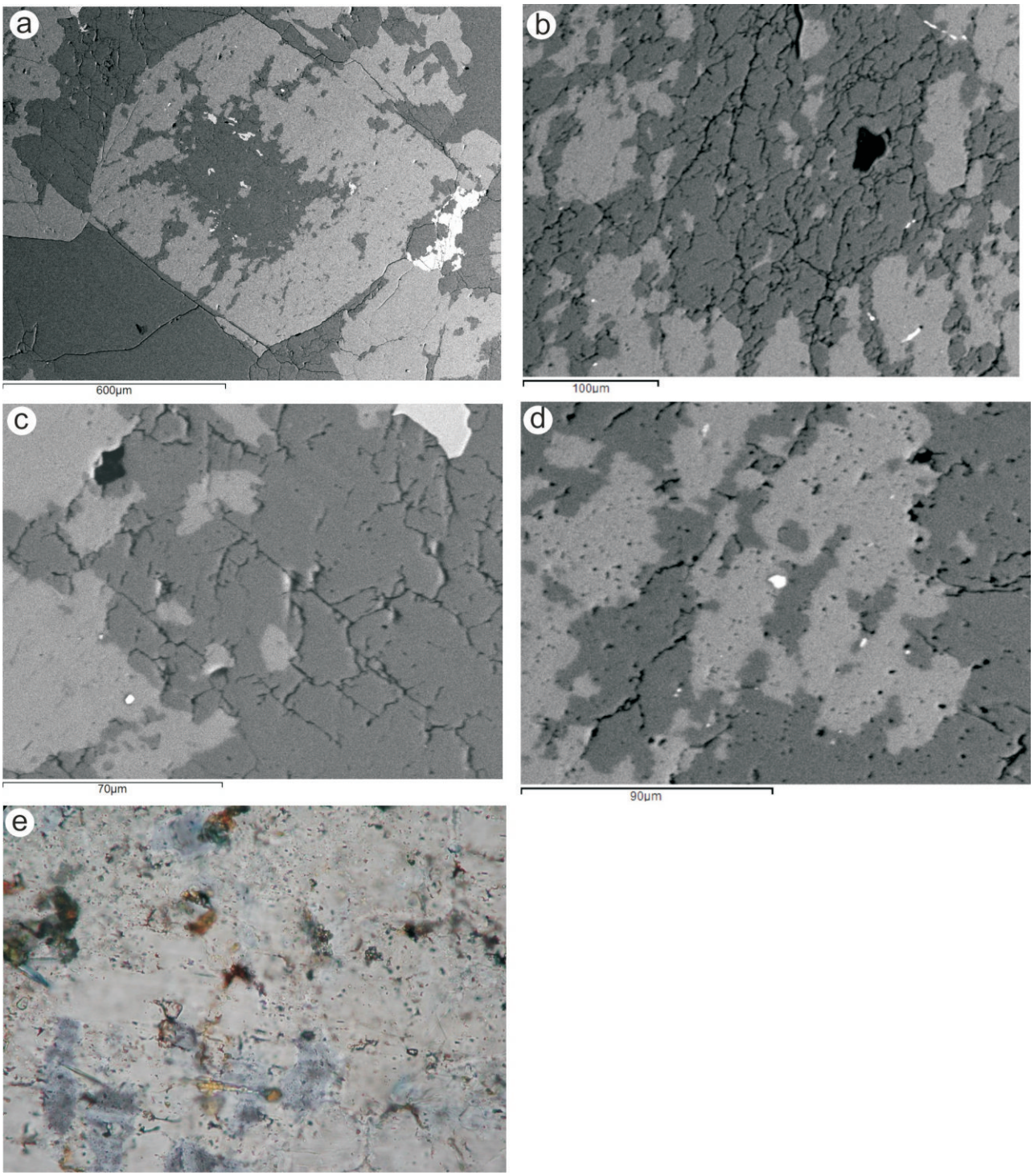

Figure 5. Alkali feldspars in granites of the Bokan complex taken as scanning electron microscope (SEM) images (a, b, c, d) and in transmitted light (e). (a) Euhedral grain of orthoclase being replaced by albite in the core and along radial fractures. (b, c) Extensively pitted and fractured albite that has replaced orthoclase. (d) Extensively pitted orthoclase and albite grains. (e) Pitted orthoclase grain with small fluid filled pits throughout, but mainly concentrated in the albite domains. Scale: (e) = FOV = 0.4 mm.

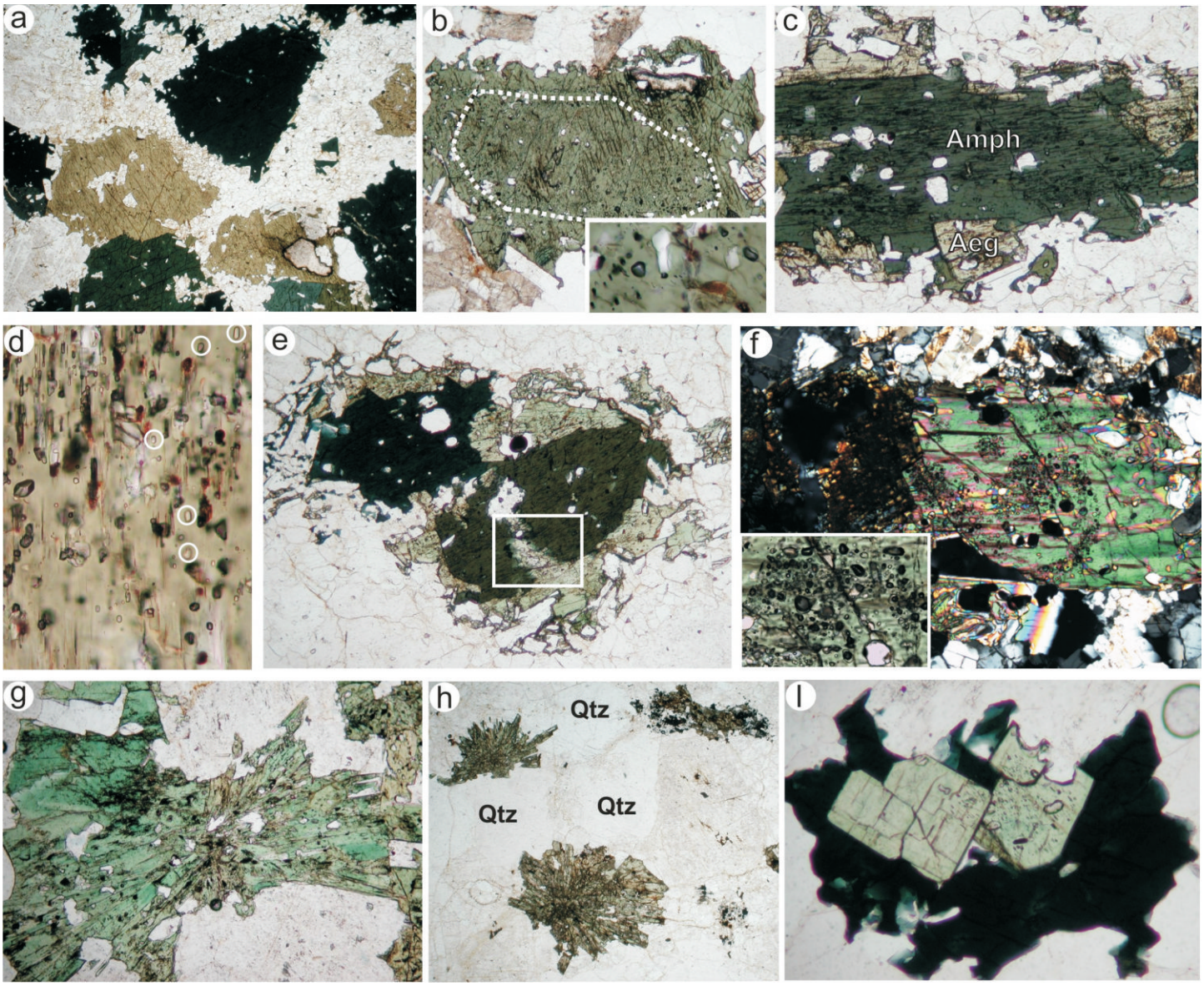

Figure 6. Photomicrographs of granitic rocks from the Bokan complex taken in plane polarized light except for f (crossed nicols). (a) Coarse subhedral amphibole grains set in a matrix of quartz and feldspar. Note the fritted edges to the amphibole grains that extend into the matrix. (b) Subhedral amphibole grain recording a two-stage growth history, as indicated by the dashed white line. Stage I is characterized by an enrichment in inclusions, including melt, fluid and mineral (see inset for detail), whereas stage II is an inclusion-free overgrowth. Again, note the fritted outline of the grain along its top. (c) A composite grain showing early, inclusion-rich amphibole (dark green; Amph) that is overgrown by inclusion-free aegirine (Aeg). Note the sharp contacts between the two phases. (d) Close up of the interior of an amphibole grain (stage I) containing low-density fluid inclusions (dark phases), possible melt inclusions and apatite grains (clear phases, some circled). Note the preferential alignment of all the inclusion types. (e) Subhedral arfvedsonitic amphibole overgrown by aegirine with ragged terminations extending into the matrix. Also note that the pyroxene partly replaces the amphibole, as outlined by the white box. (f) Inclusion-rich (low-density fluid, melt) aegirine with clear overgrowth similar to that seen in amphibole. Inset box is an enlarged area of the inclusion-rich domain. (g) Late-stage, intergranular aegirine with a bowtie-like texture between coarser quartz and feldspar grains. Note the variable development of pleochroism and alteration along cleavage directions. (h) Radial-textured aegirine clots disseminated within a quartz-feldspar matrix and surrounding subhedral quartz (Qtz). Also note the intergrowth of amphibole-pyroxene with superimposed alteration (quartz-hematite) in the upper right of image. (i) Euhedral aegirine overgrown by arfvedsonitic amphibole. The alignment (NW-SE) of secondary fluid inclusions in the pyroxene may relate to the overgrowth by the amphibole. Scales: (a) FOV = 7 mm, (b) FOV = 3.5 mm, (c) FOV = 3.5 mm, (d) FOV = 0.4 mm (long axis), (e) FOV = 3.5 mm, (f) FOV = 1.7 mm, (g) FOV = 3.5 mm, (h) FOV = 3.5 mm, (i) FOV = 1.7 mm.

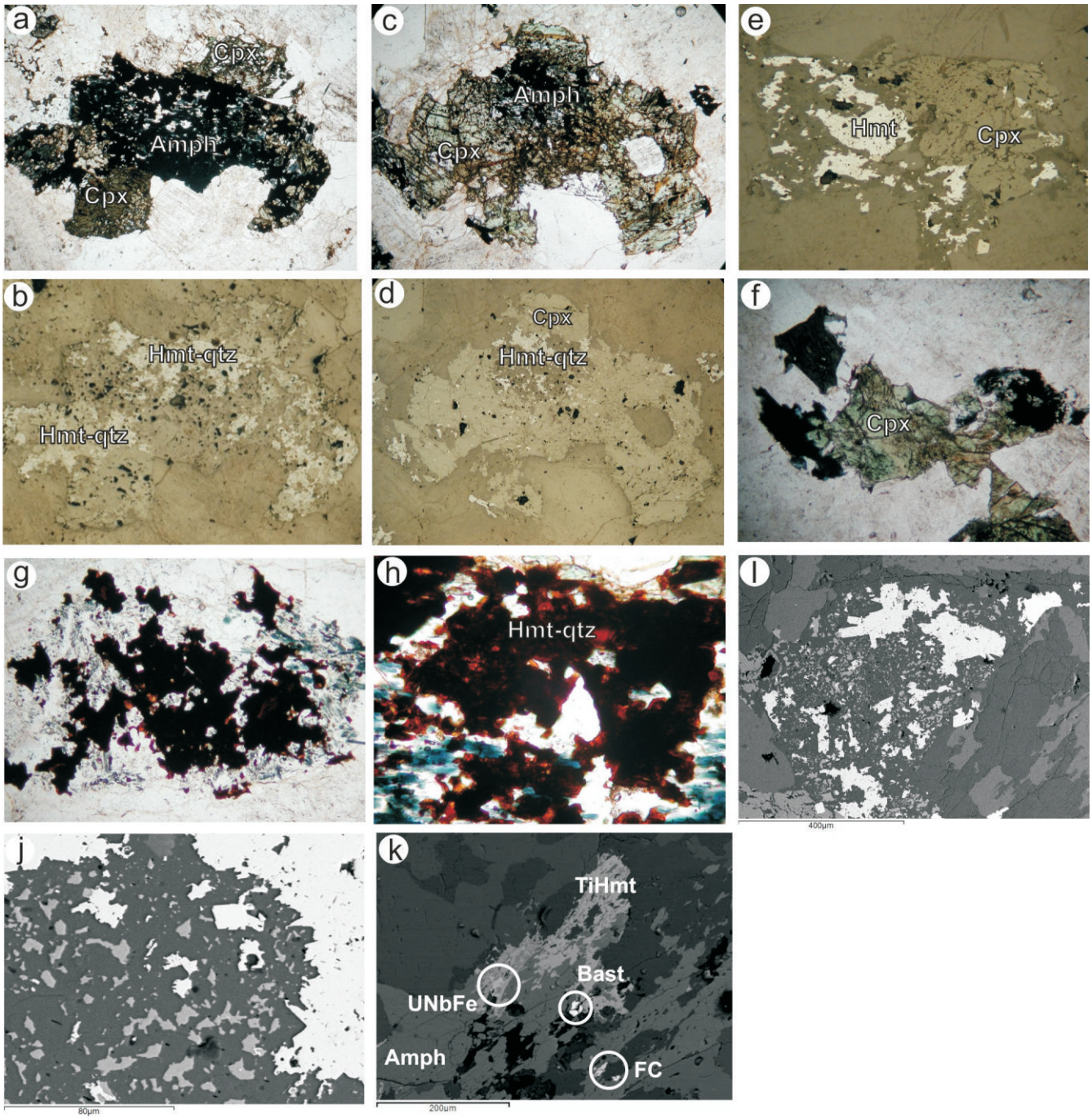

Figure 7. Photomicrographs of altered and mineralized amphibole in granitic rocks in both plane polarized light (PPL; a, c, f, g, h, i) and reflected light (RL; b, d, e); note that images a-b and c-d are paired photos. In these images the general term amphibole is used for a range of amphibole and pyroxene types present unless mentioned otherwise (e.g., arfvedsonite, reibeckite). (a, b) Subhedral outline of intergrown amphibole (Amph) and clinopyroxene (Cpx). The dark areas in the PPL image are mainly iron oxide (Hmt), whereas the low reflectance areas in the RL image are amphibole and pyroxene. Note that it is mainly the amphibole area which is altered to hematite. (c, d) As in the previous image, but in this case the sample is clinopyroxene dominant with a small core area of former amphibole. Again, note that it is the amphibole which is altered. (e) Clinopyroxene overgrown by amphibole which is now altered to a hematite-quartz mixture. (f) Subhedral clinopyroxene with amphibole overgrowths which are now altered to a hematite-quartz assemblage. Note the lack of apparent alteration or replacement of the clinopyroxene compared to amphibole. (g, h) Images of primary amphibole pseudomorphically altered to an assemblage of quartz-hematite and a reibeckite-arfvedsonite intergrowth. Note how the outline of the original amphibole grain is preserved in image g. (i, j) SEM images of altered amphibole showing coarse Fe-Ti oxides with small residual grains of resorbed amphibole disseminated in quartz. (k) SEM image of altered amphibole with intergrowth titaniferous (6 wt. % Ti) hematite and disseminated grains of a U-Nb-Pb hematite (UNbFe) phase, ferro-columbite (FC) and bastnaesite (Bast). Scales: (a-g) FOV = 3.5 mm, (h) FOV = 1.7 mm.

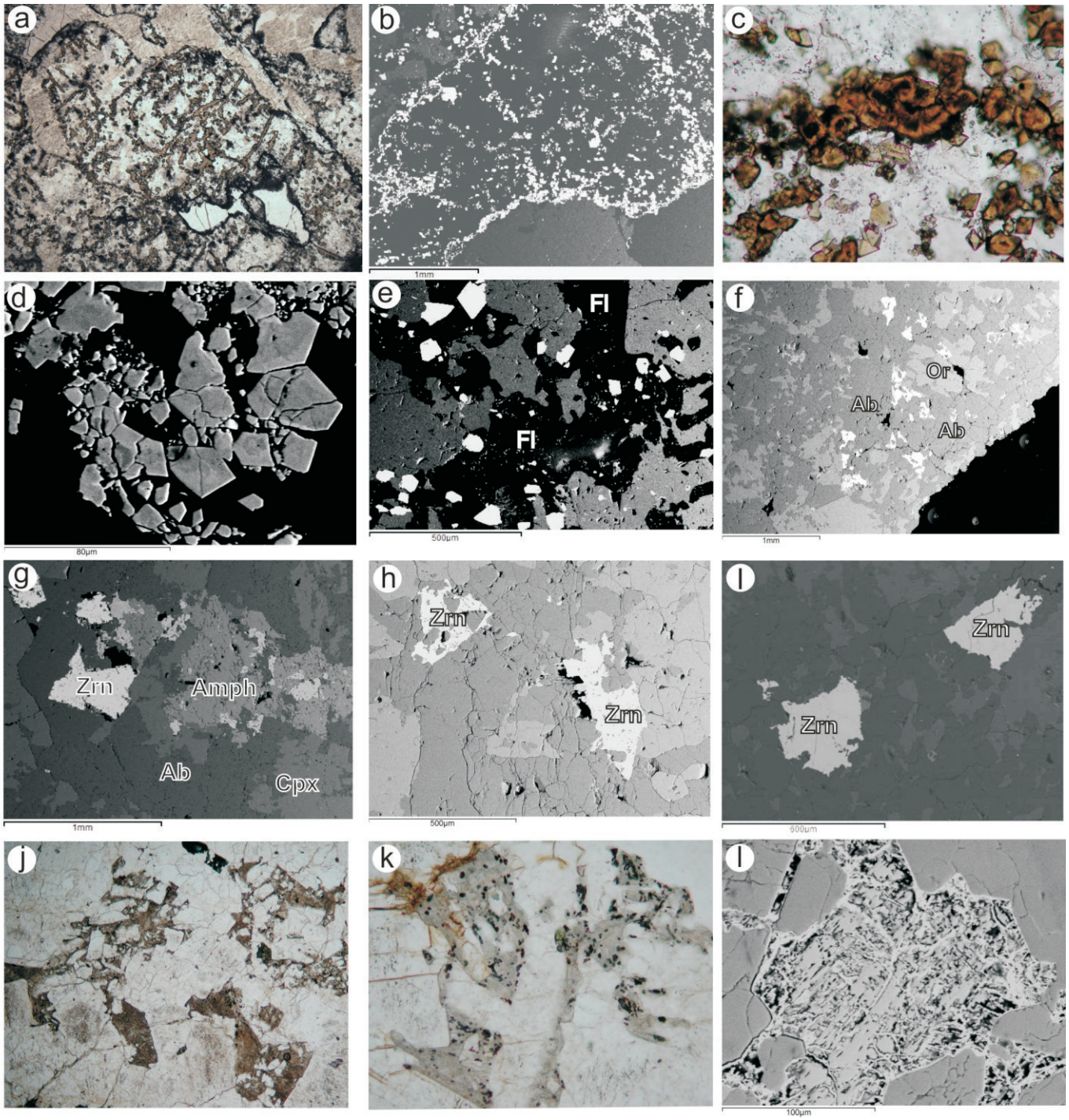

Figure 8. Examples of zircon mineralization from the Bokan complex seen in transmitted light (a, c, j, k) and SEM ((b, d, e, f, g, h, i, l). (a, b) Vein-like network of zircon in a pegmatite sample. (c, d) Close up images of the zircon euhedra from the previous images (a,b) showing that the core areas are texturally different and are Fe rich (1-2 wt. %). (e) Disseminated zircon anhedra in albite-rich granite. (e) Zircon euhedra in a fluorite-rich (Fl) part of a pegmatite sample. (f) Disseminated zircon anhedra in an albite-rich area of granite. (g) Large subhedral zircon (Zrn) grains in albite (Ab)-rich granite with anhedral amphibole (Amph) with clinopyroxene (Cpx) inclusions. (h) Anhedral to subhedral zircon as inclusions in amphibole. (i) Anhedral zircon with fritted edges in an albite-rich granite. (j, k) Zirconium-rich domains (zircon, elpidite) in intergranular domains of granite. (l) Close up image of a zirconium-rich domain showing the mixture of phases. The dull areas are an elpidite-like phase. Scales: (a) FOV = 1.7 mm, (c) FOV = 0.4 mm, (j) FOV = 1.7 mm, (k) FOV = 1.7 mm.

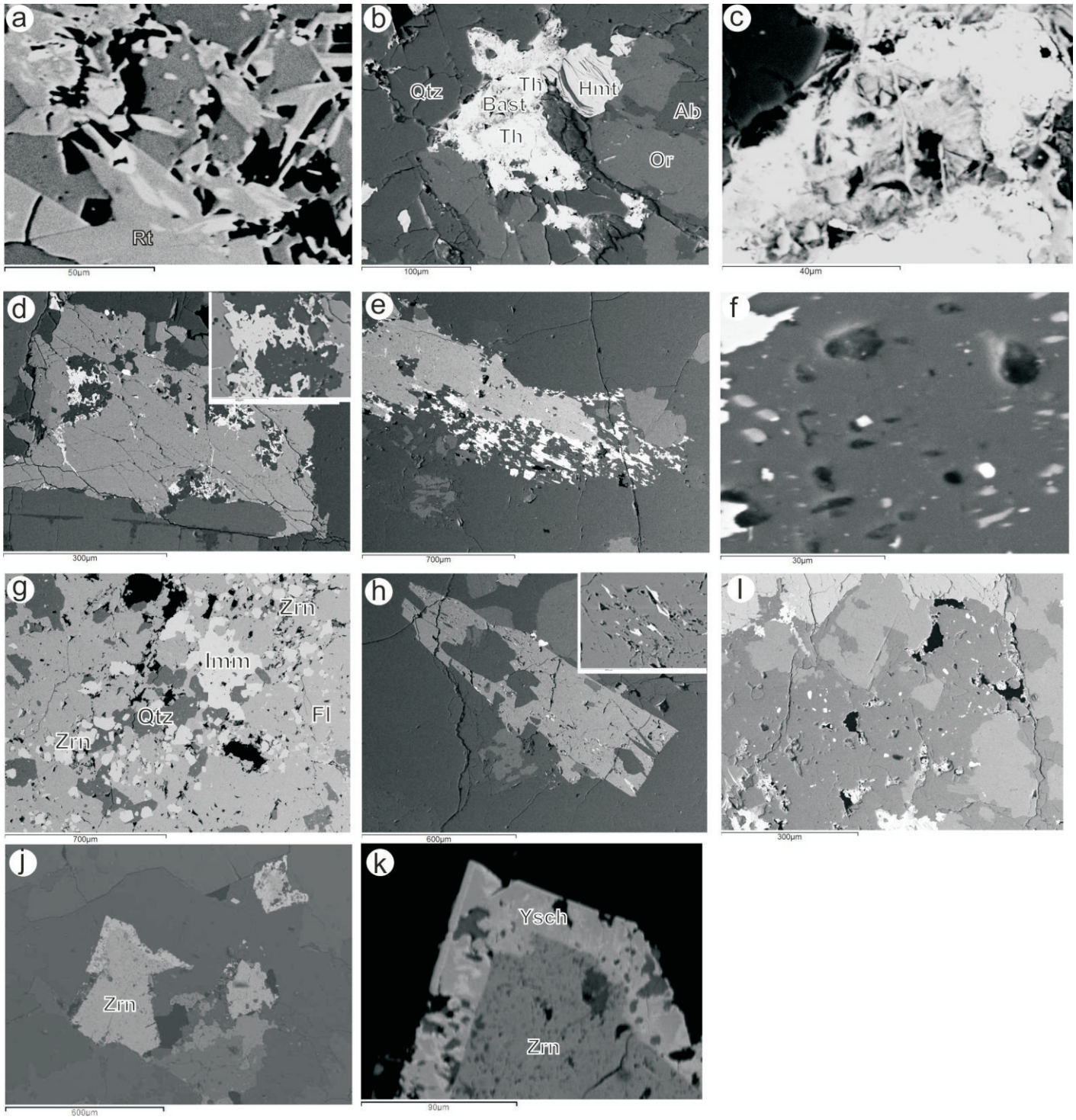

Figure 9. SEM images of mineralized phases in the Bokan complex. (a) Pegmatite sample with rutile phases enriched in Nb and Sn (bright phases in image). (b, c) Clot of bastnaesite (Bast) replaced by a Y-thorite (Th) phase in quartz (Qtz), albite (Ab), orthoclase (Or) domain. Note that image c is an enlargement of image b. (d) Quartz-hematite clot in amphibole from granite that contains zircon and REE phases, as shown in the inset. (e, f) Quartz-hematite replacement of amphibole in granite with bastnaesite (Bast) grains disseminated in the quartz areas. The grey needles in image (f) are arfvedsonitic amphibole. (g) Coarse iimoriite (Imm) with quartz-zircon (Zrn) and fluorite (Fl) in pegmatite. (h) Granite sample with a pitted clinopyroxene grain with a U-Nb-Pb-Zn rich ilmenite phase. (i) Y-synchysite phases disseminated in clinopyroxene hosted by granite. (j, k) Zircon in granite which is rimmed by a Y-synchysite (Ysch) phase that is intergrown by a Fe-Ti phase (bright irregular phases).

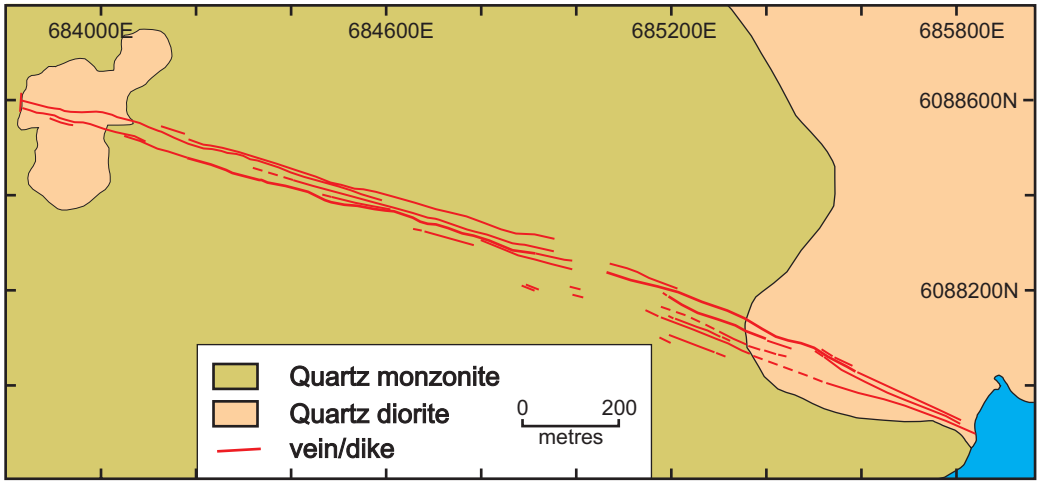

Figure 10. Geological sketch map showing the Dotson shear zone with its multitude of Jurassic vein-dikes crosscutting the Paleozoic granitoids (modified after Ucore Rare Metals Ltd.).

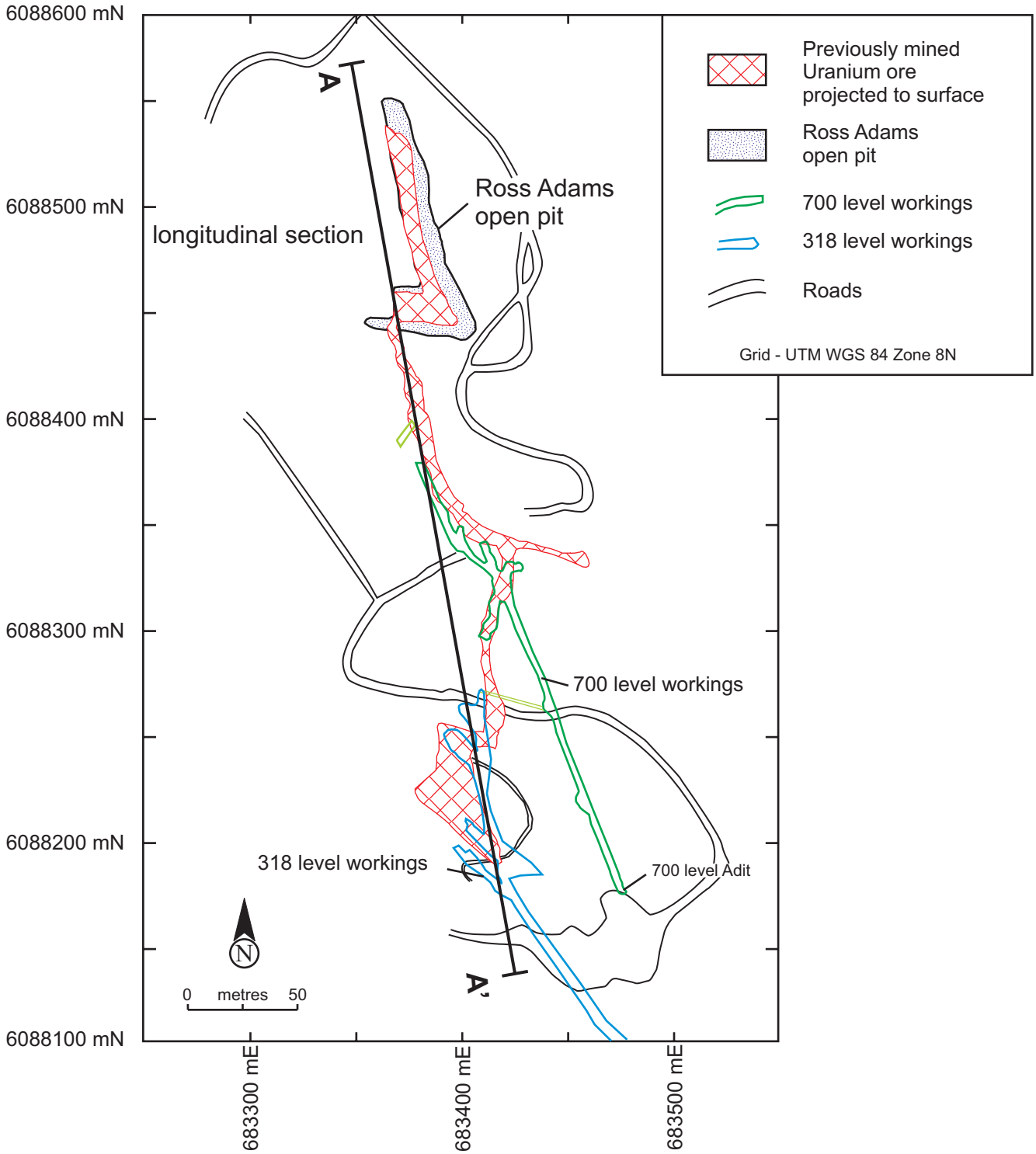

Figure 11. Sketch map of the Ross-Adams mine area showing the open pit and underground workings. Modified after Keyser and McKenney (2007). Line (A-A') shows the orientation of the cross-section (Fig. 12).

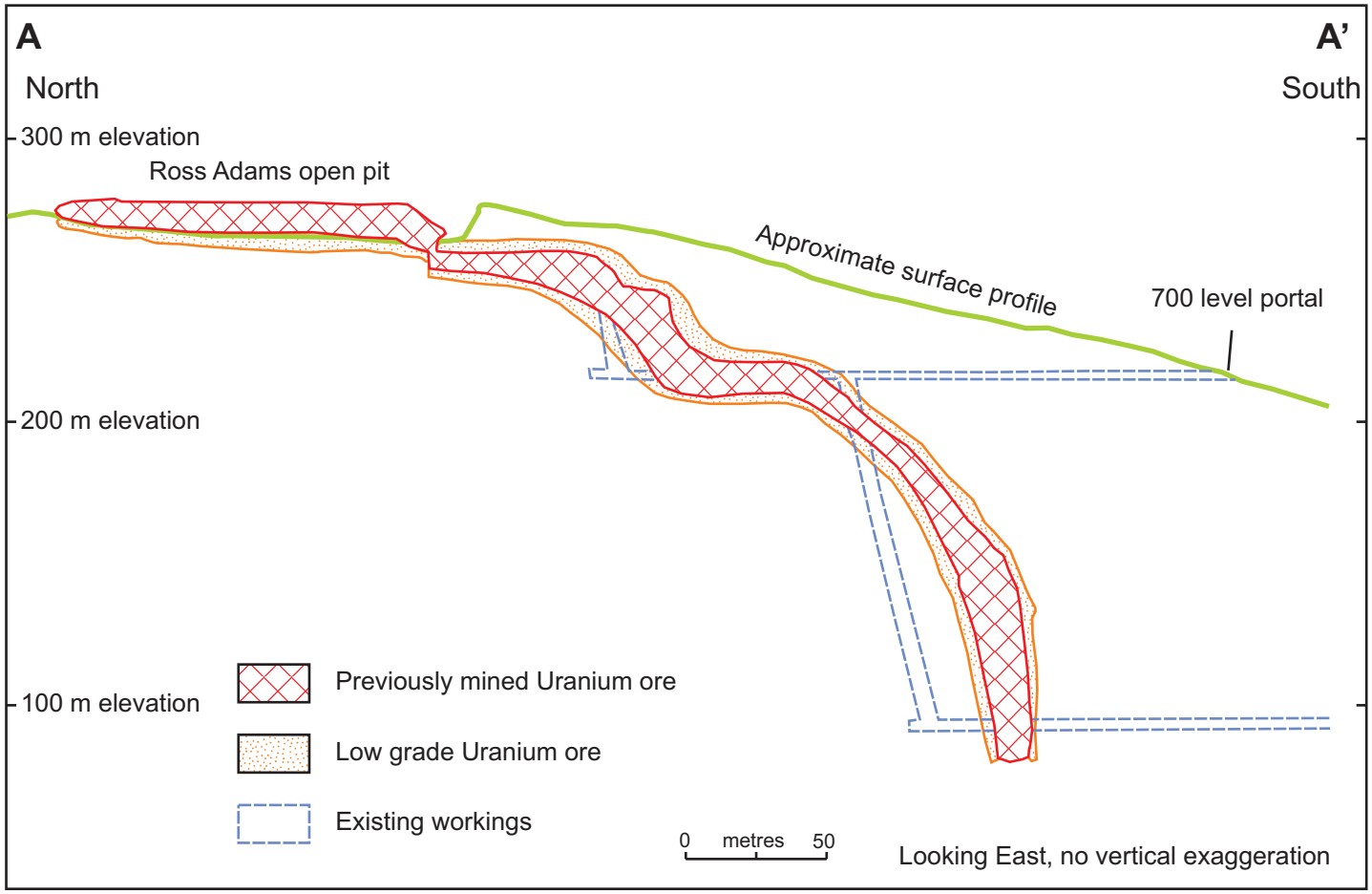

Figure 12. Cross-section of the main ore pipe of the Ross-Adams deposit showing the previously mined high grade ore (>0.5 wt. % U_3O_8) , the low grade ore envelope (< 0.5 wt. % U_3O_8) and mine workings (see Figure 11 for the location of cross-section). Modified after Keyser and McKenney (2007).

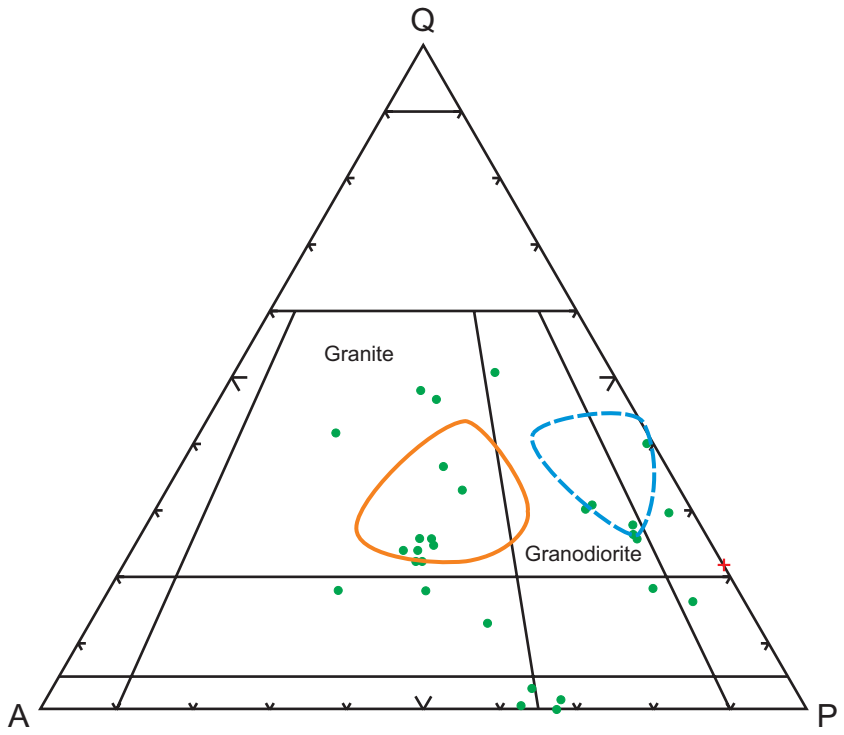

Figure 13. QAP (quartz-alkali feldspar-plagioclase) diagram of Le Maitre et al. (1989) showing the normative composition of the granitic rocks of the Bokan complex and related dikes and Paleozoic granites. There is agreement between modal and normative composition of the granites. Solid red line field: unaltered granitic rocks of the Bokan complex and its dikes; dashed blue line field: Paleozoic granitoids; the Ross-Adams mine area: green dots - altered granitic rocks; red pluses - mineralized granitic rocks.

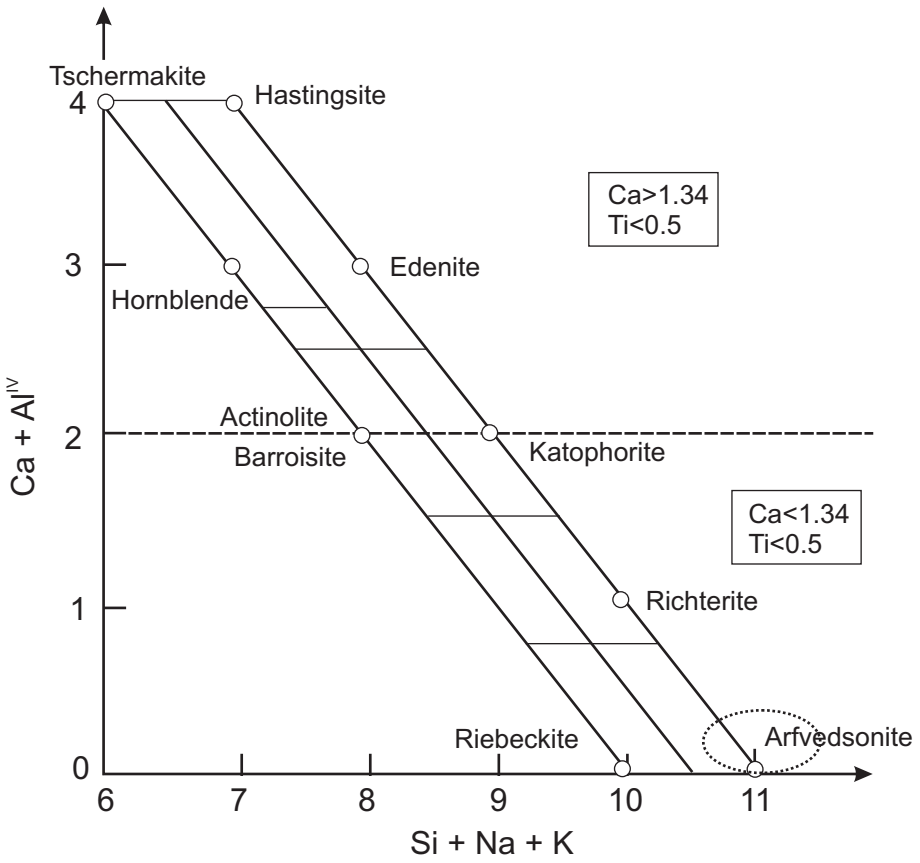

Figure 14. Amphibole classification graph. Si+Na+K versus Ca+Al^{iv}(cations) diagram showing the composition of representative amphiboles from the Bokan peralkaline granites and related dikes (Table 1b). Most of the analyzed amphiboles (dotted line field) plot near end-member arfvedsonite.

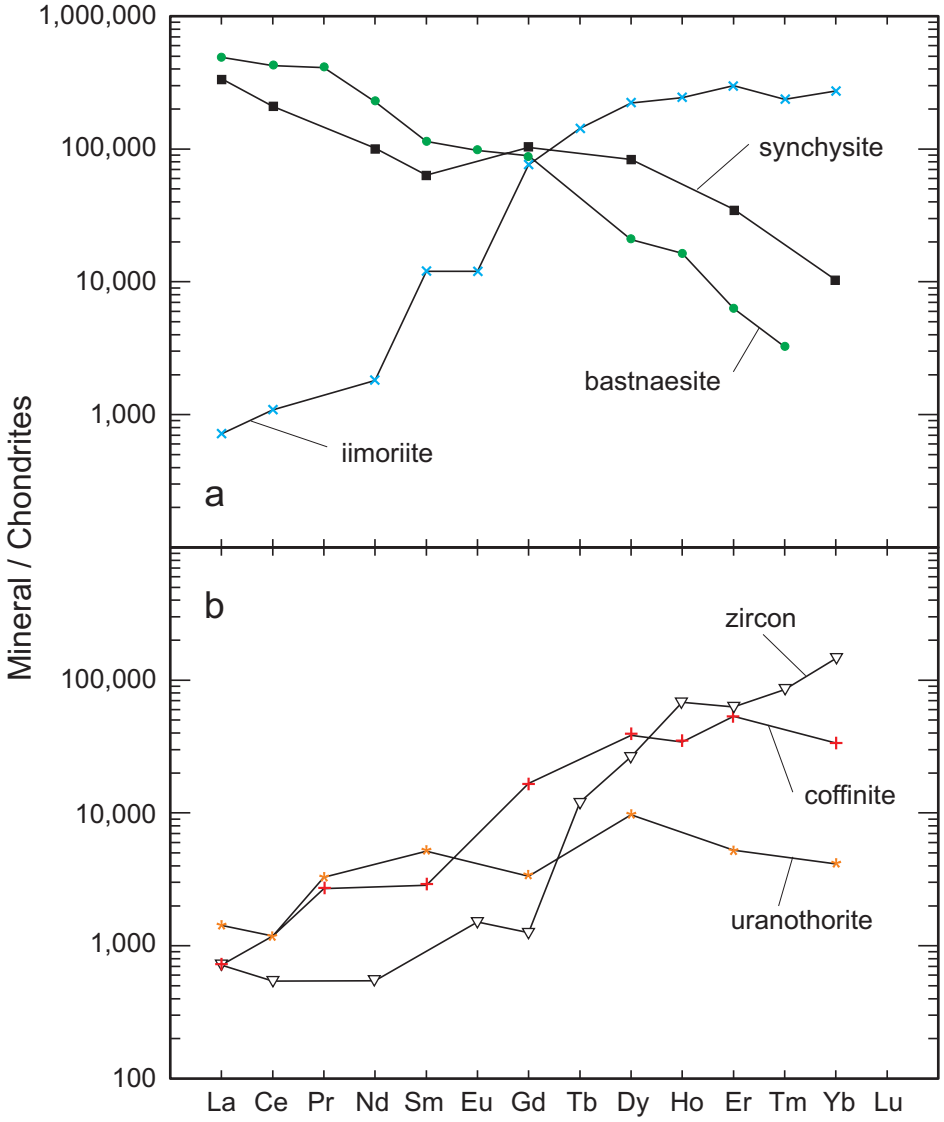

Figure 15. Chondrite-normalized REE abundances of (a) bastnaesite, synchysite and iimoriite and (b) uranothorite, coffinite and zircon from the felsic dikes of the I&L Zone. Plotted data are averages of microprobe analyses of minerals (Table 1d) separated during a processing of bulk samples for metallurgical investigations (archives of Ucore Rare Metals; microprobe analyses done at McGill University, Montreal, Quebec).

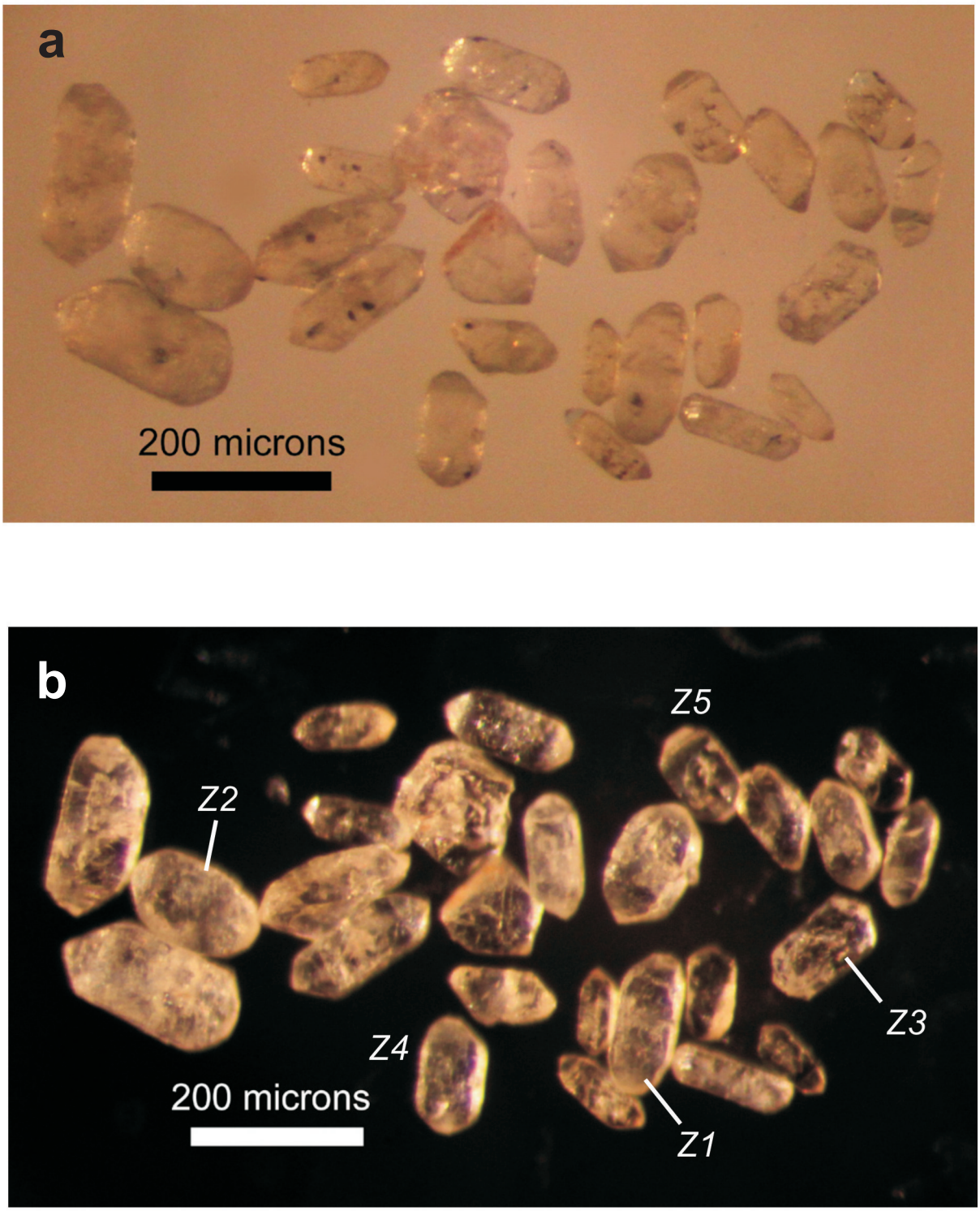

Figure 16. Photos of the retrieved zircons from the Bokan peralkaline arfvedsonite granite sample for U-Pb age dating analyses (sample G245). (a) Zircon grains selected for annealing and leaching. Note the presence of numerous opaque inclusions. (b) Labels identify single grains chosen for analysis.

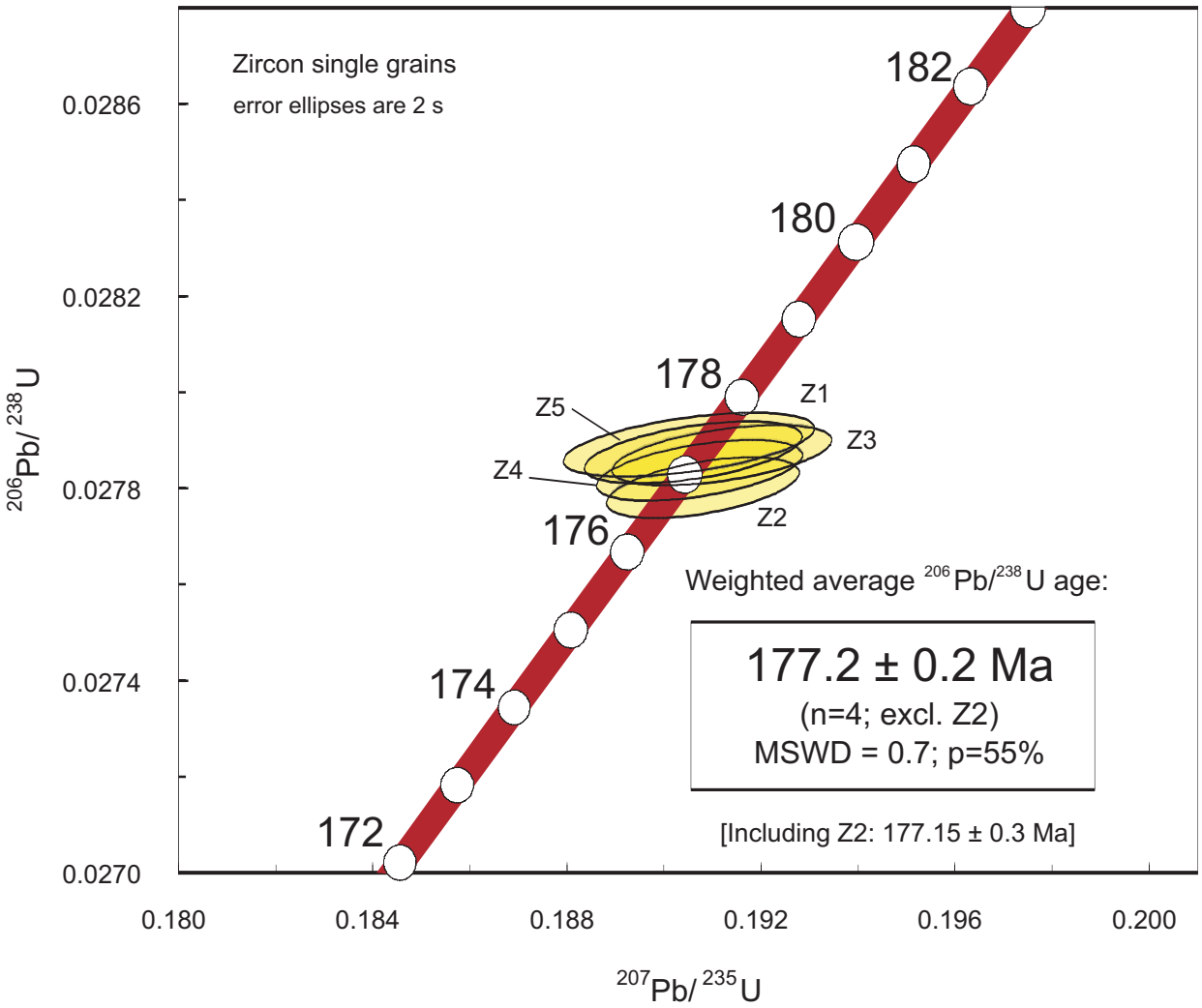

Figure 17. Concordia plot of the obtained U-Pb age dating results for zircons from the Bokan peralkaline arfvedsonite granite (G245 - core of the complex).

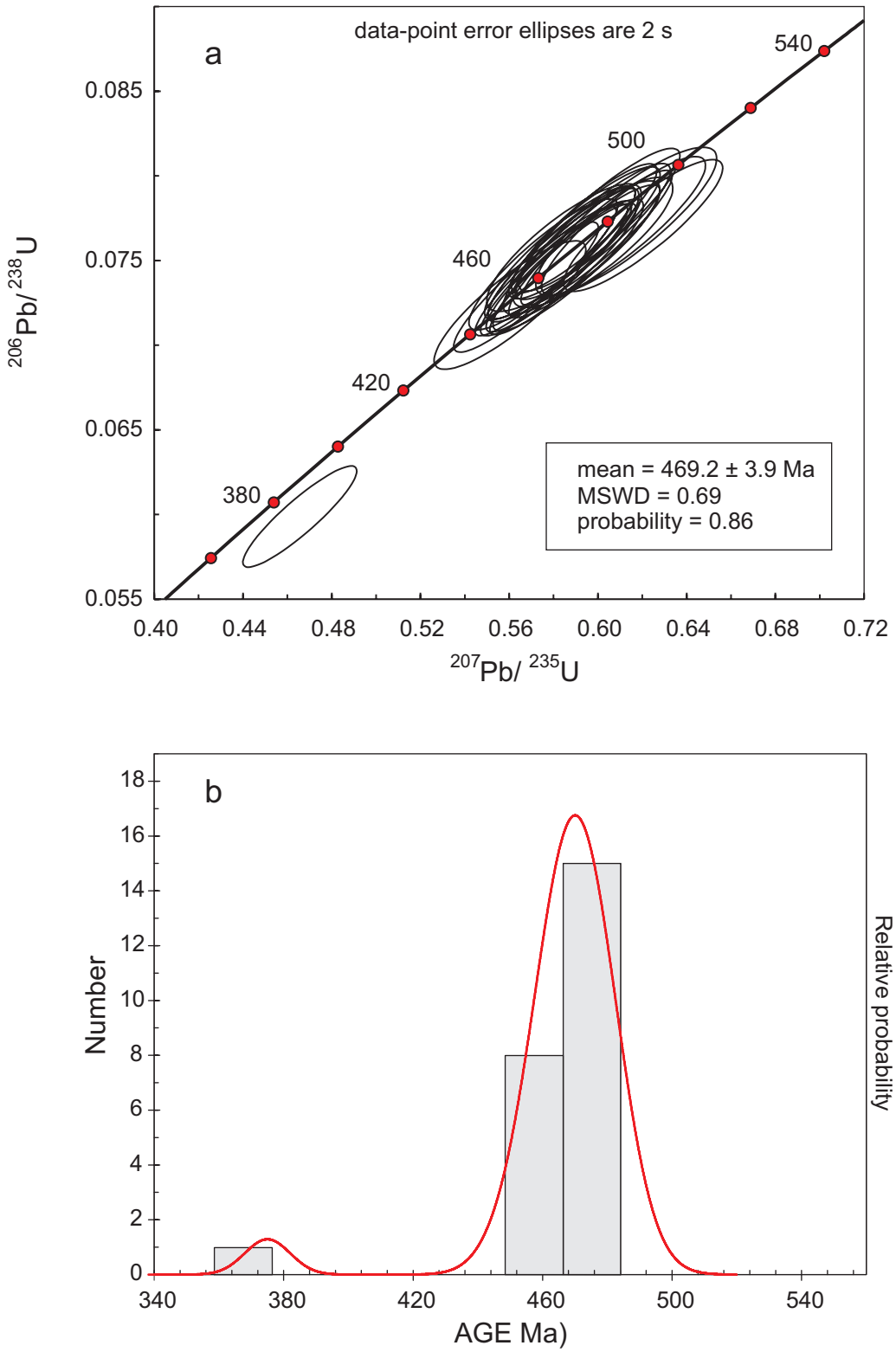

Figure 18. Results of LA-ICP-MS zircon dating of Paleozoic quartz monzonite (sample H835). (a) Concordia plot showing error ellipses (2 sigma) and (b) frequency distribution of U-Pb zircon ages.

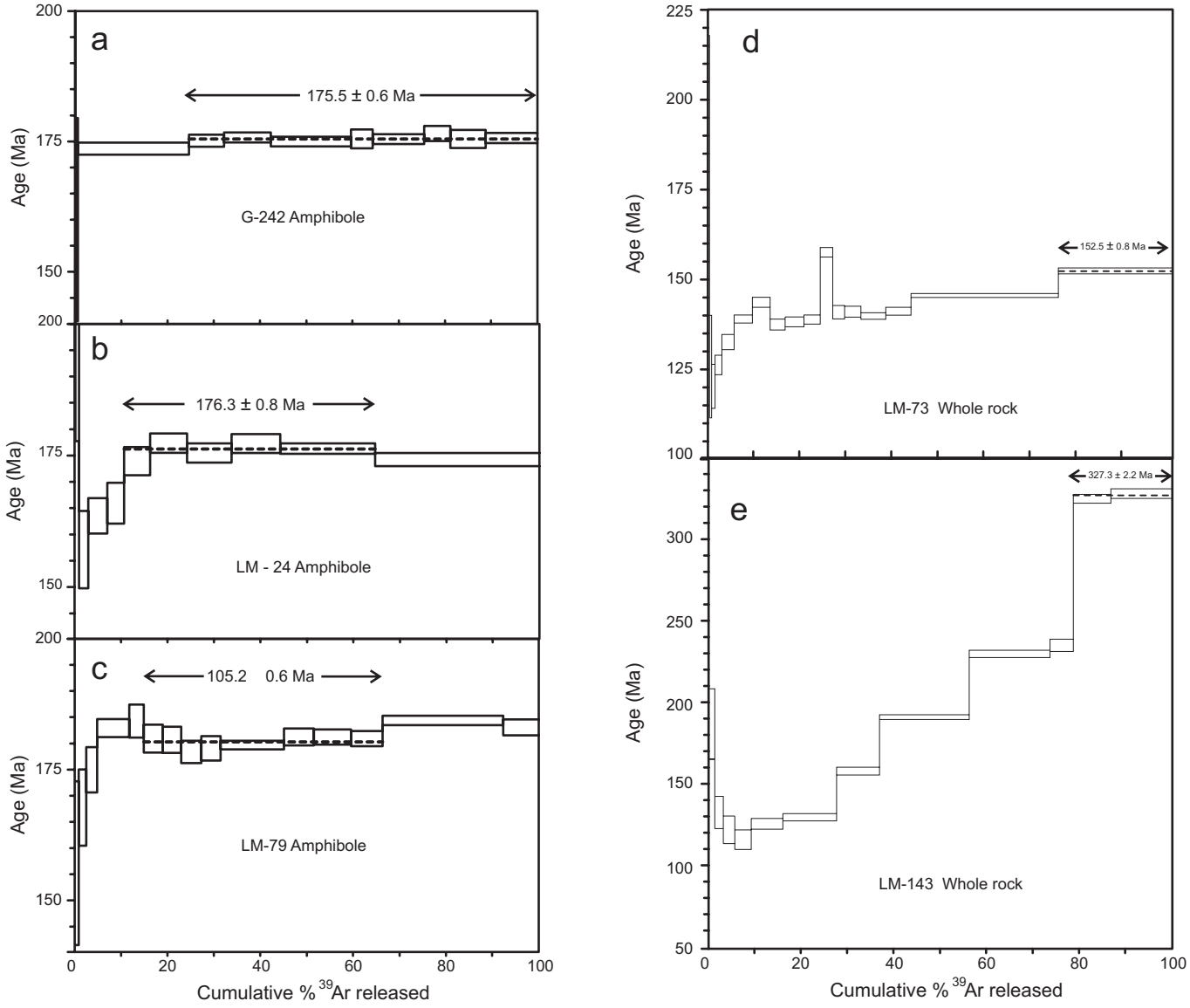

Figure 19. $^{40}Ar/^{39}Ar$ spectra from the Bokan complex area (a) amphibole (arfvedsonite) from peralkaline granite (G242; core of the intrusion); (b) amphibole (arfvedsonite) from granitic dike (LM24) at the Ross-Adams open pit; (c) amphibole from lamprophyric dike, Dotson Zone (LM79); (d) lamprophyric dike (LM73) cutting the I&L Zone. (e) dioritic dike (LM143), Geoduck Zone.

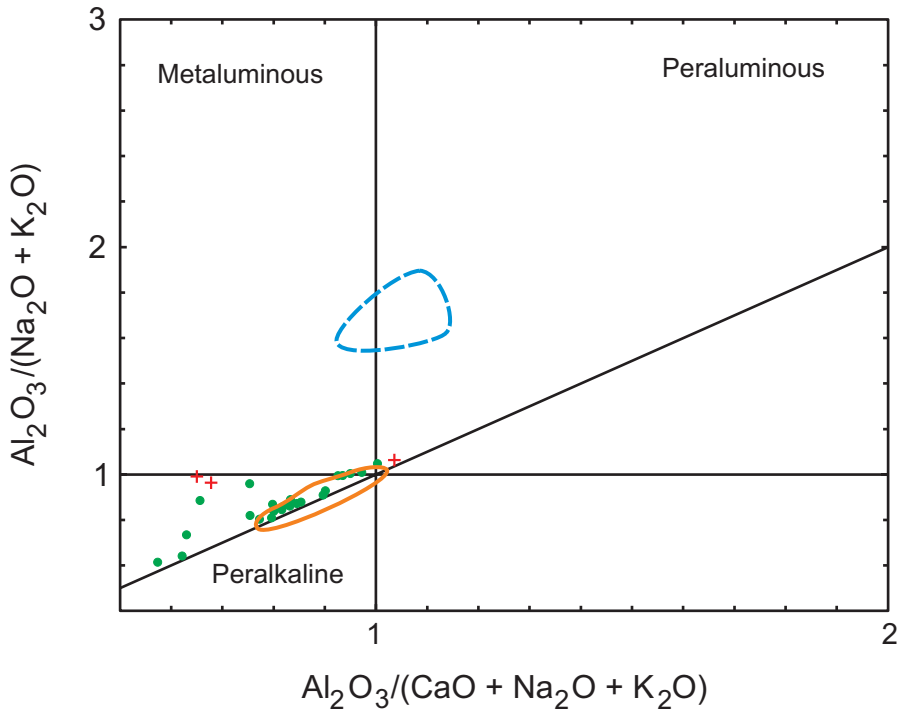

Figure 20. Molar $Al_2O_3/(Na_2O+K_2O)$ versus $Al_2O_3/(CaO+Na_2O+K_2O)$ plot of Shand (1951) discriminating metaluminous, peraluminous and peralkaline compositions for granitic rocks of the Bokan complex, related dikes and host Paleozoic granitoids. Solid red line field: unaltered granitic rocks of the Bokan complex and its dikes; dashed blue line field: Paleozoic granitoids; the Ross-Adams mine area: green dots - altered granitic rocks and red pluses - mineralized granitic rocks.

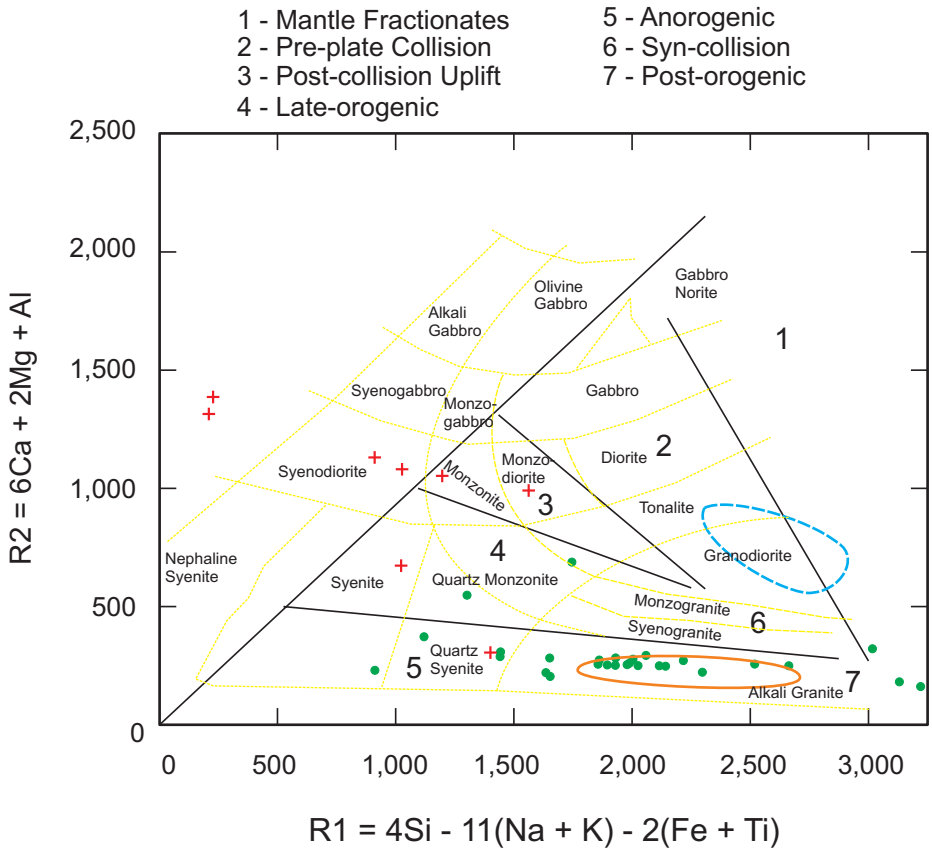

Figure 21. Multicationic classification plot of de la Roche et al. (1980) for plutonic rocks. This binary R1-R2 diagram shows the compositional fields of de la Roche et al. (1980) as well as tectonic discrimination fields (Batchelor and Bowden, 1985). R1= 4Si-11[Na+K]-2[Fe+Ti]; R2 = 6Ca+ 2Mg+Al. Solid red line field: unaltered granitic rocks of the Bokan complex and its dikes; dashed blue line field: Paleozoic granitoids; the Ross-Adams mine area: green dots - altered granitic rocks and red pluses - mineralized granitic rocks. The fresh rocks of the Bokan complex and associated dikes plot into the field of alkali granites (anorogenic or post-orogenic).

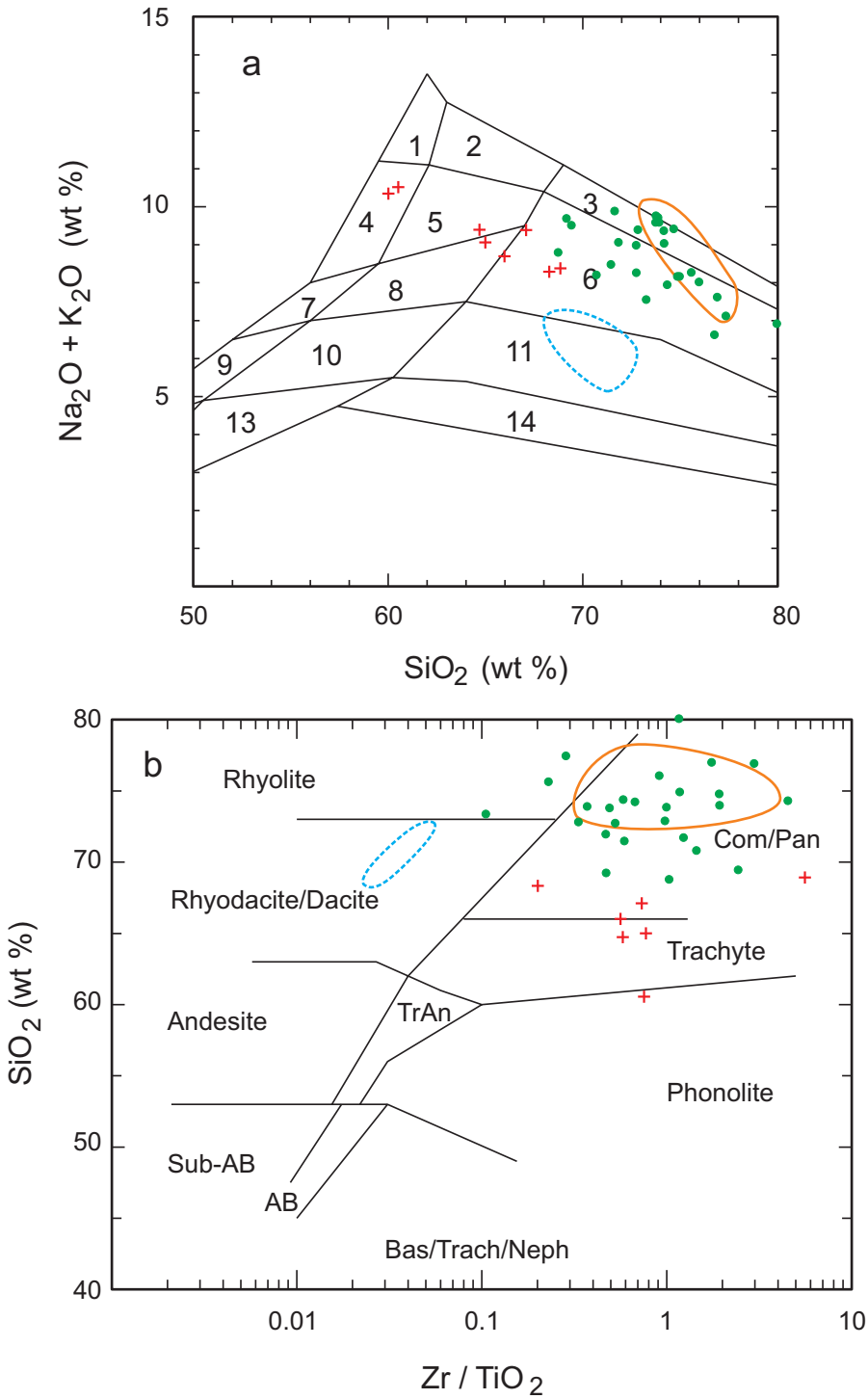

Figure 22. Classification diagrams for the rocks of the Bokan complex and its environs (a) (Na_2O+K_2O) versus SiO_2 (wt. %) diagram proposed by Middlemost (1995); fields: 1-Alkali feldspar syenite; 2-Alkali feldspar quartz syenite; 3-Alkali feldspar granite; 4-Syenite; 5-Quartz syenite; 6-Granite; 7-Monzonite; 8-Quartz monzonite; 9 Monzodiorite; 10-Quartz monzodiorite; 11-Granodiorite; 12-Diorite & gabbro; 13- Quartz diorite; 14-Tonalite and (b) Zr/TiO_2 versus SiO_2 (wt. %) diagram (after Winchester and Floyd, 1977) for the classification of volcanic rocks using incompatible element ratios. Sub-AB-subalkaline basalt; AB-alkali basalt; Bas-basanite; Trach-trachyte; Neph-nephelinite; TrAn-trachyandesite; Com-comendite; Pan-pantellerite. Solid red line field: unaltered granitic rocks of the Bokan complex; dashed blue line field: Paleozoic granitoids; the Ross-Adams mine area: green dots - altered granitic rocks and red pluses - mineralized granitic rocks. Graph (b) shows that the Bokan granites plot into the fields of alkaline volcanic rocks, thus reflecting the alkaline/peralkaline nature of the rocks.

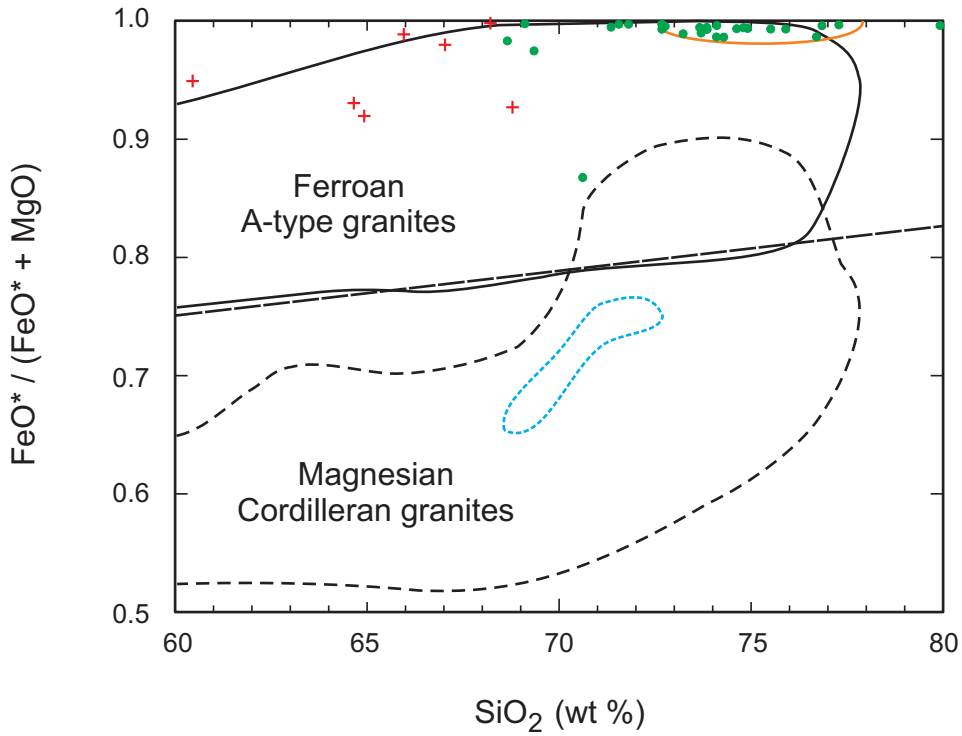

Figure 23. SiO_2 (wt.%) versus FeO*/(FeO*+MgO) diagram for the Bokan granites. Fields for ferroan (A-type) and magnesian (Cordilleran) granites are after Frost et al. (2001). Solid red line field: unaltered granitic rocks of the Bokan complex; dashed blue line field: Paleozoic granitoids; the Ross-Adams mine area: green dots - altered granitic rocks and red pluses - mineralized granitic rocks. The Bokan granites plot into the ferroan field consistent with their A-type characteristics.

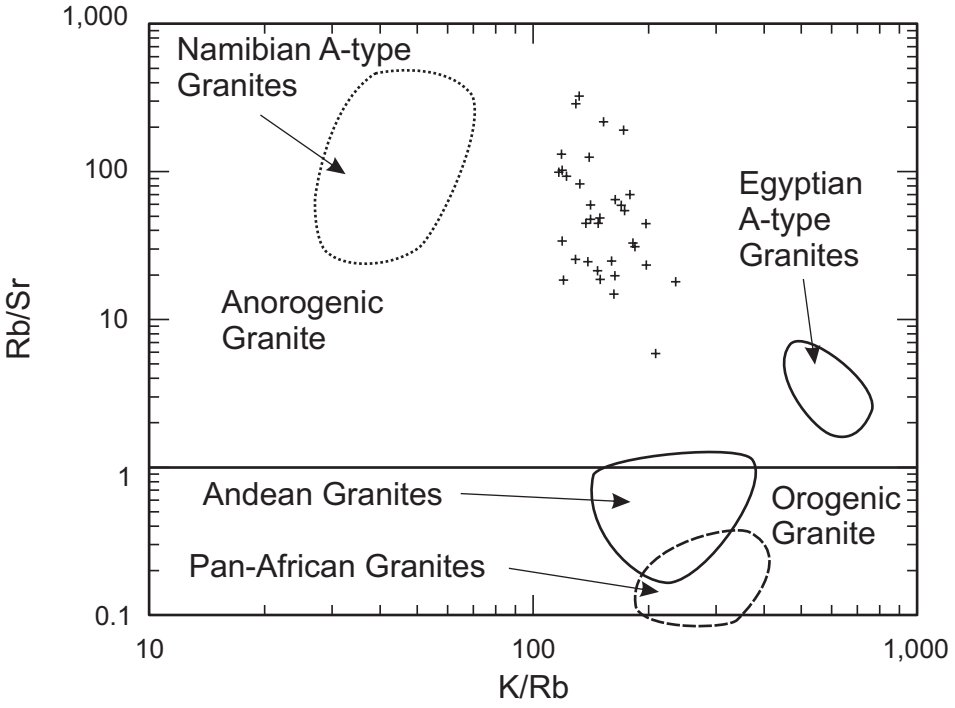

Figure 24. Rb/Sr versus K/Rb diagram showing that the Bokan peralkaline granites have Rb/Sr ratio > 1. The boundary separating the fields of orogenic and anorogenic granites as well as the fields for the orogenic Pan-African and Andean granites and for the anorogenic granites of eastern Egypt and Namibia are after Abdel-Rahman (2006). Fresh granitic rocks of the Bokan complex (pluses).

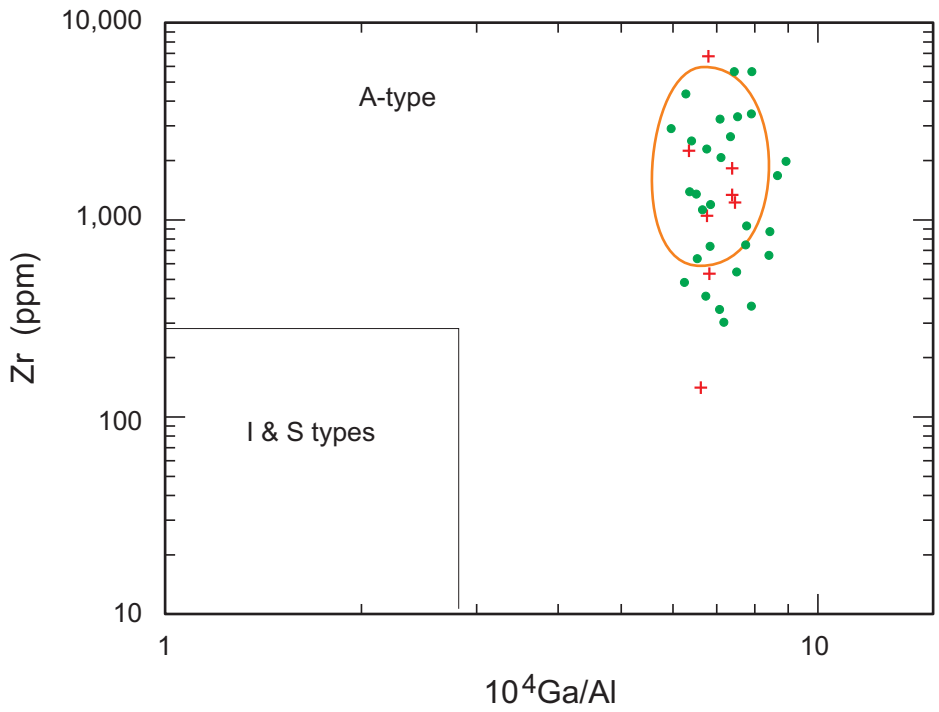

Figure 25. Plot of 10^4Ga/Al versus Zr (ppm) of Whalen et al. (1987) and Eby (1992) for the peralkaline granitic rocks of the Bokan complex and associated dikes showing the fields for I & S-types as well as for the A-type granites. Solid red line field: unaltered granitic rocks of the Bokan complex; the Ross-Adams mine area: green dots - altered granitic rocks and red pluses - mineralized granitic rocks.

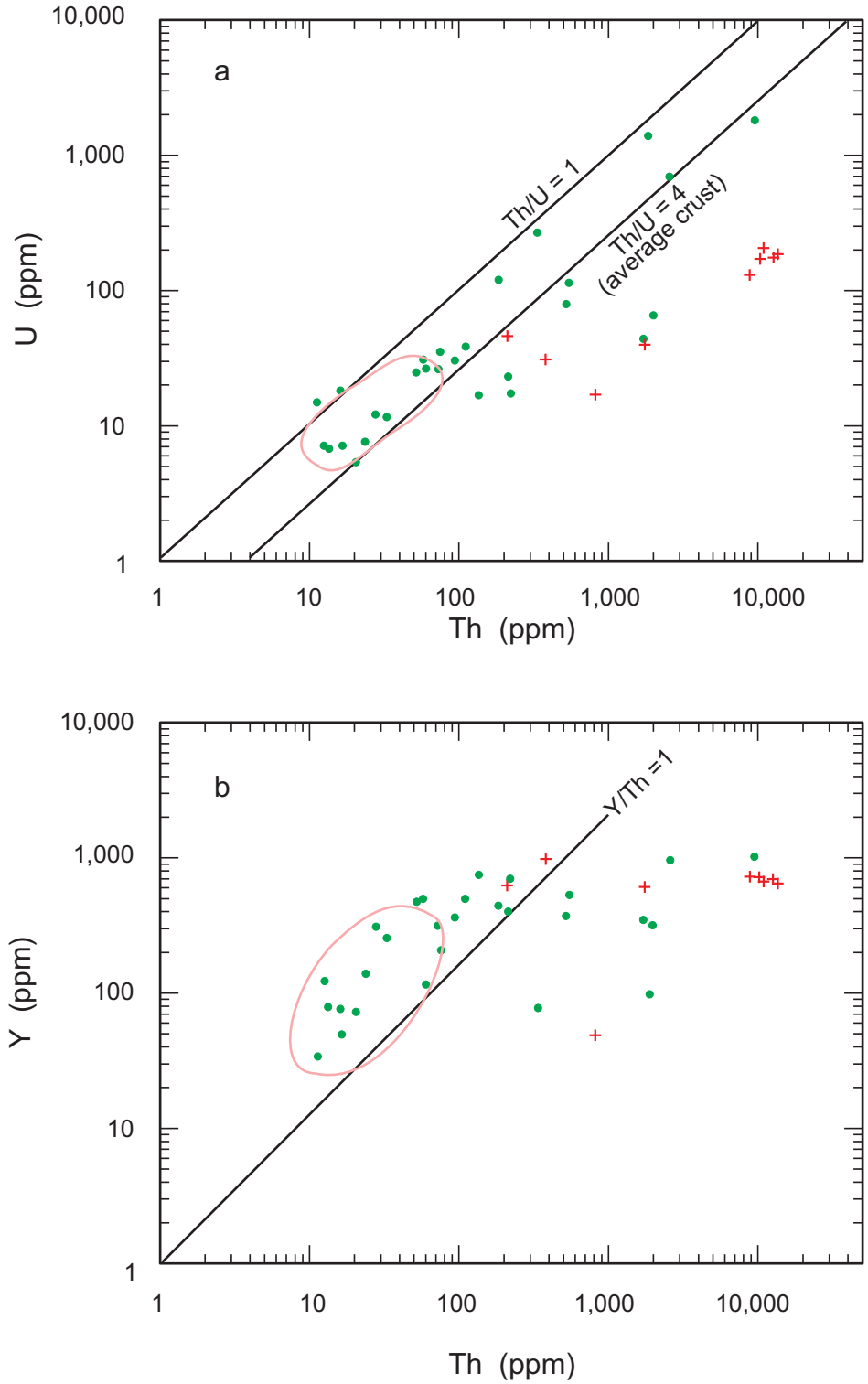

Figure 26. Relations between (a) U and Th and (b) Y and Th (ppm) in the rocks of the Bokan complex including the Ross-Adam deposit. Solid red line field: unaltered peralkaline granitic rocks of the Bokan complex; the Ross-Adams mine area: green dots - altered granitic rocks and red pluses - mineralized granitic rocks.

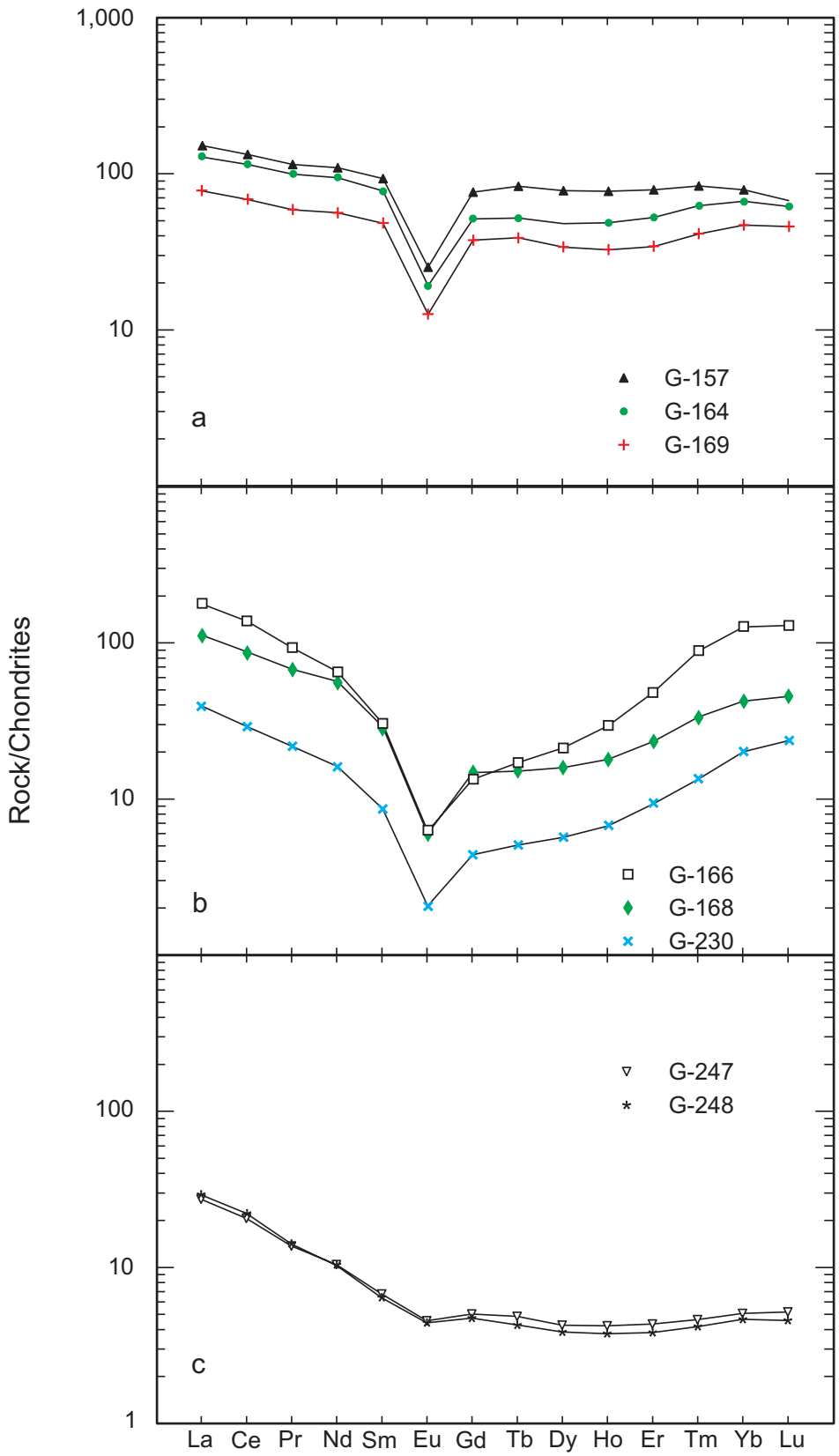

Figure 27. Chondrite-normalized REE abundances in granitic rocks of the Bokan complex and its environs. (a) Bokan peralkaline granites with relatively flat HREE and minor LREE enrichment; (b) Bokan peralkaline granites with LREE enrichment and a positive HREE slope; (c) Paleozoic quartz monzonites. Normalizing values are after Sun and McDonough (1989).

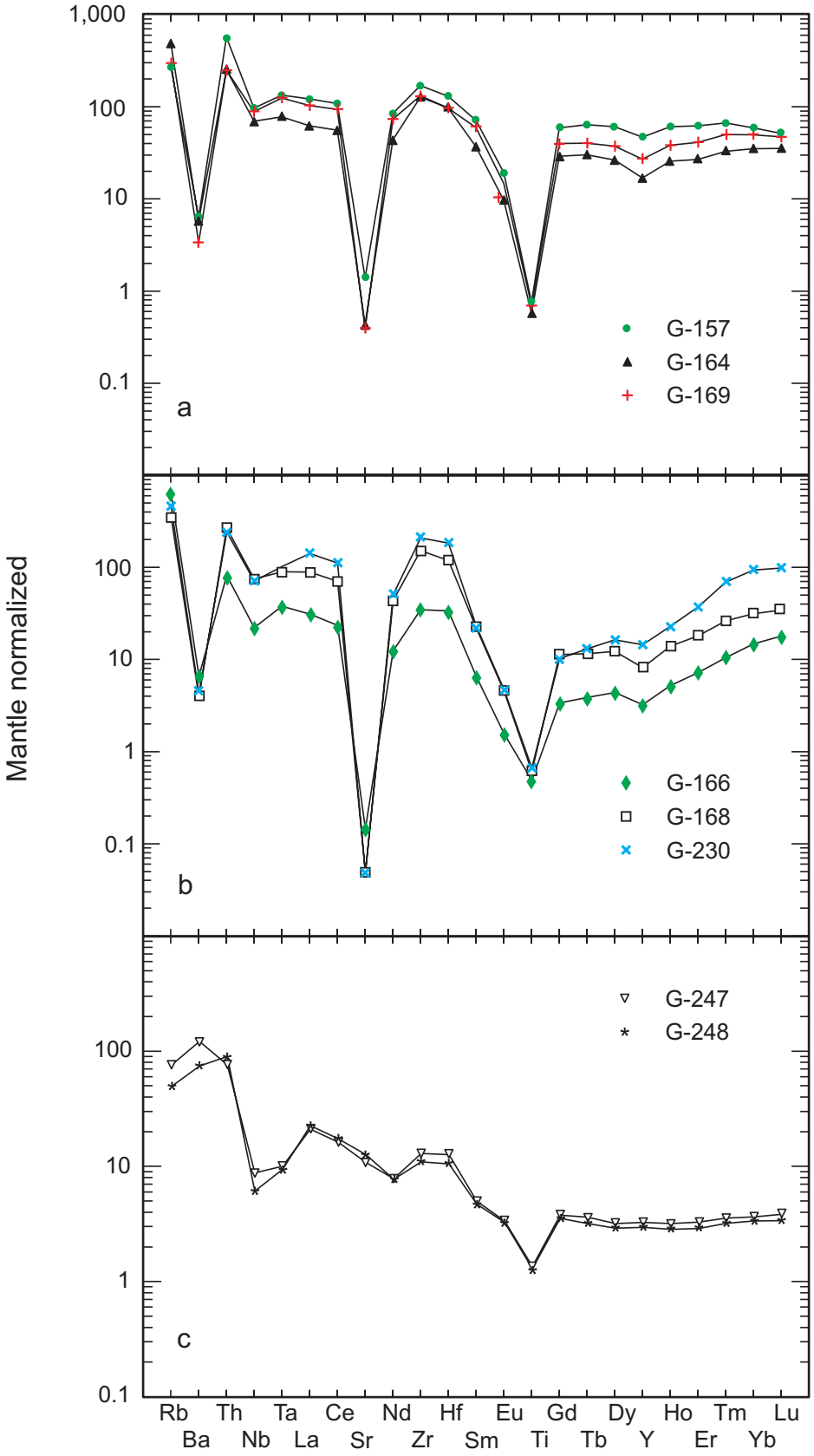

Figure 28. Primitive mantle-normalized trace element patterns of the granitic rocks of the Bokan complex and its environs. (a) Bokan peralkaline granites with relatively flat REE patterns; (b) Bokan peralkaline granites with fractionated HREE; (c) Paleozoic quartz monzonites. Normalizing values are after Sun and McDonough (1989).

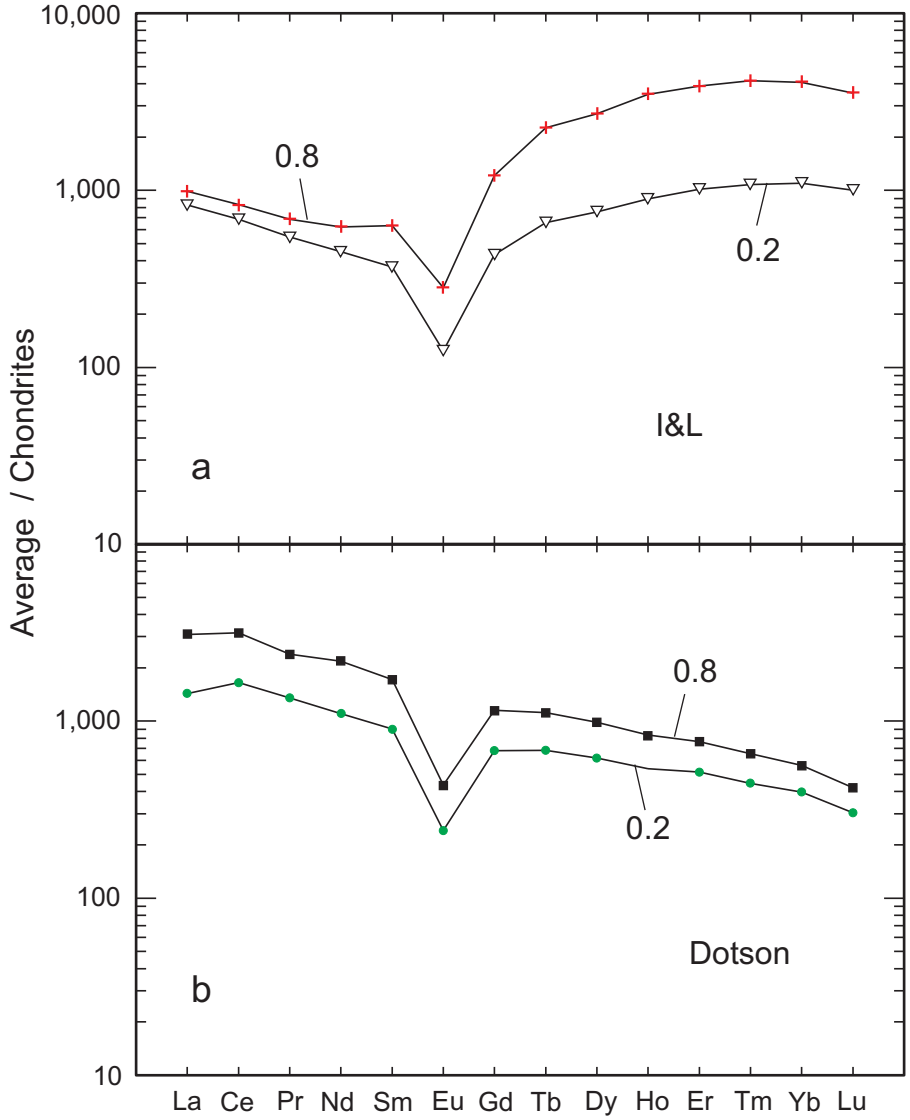

Figure 29. Chondrite-normalized REE patterns of the averages of mineralized rocks at the I&L (a) and Dotson (b) zones at the cut-off of 0.2 and 0.8 wt.% REE oxides including Y_2O_3. The data are from Robinson et al. (2011). Normalizing values are after Sun and McDonough (1989).

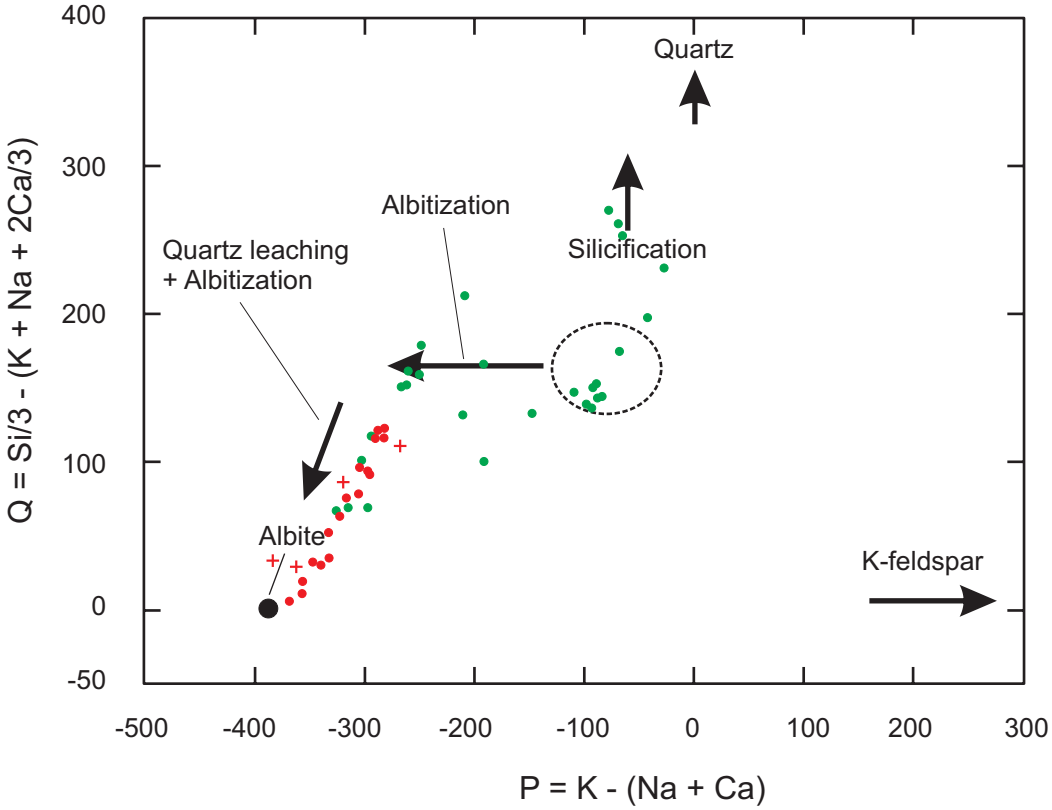

Figure 30. Q-P chemical-mineralogical diagram of Debon and LeFort (1988) showing the variations (in millications) of quartz content (Q-parameter) relative to the K-feldspar/plagioclase (P-parameter) for the Bokan granites and altered rocks associated with the Ross-Adams deposit. The horizontal arrow indicates the replacement of K-feldspar by albite while the sloping arrow represents a vector of leaching of quartz accompanied by albitization (after Cuney and Kyser, 2008). Dashed line field: unaltered peralkaline granitic rocks of the Bokan complex and its dikes; the Ross-Adams mine area: green dots - altered granitic rocks; red pluses - mineralized granitic rocks, red dots – mine area, samples of Thompson et al. (1980). Black filled circle – the composition of albite.

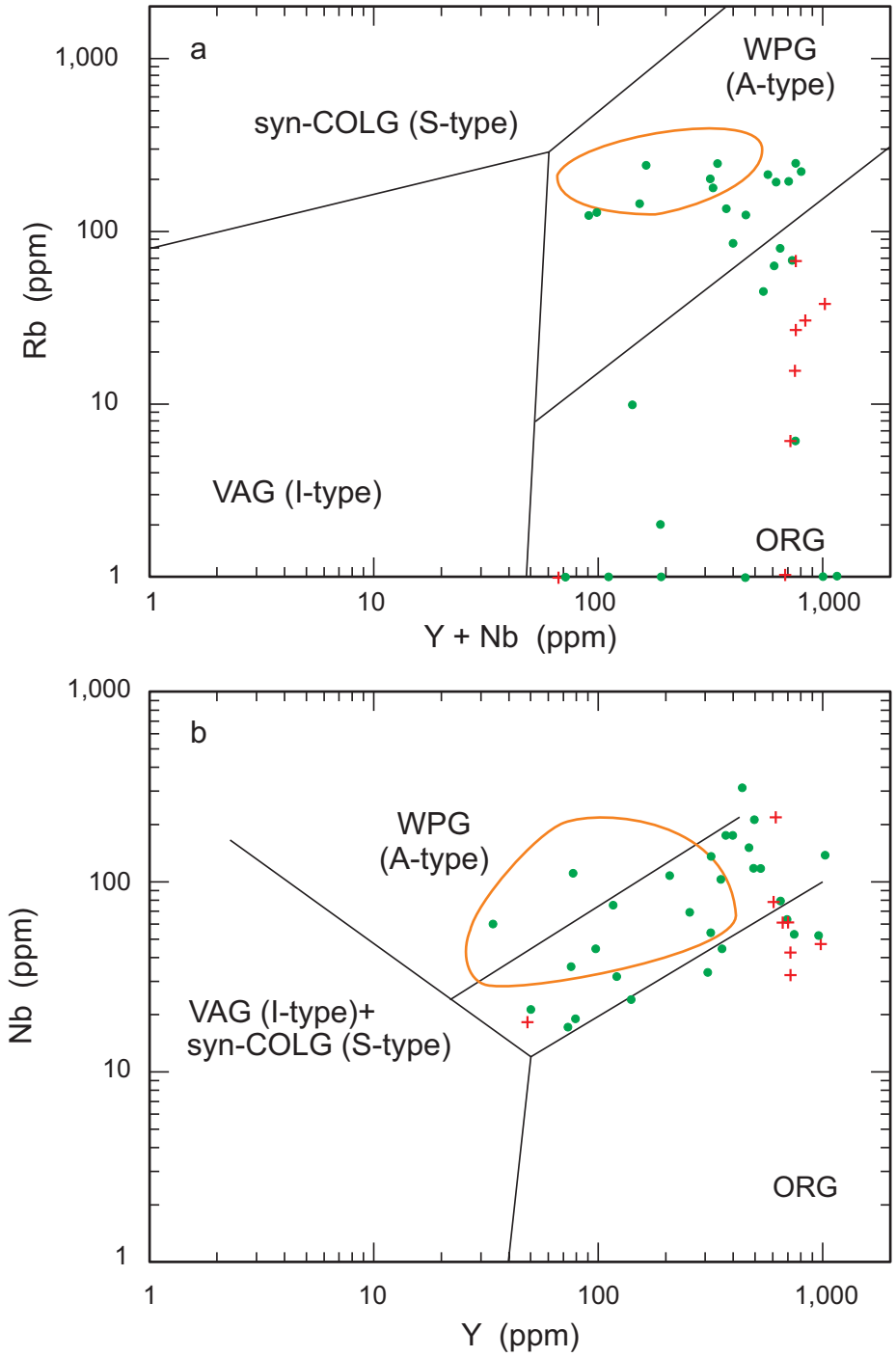

Figure 31. (a) Rb versus Nb+Y and (b) Nb versus Y (ppm) discrimination diagrams of Pearce et al. (1984) for the peralkaline granitic rocks of the Bokan complex. Fields are ORG - ocean-ridge granites; VAG - volcanic arc granites, syn-COLG - syn-collisional granites, WPG - within-plate granites. Solid red line field: unaltered granitic rocks of the Bokan complex and its dikes; the Ross-Adams mine area: green dots - altered peralkaline granitic rocks and red pluses - mineralized granitic rocks. The fresh granites of the Bokan complex plot within the WPG (A-type) granite field. Some of the altered and mineralized rocks plot outside the Bokan field, confirming the mobility of the elements.

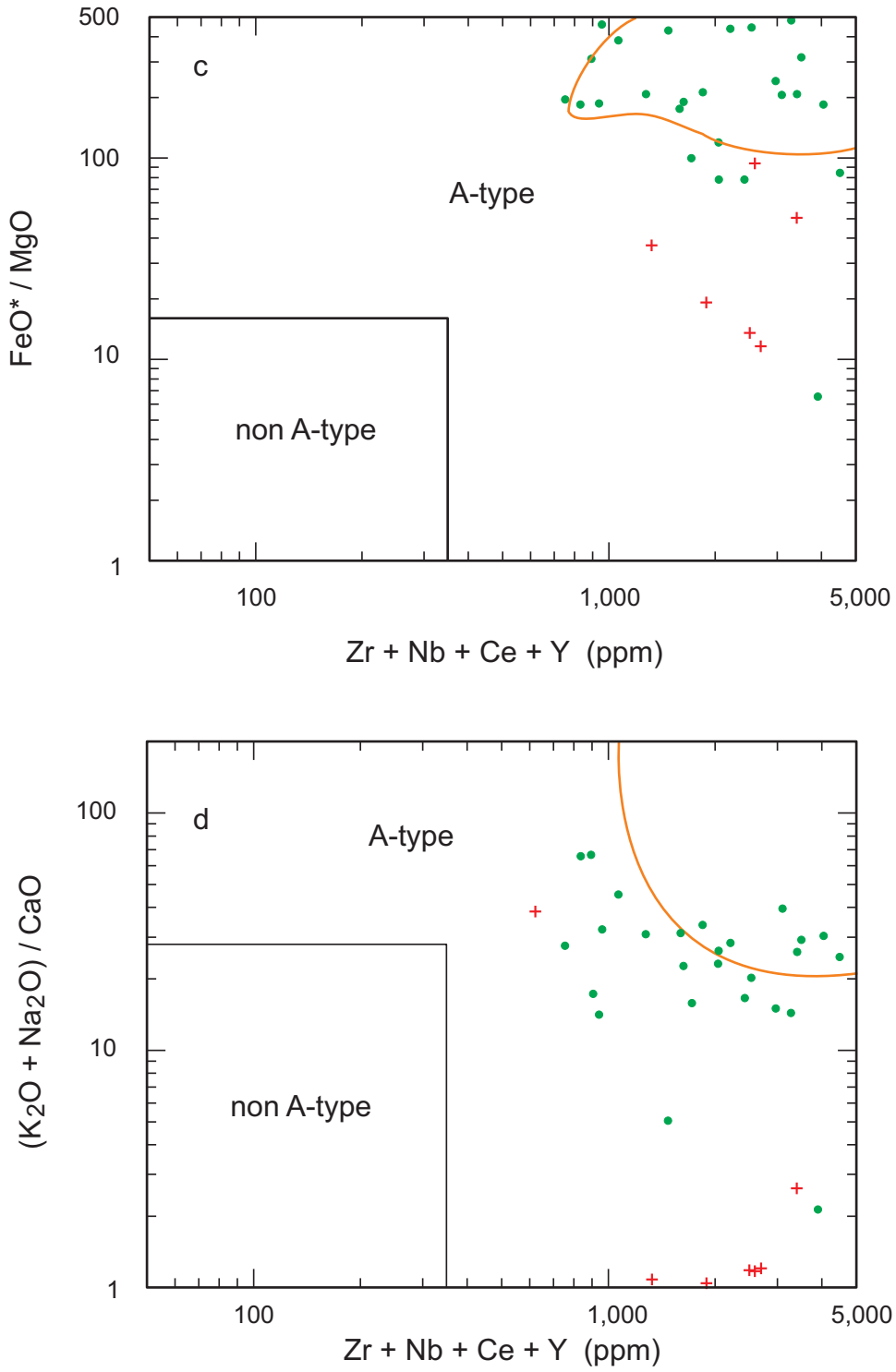

Figure 31. (c) Zr+Nb+Ce+Y (ppm) versus FeO*/MgO and (d) Zr+Nb+Ce+Y (ppm) versus (K_2O+Na_2O)/CaO diagrams of Whalen et al. (1987) for the granitic rocks of the Bokan complex. Fields for non A-type (fractionated granites and I-, S-and M-type granites) and A-type granites are shown. Solid red line field: unaltered peralkaline granitic rocks of the Bokan complex and its dikes; the Ross-Adams mine area: green dots - altered granitic rocks and red pluses - mineralized granitic rocks. The fresh granites of the Bokan complex plot within the A-type granite field. Some of the altered and mineralized rocks plot outside the Bokan field, confirming the mobility of the elements.

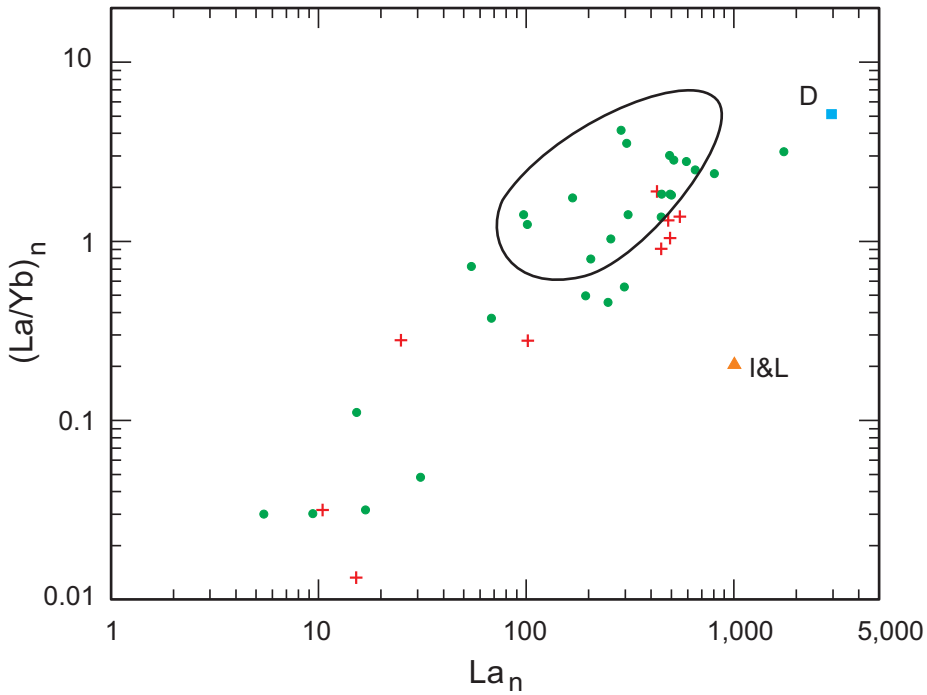

Figure 32. La_n versus $(La/Yb)_n$ diagram for granitic rocks of the Bokan complex including altered and mineralized samples. n - chondrite-normalized (normalizing values after Sun and McDonough, 1989). Solid line field: unaltered peralkaline granitic rocks of the Bokan complex and its dikes; the Ross-Adams mine area: green dots - altered granitic rocks and red pluses - mineralized granitic rocks. Average concentrations of calculated reserves at I&L (red solid triangle - I&L) and Dotson (green solid square - D) zones (with cut-off grade 0.8 wt. % REE oxides including Y_2O_3) are shown for comparison.

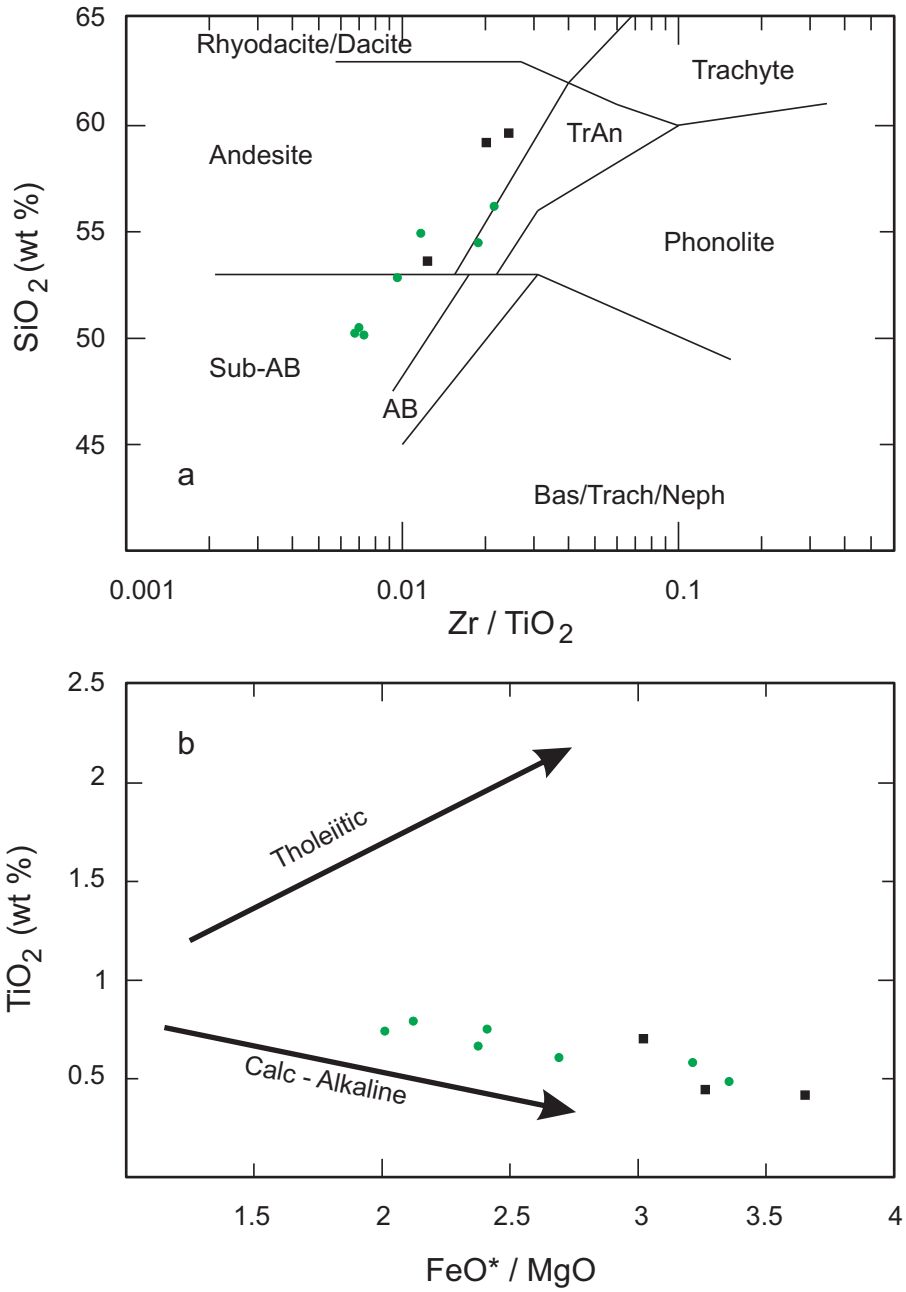

Figure 33. (a) SiO_2 (wt. %) versus Zr/TiO_2 diagram (after Winchester and Floyd, 1977) for mafic dikes (including lamprophyres) from the Bokan complex showing that the rocks have basaltic and andesitic composition. Fields are are the same as in Figure 22 b; (b) TiO_2 (wt. %) versus FeO*/MgO diagram of Miyashiro (1974) with tholeiitic and calc-alkaline vectors shows that the rocks are calc-alkaline. Samples: solid green dots-dikes from the Ross-Adams deposit area; solid squares-dikes from the I&L Zone.

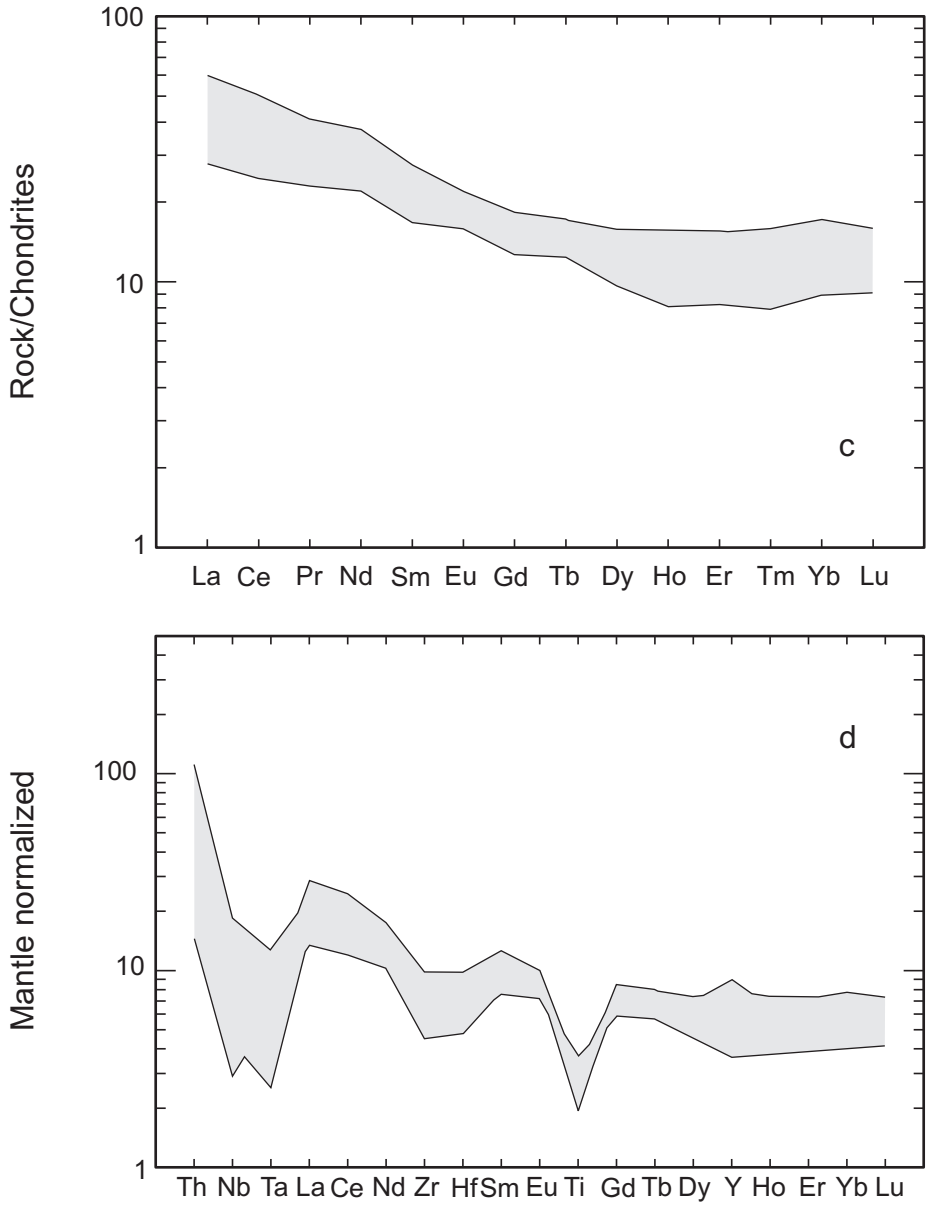

Figure 33. (c) chondrite-normalized REE patterns of the mafic dikes (normalizing values after Sun and McDonough, 1989); (d) primitive mantle-normalized trace element patterns of the mafic rocks (normalizing values after Sun and McDonough, 1989) illustrate that the rocks have distinct negative Nb-Ta and Ti anomalies.

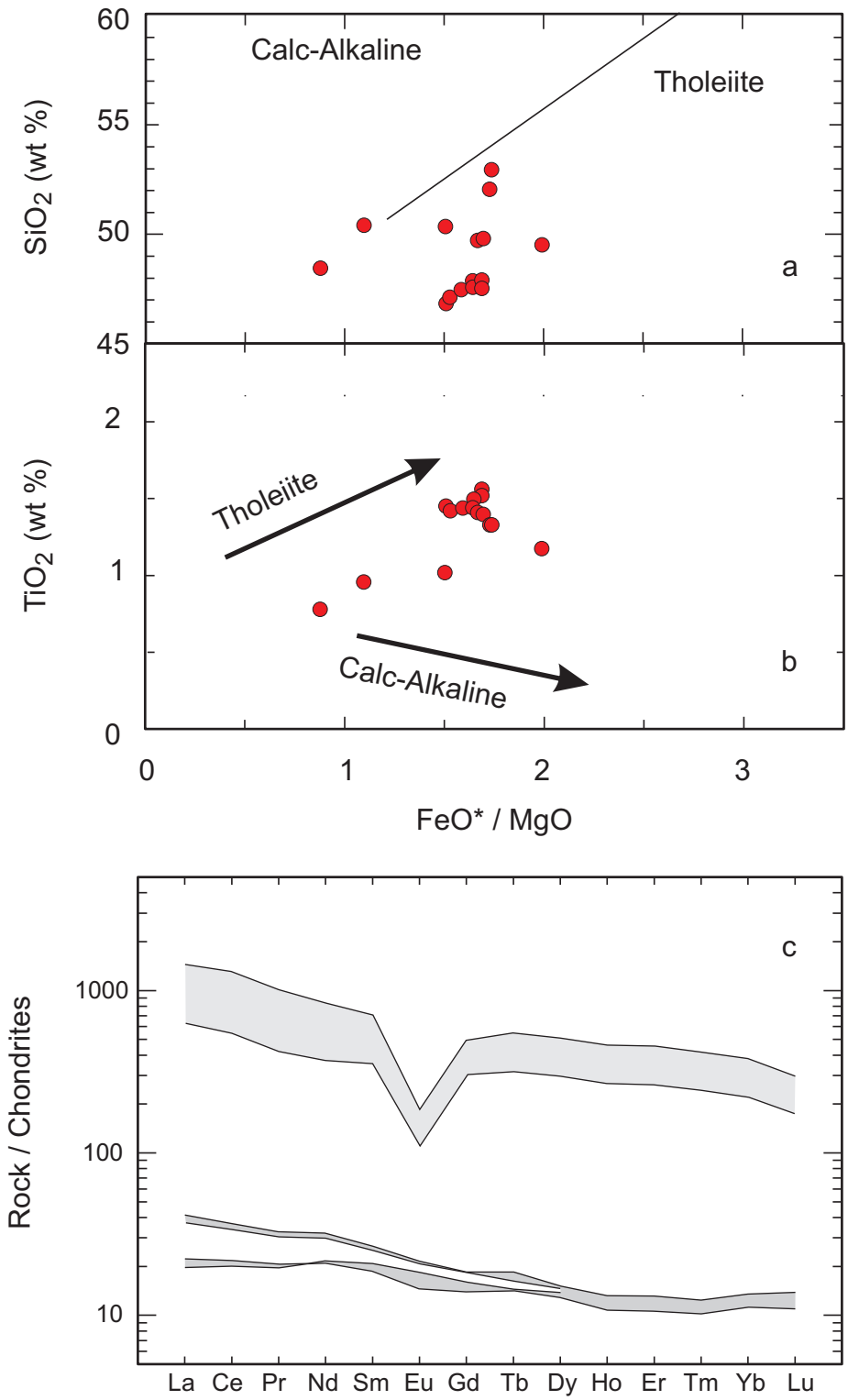

Figure 34. (a) SiO_2(wt. %) versus FeO*/MgO; (b) TiO_2 (wt. %) versus FeO*/MgO and (c) chondrite-normalized REE patterns of Paleozoic gabbroic rocks from the vicinity of the Dotson Zone (drill-core samples). (a) and (b) diagrams are after Miyashiro (1974) showing fields and vectors for calc-alkaline and tholeiitic rocks. Normalizing values for REE are after Sun and McDonough (1989). The gabbros are tholeiitic and those close to the shear zone have significantly higher REE abundances than those away from the zone, although their major element compositions do not change noticeably.

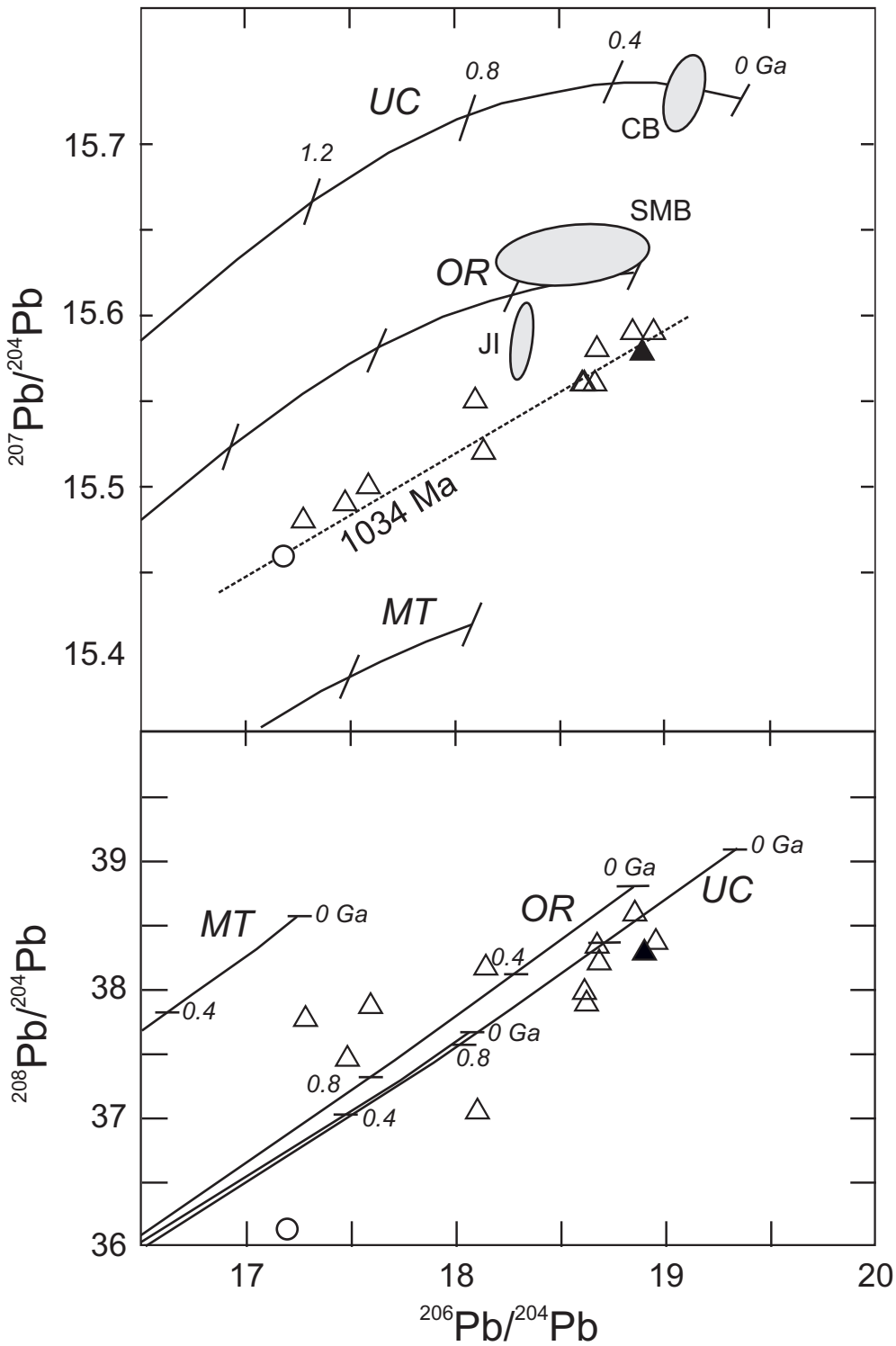

Figure 35. Plots of lead isotopic data for Bokan samples in $^{207}Pb/^{204}Pb$ versus $^{206}Pb/^{204}Pb$ (a) and $^{208}Pb/^{204}Pb$ versus $^{206}Pb/^{204}Pb$ (b) diagrams with lead evolution curves shown (from Doe and Zartman, 1979) for the mantle (MT), orogene (OR) and upper crust (UC). Also shown for comparative purposes are the lead isotopic fields for different intrusions, namely the Cassiar Batholith (CB; Driver et a., 2000), the South Mountain Batholith (SMB; Dostal and Chatterjee, 2010) and the Josephine intrusion (JI; Barth et al., 1995). The reference isochron of 1034 Ma which goes through the Bokan data is discussed in the text. Triangle - peralkaline granite; solid triangle - galena 2009; circle – lamprophyre.

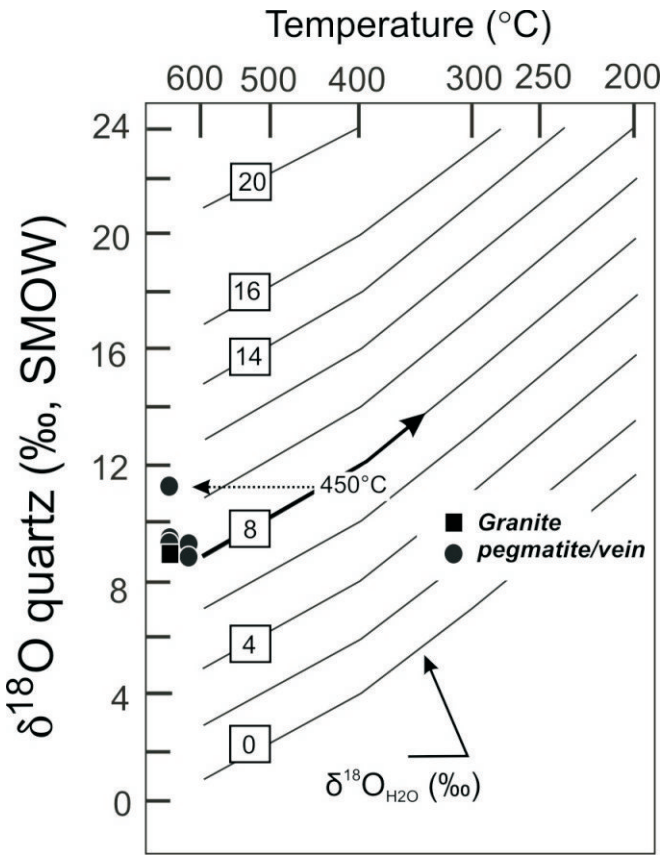

Figure 36. Plot of $\delta^{18}O_{quartz}$ versus Temperature (°C) for quartz data (granite and pegmatite/vein) from the Bokan complex. The diagram is contoured for isopleths of $\delta^{18}O_{H2O}$ using the quartz-H_2O fractionation equation of Matsuhisa et al. (1979). See text for discussion of the significance of the data and the arrow for the single sample enriched in ^{18}O.

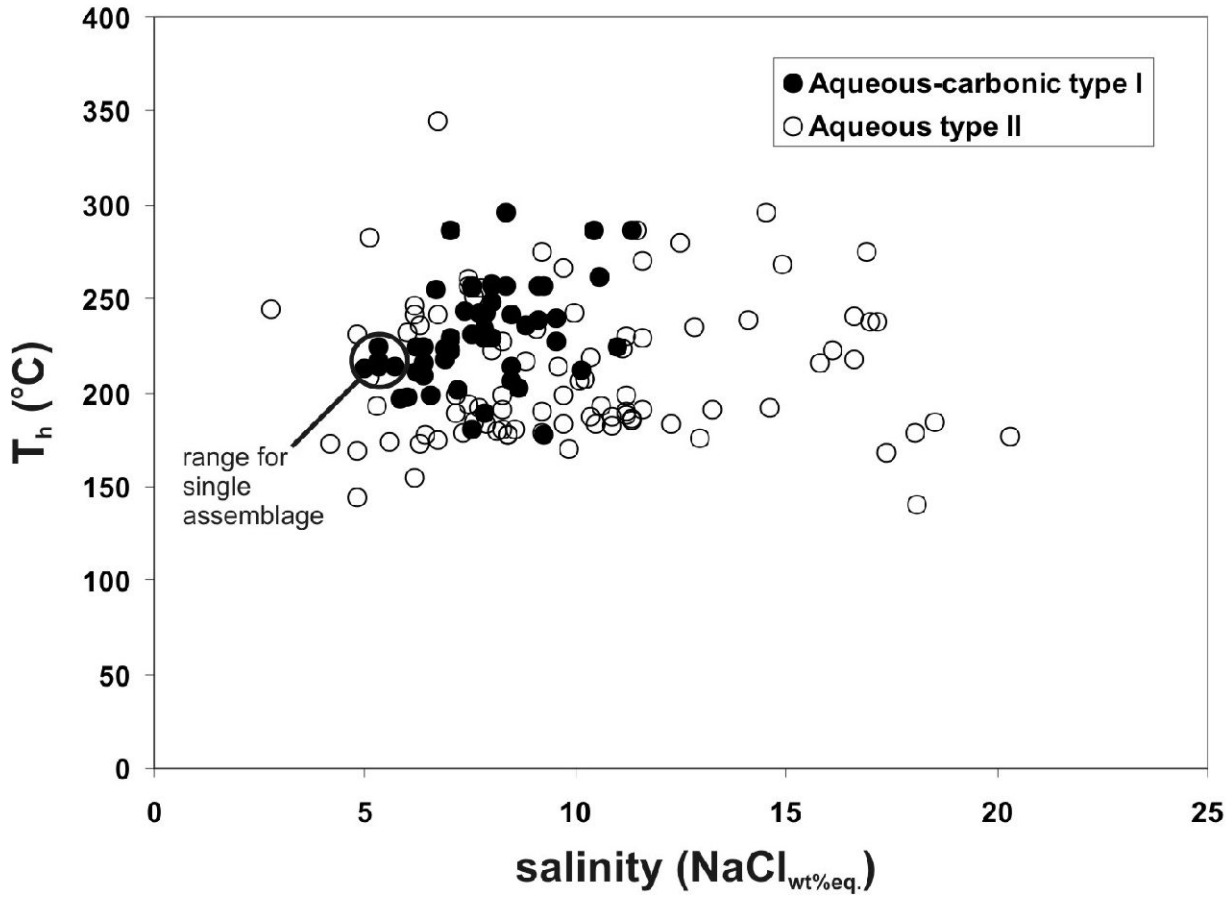

Figure 37. Plot of homogenization temperature versus bulk inclusion salinity. Data for aqueous and aqueous carbonic inclusions show a similar range in final homogenization temperature but the secondary aqueous inclusions show a wider overall range in bulk salinity. Singe fluid inclusion assemblages (circled) yield very small ranges in T_h and bulk salinity; when the entire range in data is considered relative to single assemblages, this suggests that relatively large fluctuations temperature and salinity occurred during inclusion entrapment when single fractures are compared, and when primary inclusion domains are considered. However, anomalously high T_h values in some assemblages (see Table 9), notably in type II inclusions are likely the result of post-entrapment reopening, mixing and resealing since large temperature fluctuations along single fractures is unrealistic.

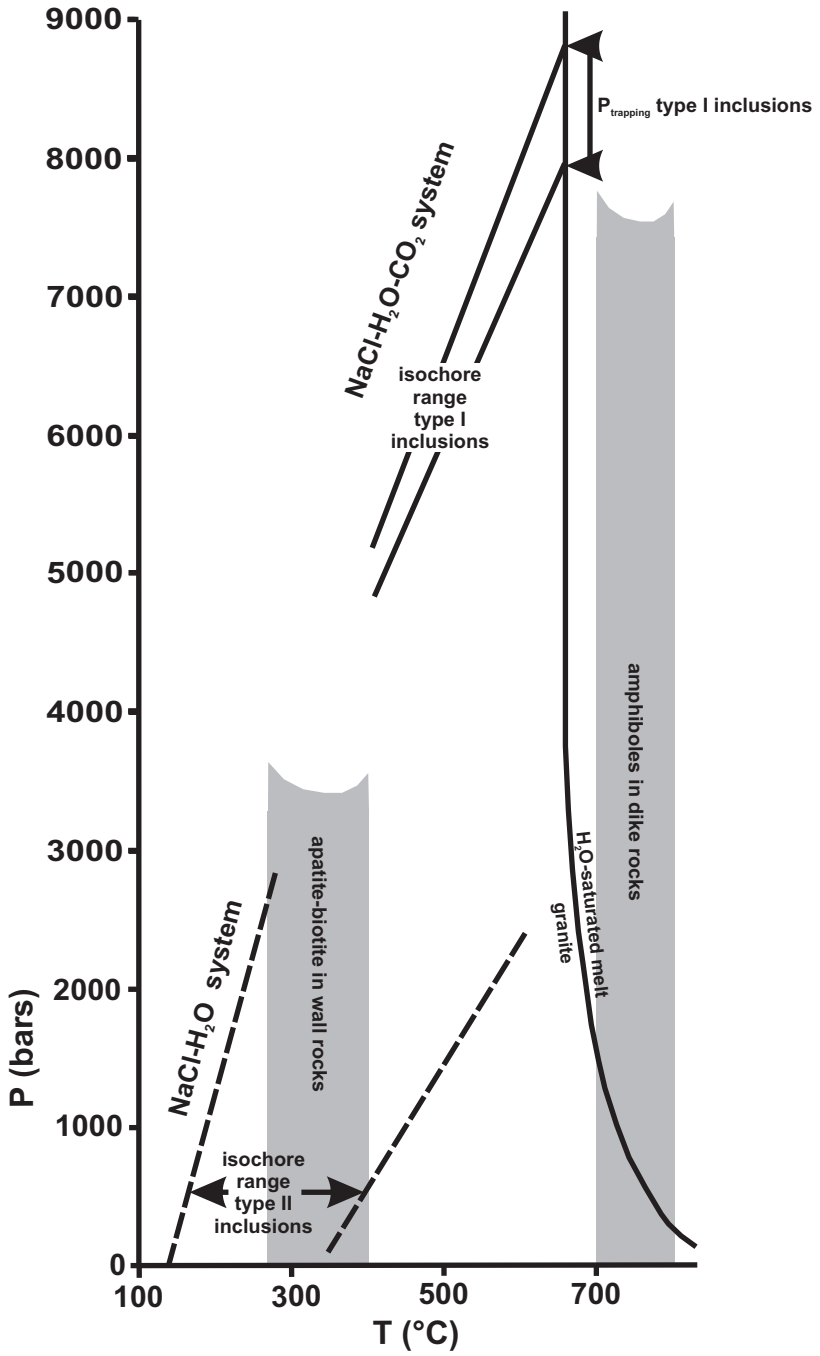

Figure 38. Estimations of range in trapping conditions for primary and secondary fluid inclusions. Type II inclusions (secondary) were modeled in the NaCl-H2O system and show a range in isochores overlaps with the final equilibration temperatures determined for biotite-apatite pairs in the wall rocks to the syn-mineralization dikes, consistent with trapping at post-solidus temperatures at P less than ~3 kbar. Type I inclusions (primary) were modeled in the NaCl-H2O-CO2 system; their isochores intersect with the minimum melting curve for a fluid-saturated granite (Holtz et al, 1992) at very high pressures (~8-9 kbar). The reasons for the discrepancy between entrapment pressure and emplacement depth are not known and are under investigation.

Photo 1. View of Bokan Mountain from the West Arm of Kendrick Bay. The bare outcrops are common for peralkaline granites.

Photo 2. Close-up of the Bokan Mountain from the I&L Zone.

Photo 3. North-western side of Bokan Mountain near the Wennie prospect. Bold, cliff-like outcrops are typical of the Bokan Mountain.

Photo 4. One of the dikes of the I&L Zone. This structurally-controlled NW-trending steeply dipping dike is about 5 meters wide and is hosted by aegirine granite. The site was described by Staatz (1978).

Photo 5. Branching mineralized pegmatite vein-dike. The dikes branch and bifurcate into thinner dikes with increasing distance from the complex. Dotson Zone.

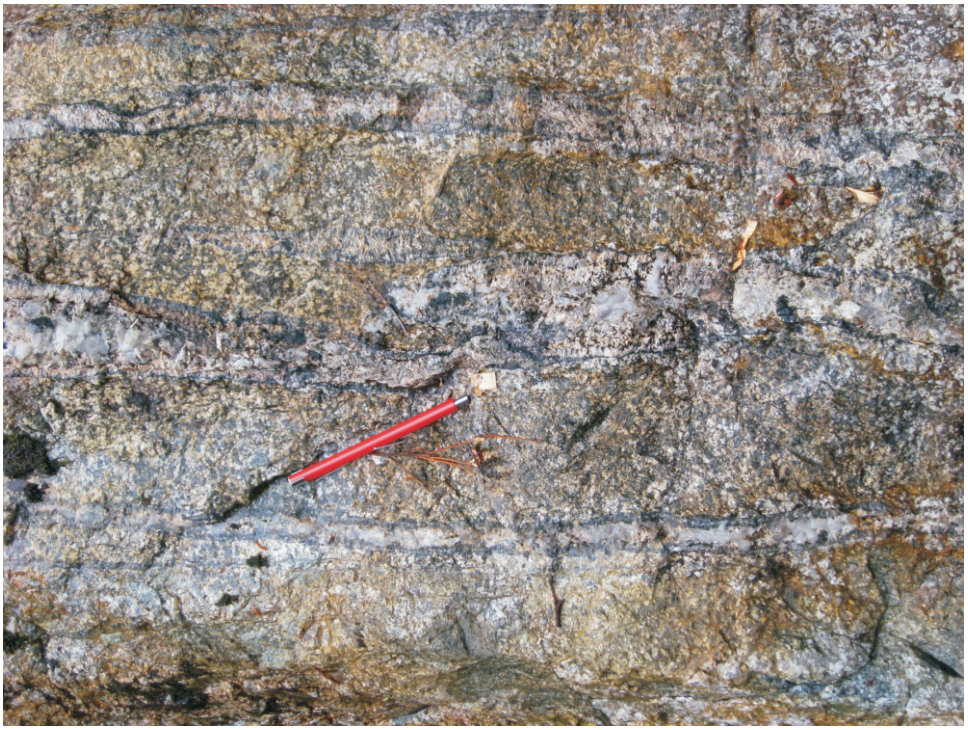

Photo 6a. The felsic vein-dikes of the Dotson Zone occur in subparallel clusters typically associated with a shear zone.

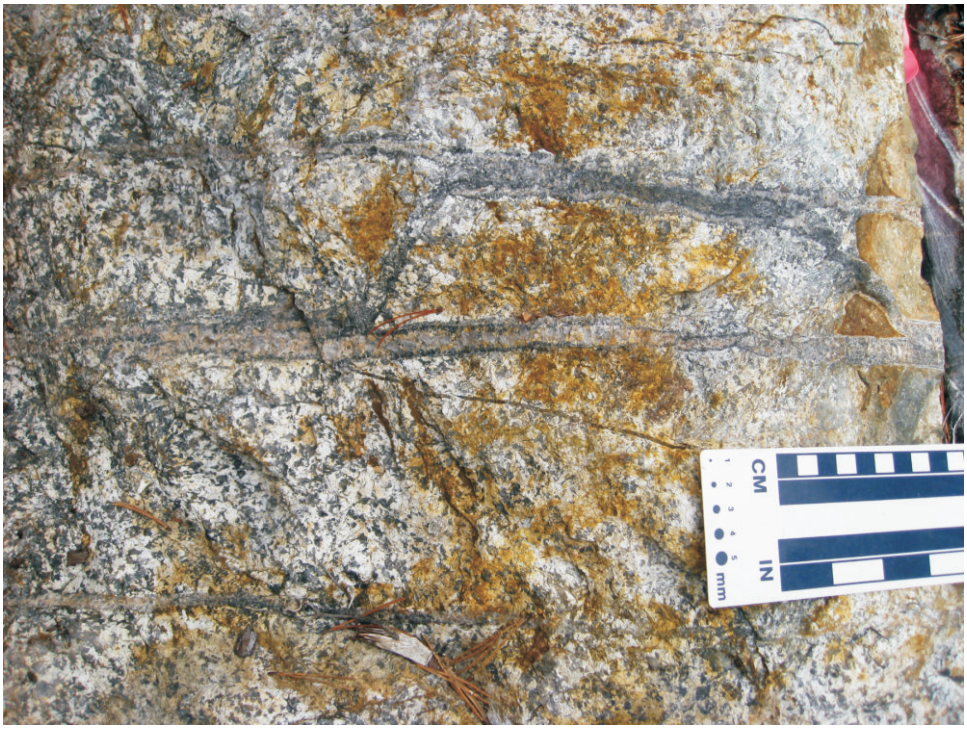

Photo 6b. The felsic vein-dikes of the Dotson Zone occur in subparallel clusters typically associated with a shear zone.

Photo 6c. The felsic vein-dikes of the Dotson Zone occur in subparallel clusters typically associated with a shear zone.

Photo 7. Mineralized aplitic dike crosscutting quartz diorite. Dotson Zone.

Photo 8. Mineralized aplitic dike (between dashed lines) is crosscut by a thin younger aplitic vein-dike (indicated by arrow). Dotson Zone.

Photo 9. Zoned mineralized aplitic vein-dike with quartz rich core. Dotson Zone.

Photo 10. Zoned mineralized pegmatite vein-dike with quartz rich core. Dotson Zone.

Photo 11. Abandoned Ross-Adams open pit.

Photo 12. Abandoned Ross-Adams mine with an audit (upper left corner). Granitic host rocks show distinct fracture-cleavages parallel to faults which controlled emplacement of the deposit.

Photo 13. Concentrically zoned mineralized aplitic pipe/vein. Dotson Zone.

Photo 14. Mineralized zoned pegmatitic vein-dike (~20 cm wide), Dotson Zone.

Photo 15. Altered and mineralized quartz monzonite (the redish altered zone is about 10 cm wide). The alteration and mineralization follows a fracture which runs parallel to the Doston Zone.

Photo 16. Deformed aplite dike (~8 cm wide) indicating that some of the dikes were already emplaced when the host rocks were still not solidified. Dotson Zone.

Table 1a. Representative analyses of pyroxene from peralkaline granitic rocks of the Bokan complex

Sample:	G151	G151	G161	G161	G242	G242	G244	G244	G244	G244	G244	LM21	LM22	LM26	LM26
(wt%)	core	core	incl	incl	incl*	incl	core	core	skeletal	skeletal	skeletal	suboph**	incl	core	rim
SiO_2	51.79	51.81	52.25	52.54	51.80	51.08	53.21	53.73	52.69	52.33	52.25	51.37	52.56	52.59	52.97
TiO_2	0.97	0.72	0.73	0.97	0.45	1.58	0.47	0.90	2.01	0.95	0.94	0.80	0.66	1.09	1.45
Al_2O_3	0.36	0.20	0.51	0.38	0.13	0.67	0.11	0.61	0.24	0.19	0.21	0.27	0.61	0.38	0.81
FeO_T	28.89	28.95	28.63	28.58	29.53	27.91	29.41	29.24	28.45	29.23	29.14	29.16	29.44	28.80	28.15
MnO	0.35	0.14	0.06	0.08	0.10	0.24	0.01	0.01	0.12	0.06	0.05	0.11	0.01	0.11	0.03
MgO	0.05	0.07	0.00	0.00	0.06	0.03	0.05	0.04	0.00	0.00	0.00	0.00	0.00	0.03	0.01
CaO	0.19	0.09	0.00	0.00	0.16	0.18	0.00	0.03	0.26	0.19	0.22	0.15	0.00	0.31	0.04
Na_2O	14.36	14.80	14.80	14.98	14.69	14.24	15.08	15.48	14.97	14.90	14.79	14.71	15.26	14.82	15.02
K_2O	0.02	0.03	0.00	0.00	0.01	0.02	0.02	0.02	0.01	0.02	0.03	0.03	0.03	0.00	0.00
Total	97.06	96.87	96.98	97.52	96.93	96.12	98.43	100.11	99.01	98.15	97.89	96.74	98.60	98.24	98.51
	cations per 6 oxygen equivalents														
Si	1.963	1.958	1.970	1.969	1.958	1.956	1.977	1.959	1.957	1.958	1.961	1.948	1.947	1.963	1.966
Ti	0.028	0.020	0.021	0.027	0.013	0.045	0.013	0.025	0.056	0.027	0.026	0.023	0.018	0.031	0.040
Al	0.016	0.009	0.023	0.017	0.006	0.030	0.005	0.026	0.011	0.009	0.009	0.012	0.026	0.017	0.036
Fe^{3+}	0.916	0.915	0.903	0.896	0.934	0.894	0.914	0.892	0.884	0.915	0.915	0.925	0.912	0.899	0.874
Mn	0.011	0.004	0.002	0.002	0.003	0.008	0.000	0.000	0.004	0.002	0.002	0.003	0.000	0.000	0.001
Mg	0.003	0.004	0.000	0.000	0.003	0.002	0.003	0.002	0.000	0.000	0.000	0.000	0.000	0.004	0.001
Ca	0.008	0.004	0.000	0.000	0.006	0.007	0.000	0.001	0.011	0.008	0.009	0.006	0.000	0.013	0.001
Na	1.055	1.084	1.082	1.088	1.076	1.057	1.087	1.094	1.078	1.081	1.076	1.081	1.095	1.073	1.081
K	0.001	0.001	0.000	0.000	0.001	0.001	0.001	0.001	0.000	0.001	0.002	0.001	0.001	0.000	0.000
Jd	13.12	15.55	16.56	17.67	13.18	15.35	15.91	18.48	17.88	15.30	14.91	14.40	16.76	16.00	19.13
Ae	86.16	84.10	83.44	82.33	86.22	83.95	84.09	81.42	81.15	83.99	84.28	85.05	83.24	82.85	80.73
Di	0.72	0.35	0.00	0.00	0.60	0.70	0.00	0.10	0.97	0.71	0.82	0.55	0.00	1.15	0.13

* inclusion in sodic amphibole

** (sub)ophitic texture (encloses or partly encloses albite crystallites); pyroxene end-members: Jd-jadeite; Ae-aegirine; Di-diopside

Table 1b. Representative analyses of amphibole from rocks of the Bokan complex

Sample:	G151	G151	G161	G161	G161	G242	G242	G244	G244	G244	LM22	LM22	LM24	LM24	LM24	LM143	LM79	LM79
(wt%)	core	core	core*	core*	core*	rim*	core	core	core	core	core	core*	core	rim	core	core	core	core
SiO_2	50.58	50.74	51.35	52.20	51.75	50.31	49.41	50.54	50.72	51.53	50.88	51.19	51.87	50.63	51.08	42.96	41.14	40.82
TiO_2	1.02	0.86	1.11	0.49	0.76	0.78	0.83	1.62	1.18	1.22	0.69	0.64	0.83	0.85	0.76	1.74	1.49	1.56
Al_2O_3	0.37	0.40	0.49	0.35	0.73	0.42	0.49	0.34	0.36	0.47	0.58	0.49	0.60	0.70	0.68	9.90	14.24	14.55
FeO	31.82	32.22	35.07	29.39	28.53	31.51	32.51	31.01	31.37	32.23	33.10	33.55	33.12	31.71	32.19	17.85	11.97	12.00
MnO	1.00	1.10	0.18	0.00	0.12	1.06	0.81	1.02	1.02	1.03	0.90	0.75	1.06	1.13	1.16	0.35	0.16	0.16
MgO	0.14	0.12	0.13	0.00	0.01	0.08	0.13	0.18	0.15	0.17	0.00	0.00	0.12	0.12	0.21	9.84	13.42	13.32
CaO	0.11	0.12	0.00	0.00	0.04	0.24	0.48	0.30	0.30	0.13	0.37	0.38	0.19	0.52	0.16	11.50	11.91	11.81
Na_2O	9.78	9.98	7.67	15.01	14.94	9.58	9.67	9.73	9.35	8.67	8.62	8.26	7.60	7.68	7.81	1.91	2.51	2.51
K_2O	2.12	2.07	0.24	0.00	0.03	1.96	1.66	1.90	1.86	1.85	1.72	1.50	1.71	1.82	1.66	0.87	0.41	0.41
F	0.89	1.02	0.15	0.00	0.01	0.96	1.17	1.08	1.07	1.19	1.22	1.12	0.76	0.87	0.79	0.08	0.00	0.00
Total	97.85	98.64	96.38	97.44	96.91	96.90	97.16	97.71	97.37	98.48	98.07	97.87	97.86	96.01	96.49	97.00	97.24	97.14
	cations per 23 oxygen equivalents; Fe^{3+} was calculated assuming 13 cations excluding Ca, Na and K																	
Si	8.275	8.253	8.099	8.749	8.720	8.303	8.163	8.294	8.309	8.262	8.214	8.222	8.227	8.254	8.232	6.507	5.996	5.951
Ti	0.126	0.106	0.131	0.062	0.096	0.096	0.103	0.200	0.145	0.147	0.084	0.077	0.099	0.104	0.092	0.198	0.163	0.171
Al	0.071	0.077	0.090	0.069	0.145	0.081	0.096	0.065	0.070	0.089	0.110	0.092	0.112	0.134	0.130	1.768	2.446	2.500
Fe^{+3}	0.000	0.000	1.054	0.000	0.000	0.000	0.000	0.000	0.000	0.000	0.115	0.298	0.491	0.164	0.387	0.362	0.729	0.783
Fe^{+2}	4.354	4.384	3.572	4.120	4.020	4.350	4.492	4.255	4.298	4.321	4.353	4.208	3.902	4.159	3.952	1.898	0.730	0.680
Mn	0.139	0.152	0.024	0.000	0.017	0.149	0.113	0.142	0.141	0.139	0.123	0.102	0.142	0.157	0.158	0.045	0.019	0.020
Mg	0.035	0.028	0.030	0.000	0.002	0.021	0.033	0.044	0.037	0.041	0.000	0.000	0.028	0.029	0.050	2.222	2.916	2.896
Ca	0.019	0.022	0.000	0.000	0.008	0.043	0.085	0.053	0.053	0.022	0.063	0.065	0.032	0.091	0.028	1.866	1.860	1.844
Na	3.103	3.147	2.347	4.879	4.881	3.066	3.099	3.094	2.969	2.694	2.699	2.573	2.336	2.427	2.439	0.560	0.709	0.710
K	0.443	0.429	0.048	0.000	0.006	0.412	0.349	0.397	0.389	0.378	0.354	0.307	0.347	0.378	0.342	0.168	0.076	0.077
F	0.449	0.506	0.759	0.000	0.000	0.485	0.593	0.536	0.536	0.587	0.607	0.559	0.380	0.439	0.398	0.039	0.000	0.000

* hosts aegirine

Samples: peralkaline granite - G151,G161, G242, G244, LM22, LM24 ; lamphophyre- LM79 ; mafic dike - LM143 (Geoduck zone)

Table 1c. Representative analyses of feldspars from rocks of the Bokan complex

Sample:	G242	G242	G244	G244	LM22	LM22	LM21	LM26	LM26*	LM145	LM143	LM73	LM113	LM113	G247	G247
(wt%)																
SiO_2	65.00	69.12	64.72	68.87	70.31	64.56	69.01	65.06	69.23	63.87	57.61	65.10	64.83	65.84	65.04	65.35
Al_2O_3	18.33	19.74	18.17	19.70	19.12	18.14	19.11	17.72	18.74	18.71	26.51	21.74	22.70	22.00	18.94	22.46
FeO	0.33	0.02	0.40	0.01	1.16	0.52	0.45	0.67	1.51	0.04	0.16	0.09	0.32	0.00	0.03	0.05
CaO	0.00	0.00	0.00	0.00	0.00	0.00	0.00	0.00	0.00	0.00	7.75	2.30	1.48	2.35	0.01	2.23
Na_2O	0.24	11.96	0.22	12.19	12.27	0.26	10.46	0.26	11.43	0.37	7.41	10.66	10.09	10.60	0.37	10.64
K_2O	16.49	0.02	16.33	0.03	0.07	16.29	0.08	15.86	0.08	15.97	0.08	0.29	1.42	0.08	15.84	0.37
Total	100.42	100.86	99.83	100.78	102.94	99.79	99.19	99.59	100.99	99.10	99.56	100.40	101.07	100.88	100.49	101.19
	cations per 8 oxygen equivalents															
Si	2.994	2.993	3.001	2.988	3.002	2.998	3.026	3.019	3.010	2.978	2.591	2.858	2.839	2.871	2.986	2.848
Al	0.996	1.007	0.993	1.007	0.962	0.993	0.988	0.970	0.961	1.029	1.406	1.126	1.172	1.130	1.025	1.154
Fe	0.013	0.001	0.015	0.000	0.042	0.020	0.016	0.026	0.055	0.002	0.006	0.003	0.012	0.000	0.002	0.002
Ca	0.000	0.000	0.000	0.000	0.000	0.000	0.000	0.000	0.000	0.000	0.374	0.108	0.070	0.110	0.001	0.104
Na	0.022	1.004	0.019	1.025	1.016	0.024	0.890	0.023	0.963	0.034	0.646	0.908	0.857	0.896	0.033	0.899
K	0.970	0.001	0.966	0.002	0.004	0.965	0.004	0.938	0.005	0.950	0.005	0.016	0.079	0.005	0.928	0.021
An	0.00	0.00	0.00	0.00	0.00	0.00	0.00	0.00	0.00	0.00	36.46	10.47	6.92	10.85	0.08	10.16
Ab	2.18	99.92	1.95	99.84	99.61	2.43	99.55	2.41	99.50	3.41	63.08	87.98	85.20	88.68	3.41	87.81
Or	97.82	0.08	98.05	0.16	0.39	97.57	0.45	97.59	0.50	96.59	0.47	1.55	7.88	0.48	96.51	2.03

*idiomorphic inclusion in aegirine or arfvedsonite; feldspar end-members: An-anorthite; Ab-albite; Or-orthoclase

Samples: peralkaline granite - G242, G244, LM21, LM22, LM26; mineralized granitic dike - LM145 (Geoduck zone); mafic dike - LM143 (Geoduck zone); lamprophyre - LM73, LM113, Paleozoic quartz monzonite - LM247

Table 1d. Microprobe analyses of ore and accessory minerals

Sample	coffinite 1	uranothorite 1	bastnaesite 1	synchysite 1	iimoriite 1	zircon 1	zircon 2	allanite-core 3	allanite-rim 3	fluorite 4
(wt%)										
SiO_2	19.69	17.52	0.06		17.08	27.95	33.43	28.65	30.03	
TiO_2							0.33	1.26	1.01	
Al_2O_3	1.06	0.43	0.02				0.08	11.64	14.20	
FeO	0.62	0.92	0.20		0.92	0.21	0.26	16.24	15.54	
CaO	0.50	1.61	2.84	16.20	0.09		0.11	8.56	11.10	69.65
ZrO_2	0.01	0.02	0.09		0.01	57.27	61.35	0.08	0.09	
HfO_2	0.27	0.10	0.06		0.51	1.65				
Nb_2O_5	0.03	0.02	0.01			0.06				
PbO	0.10	0.15			0.40	0.08				
ThO_2	0.06	39.46	0.83	0.14	0.04	1.51	0.27	0.29	0.81	
UO_2	64.94	30.34	0.07	0.03	0.06	1.57	0.38	0.20	0.26	
Y_2O_3	9.50	1.16	2.06	16.90	45.37	3.05	2.40	1.44	1.32	2.59
La_2O_3	0.02	0.04	13.73	9.51	0.04	0.02				
Ce_2O_3	0.12	0.12	31.38	15.50	0.08	0.04	0.32	10.46	7.74	0.06
Pr_2O_3	0.03	0.05	4.56		0.06	0.03				
Nd_2O_3	0.07	0.04	12.51	5.61	0.09	0.03				
Sm_2O_3	0.05	0.09	2.00	1.11	0.21					
Eu_2O_3			0.65		0.08	0.01				
Gd_2O_3	0.40	0.08	3.96	2.46	1.82	0.03				
Tb_2O_3					0.62	0.05				
Dy_2O_3	1.15	0.29	0.62	2.49	6.64	0.79				
Ho_2O_3	0.23	0.18	0.11		1.64	0.46				
Er_2O_3	1.02	0.10	0.12	0.67	5.71	1.20				
Tm_2O_3	0.07	0.03	0.23		0.73	0.26				
Yb_2O_3	0.65	0.08		0.20	5.28	2.81				
F	0.71	0.39	5.13	3.19	0.12	0.15				35.06
n	3	67	16	3	32	6				

n- number of analysed grains; analyses with n ≥ 3 are from bulk samples from felsic dikes of the I&L zone used for a mineral separation test by Ucore. 1 - mineralized granitic dikes at the I&L zone (microprobe analyses done at McGill University); 2 - Bokan peralkaline granite - sample G244; 3 - mineralized granitic dike at the Geoduck zone -sample LM145; 4 - peralkaline granite dike at the I &L Zone - sample LM135, (microprobe anaylyses done at Dalhousie Univesity).

Table 2. Zircon U-Pb isotopic data for Bokan peralkaline granite (sample G245).

Fraction	Description	Weight (mg)	U (ppm)	Pb^T (pg)	Pb_C (pg)	Th/U	$^{206}Pb/^{204}Pb$	$^{206}Pb/^{238}U$	± 2σ	$^{207}Pb/^{235}U$	± 2σ	$^{207}Pb/^{206}Pb$	± 2σ	Ages (Ma) $^{206}Pb/^{238}U$	± 2σ	$^{207}Pb/^{235}U$	± 2σ	$^{207}Pb/^{206}Pb$	± 2σ	Disc. (%)
Z1	1 cls to pale brn euh pr	1.9	1795	49.89	2.76	0.346	1182	0.027898	±0.00005417	0.19052	±0.0021118	0.049531	±0.0005066	177.4	±0.339780038	177.1	±1.801	173.0	±23.93	-2.54
Z2	1 cls to pale brn euh pr	1.8	1188	33.37	1.37	0.396	1560	0.027809	±0.00005082	0.19081	±0.0016170	0.049765	±0.0003842	176.8	±0.318761128	177.3	±1.37	184.0	±18.01	3.96
Z3	1 cls to pale brn euh pr tip	1.0	797	22.06	1.04	0.335	1381	0.027876	±0.00005128	0.19121	±0.0018371	0.049748	±0.0004389	177.2	±0.321676878	177.7	±1.566	183.3	±20.59	3.33
Z4	1 cls to pale brn euh pr	0.8	1103	31.99	0.93	0.368	1453	0.027846	±0.00005094	0.19076	±0.0017394	0.049681	±0.000402	177.1	±0.321676878	177.3	±1.44	180.1	±19.05	1.75
Z5	1 cls to pale brn euh pr	0.9	995	42.99	0.93	0.373	1612	0.027881	±0.00005199	0.19061	±0.0018339	0.049573	±0.000431	177.3	±0.330173264	177.1	±1.56	175.0	±20.12	-1.01

Notes:

All analyzed fractions represent best quality grains of zircon, free of cores and, as much as possible, cracks. Minor inclusions (fluid? melt? opaques) are ubiquitous in all grains.

Abbreviations: cls - colorless; brn - brown; pr - prism; euh - euhedral

Pb^T is total amount (in picograms) of Pb.

Pb_C is total measured common Pb (in picograms) assuming the isotopic composition of laboratory blank: 206/204 - 18.221; 207/204 - 15.612; 208/204 - 39.360 (errors of 2%).

Pb/U atomic ratios are corrected for spike, fractionation, blank, and, where necessary, initial common Pb; 206Pb/204Pb is corrected for spike and fractionation.

Th/U is model value calculated from radiogenic $^{208}Pb/^{206}Pb$ ratio and $^{207}Pb/^{206}Pb$ age, assuming concordance.

Disc. (%) - per cent discordance for the given $^{207}Pb/^{206}Pb$ age.

Table 3. LA-ICP-MS U-Pb isotopic data of zircons from a Paleozoic quartz monzonite (sample H835).

	corrected ages (Ma)		corrected ratios			
	$^{206}Pb/^{238}U$		$^{207}Pb/^{235}U$		$^{206}Pb/^{238}U$	
Grain:		1σ		1σ		1σ
ALK1-01	465	9	0.57541	0.01370	0.07477	0.00158
ALK1-02	462	9	0.57646	0.01301	0.07438	0.00156
ALK1-03	478	9	0.59384	0.01340	0.07689	0.00156
ALK1-04	464	9	0.58242	0.01341	0.07465	0.00158
ALK1-05	375	7	0.46565	0.01049	0.05988	0.00122
ALK1-06	463	9	0.58428	0.01348	0.07450	0.00158
ALK1-07	471	9	0.58477	0.01425	0.07576	0.00154
ALK1-08	450	9	0.56039	0.01397	0.07237	0.00155
ALK1-09	469	10	0.58376	0.01357	0.07546	0.00160
ALK1-10	476	10	0.59781	0.01425	0.07671	0.00164
ALK1-11	468	10	0.58446	0.01394	0.07532	0.00161
ALK1-12	463	10	0.58025	0.01354	0.07445	0.00159
ALK1-13	474	10	0.59942	0.01395	0.07634	0.00163
ALK1-14	481	10	0.60061	0.01488	0.07741	0.00172
ALK1-15	457	9	0.56763	0.01334	0.07343	0.00157
ALK1-16	469	10	0.58287	0.01389	0.07546	0.00161
ALK1-17	479	10	0.62040	0.01466	0.07707	0.00159
ALK1-18	465	10	0.58662	0.01386	0.07473	0.00159
ALK1-19	471	10	0.59267	0.01442	0.07576	0.00161
ALK1-20	478	10	0.61157	0.01511	0.07705	0.00167
ALK1-21	480	11	0.61275	0.01667	0.07731	0.00179
ALK1-22	470	10	0.59394	0.01394	0.07555	0.00160
ALK1-23	476	10	0.59397	0.01395	0.07664	0.00159
ALK1-24	473	9	0.59773	0.01474	0.07607	0.00157

Table 4. $^{40}A/^{39}Ar$ analyses of amphiboles and whole-rocks from the Bokan complex and associated dikes.

(a) Amphibole (arfvedsonite) from peralkaline granite of the core of the Bokan complex (sample G242).

Volume 39K: 1542.4 x 0.000000000001 cm3 NTP — J Value: 0.01688 ± 0.000044

Integrated Age: 175.23 ± 0.65 Ma

Initial 40/36: 369.52 ± 273.27 (MSWD = 0.78, isochron between 0.42 and 2.15)

Correlation Age: 175.06 ± 1.68 Ma (75.3% of ^{39}Ar, steps marked by >) — MSWD 0.616

Plateau Age: 175.49 ± 0.62 Ma (75.3% of ^{39}Ar, steps marked by <) — Mod. Err. 0.51

Isotope Correlation data

Power	$^{36}Ar/^{40}Ar$	$^{39}Ar/^{40}Ar$	r	Ca/K	%40Atm	$\%^{39}Ar$	$^{40}Ar^*/^{39}K$	Age		
1.8	0.002039 ± 0.000481	0.020484 ± 0.000724	0.006	4.450	60.18	0.05	19.42 ± 7.24	511.60	±	166.10
2	0.002595 ± 0.000634	0.013616 ± 0.000867	0.005	0.000	76.64	0.02	17.13 ± 13.97	458.30	±	330.00
2.5	0.001581 ± 0.000228	0.096963 ± 0.001026	0.008	0.097	46.58	0.52	5.50 ± 0.70	160.00	±	19.50
2.9	0.000303 ± 0.000019	0.152142 ± 0.000464	0.005	0.140	8.91	24.08	5.98 ± 0.04	173.60	±	1.20
<3.00>	0.000051 ± 0.000020	0.163078 ± 0.000583	-0.002	0.134	1.49	7.59	6.04 ± 0.04	175.20	±	1.20
<3.10>	0.000027 ± 0.000016	0.163608 ± 0.000519	-0.001	0.136	0.79	10.10	6.06 ± 0.03	175.80	±	1.00
<3.20>	0.000036 ± 0.000015	0.164020 ± 0.000516	0	0.147	1.03	17.31	6.03 ± 0.03	175.00	±	0.90
<3.30>	0.000055 ± 0.000032	0.162556 ± 0.000715	-0.002	0.156	1.60	4.70	6.05 ± 0.06	175.50	±	1.80
<3.40>	0.000047 ± 0.000015	0.162978 ± 0.000506	-0.002	0.167	1.37	11.20	6.05 ± 0.03	175.50	±	0.90
<3.50>	0.000023 ± 0.000026	0.163071 ± 0.000640	-0.003	0.113	0.67	5.68	6.09 ± 0.05	176.60	±	1.50
<3.60>	0.000021 ± 0.000032	0.164238 ± 0.000588	-0.001	0.120	0.60	7.61	6.05 ± 0.06	175.50	±	1.70
<.00>	0.000023 ± 0.000016	0.163947 ± 0.000483	-0.001	0.151	0.66	11.13	6.06 ± 0.04	175.70	±	1.00

Table 4. $^{40}A/^{39}Ar$ analyses of amphiboles and whole-rocks from the Bokan Mountain complex and associated dikes.

(b) Amphibole from a granitic dike associated with the mineralization at the Ross-Adams deposit (sample LM24).

Volume 39K: 912.57 x 0.000000000001 cm3 NTP — J Value: 0.01684 ± 0.000034

Integrated Age: 175.78 ± 0.82 Ma

Initial 40/36: 298.14 ± 71.61 (MSWD = 2.14, isochron between 0.18 and 2.63)

Correlation Age: 176.21 ± 2.99 Ma ((54.00% of 39Ar, steps marked by >) — MSWD 1.606

Plateau Age: 175.28 ± 0.81 Ma (54.00% of 39Ar, steps marked by <) — Mod. Err. 0.88

Isotope Correlation data

Power	$^{36}Ar/^{40}Ar$	$^{39}Ar/^{40}Ar$	r	Ca/K	%40Atm	$\%^{39}Ar$	$^{40}Ar^*/^{39}K$	Age
2	0.002520 ± 0.000161	0.009082 ± 0.000308	0.004	0.471	74.40	0.22	28.16 ± 5.36	700.20 ± 110.50
2.4	0.001514 ± 0.000185	0.081014 ± 0.000952	0.006	0.330	44.60	0.80	6.82 ± 0.68	196.30 ± 18.50
2.7	0.000747 ± 0.000126	0.144218 ± 0.001241	0.001	0.462	21.96	1.93	5.40 ± 0.26	157.10 ± 7.40
2.9	0.000344 ± 0.000063	0.159449 ± 0.000918	0.002	0.339	10.10	4.11	5.64 ± 0.12	163.60 ± 3.40
3	0.000359 ± 0.000071	0.156274 ± 0.000982	0.001	0.305	10.54	3.65	5.72 ± 0.14	166.00 ± 3.90
<3.10>	0.000209 ± 0.000048	0.156112 ± 0.000764	0	0.285	6.13	5.58	6.01 ± 0.10	174.00 ± 2.70
<3.20>	0.000142 ± 0.000032	0.156170 ± 0.000732	0	0.299	4.17	7.93	6.14 ± 0.07	177.40 ± 1.90
<3.30>	0.000327 ± 0.000031	0.148951 ± 0.000580	0.002	0.407	9.60	9.58	6.07 ± 0.07	175.50 ± 1.80
<3.40>	0.000370 ± 0.000030	0.145266 ± 0.000514	0.004	0.469	10.87	10.50	6.13 ± 0.07	177.30 ± 1.80
<3.50>	0.000197 ± 0.000015	0.154504 ± 0.000483	0.005	0.344	5.77	20.40	6.10 ± 0.04	176.30 ± 1.00
6	0.000235 ± 0.000021	0.154549 ± 0.000522	0.003	0.397	6.90	35.30	6.02 ± 0.05	174.20 ± 1.30

Table 4. $^{40}A/^{39}Ar$ analyses of amphiboles and whole-rocks from the Bokan complex and associated dikes.

(c) Amphibole from lamprophyric dike crosscutting granite of the Dotson Zone (sample LM79).

Volume 39K: 1531.58 x 0.000000000001 cm3 NTP — J Value: 0.016847 ± 0.000034

Integrated Age: 106.31 ± 0.52 Ma

Initial 40/36: 713.57 ± 273.74 (MSWD = 0.85, isochron between 0.53 and 1.506)

Correlation Age: 100.54 ± 3.55 Ma ((88.20% of ^{39}Ar, steps marked by >) — MSWD 1.506

Plateau Age: 105.18 ± 0.62 Ma (51.40% of ^{39}Ar, steps marked by <) — Mod. Err. 0.66

Isotope Correlation data

Power	$^{36}Ar/^{40}Ar$	$^{39}Ar/^{40}Ar$	r	Ca/K	$\%^{40}Atm$	$\%^{39}Ar$	$^{40}Ar^*/^{39}K$	Age
2	0.002325 ± 0.000517	0.086018 ± 0.001849	0.011	1.238	68.46	0.19	3.65 ± 1.78	107.5 ± 51.0
2.4	0.001019 ± 0.000459	0.253269 ± 0.003427	0.002	1.473	29.83	0.64	2.76 ± 0.54	82.0 ± 15.6
2.7	0.000445 ± 0.000235	0.277691 ± 0.002144	-0.001	1.978	13.03	1.57	3.13 ± 0.25	92.6 ± 7.3
2.9	0.000312 ± 0.000135	0.268747 ± 0.001678	-0.002	2.184	9.14	2.34	3.38 ± 0.15	99.9 ± 4.3
3	0.000186 ± 0.000051	0.258584 ± 0.001052	0.000	2.119	5.45	7.01	3.65 ± 0.06	107.8 ± 1.7
3.10>	0.000137 ± 0.000094	0.259172 ± 0.001640	-0.002	1.303	4.02	3.06	3.70 ± 0.11	109.1 ± 3.2
<3.20>	0.000179 ± 0.000082	0.264130 ± 0.001296	-0.001	1.048	5.24	4.14	3.59 ± 0.09	105.8 ± 2.7
<3.30>	0.000143 ± 0.000077	0.267736 ± 0.001227	-0.002	0.603	4.18	3.91	3.58 ± 0.09	105.6 ± 2.5
<3.40>	0.000163 ± 0.000067	0.272243 ± 0.001336	-0.002	0.189	4.76	4.33	3.50 ± 0.07	103.3 ± 2.1
<3.50>	0.000164 ± 0.000072	0.270337 ± 0.001379	-0.003	0.130	4.81	4.16	3.52 ± 0.08	103.9 ± 2.3
<3.70>	0.000086 ± 0.000025	0.275169 ± 0.000874	0.000	0.121	2.51	13.59	3.54 ± 0.03	104.6 ± 0.8
<3.90>	0.000114 ± 0.000048	0.268733 ± 0.001272	0.000	0.129	3.33	6.45	3.60 ± 0.06	106.1 ± 1.6
<4.10>	0.000092 ± 0.000045	0.270558 ± 0.000914	-0.002	0.399	2.69	7.97	3.60 ± 0.05	106.1 ± 1.5
4.30>	0.000100 ± 0.000045	0.270842 ± 0.001032	-0.002	1.886	2.86	6.83	3.59 ± 0.05	105.8 ± 1.5
4.80>	0.000170 ± 0.000025	0.257520 ± 0.000734	0.004	15.004	4.51	26.15	3.71 ± 0.03	109.3 ± 0.9
6.00>	0.000155 ± 0.000046	0.261991 ± 0.001033	0.000	13.357	4.07	7.66	3.66 ± 0.05	108.0 ± 1.5

Table 4. $^{40}A/^{39}Ar$ analyses of amphiboles and whole-rocks from the Bokan complex and associated dikes.

(d) Biotite-rich lamprophyric dike crosscutting granite at the I&L Zone (whole-rock sample LM73).

Volume 39K: 3209.25 x 0.000000000001 cm3 NTP — J Value: 0.016863 ± 0.000034

Integrated Age: 144.92 ± 0.45 Ma

Initial 40/36; 416.03 ± 228.09 (MSWD = 0.56, isochron between 0.18 and 2.63)

Correlation Age: 109.43 ± 19.74 Ma ((1.30% of ^{39}Ar, steps marked by >) — MSWD

Plateau Age: 152.49 ± 0.81 Ma (24.10% of ^{39}Ar, steps marked by <) — Mod. Err.

120.4 ± 6.18 Ma (0.70% of 39Ar, steps marked by [)

Isotope Correlation data

Power	$^{36}Ar/^{40}Ar$	$^{39}Ar/^{40}Ar$	r	Ca/K	%40Atm	$\%^{39}Ar$	$^{40}Ar^*/^{39}K$	Age
1.60>	0.002672 ± 0.001140	0.028658 ± 0.001933	0.009	1.417	78.84	0.01	7.36 ± 11.84	211.0 ± 320.4
2.00>	0.001948 ± 0.000323	0.055287 ± 0.001199	0.009	0.399	57.36	0.09	7.69 ± 1.74	220.1 ± 46.9
2.30>	0.001463 ± 0.000401	0.090492 ± 0.001600	0.006	0.473	43.02	0.12	6.28 ± 1.32	181.7 ± 36.2
2.60>	0.001050 ± 0.000273	0.160912 ± 0.001588	0.002	1.035	30.80	0.40	4.29 ± 0.50	126.0 ± 14.3
[2.80>	0.000630 ± 0.000145	0.198960 ± 0.001384	0.001	1.799	18.46	0.71	4.09 ± 0.22	120.4 ± 6.2
3	0.000333 ± 0.000069	0.209708 ± 0.001191	0.001	1.555	9.73	1.56	4.30 ± 0.10	126.3 ± 2.8
3.2	0.000182 ± 0.000050	0.208997 ± 0.000869	0.000	0.806	5.30	2.59	4.53 ± 0.07	132.8 ± 2.1
3.4	0.000120 ± 0.000024	0.202972 ± 0.000690	0.001	0.621	3.48	4.04	4.75 ± 0.04	139.1 ± 1.1
3.5	0.000088 ± 0.000031	0.198162 ± 0.000673	0.000	0.662	2.55	3.88	4.92 ± 0.05	143.7 ± 1.4
3.6	0.000070 ± 0.000033	0.208467 ± 0.000751	-0.001	0.353	2.02	3.21	4.70 ± 0.05	137.6 ± 1.4
3.7	0.000085 ± 0.000030	0.206498 ± 0.000918	-0.001	0.204	2.43	4.03	4.72 ± 0.05	138.3 ± 1.4
3.8	0.000064 ± 0.000027	0.206560 ± 0.000689	-0.001	0.229	1.82	3.65	4.75 ± 0.04	139.1 ± 1.2
3.9	0.000063 ± 0.000028	0.181302 ± 0.000750	-0.001	0.246	1.80	2.75	5.42 ± 0.05	157.7 ± 1.4
4	0.000093 ± 0.000042	0.201721 ± 0.001085	-0.001	0.342	2.69	2.57	4.82 ± 0.07	141.1 ± 1.9
4.2	0.000065 ± 0.000031	0.203304 ± 0.000860	-0.001	0.376	1.86	3.51	4.83 ± 0.05	141.2 ± 1.4
4.5	0.000058 ± 0.000022	0.205375 ± 0.000796	0.000	0.345	1.65	5.35	4.79 ± 0.04	140.1 ± 1.0
4.8	0.000065 ± 0.000022	0.203193 ± 0.000665	0.000	0.192	1.86	5.57	4.83 ± 0.04	141.2 ± 1.0
5.1	0.000028 ± 0.000011	0.198939 ± 0.000598	0.001	0.114	0.78	31.91	4.99 ± 0.02	145.7 ± 0.6
<6	0.000039 ± 0.000013	0.189052 ± 0.000647	0.001	0.153	1.11	24.07	5.23 ± 0.03	152.5 ± 0.8

Table 4. $^{40}A/^{39}Ar$ analyses of amphiboles and whole-rocks from the Bokancomplex and associated dikes.

(e) Dioritic dike crosscutting the Geoduck Zone (whole-rock sample LM143).

Volume 39K: 769.88 x 1E-12 cm3 NTP — J Value: 0.016852 ± 0.000034

Integrated Age: 212.90 ± 1.05 Ma

Initial 40/36: 401.58 ± 119.24 (MSWD = 2.59, isochron between 0.00 and 3.00)

Correlation Age: 314.34 ± 11.85 Ma (21.9% of ^{39}Ar, steps marked by >) — MSWD 2.605

Plateau Age: 327.28 ± 2.19 Ma (21.4% of ^{39}Ar, steps marked by <) — Mod. Err. 3.26

117.03 ± 6.08 Ma (3.5% of 39Ar, steps marked by [)

Isotope Correlation data

Power	$^{36}Ar/^{40}Ar$	$^{39}Ar/^{40}Ar$	r	Ca/K	%40Atm	$\%^{39}Ar$	$^{40}Ar^*/^{39}K$	Age
1.60>	0.002517 ± 0.000436	0.015791 ± 0.000754	0.005	3.690	74.29	0.07	16.26 ± 8.27	436.8 ± 197.3
2.10>	0.001861 ± 0.000131	0.020680 ± 0.000371	0.009	2.425	54.87	0.42	21.80 ± 1.93	564.6 ± 42.9
2.5	0.002033 ± 0.000162	0.061570 ± 0.000715	0.012	5.231	59.91	0.99	6.49 ± 0.78	187.3 ± 21.5
2.8	0.001700 ± 0.000128	0.109278 ± 0.000893	0.013	2.792	50.02	1.83	4.56 ± 0.35	133.5 ± 9.8
3.1	0.001613 ± 0.000124	0.125017 ± 0.000930	0.008	2.152	47.46	2.47	4.19 ± 0.30	123.0 ± 8.4
[3.40	0.001482 ± 0.000101	0.141388 ± 0.000943	0.012	2.028	43.58	3.54	3.98 ± 0.21	117.0 ± 6.1
3.7	0.000978 ± 0.000062	0.164915 ± 0.000829	0.008	2.655	28.69	6.75	4.32 ± 0.11	126.6 ± 3.2
4	0.000629 ± 0.000046	0.182756 ± 0.000729	0.005	2.981	18.41	11.67	4.46 ± 0.08	130.7 ± 2.2
4.3	0.000535 ± 0.000041	0.154439 ± 0.000644	0.005	5.678	15.62	9.19	5.46 ± 0.08	158.8 ± 2.3
4.5	0.000483 ± 0.000020	0.129051 ± 0.000451	0.008	5.785	14.02	19.34	6.66 ± 0.05	191.9 ± 1.4
4.7	0.000437 ± 0.000028	0.107983 ± 0.000369	0.004	6.864	12.63	17.36	8.09 ± 0.08	230.5 ± 2.2
4.9	0.000375 ± 0.000049	0.107693 ± 0.000559	0.003	7.241	10.79	5.01	8.28 ± 0.14	235.7 ± 3.8
< 5.10>	0.000285 ± 0.000026	0.078407 ± 0.000343	0.003	10.514	8.06	8.06	11.72 ± 0.11	325.3 ± 2.8
< 6.00>	0.000367 ± 0.000026	0.075488 ± 0.000289	0.003	13.679	10.51	13.30	11.85 ± 0.11	328.5 ± 2.9

Table 5a. Composition of representative granitic rocks of the Bokan complex

Sample	G151	G154	G155	G156	G157	G158	G159	G160	G161	G162	G163	G164
(wt%)												
SiO_2	74.83	73.25	72.75	73.97	74.05	73.04	72.29	73.90	74.23	74.84	74.25	73.08
TiO_2	0.12	0.18	0.12	0.18	0.16	0.16	0.15	0.11	0.10	0.11	0.15	0.12
Al_2O_3	11.63	11.68	11.26	11.19	11.45	11.55	11.55	11.15	11.24	11.62	10.51	11.45
Fe_2O_3	3.91	4.34	4.61	4.05	3.94	4.00	4.72	3.69	3.53	3.82	4.36	4.58
MnO	0.08	0.08	0.08	0.05	0.06	0.06	0.08	0.08	0.03	0.05	0.05	0.04
MgO	0.02	0.01	0.02	0.01	0.02	0.02	0.02	0.01	0.01	0.03	0.02	0.01
CaO	0.11	0.12	0.06	0.02	0.30	0.08	0.10	0.04	0.24	0.03	0.03	0.11
Na_2O	5.51	4.52	4.97	4.35	4.70	4.85	4.64	4.81	5.25	4.94	4.37	4.72
K_2O	3.56	4.13	4.53	4.55	4.30	4.22	4.32	4.18	3.47	4.11	4.24	4.39
P_2O_5	0.03	0.01	0.01	0.01	0.01	0.02	0.01	0.01	0.01	0.01	0.01	0.01
LOI	0.34	0.57	0.19	0.49	0.80	0.53	0.74	0.36	0.29	0.31	0.38	0.48
Total	100.15	98.89	98.60	98.87	99.80	98.53	98.61	98.34	98.40	99.87	98.37	98.99
(ppm)												
Pb	21	16	14	47	28	14	27	16	81	15	42	24
Zn	170	190	310	330	190	110	320	190	220	100	200	280
Sn	30	12	15	25	24	17	18	17	25	26	19	17
Rb	229	186	210	218	171	178	197	297	240	279	251	306
Cs	0.90	0.50	0.60	0.60	0.30	0.40	0.50	1.10	0.60	0.70	1.10	1.00
Ba	49	37	23	29	44	62	19	36	19	26	33	40
Sr	9	6	3	4	29	4	6	3	13	3	2	9
Ga	39	40	42	41	40	38	43	40	42	38	39	42
Ta	7.74	4.64	3.49	7.32	5.44	5.52	3.73	2.99	9.47	6.34	5.45	3.15
Nb	105.0	63.1	34.9	117.0	68.3	77.0	36.9	36.0	137.0	87.2	70.6	49.0
Hf	34.60	23.70	26.80	29.50	39.80	42.40	23.10	81.10	58.30	64.20	50.70	29.60
Zr	1520	1220	1080	1310	1880	2030	909	3720	2750	3000	2470	1400
Y	182	92	32	52	211	129	94	253	264	150	39	76
Th	57.90	24.30	18.20	24.00	48.00	30.30	18.40	14.00	43.10	19.00	27.00	21.20
U	14.90	9.75	7.63	7.97	11.30	12.80	6.69	8.27	23.70	15.90	11.80	8.63
La	83.90	154.00	33.50	74.30	82.70	39.40	140.00	84.70	131.00	36.90	96.50	42.10
Ce	174.00	315.00	76.50	189.00	191.00	89.20	246.00	217.00	215.00	92.70	189.00	97.60
Pr	22.40	33.90	8.17	24.20	24.70	11.00	27.70	26.20	46.40	12.40	21.00	12.60
Nd	98.80	138.00	29.30	111.00	114.00	48.20	102.00	126.00	228.00	58.30	83.30	58.50
Sm	25.50	26.10	5.26	26.10	31.30	12.70	18.60	34.00	70.80	17.30	14.60	16.10
Eu	2.50	2.22	0.42	2.20	3.22	1.25	1.60	3.39	8.95	1.81	1.18	1.60
Gd	27.30	19.70	3.38	19.80	34.90	14.00	14.20	37.90	68.60	20.30	10.10	17.10
Tb	5.40	3.32	0.73	3.00	6.86	3.30	2.51	7.06	11.90	4.88	1.68	3.20
Dy	33.20	20.50	5.38	16.80	44.30	25.30	15.90	44.50	66.60	35.80	10.50	19.20
Ho	7.00	4.64	1.41	3.40	9.86	6.32	3.64	10.30	13.70	8.81	2.44	4.14
Er	19.70	15.90	5.47	10.40	29.50	20.00	11.30	31.80	40.20	29.40	8.85	12.70
Tm	3.25	3.37	1.25	1.93	4.88	3.59	1.99	5.64	7.02	5.58	2.00	2.39
Yb	20.70	26.20	11.10	14.20	28.80	23.60	14.40	37.40	45.00	37.90	16.90	17.00
Lu	2.82	3.99	1.96	2.20	3.78	3.43	2.25	5.52	5.91	5.36	2.88	2.57

Table 5a. Composition of representative granitic rocks of the Bokan complex

Sample	G166	G167	G168	G169	G172	G230	G231	G232	G233	G234	G235	G236
(wt%)												
SiO_2	73.04	73.72	74.62	73.94	74.40	73.94	74.11	74.45	74.72	73.94	75.27	75.23
TiO_2	0.10	0.14	0.13	0.15	0.18	0.14	0.26	0.13	0.10	0.13	0.12	0.10
Al_2O_3	11.33	11.07	10.75	11.29	11.55	11.03	11.02	10.73	10.17	10.76	11.54	11.34
Fe_2O_3	4.03	4.09	3.99	4.20	4.51	4.15	4.35	4.83	4.45	4.35	4.16	4.43
MnO	0.07	0.05	0.05	0.01	0.04	0.04	0.03	0.09	0.08	0.03	0.02	0.05
MgO	0.03	0.03	0.02	0.01	0.03	0.01	0.01	0.02	0.02	0.02	0.02	0.02
CaO	0.03	0.04	0.02	0.17	0.06	0.02	0.34	0.06	0.05	0.07	0.11	0.04
Na_2O	4.11	5.02	4.81	3.95	5.34	5.06	4.17	6.16	4.61	5.66	5.93	5.25
K_2O	5.62	3.96	3.99	4.45	4.45	4.49	4.81	2.27	3.64	3.49	3.30	4.05
P_2O_5	0.01	0.02	0.01	0.01	0.02	0.01	0.01	0.01	1.00	0.01	0.01	0.01
LOI	0.34	0.37	0.33	0.40	0.33	0.28	0.72	0.29	0.25	0.33	0.30	0.19
Total	98.71	98.51	98.72	98.58	100.91	99.17	99.83	99.04	99.10	98.79	100.79	100.71
(ppm)												
Pb	7	16	9	29	43	32	14	12	13	22	8	11
Zn	270	140	160	110	80	110	220	250	170	80	40	160
Sn	9	19	17	22	23	33	17	18	16	17	19	19
Rb	393	248	217	187	269	288	249	128	178	194	197	238
Cs	1.20	1.00	0.80	0.30	0.50	0.40	0.70	0.80	0.40	0.60	0.40	0.60
Ba	45	31	27	23	16	29	29	28	22	28	19	29
Sr	3	3	1	8	6	1	10	6	3	4	8	4
Ga	43	38	40	42	38	40	35	46	36	40	44	43
Ta	1.52	6.05	3.61	5.00	10.20	4.13	5.76	5.03	3.19	2.93	5.32	4.65
Nb	15.5	41.6	52.3	62.2	165.0	49.8	67.5	70.9	30.0	45.0	83.6	57.7
Hf	10.20	86.40	35.90	29.40	71.30	55.90	52.10	34.40	77.10	25.20	26.00	28.60
Zr	380	4480	1670	1450	3640	2300	2250	1350	3020	1050	1040	1150
Y	14	150	36	121	77	65	349	107	148	61	88	34
Th	6.79	42.70	22.20	20.80	16.60	20.20	25.60	54.60	11.60	16.00	38.50	11.40
U	2.27	23.90	7.30	11.50	27.40	18.70	22.10	9.81	15.80	9.05	14.20	11.00
La	21.00	89.30	59.80	69.30	0.00	95.40	64.80	129.00	38.10	84.70	106.00	36.40
Ce	40.70	204.00	123.00	163.00	269.00	194.00	130.00	279.00	94.70	176.00	240.00	95.70
Pr	4.57	25.30	14.30	21.20	29.90	19.70	17.20	30.50	9.40	20.10	29.50	10.90
Nd	16.50	113.00	57.90	97.70	124.00	67.20	74.90	110.00	36.60	77.80	115.00	39.60
Sm	2.85	26.40	9.56	25.90	20.10	10.10	26.30	17.70	9.02	16.50	25.00	6.64
Eu	0.26	2.37	0.75	2.43	1.44	0.78	3.16	1.33	0.95	1.41	2.12	0.53
Gd	1.97	24.20	6.61	23.30	11.00	6.01	38.00	11.60	10.40	11.70	16.60	4.35
Tb	0.41	5.09	1.22	4.26	2.72	1.39	8.37	2.32	2.62	2.01	2.91	0.95
Dy	3.16	36.50	8.84	27.00	23.70	11.90	56.00	17.80	20.70	13.00	19.10	7.40
Ho	0.84	8.70	2.24	6.15	6.88	3.70	13.90	4.76	5.70	2.98	4.71	1.84
Er	3.39	28.40	8.54	19.40	28.90	17.70	50.10	18.30	21.00	8.95	17.50	6.67
Tm	0.76	5.39	1.91	3.62	7.18	5.08	10.60	3.86	4.32	1.94	3.71	1.38
Yb	7.15	37.60	15.10	24.10	59.80	45.40	79.10	29.60	31.61	14.00	27.90	11.00
Lu	1.30	5.46	2.50	3.44	9.22	7.16	11.80	4.45	4.77	2.19	4.11	1.78

Table 5a. Composition of representative granitic rocks of the Bokan complex

Sample	G237	G238	G239	G240	G241	G242	G243	G244	G245	G246
(wt%)										
SiO_2	74.90	76.95	76.44	74.22	77.56	72.09	73.95	72.83	73.02	72.67
TiO_2	0.16	0.12	0.11	0.17	0.12	0.14	0.16	0.13	0.20	0.17
Al_2O_3	11.87	10.28	10.84	11.86	9.20	11.08	11.98	12.02	12.27	12.33
Fe_2O_3	3.75	4.19	4.63	4.18	5.99	5.32	4.52	3.63	3.43	3.39
MnO	0.04	0.03	0.01	0.09	0.13	0.11	0.06	0.08	0.09	0.07
MgO	0.02	0.02	0.01	0.02	0.01	0.02	0.02	0.02	0.02	0.02
CaO	0.29	0.04	0.02	0.17	0.05	0.06	0.03	0.07	0.06	0.27
Na_2O	4.99	4.15	4.04	4.77	6.66	5.16	4.76	5.35	5.62	5.48
K_2O	4.37	3.83	3.96	4.38	0.51	4.41	5.15	4.05	3.99	3.90
P_2O_5	0.01	0.02	0.01	0.02	0.01	0.01	0.01	0.01	0.01	0.10
LOI	0.39	0.25	0.44	0.55	0.25	0.32	0.12	0.30	0.33	0.45
Total	100.79	99.87	100.51	100.44	100.49	98.71	100.76	98.49	99.04	98.85
(ppm)										
Pb	29	9	11	88	18	32	7	48	37	46
Zn	300	130	60	220	390	330	160	300	200	180
Sn	19	13	20	23	10	21	18	22	33	14
Rb	223	194	191	243	18	307	324	238	224	198
Cs	0.90	0.70	0.90	0.70	1.00	1.80	1.30	0.80	1.10	1.70
Ba	26	34	25	114	6	29	28	46	55	82
Sr	15	3	1	13	1	3	1	5	5	10
Ga	44	41	42	45	45	45	39	43	40	40
Ta	4.31	2.82	3.68	4.22	2.36	5.03	2.38	4.72	6.32	6.02
Nb	58.6	39.1	51.9	58.5	36.3	64.8	37.0	44.5	83.0	74.5
Hf	45.30	23.80	27.90	39.80	14.20	72.90	17.80	37.90	45.90	32.90
Zr	1840	931	1060	1530	607	2720	707	1430	1810	1080
Y	111	37	46	131	30	341	43	113	238	286
Th	17.10	21.40	27.70	29.50	13.50	23.40	16.90	21.20	39.50	49.60
U	14.30	6.73	8.72	15.60	5.99	17.40	5.32	8.54	20.00	27.20
La	73.80	56.60	48.70	205.00	33.30	110.00	21.40	70.80	113.00	113.00
Ce	172.00	137.00	121.00	450.00	109.00	200.00	55.80	168.00	322.00	314.00
Pr	23.40	17.50	14.90	52.30	7.52	34.90	4.76	17.30	31.00	37.90
Nd	95.30	67.70	58.50	208.00	23.90	144.00	17.10	65.80	124.00	154.00
Sm	23.00	13.80	11.60	40.50	3.85	42.70	3.48	14.80	31.70	44.30
Eu	2.05	1.11	0.94	3.41	0.34	4.46	0.34	1.41	3.12	4.48
Gd	18.40	8.68	8.20	31.00	2.78	47.00	3.30	14.00	32.20	43.30
Tb	3.10	1.39	1.58	5.06	0.68	10.30	0.87	3.07	6.49	9.29
Dy	19.90	8.52	11.00	30.40	5.70	66.60	6.97	21.30	42.10	58.40
Ho	5.21	1.94	2.64	8.25	1.63	14.90	1.83	5.07	9.39	12.20
Er	19.70	7.00	9.38	19.10	6.94	45.50	6.44	16.10	28.10	35.60
Tm	4.17	1.59	1.94	3.40	1.77	7.88	1.31	2.96	4.55	6.12
Yb	30.10	13.30	15.50	24.10	15.00	51.80	10.00	20.40	28.30	40.20
Lu	4.33	2.20	2.41	3.43	2.42	7.39	1.58	3.06	3.74	4.92

Table 5b. Composition of representative granitic rocks from I&L, Dotson and Geoduck zones

Sample	LM11	LM12	LM13	LM14	LM15	LM16	LM17	LM18	LM19	LM93	LM94	LM95
(wt%)												
SiO_2	79.27	70.25	69.67	74.14	73.56	74.51	73.67	76.27	73.86	72.53	74.65	73.76
TiO_2	0.06	0.36	0.34	0.13	0.14	0.15	0.15	0.06	0.16	0.15	0.45	0.14
Al_2O_3	8.68	13.84	14.24	11.23	10.69	10.72	10.97	12.17	11.50	11.32	9.00	11.10
Fe_2O_3	3.52	3.37	3.27	3.72	4.13	4.22	4.12	1.30	4.46	5.27	6.84	4.52
MnO	0.05	0.10	0.12	0.14	0.07	0.04	0.08	0.02	0.14	0.04	0.12	0.02
MgO	0.01	0.36	0.32	0.02	0.01	0.01	0.01	0.09	0.03	0.02	0.03	0.01
CaO	0.10	1.07	0.99	0.18	0.30	0.28	0.40	0.72	0.58	0.38	0.37	0.51
Na_2O	4.16	4.80	4.87	3.52	4.45	5.25	4.49	4.06	4.53	4.15	6.72	3.99
K_2O	2.87	4.17	4.36	5.44	4.58	3.75	4.75	4.06	3.38	4.50	0.35	4.26
P_2O_5	0.01	0.13	0.10	0.04	0.01	0.01	0.01	0.01	0.01	0.01	0.01	0.01
LOI	0.26	0.50	0.55	0.51	0.50	0.47	0.58	0.69	0.78	0.50	0.52	0.45
Total	98.99	98.94	98.83	99.07	98.44	99.40	99.23	99.45	99.43	98.87	99.06	98.77
(ppm)												
Pb	11	10	13	5	52	6	8	5	9	10	5	15
Zn	150	40	50	50	300	210	260	230	290	140	210	250
Sn	9	8	7	16	22	28	20	1	30	14	5	21
Rb	171	139	159	222	236	180	234	75	141	206	12	182
Cs	0.30	3.50	4.70	0.40	0.40	0.30	0.40	0.20	0.20	0.40	0.10	0.40
Ba	9	612	668	43	26	28	24	273	32	45	5	43
Sr	6	129	131	10	9	10	20	39	37	27	16	24
Ga	39	19	21	36	37	40	39	14	43	37	37	41
Ta	2.38	2.27	2.24	5.33	10.90	11.10	10.70	0.60	15.50	7.18	0.36	2.89
Nb	30.6	29.6	28.0	90.7	180.0	166.0	180.0	5.3	237.0	96.9	15.9	53.5
Hf	24.80	9.70	9.20	29.00	29.40	47.90	42.90	3.90	21.90	7.80	3.70	11.70
Zr	1220	386	343	1420	1270	2160	1990	85	1240	249	131	369
Y	104	58	65	239	237	244	263	41	405	269	33	429
Th	27.20	21.50	26.70	186.00	44.80	17.60	22.40	13.00	47.10	29.70	5.42	17.20
U	6.38	8.28	9.67	17.90	20.90	20.00	20.80	4.12	33.90	11.90	0.77	5.45
La	38.30	33.70	39.00	63.20	79.60	101.00	95.00	12.70	231.00	68.70	6.82	95.90
Ce	78.70	71.10	80.60	158.00	187.00	241.00	224.00	30.70	616.00	164.00	15.30	221.00
Pr	12.00	8.60	9.47	21.00	23.20	30.30	27.90	4.06	69.10	21.50	2.18	28.50
Nd	58.10	36.50	39.90	96.40	102.00	137.00	124.00	19.60	306.00	99.30	11.10	130.00
Sm	17.70	8.37	8.83	25.20	29.30	37.70	34.80	5.25	76.20	29.40	3.30	38.60
Eu	1.80	1.27	1.40	2.61	3.14	3.82	3.49	0.46	7.21	3.18	0.35	4.27
Gd	20.90	8.42	8.95	30.00	34.90	40.30	36.20	5.98	73.80	35.70	3.83	50.70
Tb	4.15	1.59	1.70	6.81	7.75	8.01	7.84	1.14	13.30	7.53	0.72	10.60
Dy	25.40	10.10	11.00	48.40	51.80	49.50	52.50	7.44	77.90	48.50	4.68	67.00
Ho	5.18	2.33	2.50	12.00	11.20	10.30	11.90	1.71	15.80	10.40	1.13	14.10
Er	13.80	7.10	7.72	40.20	30.60	27.30	33.00	5.32	43.20	28.10	3.93	36.40
Tm	2.08	1.27	1.37	7.39	4.39	4.01	4.86	1.00	6.91	4.01	0.92	5.09
Yb	12.60	8.55	9.00	47.00	25.70	23.60	27.50	7.04	42.20	23.20	7.90	28.80
Lu	1.77	1.25	1.32	6.63	3.62	3.28	3.72	1.05	5.61	3.18	1.58	4.10

Table 5b. Composition of representative granitic rocks from I&L, Dotson and Geoduck zones

Sample	LM96	LM97	LM99	LM100	LM101	LM102	LM103	LM105	LM106	LM135	LM145
(wt%)											
SiO_2	73.29	72.46	73.58	73.54	73.95	75.20	74.55	73.22	76.76	76.56	73.35
TiO_2	0.19	0.18	0.16	0.15	0.17	0.11	0.14	0.11	0.09	0.04	0.15
Al_2O_3	9.50	11.27	10.93	10.84	7.92	11.65	10.53	10.95	10.97	12.14	10.65
Fe_2O_3	6.89	3.92	4.08	4.36	4.97	3.42	4.56	4.57	3.33	0.67	4.82
MnO	0.09	0.02	0.05	0.08	0.04	0.03	0.05	0.07	0.04	0.01	0.03
MgO	0.01	0.01	0.01	0.01	0.01	0.02	0.01	0.02	0.02	0.03	0.02
CaO	0.20	1.45	0.36	0.37	0.31	0.27	0.88	0.43	0.29	0.04	0.30
Na_2O	5.69	3.94	5.09	5.10	2.47	4.90	3.84	4.87	3.68	4.71	4.59
K_2O	2.99	4.22	4.02	4.02	6.03	3.73	3.75	3.73	4.08	3.55	4.28
P_2O_5	0.01	0.01	0.01	0.02	0.01	0.01	0.01	0.01	0.02	0.01	0.01
LOI	0.59	0.95	0.53	0.51	0.56	0.40	0.92	0.57	0.93	0.47	0.51
Total	99.45	98.43	98.82	99.01	96.44	99.73	99.24	98.56	100.21	98.23	98.71
(ppm)											
Pb	18	13	40	7	18	8	8	16	25	11	7
Zn	220	90	340	290	260	140	240	190	290	10	300
Sn	30	29	29	25	36	11	18	16	9	6	29
Rb	162	212	224	223	323	246	197	196	219	138	225
Cs	0.40	0.40	0.50	0.80	0.70	0.60	0.30	0.90	0.70	0.90	0.40
Ba	23	20	31	27	46	44	15	20	25	37	35
Sr	9	33	19	1616	9	15	18	28	14	12	8
Ga	38	36	43	39	28	39	39	40	43	21	41
Ta	4.09	4.03	9.34	7.25	6.04	2.48	0.00	0.00	0.00	2.78	8.58
Nb	69.8	60.6	134.0	113.0	60.4	39.0	62.2	58.3	49.5	18.8	119.0
Hf	11.50	50.10	58.00	60.80	672.00	11.80	57.60	15.50	5.80	7.20	37.90
Zr	376	2450	2520	2990	30000	416	2920	649	254	177	1820
Y	98	151	149	194	777	230	144	110	125	55	294
Th	12.80	28.60	59.00	25.80	64.30	10.60	22.80	22.20	25.20	30.30	49.00
U	8.81	17.00	16.60	22.00	52.10	7.44	26.00	7.81	7.12	12.90	23.00
La	57.40	95.00	345.00	138.00	74.60	45.40	96.40	106.00	267.00	7.43	178.00
Ce	139.00	202.00	846.00	366.00	161.00	112.00	213.00	227.00	577.00	23.20	431.00
Pr	18.00	24.40	92.80	47.10	20.60	15.10	26.30	27.40	56.70	3.81	54.40
Nd	81.80	108.00	408.00	214.00	97.70	73.10	117.00	119.00	228.00	19.70	246.00
Sm	21.00	26.20	90.10	61.30	26.50	20.10	27.80	25.20	41.10	6.80	62.90
Eu	1.98	2.42	7.66	5.68	2.79	2.02	2.54	2.33	3.42	0.38	5.74
Gd	19.90	24.50	64.60	57.90	36.60	23.40	24.80	23.20	31.70	7.84	55.90
Tb	3.67	4.34	8.55	8.68	10.20	5.56	4.57	4.12	4.91	1.61	9.82
Dy	22.10	29.80	42.20	48.00	95.30	40.00	30.60	24.40	27.70	10.60	60.60
Ho	4.57	7.49	7.74	9.49	29.90	9.51	7.20	5.04	5.45	2.37	13.60
Er	13.00	25.10	22.70	26.60	123.00	28.90	23.10	14.10	14.90	7.35	42.00
Tm	2.28	4.71	4.02	4.39	28.90	5.10	4.65	2.33	2.25	1.39	7.43
Yb	16.60	32.00	27.70	29.20	231.00	33.60	36.10	15.20	13.30	9.01	49.30
Lu	2.76	4.49	3.92	4.27	36.30	4.77	5.56	2.19	1.82	1.27	6.79

Table 5c. Composition of representative Paleozoic igneous rocks

Sample	371	372	373	374	379	380	381	382	384	385	411	G247	G248	G249
(wt%)														
SiO_2	50.24	47.86	51.03	46.06	46.75	46.71	48.75	46.75	47.55	45.89	46.88	70.19	70.52	46.25
TiO_2	1.28	1.34	1.28	1.47	1.41	1.46	1.38	1.42	1.13	1.42	0.75	0.28	0.28	0.82
Al_2O_3	14.28	15.01	14.03	16.13	16.49	16.56	15.80	16.63	16.21	16.93	14.36	13.98	14.71	15.94
Fe_2O_3	11.35	11.75	11.27	12.69	12.66	12.68	12.02	12.76	10.13	12.70	10.85	3.46	3.53	10.66
MnO	0.30	0.29	0.30	0.21	0.19	0.19	0.24	0.19	0.28	0.19	0.21	0.07	0.06	0.15
MgO	5.91	6.23	5.83	6.76	6.93	6.94	6.48	7.21	4.58	7.58	11.14	1.02	1.07	8.31
CaO	8.38	8.49	8.11	9.64	9.61	9.67	8.87	9.71	12.73	10.16	9.28	2.31	3.04	11.59
Na_2O	3.13	3.18	3.02	3.00	2.90	3.08	3.01	2.86	2.34	2.42	1.85	3.47	4.02	2.27
K_2O	1.53	1.80	1.36	0.67	0.55	0.53	1.32	0.68	0.94	0.47	1.25	2.46	1.41	0.59
P_2O_5	0.22	0.21	0.21	0.23	0.24	0.25	0.24	0.23	0.15	0.17	0.16	0.04	0.04	0.15
LOI	3.20	3.03	2.58	2.83	2.43	2.71	2.20	2.10	3.44	2.88	2.31	1.19	0.97	2.30
Total	99.82	99.19	99.02	99.69	100.16	100.78	100.31	100.54	99.47	100.81	99.04	98.47	99.65	99.03
Mg#	50.77	51.22	50.60	51.34	52.02	52.01	51.64	52.81	47.24	54.17	67.03	36.86	37.51	60.69
(ppm)														
Cr	50	50	50	60	60	50	50	60	50	60	590			110
Ni	70	70	70	80	80	80	70	90	70	90	220			80
Co	46	50	46	55	54	53	49	56	33	55	43			44
Sc	24	25	24	28	28	27	25	27	22	29	34			42
V	221	234	220	261	257	258	236	247	198	255	265			312
Pb	191	291	334	26	8	7	197	13	77	0	0	2	10	2
Zn	0	620	1340	140	90	90	570	90	980	80	110	20	50	50
Rb	187	276	149	43	24	22	84	23	76	12	49	47	31	10
Cs	7.10	9.70	0.00	1.50	0.90	0.90	4.00	1.10	2.80	0.00	0.90	0.50	0.30	0.20
Ba	265	290	278	207	202	219	288	232	174	139	282	827	512	257
Sr	519	509	415	522	475	492	511	495	887	413	226	222	263	335
Ga	28	24	25	19	19	19	23	19	26	18	14	13	13	15
Ta	22.80	13.00	11.90	0.40	0.05	0.05	10.90	0.05	22.00	0.05	0.05	0.40	0.38	0.03
Nb	483.0	252.0	341.0	15.0	6.0	5.0	185.0	4.0	464.0	4.0	3.0	6.1	4.3	1.9
Hf	21.90	13.90	16.10	2.50	2.40	2.50	19.10	2.40	19.80	2.20	1.40	3.80	3.20	1.70
Zr	1281	786	929	111	106	106	1070	102	1128	92	50	141	121	58
Y	1031	590	776	35	27	28	766	28	879	25	0	14	13	19
Th	171.00	86.70	103.00	3.20	1.90	1.80	63.80	1.50	109.00	0.80	1.20	6.30	7.53	0.83
U	89.70	52.90	62.70	2.00	0.70	0.80	46.10	0.70	76.50	0.30	0.70	1.94	1.94	0.45
La	459.00	294.00	413.00	17.70	12.10	13.31	203.00	12.10	390.00	6.30	7.00	14.10	15.30	4.86
Ce	1090.00	716.00	976.00	42.90	29.30	31.30	461.00	28.90	929.00	16.90	17.90	28.00	30.50	13.60
Pr	126.00	83.90	112.00	5.56	3.90	4.16	53.90	3.87	109.00	2.47	2.53	2.79	2.92	2.09
Nd	510.00	342.00	457.00	25.80	19.00	19.90	230.00	18.60	453.00	13.40	12.90	10.30	10.30	10.60
Sm	137.00	86.90	111.00	7.00	5.00	5.30	71.10	5.00	129.00	4.10	3.70	2.15	2.06	3.23
Eu	13.80	9.02	11.00	1.78	1.56	1.62	8.29	1.60	13.20	1.39	1.08	0.55	0.54	1.11
Gd	131.00	80.50	102.00	6.70	4.90	5.00	81.60	5.00	123.00	4.30	3.70	2.18	2.08	3.62
Tb	25.90	15.30	19.30	1.20	0.80	0.90	17.10	0.80	22.90	0.70	0.70	0.38	0.34	0.62
Dy	168.00	97.80	125.00	6.60	4.90	5.10	119.00	5.00	147.00	4.60	4.30	2.29	2.11	3.64
Ho	34.10	19.80	25.80	1.30	1.00	1.00	25.80	1.00	29.40	0.90	0.80	0.51	0.46	0.74
Er	98.00	56.90	75.10	3.50	2.80	2.90	77.30	2.90	82.50	2.60	2.30	1.53	1.37	2.03
Tm	14.10	8.13	10.80	0.50	0.41	0.42	11.20	0.43	11.70	0.38	0.35	0.26	0.23	0.29
Yb	81.10	46.80	62.50	3.20	2.70	2.90	64.70	2.90	67.50	2.60	2.40	1.75	1.63	1.86
Lu	9.71	5.66	7.82	0.49	0.44	0.46	7.99	0.46	8.12	0.42	0.36	0.28	0.25	0.28

371, 372, 373, 374, 379, 380, 381, 382, 384, 385, 411 - drill core samples from mafic bodies around the Dotson zone;
G-249 - diabase dike collected ~5 km East of the Bokan complex
G-247, G-248 - granitic rocks (country rocks of the Bokan complex)
Mg# = mol 100 x MgO/(MgO + FeO*)

Table 5d. Composition of granitic rocks from the Ross-Adams deposit

Sample	754	755	756	757	758	759	760	761	762	763
(wt%)										
SiO_2	66.96	67.36	71.51	73.99	71.70	64.75	58.63	57.10	67.70	67.32
TiO_2	0.33	0.22	0.20	0.13	0.12	0.30	0.14	0.28	0.26	0.17
Al_2O_3	12.45	10.90	12.11	11.48	10.95	14.31	15.08	14.26	14.37	12.60
Fe_2O_3	6.26	7.58	5.30	4.31	6.21	4.47	2.97	4.48	8.26	2.93
MnO	0.12	0.27	0.15	0.11	0.06	0.17	0.05	0.10	0.15	0.33
MgO	0.09	0.17	0.01	0.02	0.03	0.08	0.14	0.11	0.01	0.40
CaO	2.69	1.35	0.68	0.35	0.62	3.44	9.77	9.06	0.21	3.66
Na_2O	8.44	8.62	7.26	5.59	5.32	9.00	10.10	9.75	8.17	7.58
K_2O	0.14	0.63	2.62	4.18	3.55	0.06	0.12	0.11	0.05	0.25
P_2O_5	0.01	0.00	0.01	0.01	0.01	0.01	0.01	0.01	0.01	0.01
LOI	1.65	1.06	0.59	0.35	1.49	1.64	1.13	1.50	0.92	1.98
Total	99.14	98.17	100.44	100.52	100.06	98.23	98.14	96.76	100.11	97.23
(ppm)										
Pb	50	22	68	11	16	375	31	205	690	62
Zn	80	690	280	320	120	460	60	280	220	510
Rb	6	44	138	246	179	6	30	15	1	66
Ba	477	61	37	101	65	35	16	35	7	45
Sr	70	40	25	19	6	53	85	95	9	66
Ga	52	43	41	38	39	48	54	50	52	49
Ta	27.30	14.90	4.10	1.40	2.70	8.00	30.90	1.60	0.90	8.40
Nb	306.0	170.0	54.0	24.0	68.0	59.0	212.0	31.0	18.0	76.0
Hf	81.00	132.00	60.80	11.20	11.90	59.10	27.20	4.60	14.40	69.30
Zr	3358	5461	2509	481	401	2166	1012	134	524	2504
Y	429	360	316	140	251	638	599	686	48	619
Th	180.00	506.00	1980.00	23.70	32.10	10500.00	204.00	8400.00	805.00	13000.00
U	117.00	77.10	65.20	7.50	11.30	200.00	44.80	124.00	16.80	178.00
La	565.00	264.00	172.00	56.30	101.00	145.00	3.40	136.00	8.30	158.00
Ce	1120.00	549.00	391.00	110.00	206.00	425.00	9.90	413.00	26.50	518.00
Pr	127.00	64.80	50.90	12.20	23.90	68.10	1.61	66.20	4.38	88.80
Nd	453.00	248.00	221.00	44.40	92.10	351.00	8.90	339.00	22.80	474.00
Sm	88.10	55.20	70.00	9.30	22.70	170.00	9.80	148.00	9.90	223.00
Eu	7.44	5.26	7.23	0.95	2.33	19.70	1.95	16.00	1.02	23.10
Gd	63.30	51.10	74.80	10.70	25.40	240.00	30.70	171.00	9.20	234.00
Tb	9.50	9.30	13.40	2.60	5.30	45.30	8.90	28.00	1.60	38.20
Dy	52.60	56.40	68.40	19.00	33.30	238.00	60.70	131.00	9.30	177.00
Ho	11.80	12.20	12.60	4.60	6.90	38.60	13.60	21.00	2.20	29.00
Er	46.00	40.60	35.30	15.40	19.10	91.70	45.30	53.10	8.20	76.70
Tm	11.00	7.88	5.49	2.73	2.75	13.80	8.50	7.23	1.88	12.60
Yb	108.00	67.00	37.00	19.60	17.40	97.40	65.00	44.00	18.00	92.80
Lu	20.70	12.50	6.03	3.42	2.83	15.90	9.82	5.75	3.94	14.50

Table 5d. Composition of granitic rocks from the Ross-Adams deposit

Sample	764	765	766	767	768	769	770	771	772	773	774
(wt%)											
SiO_2	61.84	65.93	61.24	63.03	68.00	73.30	72.91	75.32	72.79	79.57	74.02
TiO_2	0.16	0.12	0.20	0.31	0.18	0.08	0.07	0.12	0.12	0.09	0.19
Al_2O_3	12.79	12.22	13.41	12.54	10.07	14.15	12.57	9.85	11.64	7.65	8.46
Fe_2O_3	4.11	2.70	3.16	4.17	10.11	3.43	3.49	4.82	3.96	4.08	7.25
MnO	0.24	0.07	0.10	0.07	0.13	0.06	0.04	0.05	0.08	0.07	0.09
MgO	0.32	0.19	0.21	0.04	0.02	0.01	0.01	0.01	0.03	0.02	0.01
CaO	7.13	6.57	7.48	7.09	0.29	0.14	0.30	0.26	0.41	0.10	0.19
Na_2O	8.42	7.88	8.74	8.26	9.48	9.40	8.83	7.42	5.44	3.89	5.04
K_2O	0.21	0.14	0.15	0.06	0.06	0.07	0.06	0.06	4.21	2.80	3.01
P_2O_5	0.01	0.01	0.01	0.01	0.01	0.01	0.01	0.01	0.01	0.01	0.01
LOI	1.69	1.28	1.63	1.32	0.26	0.25	0.23	0.27	0.41	0.14	0.09
Total	96.92	97.11	96.34	96.89	98.61	100.90	98.52	98.19	99.10	98.42	98.36
(ppm)											
Pb	78	27	69	29	84	1250	37	26	7	6	38
Zn	260	70	240	280	810	1250	70	140	390	290	0
Rb	65	37	26	1	1	1	1	1	195	124	138
Ba	39	17	42	16	5	10	8	7	39	32	50
Sr	109	90	124	85	8	4	2	3	18	1	6
Ga	50	44	53	49	45	58	50	37	42	34	0
Ta	3.40	3.60	4.20	7.10	1.90	5.20	5.60	3.80	7.60	1.30	3.80
Nb	58.0	45.0	40.0	75.0	21.0	60.0	74.0	35.0	149.0	17.0	53.0
Hf	33.70	171.00	31.10	40.60	23.40	18.30	81.80	47.70	28.00	17.00	25.50
Zr	1258	6397	1165	1727	860	747	3248	2041	1177	652	959
Y	666	936	680	578	49	34	114	74	462	72	120
Th	12000.00	363.00	9660.00	1670.00	16.30	11.50	59.10	15.70	50.90	20.00	143.00
U	166.00	29.60	163.00	38.30	7.00	14.80	25.90	17.70	24.40	5.30	12.20
La	176.00	4.90	154.00	32.80	5.00	32.90	3.10	1.80	103.00	33.30	129.00
Ce	590.00	16.80	486.00	96.30	11.90	58.30	9.10	5.00	228.00	78.20	281.00
Pr	102.00	3.10	80.80	15.10	1.50	5.87	1.26	0.73	26.90	10.30	32.20
Nd	553.00	19.60	432.00	76.30	6.20	19.10	5.80	3.50	104.00	43.10	128.00
Sm	267.00	22.40	191.00	35.30	2.00	3.90	2.90	1.90	29.00	12.10	29.00
Eu	28.30	4.82	19.80	3.97	0.25	0.34	0.41	0.27	3.12	1.21	2.63
Gd	277.00	96.60	194.00	46.80	3.00	3.10	5.10	3.80	36.50	13.10	25.50
Tb	39.80	26.60	29.10	9.50	0.80	0.60	1.80	1.20	8.60	2.80	4.80
Dy	168.00	184.00	129.00	58.70	6.60	4.50	16.30	10.40	60.90	17.50	30.00
Ho	26.10	37.20	21.40	12.80	1.80	1.30	5.00	3.00	14.20	3.70	6.20
Er	68.80	120.00	59.50	42.90	8.40	5.40	23.70	13.10	45.10	11.50	19.70
Tm	10.90	26.40	9.70	8.60	2.44	1.34	6.25	3.45	7.16	2.10	3.63
Yb	77.90	224.00	70.70	71.50	27.50	14.20	62.30	36.40	44.40	16.20	27.70
Lu	11.70	36.50	10.70	11.80	6.30	3.11	12.60	7.78	6.41	2.75	4.39

Table 5d. Composition of granitic rocks from the Ross-Adams deposit

Sample	775	776	777	778	780	781	782	783	784	785	786
(wt%)											
SiO_2	70.40	73.35	72.51	72.99	74.07	73.57	73.07	73.75	74.54	72.64	70.27
TiO_2	0.33	0.16	0.19	0.15	0.19	0.12	0.16	0.15	0.17	0.23	0.28
Al_2O_3	8.04	10.89	10.70	11.07	11.25	10.92	11.15	10.95	11.56	11.30	11.85
Fe_2O_3	10.61	4.62	4.81	4.60	4.57	3.96	4.88	4.18	4.58	5.17	5.53
MnO	0.24	0.09	0.05	0.08	0.07	0.12	0.15	0.11	0.17	0.10	0.23
MgO	0.04	0.05	0.01	0.02	0.02	0.02	0.03	0.02	0.02	0.06	0.05
CaO	0.55	0.39	0.38	0.36	0.31	0.28	0.31	0.35	0.26	0.46	0.45
Na_2O	7.01	5.21	5.28	5.18	6.21	5.51	5.55	3.86	8.08	7.71	7.20
K_2O	1.36	3.82	4.18	4.30	3.18	3.63	4.02	4.20	0.05	0.05	0.04
P_2O_5	0.01	0.01	0.01	0.01	0.01	0.01	0.01	0.01	0.01	0.01	0.01
LOI	0.90	0.47	0.30	0.33	0.30	0.33	0.32	1.10	0.59	0.87	1.38
Total	99.49	99.06	98.42	99.09	100.18	98.47	99.65	98.68	100.03	98.61	97.29
(ppm)											
Pb	54	55	183	14	21	5	24	66	47	123	418
Zn	850	430	110	290	140	300	540	220	360	170	280
Rb	63	191	231	248	238	265	282	220	1	1	1
Ba	52	37	17	25	51	15	113	62	120	56	71
Sr	21	25	21	8	8	4	9	107	11	17	29
Ga	38	39	37	35	40	38	38	41	40	38	45
Ta	8.60	7.00	5.80	2.80	6.80	2.70	4.80	2.40	7.30	3.50	8.40
Nb	116.0	81.0	87.0	33.0	93.0	37.0	75.0	52.0	102.0	51.0	132.0
Hf	44.50	86.50	23.30	57.00	18.50	47.40	21.00	11.00	17.30	32.60	11.30
Zr	1960	3765	963	2857	575	2114	867	344	633	1358	291
Y	487	399	255	304	307	109	441	728	348	932	978
Th	56.70	53.70	50.10	27.50	63.80	51.20	62.80	133.00	1700.00	2510.00	9120.00
U	30.50	28.70	18.70	11.90	21.50	24.80	47.50	16.50	43.90	686.00	1750.00
La	165.00	162.00	111.00	84.70	97.10	88.50	111.00	214.00	68.60	10.10	79.90
Ce	358.00	344.00	250.00	177.00	210.00	181.00	237.00	465.00	186.00	29.30	247.00
Pr	43.70	42.40	31.10	21.10	24.70	19.90	28.80	60.20	25.40	4.25	37.30
Nd	171.00	169.00	120.00	81.60	92.50	68.80	112.00	244.00	114.00	21.20	197.00
Sm	44.70	44.70	29.20	21.10	23.60	12.40	33.70	68.60	44.20	18.40	102.00
Eu	4.75	4.63	3.05	2.36	2.48	1.08	3.94	7.29	5.25	3.74	13.20
Gd	55.40	50.80	33.90	27.40	30.40	10.40	49.10	84.30	63.80	66.50	188.00
Tb	12.10	10.40	7.10	6.40	6.50	2.00	11.70	18.50	13.50	19.60	43.10
Dy	80.00	66.90	45.40	44.90	43.00	13.70	78.00	122.00	85.60	151.00	275.00
Ho	17.40	14.20	9.50	11.00	9.30	3.50	16.90	25.30	16.80	34.60	51.70
Er	51.60	40.20	27.10	38.50	28.70	16.00	50.90	70.80	47.90	108.00	131.00
Tm	8.08	5.69	4.00	7.24	4.87	4.85	8.54	9.51	7.76	18.50	18.50
Yb	55.90	33.70	26.40	49.90	36.50	55.80	59.20	51.90	52.20	127.00	106.00
Lu	9.59	5.09	4.49	7.83	6.06	11.20	8.80	7.06	8.28	20.00	14.70

Table 5d. Composition of granitic rocks from the Ross-Adams deposit

Sample	788	794	795	796	797	798	799	800	802	803	805
(wt%)											
SiO_2	73.08	76.29	70.92	79.26	76.93	79.93	70.99	74.91	74.68	74.27	74.50
TiO_2	0.19	0.12	0.10	0.08	0.10	0.08	0.35	0.16	0.14	0.14	0.15
Al_2O_3	11.44	8.83	11.09	8.84	9.86	8.50	8.05	11.03	11.31	10.92	11.10
Fe_2O_3	4.54	4.76	6.34	4.19	4.84	4.23	9.87	4.40	3.90	3.73	4.12
MnO	0.17	0.20	0.53	0.11	0.07	0.09	0.09	0.13	0.08	0.10	0.02
MgO	0.02	0.01	0.01	0.01	0.02	0.01	0.02	0.02	0.02	0.03	0.03
CaO	0.20	1.38	0.46	0.17	0.21	0.15	0.44	0.36	0.25	0.30	0.34
Na_2O	6.59	2.84	4.28	3.81	4.48	3.91	6.13	5.14	7.84	4.95	5.26
K_2O	1.38	4.19	3.79	2.32	3.57	3.01	2.85	4.12	0.06	4.12	4.18
P_2O_5	0.01	0.01	0.01	0.01	0.01	0.01	0.02	0.01	0.01	0.02	0.01
LOI	0.67	0.89	2.22	1.06	0.37	0.17	0.42	0.34	0.29	0.29	0.27
Total	98.29	99.52	99.75	99.86	100.46	100.08	99.24	100.62	98.59	98.87	99.98
(ppm)											
Pb	27	14	98	2810	15	16	89	39	23	109	30
Zn	360	110	390	2220	250	350	470	400	390	340	290
Rb	79	194	144	86	147	131	126	215	2	218	226
Ba	18	67	79	49	16	29	39	28	12	25	26
Sr	5	16	19	61	9	8	12	31	2	7	20
Ga	41	37	44	37	38	35	37	40	39	38	39
Ta	8.10	14.70	2.20	2.10	2.00	1.70	9.80	5.20	8.10	4.60	8.20
Nb	115.0	209.0	31.0	44.0	30.0	19.0	134.0	94.0	109.0	50.0	97.0
Hf	53.30	11.00	13.00	124.00	20.40	22.40	44.70	31.90	27.60	62.90	76.30
Zr	2236	353	529	5548	801	927	1665	1229	1328	3164	3157
Y	515	489	118	351	48	79	314	250	76	195	139
Th	532.00	109.00	12.30	91.80	14.50	13.30	71.00	53.40	334.00	48.10	36.90
U	111.00	37.40	6.90	30.10	5.80	6.80	26.10	16.60	264.00	25.10	26.10
La	63.60	163.00	94.70	98.60	26.60	18.40	163.00	127.00	22.40	102.00	151.00
Ce	151.00	403.00	204.00	223.00	61.40	41.20	389.00	296.00	59.00	233.00	326.00
Pr	18.60	47.20	22.60	25.70	6.90	4.91	46.80	33.80	6.88	25.90	36.50
Nd	73.20	187.00	90.70	106.00	27.40	20.80	194.00	135.00	27.10	102.00	143.00
Sm	23.00	54.20	21.50	28.40	7.50	6.50	51.30	35.50	7.20	29.20	30.90
Eu	2.93	5.55	1.88	2.83	0.75	0.74	4.89	3.53	0.73	3.11	2.80
Gd	42.40	62.00	18.80	32.00	7.10	8.20	48.50	34.60	6.90	32.20	25.80
Tb	12.90	13.50	3.30	7.90	1.20	1.80	9.30	6.90	1.40	6.50	4.40
Dy	94.80	85.90	19.80	63.40	7.70	13.20	59.00	44.40	9.40	42.60	26.90
Ho	20.80	17.30	4.20	16.60	1.70	3.10	12.50	9.40	2.40	8.90	5.60
Er	61.40	45.10	13.10	65.30	6.00	11.00	38.60	27.90	11.40	27.30	17.90
Tm	10.40	6.01	2.14	14.30	1.29	2.19	6.95	4.32	3.45	4.65	3.16
Yb	77.60	33.00	13.80	107.00	11.60	15.50	54.10	26.00	36.50	31.80	21.70
Lu	13.90	4.15	1.97	15.20	1.96	2.22	9.29	3.57	6.42	4.43	3.23

Table 5d. Composition of granitic rocks from the Ross-Adams deposit

Sample	807	808	809	810	411	812	415	816	817
(wt%)									
SiO_2	73.50	75.16	73.57	72.08	73.45	73.14	73.44	74.14	75.67
TiO_2	0.15	0.17	0.17	0.17	0.16	0.17	0.19	0.13	0.14
Al_2O_3	11.35	11.24	11.36	11.04	10.69	10.97	8.68	10.83	11.16
Fe_2O_3	4.64	3.66	4.33	4.32	4.60	4.08	7.99	4.40	4.65
MnO	0.14	0.11	0.05	0.03	0.05	0.03	0.15	0.11	0.08
MgO	0.02	0.02	0.05	0.03	0.03	0.02	0.01	0.02	0.05
CaO	0.28	0.43	0.35	0.43	0.42	0.30	0.29	0.45	0.26
Na_2O	5.36	3.90	5.28	5.20	5.10	5.19	5.24	4.92	6.35
K_2O	4.24	4.22	4.03	4.19	3.97	4.04	2.89	4.26	0.19
P_2O_5	0.01	0.01	0.02	0.01	0.01	0.01	0.01	0.01	0.01
LOI	0.50	1.43	0.49	0.76	0.42	0.30	0.12	0.40	1.13
Total	100.19	100.35	99.70	98.26	98.90	98.24	99.01	99.67	99.69
(ppm)									
Pb	23	149	29	28	18	60	11	9	123
Zn	350	660	160	180	220	390	550	360	130
Rb	250	170	215	216	206	200	124	215	10
Ba	46	43	35	29	33	24	46	50	61
Sr	10	60	13	10	7	14	12	34	21
Ga	41	40	40	39	37	41	38	39	37
Ta	2.90	10.70	7.50	4.80	5.20	7.70	2.40	6.50	2.80
Nb	63.0	259.0	174.0	118.0	82.0	106.0	38.0	93.0	44.0
Hf	20.60	38.30	26.70	54.10	99.20	77.20	22.30	20.40	101.00
Zr	733	1691	1113	2178	4115	3203	908	845	4282
Y	692	561	393	2297	463	203	93	271	96
Th	219.00	245.00	211.00	264.00	64.80	73.80	12.10	34.00	1840.00
U	17.40	40.20	22.70	25.50	26.30	34.50	7.70	20.00	1360.00
La	150.00	158.00	149.00	182.00	83.60	194.00	40.00	224.00	5.60
Ce	348.00	378.00	352.00	434.00	194.00	452.00	96.70	501.00	14.50
Pr	39.60	42.70	41.40	50.90	21.70	52.60	11.60	55.80	1.69
Nd	159.00	168.00	167.00	214.00	88.40	206.00	49.40	219.00	7.20
Sm	52.60	50.90	45.70	70.50	24.80	48.70	13.50	49.20	3.60
Eu	6.14	5.33	4.56	8.61	2.65	4.29	1.34	4.35	0.61
Gd	70.60	57.20	43.50	109.00	28.30	36.70	14.00	40.80	8.50
Tb	18.30	14.50	10.30	30.40	7.40	7.20	2.70	7.40	2.70
Dy	132.00	108.00	76.20	250.00	59.10	48.60	16.60	45.40	22.50
Ho	29.00	24.90	17.50	64.50	15.30	11.00	3.50	9.30	6.10
Er	83.90	77.00	54.40	208.00	52.80	36.80	11.50	26.30	30.50
Tm	12.00	11.80	8.19	29.90	8.91	6.38	2.36	3.86	9.98
Yb	66.30	71.30	49.90	156.00	54.60	42.60	19.30	23.30	108.00
Lu	8.15	9.06	6.56	17.70	7.10	5.98	3.28	3.12	19.20

Table 5e. Composition of representative mafic (lamprophyric) dikes

Sample	LM90	LM92	LM113	752	779	801	804	806	824	828
(wt%)										
SiO_2	55.75	50.29	56.16	47.62	48.66	51.38	52.21	50.81	48.64	52.12
TiO_2	0.42	0.65	0.39	0.71	0.72	0.65	0.45	0.54	0.76	0.57
Al_2O_3	18.17	17.15	17.58	17.65	19.93	19.05	16.56	17.22	18.30	18.95
Fe_2O_3	5.15	8.26	4.79	10.31	9.11	8.58	6.52	6.32	9.92	7.57
MnO	0.17	0.32	0.16	0.19	0.17	0.18	0.23	0.22	0.21	0.22
MgO	1.42	2.46	1.18	3.85	4.08	3.25	1.75	1.77	4.21	2.53
CaO	5.56	6.16	5.97	10.08	9.80	9.36	7.66	6.99	10.29	8.54
Na_2O	5.31	6.07	6.88	2.65	3.32	3.46	5.11	5.80	3.10	3.04
K_2O	1.94	2.14	0.92	1.01	1.00	1.08	2.15	3.25	0.74	1.18
P_2O_5	0.24	0.31	0.21	0.71	0.19	0.21	0.29	0.34	0.21	0.21
LOI	5.37	5.29	5.31	4.91	3.22	3.35	6.61	7.08	3.34	4.71
Total	99.50	99.10	99.55	99.69	100.20	100.55	99.54	100.34	99.72	99.65
Mg#	35.32	37.10	32.79	42.51	47.00	42.86	34.71	35.68	45.67	39.83
(ppm)										
Rb	85	116	45	46	37	36	99	218	33	53
Ba	1219	457	237	252	477	439	536	444	250	642
Sr	781	708	12	738	783	838	621	903	813	841
Ga	17	18	18	18	17	19	19	16	18	19
Ta	0.32	0.32	0.49	0.10	0.10	0.20	0.30	0.20	0.10	1.00
Nb	4.5	4.3	12.4	2.0	2.0	5.0	8.0	5.0	3.0	4.0
Hf	2.50	2.20	2.80	1.40	1.60	1.80	2.80	2.80	1.60	2.40
Zr	85	81	96	48	52	62	97	102	53	67
Y	20	34	23	16	16	25	38	30	27	556
Th	2.51	1.94	8.98	5.80	1.20	3.70	2.60	2.70	1.50	1.90
U	0.98	6.96	2.12	1.70	0.50	0.80	2.60	2.00	0.70	1.50
La	11.70	14.10	15.30	9.20	8.90	11.10	18.20	17.70	9.80	13.60
Ce	25.40	31.10	33.30	20.80	20.60	25.60	40.50	40.40	23.00	29.00
Pr	3.61	4.25	4.53	2.88	2.90	3.31	4.91	4.96	2.97	4.31
Nd	17.70	19.00	21.40	13.30	13.50	15.20	21.60	22.00	14.10	21.20
Sm	4.19	4.57	4.82	3.30	3.30	3.70	4.60	5.20	3.50	10.90
Eu	1.35	1.44	1.54	1.18	1.18	1.21	1.37	1.57	1.17	2.64
Gd	3.89	4.44	4.67	3.40	3.40	3.60	4.30	4.70	3.40	29.60
Tb	0.64	0.80	0.78	0.60	0.60	0.60	0.70	0.80	0.60	8.40
Dy	3.76	5.05	4.70	3.20	3.20	3.50	4.80	4.50	3.60	65.00
Ho	0.80	1.13	0.99	0.70	0.60	0.70	1.00	0.90	0.80	14.70
Er	2.36	3.29	2.87	1.90	1.80	2.00	3.20	2.70	2.10	39.30
Tm	0.37	0.47	0.46	0.29	0.27	0.29	0.52	0.40	0.33	4.72
Yb	2.43	3.38	2.89	1.90	1.90	1.90	3.50	2.60	2.00	20.10
Lu	0.36	0.50	0.43	0.31	0.30	0.30	0.50	0.39	0.30	2.00

Mg# = mol 100 x MgO/(MgO+FeO*)

Table 6. Nd isotopic composition of rocks of the Bokan complex

Sample	Nd (ppm)	Sm (ppm)	$^{147}Sm/^{144}Nd$	$^{143}Nd/^{144}Nd$		2σ	ε_{Nd}	T_{DMI} (Ma)	T_{DM2} (Ma)
G 151	94.64	23.59	0.1507	0.512839	±	7	5.0	523	752
G 155	28.62	4.833	0.1021	0.512809	±	6	5.5	344	467
G 231	73.41	25.87	0.2131	0.512906	±	6	4.9	-	-
G 234	77.21	15.97	0.1250	0.512819	±	6	5.2	412	569
G 237	83.26	20.04	0.1455	0.512856	±	14	5.4	452	657
G 244	62.07	13.77	0.1341	0.512810	±	8	4.8	474	651
G 165	422.7	94.73	0.1355	0.512706	±	12	2.7	674	865
LM 99	410.1	85.75	0.1264	0.512729	±	8	3.4	568	733
LM 101	90.91	21.08	0.1402	0.512849	±	7	5.4	433	624
LM 104	15.57	3.508	0.1362	0.512829	±	6	5.1	450	632
LM 92	18.36	4.367	0.1458	0.512911	±	5	6.5	329	537
LM 113	17.43	3.869	0.1342	0.512903	±	6	6.6	305	474

Samples: Bokan peralkaline granite - G151, G155, G231, G234, G237, G244; mineralized granite - G165, LM 99, LM 101, LM 104; lamprophyre dike - LM 92, LM 113.

$^{143}Nd/^{144}Nd$ are measured Nd isotopic ratios and ε_{Nd} is the fractional difference between the $^{143}Nd/^{144}Nd$ of rock and the bulk earth at the time of crystallization. The ε_{Nd} values were calculated assuming bulk earth today has $^{143}Nd/^{144}Nd$=0.512637 and $^{147}Sm/^{144}Nd$=0.1967 and an age of 177 Ma. Concentrations of Nd and Sm were determined by isotope dilution. Precision of concentrations of Nd and Sm is ± 1%. Nd model ages were calculated based upon De Paolo's (1981) depleted mantle model (TDM1), and on a depleted mantle model (TDM2) separated from the CHUR (chondrite-uniform reservoir) at 4.55 Ga, with linear evolution and a present-day epsilon value of +10. $^{143}Nd/^{144}Nd$ values were corrected from the deviation from JNdi-1. Mean values of Memorial University TIMS lab is $^{143}Nd/^{144}Nd$ = 0.512094; stdv=11 and n=27

Table 7a. U-Th-Pb isotopic and concentration data for the rocks of the Bokan complex.

Sample	U (ppm)	Th (ppm)	Pb (ppm)	$(206/204)_C$	2σ	$(207/204)_C$	2σ	$(208/204)_C$	2σ	$(206/204)_I$	$(207/204)_I$	$(208/204)_I$
G151	14.90	57.90	21.0	19.378	± 0.001	15.616	± 0.001	38.666	± 0.002	18.104	15.553	37.049
G155	7.63	18.20	14.0	19.597	± 0.001	15.607	± 0.001	38.744	± 0.003	18.614	15.558	37.979
G162	15.90	19.00	15.0	19.495	± 0.001	15.599	± 0.001	38.611	± 0.003	17.590	15.504	37.868
G231	22.10	25.60	14.0	20.150	± 0.002	15.619	± 0.001	38.856	± 0.004	17.279	15.477	37.770
G234	9.05	16.00	22.0	19.419	± 0.002	15.612	± 0.002	38.634	± 0.006	18.680	15.575	38.208
G237	14.30	17.10	29.0	19.555	± 0.001	15.609	± 0.001	38.684	± 0.003	18.667	15.565	38.377
G244	8.54	21.20	48.0	19.270	± 0.001	15.605	± 0.001	38.630	± 0.002	18.951	15.589	38.372
G165	34.20	56.40	89.0	19.546	± 0.001	15.626	± 0.001	38.959	± 0.004	18.852	15.592	38.585
LM99	16.60	59.00	40.0	19.361	± 0.001	15.601	± 0.001	38.760	± 0.002	18.615	15.564	37.894
LM101	52.10	64.30	18.0	23.012	± 0.001	15.765	± 0.001	39.685	± 0.002	17.481	15.491	37.456
LM104	127.00	17.40	201.0	19.268	± 0.001	15.574	± 0.001	38.222	± 0.002	18.142	15.518	38.172
LM 92	6.96	1.94	6.0	19.200	± 0.001	15.556	± 0.001	38.317	± 0.002	17.189	15.456	36.134
LM113	2.12	8.98	2.0	19.168	± 0.001	15.587	± 0.001	38.443	± 0.003	14.352	15.497	35.932

Samples: Bokan peralkaline granite - G151, G155, G162, G231, G234, G237, G244; mineralized granite - G165, LM 99, LM 101, LM 104; lamprophyre dike - LM 92, LM 113.

$(206/204)_c$, $(207/204)_c$ and $(208/204)_c$ are measured $^{206}Pb/^{204}Pb$, $^{207}Pb/^{204}Pb$ and $^{208}Pb/^{204}Pb$ isotopic ratios respectively, corrected for mass fractionation. (206/204)i, (207/204)i and (208/204)i are initial (time corrected) $^{206}Pb/^{204}Pb$, $^{207}Pb/^{204}Pb$ and $^{208}Pb/^{204}Pb$ ratios, respectively (assumed age 177 Ma). Deviation from the certified values of repeated analyses of standard NBS 981 yield at the isotopic laboratory of the Memorial University to a correction factor of 0.00107 ±3 per amu. At Memorial, the mean of NBS 981 measurements (n=23) of $(^{206}Pb/^{204}Pb)_m$, $(^{207}Pb/^{204}Pb)_m$ and $(^{208}Pb/^{204}Pb)_m$ are 16.900 (stdv. 0.007), 15.439 (0.010) and 36.539 (0.033) respectively.

Table 7b Pb-isotopic data for galena from the Bokan complex

Pb ratios	206/204	2σ	207/204	2σ	208/204	2σ	208/206	2σ	207/206	2σ
2009	18.896	± 0.003	15.578	± 0.004	38.286	± 0.038	2.0265	± 0.0004	0.82443	± 0.0001
McK	48.776		17.089		50.4		1.0333		0.3504	

Sample 2009 is galena from a pegmatite dike of the I&L Zone; 206/204, 207/204, 208/204, 208/206 and 207/206 are measured $^{206}Pb/^{204}Pb$, $^{207}Pb/^{204}Pb$, $^{208}Pb/^{204}Pb$, $^{208}Pb/^{206}Pb$ and $^{207}Pb/^{206}Pb$ isotopic ratios respectively, corrected for mass fractionation to the values of Todt et al. (1996); 2 σ – reproducibility of NBS 981; McK- Pb isotope data for galena from the Ross-Adams deposit given by MacKevett (1963).

Table 8. Oxygen isotopic composition of quartz from Bokan complex.

			$\delta^{18}O$ (‰)			
			measured	calculated		
Sample	**Rock**	**Mineral**		**(H_2O) @ 600°C (‰)**	**(H_2O) @ 500°C (‰)**	**(H_2O) @ 400°C (‰)**
LM66	granite	quartz	9.0	7.5	6.7	5.0
LM78	granite	quartz	8.9	7.4	6.6	4.8
Average			9.0	7.5	6.7	4.9
LM58	vein/pegmatite	quartz	11.3	9.8	9.0	7.3
LM61	vein/pegmatite	quartz	9.2	7.7	6.9	5.2
LM70	vein/pegmatite	quartz	8.9	7.4	6.6	4.8
LM71	vein/pegmatite	quartz	9.6	8.1	7.3	5.5
LM77	vein/pegmatite	quartz	9.3	7.8	7.0	5.2
Average			9.7	8.2	7.4	5.6

Table 9 - Microthermometric data for primary and secondary fluid inclusions

Sample #	Chip	T_m^{CO2} (°C)	T_m^{ice} (°C)	T_m^{clath} (°C)	NaCl wt% eq.	T_h^{CO2} (°C)	$T_h^{L+V>L}$ (°C)	Size (μm)	Ass.
Aqueous-carbonic, type I									
LM111	1			3.7	10.9	31.3		15	j
LM111	1			5.8	7.7	24.5		12	
LM111	1			6.2	7.0		286.0	25	
LM111	1			3.4	11.3		286.0	15	
LM111	1			4.0	10.5		286.0	20	
LM111	1			6.1	7.2	27.6		15	t
LM111	1			6.5	6.6	30.6		15	t
LM111	1			6.5	6.6			15	
LM111	3			4.6	9.6		240.0	15	j
LM111	3			6.8	6.0		197.6	25	j
LM111	3			6.9	5.9		196.2	15	
LM111	3			7.0	5.7	24.7		20	
LM111	3			6.0	7.4	30.7		20	
LM111	3			5.1	8.8	31.4	236.1	15	
LM111	3			5.6	8.0		229.2	15	g
LM111	3			5.7	7.9		233.9	15	g
LM111	3			6.0	7.4		243.4	20	
LM111	3			3.6	11.0		223.9	15	
LM111	3			5.3	8.5		241.7	25	
LM111	3			5.3	8.5		213.7	15	
LM111	3			4.9	9.1		238.7	20	
LM111	3			2.6	12.4			15	
LM111	2			6.2	7.0		228.9	15	
LM111	2			5.7	7.9		228.9	15	
LM111	2			5.6	8.0	30.9	257.7	15	
LM111	2			4.8	9.3		256.5	20	
LM111	2			6.4	6.7		255.0	15	
LM111	2			5.6	8.0		256.5	15	
LM111	2			6.6	6.4		224.7	15	
LM111	2			5.9	7.5		256.5	30	
LM111	2			5.7	7.9		188.8	15	
LM111	2			4.9	9.1		256.5	15	
LM111	2			5.4	8.3		256.5	15	
LM111	2			5.4	8.3			25	
LM111	2			5.4	8.3			15	
LM111	2			5.6	8.0			15	
LM111	2			4.6	9.6	29.2		15	
LM111	2			6.0	7.4	30.9		15	
LM111	2			5.4	8.3			15	
LM111	1			5.6	8.0			15	
LM111	1			5.4	8.3			10	
LM111	1			4.8	9.3		178.0	10	
LM111	1			6.6	6.4		208.8	10	
LM111	1			7.0	5.7		213.6	8	
LM111	1			6.6	6.4		216.1	8	
LM111	1			4.6	9.6		227.5	10	
LM111	1			6.5	6.5		199.0	8	
LM111	1			5.3	8.5		206.2	13	
LM111	1			5.2	8.6		202.0	8	
LM111	1			6.7	6.2		224.2	8	vv
LM111	1			6.3	6.9		223.6	15	xx
LM111	1			5.6	8.0	30.8	248.1	15	bb
LM111	1			6.3	6.9	31.2	217.8	15	bb
LM111	1			7.2	5.3	31.2	216.3	15	aa
LM111	1			7.4	5.0	31.2	213.3	10	aa
LM111	1			7.2	5.3	31.2	214.1	12	aa
LM111	1			7.2	5.3	31.1	224.0	10	cc
LM111	1			6.7	6.2		210.7	8	cc
LM111	2			6.1	7.2		201.0	10	dd
LM111	2			5.9	7.5		180.5	8	dd
LM111	2			3.9	10.6		261.6	8	
LM111	2			5.8	7.7	31.2	242.4	10	
LM111	2			5.7	7.9		242.3	8	ff
LM111	2			5.4	8.3	30.7	295.8	8	ff
LM111	2			5.9	7.5		255.6	6	
LM111	2			4.2	10.1		211.8	10	
LM111	3			5.9	7.5		230.8	10	ii
LM111	3			6.2	7.0		222.5	10	ii

Notes and abbreviations:

T_m^{CO2} = Final melting temperature of carbonic phase (CO_2)

T_m^{ice} = Final melting temperature of water ice

T_m^{clath} = Final decompositional temperature of clathrate

NaCl wt% eq. = bulk fulid inclusion salinity in wt% NaCl equivalent (calculated using the equation of Bodnar, 1994)

T_h^{CO2} = homogenization temperature for the carbonic phase

$T_h^{L+V>L}$ = homogenization of from two phase liquid + vapour to single phase liquid (total homogenization)

Ass. = assemblage #; inclusions in a group that was trapped along a single, texturally constrained growth feature (either secondary or primary) and show consistent microthermometric behavior

Table 9 - Microthermometric data for primary and secondary fluid inclusions

Sample #	Chip	T_m^{CO2} (°C)	T_m^{ice} (°C)	T_m^{clath} (°C)	NaCl wt% eq.	T_h^{CO2} (°C)	$T_h^{L+V>L}$ (°C)	Size (μm)	Ass.
Aqueous, type II									
LM111	1		-6.0		9.2		190.1	20	
LM111	1		-7.8		11.5		286.2	20	
LM111	1		-4.9		7.7		255.9	15	
LM111	1		-5.1		8.0		222.0	15	
LM111	1		-6.0		9.2		275.4	15	
LM111	1		-4.7		7.5		261.1	15	
LM111	1		-4.0		6.5			15	
LM111	1		-3.6		5.9			20	
LM111	1		-4.3		6.9			20	
LM111	1		-5.2		8.1			30	
LM111	3		-4.0		6.5		177.4	25	
LM111	3		-5.4		8.4		177.9	15	
LM111	3		-3.8		6.2		241.7	20	
LM111	3		-4.2		6.7		241.7	20	
LM111	3		-6.9		10.4			30	
LM111	3		-3.4		5.6		174.2	30	
LM111	3		-4.2		6.7		174.8	15	
LM111	3		-5.4		8.4		177.3	15	
LM111	3		-5.7		8.8		217.1	15	
LM111	3		-4.0		6.5			15	
LM111	3		-4.2		6.7			15	
LM111	3		-4.1		6.6			15	
LM111	2		-7.9		11.6		228.9	15	
LM111	2		-4.7		7.5		193.8	15	
LM111	2		-4.5		7.2		198.5	20	
LM111	2		-4.7		7.5		256.5	15	
LM111	2		-7.5		11.1		223.1	15	
LM111	2		-7.9		11.6		191.1	15	
LM111	2		-3.7		6.0		232.1	30	
LM111	2		-3.5		5.7			15	
LM111	2		-3.9		6.3			20	
LM111	1		-3.1		5.1		207.9	10	vv
LM111	1		-5.3		8.3		180.5	12	vv
LM111	1		-3.0		4.8		168.6	15	xx
LM111	1		-3.0		4.8		143.7	20	xx
LM111	2		-6.4		9.7		183.6	18	dd
LM111	2		-3.9		6.3		236.1	15	
LM111	3		-4.6		7.3		179.0	25	gg
LM111	3		-5.0		7.9		183.3	15	gg
LM111	3		-4.8		7.6		183.9	9	gg
LM111	3		-5.5		8.5		180.5	30	hh
LM111	3		-5.2		8.1		179.2	10	hh
LM111	3		-3.9		6.3		172.8	12	
LM111	3		-6.0		9.2		178.3	10	nn
LM111	3		-4.5		7.2		188.9	12	nn
LM111	3		-6.5		9.9		169.9	15	nn
G191	2		-7.3		10.9		187.3	7	a
G191	2		-7.7		11.3		186.3	6	a
G191	2		-7.6		11.2		187.6	6	a
G191	2		-8.5		12.3		183.0	5	a
G191	2		-7.7		11.3		185.5	4	a
G191	2		-4.9		7.7		191.9	10	b
G191	2		-5.3		8.3		191.3	7	b
G191	3		-6.9		10.4		218.2	10	a
G191	3		-6.2		9.5			10	a
G191	3		-9.0		12.8		234.7	9	b
G191	3		-6.6		10.0		242.3	10	d
G191	3		-6.4		9.7		266.1	12	e
G191	4		-6.4		9.7		198.4	10	a
G191	4		-6.3		9.6		213.4	8	b
G191	4		-6.8		10.2		207.5	11	c
G191	4		-6.7		10.1		206.6	12	c
G191	4		-5.3		8.3		198.8	25	d
G191	4		-5.9		9.1		233.7	15	d
G198	4		-1.7		2.8		244.1	10	a
G198	4		-7.6		11.2		198.4	15	b
G198	4		-5.3		8.3		227.5		c
G198	1		-3.2		5.3		192.4		d

Notes and abbreviations:

T_m^{CO2} = Final melting temperature of carbonic phase (CO_2)

T_m^{ice} = Final melting temperature of water ice

T_m^{clath} = Final decompositional temperature of clathrate

NaCl wt% eq. = bulk fulid inclusion salinity in wt% NaCl equivalent (calculated using the equation of Bodnar, 1994)

T_h^{CO2} = homogenization temperature for the carbonic phase

$T_h^{L+V>L}$ = homogenization of from two phase liquid + vapour to single phase liquid (total homogenization)

Ass. = assemblage #; inclusions in a group that was trapped along a single, texturally constrained growth feature (either secondary or primary) and show consistent

Table 9 - Microthermometric data for primary and secondary fluid inclusions

Sample #	Chip	T_m^{CO2} (°C)	T_m^{ice} (°C)	T_m^{clath} (°C)	NaCl wt% eq.	T_h^{CO2} (°C)	$T_h^{L+V>L}$ (°C)	Size (μm)	Ass.
Aqueous, type II (cont'd)									
G198	1		-7.0		10.5		183.1	15	d
G198	1		-12.2		16.1		222.1	20	
G198	1		-4.8		7.6		251.0	15	
G199	2		-13.2		16.9		274.8	25	
G199	2		-13.5		17.2		237.6	20	
G199	2		-12.8		16.6		217.7	17	
G199	2		-11.9		15.8		215.9	12	
G199	2		-13.3		17.0		237.6	15	
G199	2		-12.8		16.6		240.6	15	
G199	3		-7.9		11.6		270.1	15	
G199	3		-10.9		14.9		268.5	15	
G199	3		-8.7		12.5		280.2	12	
G199	3		-7.6		11.2		229.9	20	
G199	3		-10.5		14.5		295.8	40	
G199	3		-10.1		14.1		238.3	12	
G199	1		-10.6		14.6		191.9	12	
G199	1		-13.8		17.4		168.4	15	
G199	1		-6.8		10.2		206.9	30	
G199	1		-9.1		12.9		176.1	25	
G199	1		-6.9		10.4		187.0	20	
G199	1		-7.6		11.2		189.7	18	
G199	1		-9.4		13.3		191.3	12	
G199	1		-7.1		10.6		193.0	12	
H923	2		-7.3		10.9		182.3		
H923	2						196.0		
H923	3		-3.8		6.2		154.5	15	
H923	3		-2.6		4.2		172.8	15	
H923	3		-4.2		6.7		345.1	25	
H923	3		-3.8		6.2		245.8	15	
H923	3		-3.1		5.1		282.8	15	
H923	3		-3.0		4.8		231.4	20	
G200	3		-14.8		18.1		140.6	12	x
G200	3		-14.7		18.0		178.9	6	x
G200	3		-18.7		20.3		176.5	10	a
G200	3		-15.4		18.5		184.3	8	a
Carbonic, type III									
H923	3	-56.4				10.4		12	
H923	1	-56.3				20.7			
H923	1	-56.5				21.3		12	
H923	1	-56.4				21.6		10	
H923	1	-56.3				22.1		8	
H923	1	-56.4				21.5		9	
H923	1	-56.4				19.9		25	
H923	1	-56.3				19.0		15	
H923	1	-56.7				22.0			
H923	1	-56.6				21.3			
H923	1	-56.5				21.1			
G198	3	-56.4				24.6		10	
G198	3	-56.4				25.3		6	
G199	2	-56.5				14.5		10	
G199	2	-56.5				20.2		10	
G199	2	-56.6				16.7		10	

Notes and abbreviations:

T_m^{CO2} = Final melting temperature of carbonic phase (CO_2)

T_m^{ice} = Final melting temperature of water ice

T_m^{clath} = Final decompositional temperature of clathrate

NaCl wt% eq. = bulk fulid inclusion salinity in wt% NaCl equivalent (calculated using the equation of Bodnar, 1994)

T_h^{CO2} = homogenization temperature for the carbonic phase

$T_h^{L+V>L}$ = homogenization of from two phase liquid + vapour to single phase liquid (total homogenization)

Ass. = assemblage #; inclusions in a group that was trapped along a single, texturally constrained growth feature (either secondary or primary) and show consistent

APPENDIX

1. History of Mining and Exploration

The history of mineral exploration of the Bokan Mountain area has been reported in numerous publications including MacKevett (1963), Thompson (1988, 1997), Thompson et al. (1980, 1982), Warner and Barker (1989), Kent and Sullivan (2004), Keyser and McKenney (2007), Long et al. (2010) and many others.

Uranium was discovered in 1955 in the shear zones and fractures of the Bokan Mountain (MacKevett, 1963). Mining commenced in 1957 at the Ross-Adams mine which was operated sporadically between 1957 and 1971 by several different companies. The mine produced about 77,000 metric tons of ore with an average grade of about 1 wt. % uranium oxide and 3 wt. % of thorium oxide (Long et al., 2010). The ore was mined initially in a small open pit (Fig. 11) located on the southeastern flank of the Bokan Mountain. As the ore body plunged steeply at the end of pit (Fig. 12), the deposit was subsequently developed as an underground operation through the establishment of haulage adits at the 700 and 318 foot level elevations (i.e. 700 and 318 feet above sea level). Ore with >0.5 wt. % U_3O_8 was shipped by barge from the property and the Kendrick Bay to continental U.S. for processing, primarily to fulfill contracts with the U.S. Atomic Energy Commission (Long et al., 2010).

The Ross-Adams uranium deposit was discovered after prospectors Don and Jane Ross detected anomalous radioactivity at the Bokan Mountain using an airborne Geiger counter in a Piper Cub airplane (Kiffer, 2005; Keyser and McKenney, 2007). This finding led Don Ross and Kelly Adams to the discovery of bedrock uranium mineralization and staking near what is now known as the Ross-Adams mine. The Climax Molybdenum Company subsequently leased a portion of these holdings and in 1957 started mining of the uranium ore in the open pit (Stephens, 1971). However, the company relinquished its interest in 1958. Bay West Inc. optioned the property in 1961 and during the 1961-1962 period renewed open pit mining operations and initiated underground mining from an audit driven under the mineralized zone (the “700 level”; Fig. 11). In 1963, Standard Metals Corporation purchased an interest in the property and continued with mining of the deposit till 1964 when the mine filled the allotment given by the U.S. Atomic Energy Commission. Afterwards, the mine again became dormant (Stephens, 1971). In 1968, Newmont Exploration Ltd. acquired leases of the area and after two years of exploration, the Ross-Adams mine was re-opened and the deposit was accessed at a deeper level by another audit (the “318 level”; Figs. 11 and 12), located below the older level of the Bay West/Standard Metals. After production during 1970-1971, the mine ceased operations in September 1971, leaving a significant amount of uranium ore unmined (~331,000 metric tons with an average grade of 0.17 wt. % U_3O_8 and 0.46 wt. % ThO_2; Warner and Barker, 1989).

Several companies, including Occidental Minerals Corporation, Standard Metals, Cotter Corporation, Setraphim Engineers, Union Carbide, Santa Fe Minerals, Dome Minerals and Humble Oil, conducted exploration including drilling on the Bokan Mountain Property during 1971-1981 (Kent and Sullivan, 2004; Keyser and McKenney, 2007).

Historic exploration of the Bokan Mountain area has resulted in the delineation of at least fifteen named bedrock prospects, mostly of the vein-dike and shear systems. Particularly noteworthy of these systems are the I&L and Dotson systems. Other named and prominent uraniferous prospects at Bokan Mountain include Sunday Lake, Boots, ILM, Little Jim, Little Joe, Geiger, Cheri and Upper Cheri prospects and the Geoduck Zone (Fig. 3).

In addition to U and Th, historic exploration and development activities at Bokan Mountain identified economically significant levels of REE, Y, Nb and Zr mineralization in association with some of the known uranium prospects (MacKevett 1963; Warner and Barker, 1989). Assessment of the REE and niobium potential of the area was the focus of the detailed study of Warner and Baker (1989) which highlighted the Bokan Mountain area as comprising one of the most significant REE and HFSE resource areas in the United States. Warner and Baker (1989) suggested that the vein-dike and shear systems related to the Bokan complex contain a resource of 6.2 million metric tons of ore that average 0.264 wt. % REE, about one-third of which is yttrium. They also predicted significant resources of Th, Nb, Ta and Zr.

After several years of exploration hiatus, new exploration activities by Ucore Rare Metals started in the district in 2007 and have continued into the present. Up to now Ucore produced a database of 143 drill holes and channel samples totaling 8728.76 m of diamond drilling and sampling on the Dotson and I&L zones. In the Spring of 2011, Ucore released the National Instrument 43-101 technical report with the initial mineral resource estimation for the REE ore at the Dotson and I&L zones. The calculations suggest that these two zones encompass 3.7 million metric tons of ore containing 0.75 wt. % oxides of REE and Y (Robinson et al., 2011).

2. Analytical Methods

2.1. Mineral Analyses

The compositions of various mineral phases from the Bokan and associated dikes were determined by electron microprobe at Dalhousie University (Halifax, Nova Scotia, Canada) using a JEOL Superprobe 8200 equipped with five wavelength-dispersive (WD) spectrometers and an Oxford Link eXL energy-dispersive (ED) system. The WD system was used in the present study. The beam current was 15 nA; the accelerating voltage was 15 kV. The count times for major and minor elements were 20 s on peak and 10 s on background. The count times for trace elements were 40 s on peak and 20 s on background. One to three spots per heavy mineral grain were analysed.

The phases were analysed using a tightly focussed (~1 μm) beam. The standards used for calibration purposes included sanidine (for Si, Al, K), garnet (Fe), jadeite (Na), hornblende (Ca, Mg, Ti), pyrolusite (Mn), F-apatite (F, P), Cl (tugtupite), pyrrhotite (S), zirconia (Zr), Y-Al garnet (Y), Ce ($CePO_4$), Th (ThO_2), U (UO_2). The data were reduced using Link's ZAF matrix correction program. The accuracy for major elements was $\pm$1.5-2.0 relative %.

2.2. Major and Trace Element Analyses

Whole rock major and trace elements were determined using lithium tetraborate fusion at the Activation Laboratories, Ancaster, Ontario, Canada. Major elements and some trace elements (Ba, Sr, Y and Zr were determined by inductively coupled plasma-optical emission spectrometry, whereas other trace elements were analyzed using a Perkin Elmer Optima 3000 inductively coupled plasma mass spectrometer. Based on replicate analyses, the precision is generally between 2 and 10 % for trace elements and 3-5 % for major elements.

2.3. U-Pb Zircon Geochronology

U-Pb ages were determined in zircons from two samples. Zircons from an amphibole-bearing peralkaline granite sample (G245) from the core of the complex were dated using a solid state mass spectrometer while those from a granitic country rock sample were dated by laser-ablation ICP-MS (LA-ICP-MS).

In the first case, zircon separation from the Bokan granite was done at the Jack Satterly Geochronology Laboratory at the University of Toronto (Ontario, Canada) using standard techniques, including heavy liquids, a Wifley table and a Frantz magnetic separator followed by hand picking under a binocular microscope. Sample preparation and analytical methods used in this study broadly followed previously described procedures (Gutierrez-Alonso et al., 2008) and are only briefly summarized here. The selected grains were washed and loaded into Teflon bombs with HF along with a mixed $^{205}Pb/^{235}U$ isotopic tracer solution (Krogh, 1973). Dissolution occurred over 4 to 5 days at 195°C. U and Pb were separated using 50 ml anion exchange columns. The isotopic compositions of Pb and U were measured using a single Daly collector with a pulse counting detector with a solid source VG354 mass spectrometer. A detector mass discrimination of 0.033% per atomic mass unit and a dead time of 24 ns were employed for Daly detector measurements. A thermal source mass discrimination correction of 0.1% per atomic mass unit was applied for both Pb and U. Amplifier gains and Daly characteristics were monitored using the SRM982 Pb standard.

The assigned laboratory blank for U was 0.2 pg, while that for Pb is routinely measured below 1 pg. Error estimates were calculated by propagating known sources of analytical

uncertainty for each analysis including within-run ratio variability, uncertainty in the fractionation correction and uncertainties in the isotopic composition of laboratory blank. Decay constants used are those of Jaffey et al. (1971). Uncertainties are given at the 95% confidence level. Initial corrections were made using the in-house data reduction program Utilage; graphical data presentation and quoted ages were generated using the Microsoft Excel Add-in Isoplot Ex. 3.00 of Ludwig (2003).

Zircons were also separated from one sample (H835) of the granitic country rock (quartz monzonite) by conventional magnetic and heavy liquid technique and subsequently mounted to perform cathode luminescence and backscatter imaging. The U and Pb isotopic analyses were performed using LA-ICP-MS at the Beijing SHRIMP Centre, Institute of Geology, Chinese Academy of Geological Sciences. Standard analytical procedures were utilized for LA-ICP-MS (Chiu et al., 2009) with results calibrated to the GJ-1 zircon standard obtained from the Australian Research Council National Key Centre for Geochemical Evolution (Jackson et al., 2004). The final isotopic ratios were determined by GLITTER 4.0 (GEOMOC) software and age corrected based on the procedure established by Anderson (2002).

2.4. $^{40}Ar/^{39}Ar$ Geochronology

Three amphibole and two whole-rock samples were dated at Queen's University (Kingston, Ontario, Canada) by the $^{40}Ar/^{39}Ar$ method. Amphibole was concentrated by standard techniques and finally grains were selected by handpicking under a binocular microscope from fractions that ranged in size from 40 to 60 mesh. Mineral separates and whole-rock samples were loaded into Al-foil packets and irradiated together with Hb3GR as a neutron-fluence monitor at the McMaster Nuclear Reactor (Hamilton, Ontario, Canada). $^{40}Ar/^{39}Ar$ analyses were performed by standard laser step-heating techniques described in detailed by Clarke et al (1998) at the Geochronology Research Laboratory of Queen's University. The data are given in Table 4 and plotted in Fig. 19. All the data have been corrected for blanks, mass discrimination, and neutron-induced interferences. Errors shown in Table 4 and on the age spectrum and isotope-correlation diagrams, represent the analytical precision at ±2 σ.

2.5. Nd Isotopes

Twelve whole rock samples were selected for Nd isotopic analyses (Table 6). Samarium and Nd abundances and Nd isotopic ratios were determined by isotope dilution mass spectrometry in the laboratory of the Department of Earth Sciences at the Memorial University of Newfoundland (St. John's, Newfoundland, Canada). The isotopic ratios were determined using a multicollector Finnigan MAT 262V thermal ionization mass spectrometer operated in a static mode. Measured $^{143}Nd/^{144}Nd$ values were normalized to a natural $^{146}Nd/^{144}Nd$ values of 0.721903, calibrated to the JNdi-1 standard ($^{143}Nd/^{144}Nd$=0.512115; Tanaka et al., 2000) with Nd values accurate to <0.002% and $^{147}Sm/^{144}Nd$ ratio accurate to <0.1%. Replicate analyses of JNdi-1standard yielded $^{143}Nd/^{144}Nd$=0.512137± 1 (n=112). The ε_{Nd} values were calculated for t = 177 Ma using a $^{147}Sm/^{144}Nd$ = 0.1967 and $^{143}Nd/^{144}Nd$ = 0.512638 values for the present day chondrite uniform reservoir (CHUR). ^{147}Sm decay constant is 6.54 10^{-12} y^{-1} (Steiger and Jäger, 1977). Nd model ages (Table 6) were calculated based upon De Paolo's (1988) depleted mantle model (T_{DM1}), and on a depleted mantle model (T_{DM2}) separated from the CHUR (chondrite-uniform reservoir) at 4.55 Ga, with linear evolution and a present-day epsilon value of +10.

2.6. Pb Isotopes

2.6.1. *Whole Rocks*

Thirteen whole rock samples were analyzed for Pb isotopes with thermal ionization mass spectrometry. For Pb isotopic analysis, about 0.2 g of rock powder was dissolved. Separation of Pb was done by the standard anionic HBr-HCl chromatography. Isotopic ratios were obtained using a multicollector Finnigan Mat 262 mass spectrometer in static or dynamic mode depending on the ratios measured at the Department of Earth Sciences, Memorial University of Newfoundland (St. John's, Newfoundland, Canada). Pb isotopic ratios are reported corrected for mass fractionation (Table 7a). A correction factor of 0.107% per amu was obtained by measuring the deviation from repeated (n=12) analyses of the NBS 981 standard. In-run precisions on all isotopic ratios are given at a 95% confidence level.

2.6.2. *Galena*

Galena from a pegmatite dike of the I&L Zone was separated from a crushed sample by handpicking mm-size grains using a binocular microscope. The galena was dissolved in 8N HNO_3, dried and re-dissolved in HBr for Pb separation and isotopic analyses at the Department of Earth Sciences of Carleton University, Ottawa, Ontario, Canada. Pb isotopic analysis was done using standard anion exchange techniques, followed by thermal ionization mass spectrometry (Table 7b). Pb mass spectrometer data were corrected for fractionation using NIST SRM981. The average ratios measured for NIST SR981 are $^{206}Pb/^{204}Pb=16.891\pm0.011$, $^{207}Pb/^{204}Pb=15.430\pm0.014$, and $^{208}Pb/^{204}Pb=36.505\pm0.048$ (2σ). The fractionation correction is +0.13%/amu (based on the values of Todt et al (1996).

2.7. Oxygen Isotopes

Seven samples of granitic material were analyzed for ^{18}O at the Queens's Facility for Isotope Research, Kingston (Ontario) using conventional methods, as summarized in Kontak and Kyser (2009). The samples were lightly crushed and sieved and pure grains of liberated quartz were handpicked under a high power binocular microscope. The separates were made up of vitreous, glassy and fresh quartz without impurities. Briefly, oxygen was extracted from quartz using the BrF_5 method of Clayton and Mayeda (1963) and isotopic measurements run on a dual inlet using a Finnigan MAT 252 isotope ration mass spectrometer. All values are reported using the δ notation (per mil; ‰) relative to V-SMOW (Vienna standard mean ocean water) and replicate $\delta^{18}O$ analyses were reproducible to $\pm$ 0.3‰.

2.8. Fluid Inclusions

Fluid inclusion observation and microthermometry were conducted at Saint Mary's University, Department of Geology (Hanley laboratory), Halifax, Nova Scotia, Canada, using an Olympus BX51 research grade microscope and a Linkam Scientific Instruments FTIR-600 heating- freezing stage.

2.9. Additional Analyses

Tables 1-9 report representative analyses. Additional data are available on request from the authors.

3. Sample Locations

3.1. Outcrop Sample Locations

Sample	Easting	Northing
G151	681442	6089938
G152	680898	6091383
G153	680901	6091407
G154	681597	6090904
G155	681603	6090977
G156	681579	6090906
G157	681687	6090906
G158	681685	6090936
G159	681594	6090966
G160	682916	6089577
G161	682833	6089568
G162	682758	6089537
G163	681656	6088611
G164	681719	6088646
G165	681719	6088643
G166	681661	6088609
G167	681667	6088621
G168	681691	6088619
G169	683567	6089013
G170	683584	6088774
G171	683599	6088760
G172	683460	6088503
LM21	683421	6088495
LM22	683473	6088391
LM24	683419	6088558
LM26	683393	6088382
2009	683550	6088952

Sample	Easting	Northing
G230	683240	6088450
G231	683185	6088447
G232	683139	6088436
G233	683106	6088409
G234	683103	6088367
G235	683064	6088338
G236	683029	6088403
G237	681113	6090526
G238	681173	6090507
G239	681230	6090560
G240	681187	6090632
G241	681067	6090593
G242	681149	6089302
G243	681163	6089333
G244	681169	6089263
G245	681197	6089208
G246	681216	6089196
G247	687866	6090340
G248	687902	6090367
G249	687897	6090357
G250	685331	6089884

coordinates UTM WGS84

Appendix 3.2. Drill Holes of Ucore Rare Metals

Sample Locations

Sample	Drill Hole	Depth (metres)
LM11	LM-08-28	1.5
LM-2	LM-08-28	8
LM13	LM-08-28	10
LM14	LM-08-28	13
LM15	LM-08-28	14
LM16	LM-08-28	16
LM17	LM-08-28	17
LM18	LM-08-28	22.7
LM19	LM-08-28	28
LM58	LM-08-23	48.8
LM61	LM-08-31	6.5
LM66	LM-08-31	30.4
LM70	LM-08-40	23.3
LM71	LM-08-44	18.9
LM73	LM-08-44	27
LM77	LM-08-44	53.7
LM78	LM-08-44	57
LM79	LM-09-56	4.4
LM90	LM- 08-22	36
LM-2	LM-08-18	18.5
LM93	LM-08-18	19
LM94	LM-08-18	3
LM95	LM-08-18	15.8
LM96	LM-08-18	28
LM97	LM-08-18	41
LM99	LM-08-18	43.5
LM100	LM-08-18	49
LM101	LM-08-18	65.8
LM102	LM-08-18	64.2
LM103	LM-08-18	67.4
LM105	LM-08-18	122
LM106	LM-08-18	119
LM111	LM-08-34	40.6
LM113	LM-08-34	44
LM135	LM-08-45	15
LM143	LM-08-46	23.8
LM145	LM-08-46	27
H923	LM -08-34	150
H835	LM -09-48	72.5
H350	LM-10-77	76.3
H361	LM-10-77	126
H369	LM-10-77	131
H370	LM-10-77	146
H371	LM-10-77	146.4
H372	LM-10-77	146.6
H373	LM-10-77	146.9
H374	LM-10-77	147.5
H379	LM-10-77	149.5
H380	LM-10-77	150.3
H381	LM-10-77	151
H382	LM-10-77	151.5
H384	LM-10-77	175
H385	LM-10-77	175.5
H411	LM-10-77	223
G191	LM-08-12	23.5
G198	LM-08-11	43.5
G199	LM-08-11	45
G200	LM-08-11	50.4

Drill Hole Locations

Drill Hole	Easting	Northing	azimuth	dip
LM-08-11	683610.7	6088894.1	212	63
LM-08-12	683596.1	6088908.3	212	71
LM-08-18	683550.5	6088952.4	212	75
LM-08-22	683516.8	6088972.5	212	62
LM-08-23	683556.7	6088937.7	212	65
LM-08-28	683516.6	6088974.1	262	57
LM-08-31	683661.7	6088874.5	212	76
LM-08-34	683563.6	6089004.6	212	65
LM-08-39	683623.1	6088917.5	212	45
LM-08-40	683529.7	6088950.3	212	45
LM-08-44	683697.8	6088848.0	212	60
LM-08-45	683697.8	6088848.0	255	45
LM-08-46	686437.7	6086865.2	37	45
LM-09-48	684509.9	6088430.1	200	62
LM-09-56	685377.6	6088182.2	220	58
LM-10-77	685270.1	6088042.7	18	60

coordinates UTM WGS84

Appendix 3.3. Drill Holes of Standard Metals Corporation
Sample Locations

Sample	Drill hole	Depth (feet)
752	KS-121	92
754	KS-121	110
755	KS-121	122
756	KS-121	179.5
757	KS-121	141.5
758	KS-121	202
759	KS-121	207.3
760	KS-121	261
761	KS-121	266
762	KS-121	272
763	KS-121	284
764	KS-121	291
765	KS-121	293
766	KS-121	295
767	KS-121	299
768	KS-121	312
769	KS-121	316.5
770	KS-121	335
771	KS-121	357.1
772	KS-53	23
773	KS-53	36.5
774	KS-53	43
775	KS-53	48
776	KS-53	51
777	KS-53	63
778	KS-53	78.9
779	KS-53	88.9
780	KS-53	110.8
781	KS-53	119
782	KS-53	126
783	KS-53	180
784	KS-53	205
785	KS-53	210
786	KS-53	220
788	KS-53	250
794	KS-90	565
795	KS-90	619
796	KS-90	664
797	KS-90	669
798	KS-50	38
799	KS-50	42
800	KS-50	52
801	KS-50	89.4
802	KS-50	115.3
803	KS-50	262.2
804	KS-50	286
805	KS-50	314.5
806	KS-50	344.8
807	KS-50	175
808	KS-50	181
809	KS-50	185.5
810	KS-50	189
811	KS-50	192
812	KS-50	223
415	KS-44	18
816	KS-44	47.3
817	KS-44	166.5
824	KS-44A	60
828	KS-45	110

Drill Hole Locations

Drill holes KS-44, KS-44A, KS-45, KS-50, KS-53, KS-90 and KS-121 were drilled by Standard Metals Corporation in 1963-64 within the Ross-Adams deposit and its immediate vicinity; the locations of the drill holes were reported by Thompson et al. (1980).